DAVIS

NATIONAL ACADEMY OF SCIENCES
NATIONAL RESEARCH COUNCIL
of the
UNITED STATES OF AMERICA

UNITED STATES NATIONAL COMMITTEE
International Union of Radio Science

INTERNATIONAL SCIENTIFIC
RADIO UNION

1977 Meeting
June 22 - 24

Sponsored by USNC/URSI

Held in conjunction with the

URSI Symposium on Electromagnetic Wave Theory

and the

Institute of Electrical and Electronics Engineers
Society of Antennas and Propagation
International Symposium

Stanford University
Stanford, California

1977 MEETING - CONDENSED PROGRAM

MONDAY MORNING, JUNE 20, 0900-1215

		Bldg Rm
AP-S 1	Various Topics in Measurements	120 121
AP-S 2	High Frequency Diffraction	POL 161J
AP-S 3	Arrays I	JOR 041
AP-S 4	Antenna Design I	QUA 370
IEMS 1	EM Theory I	JOR 040

MONDAY AFTERNOON, JUNE 20, 1400-1720

AP-S 5	Measurements of the Environment	120 121
AP-S 6	Electromagnetic Theory	POL 161J
AP-S 7	Arrays II	JOR 041
AP-S 8	Antenna Design II	QUA 370
IEMS 2	Waveguides	JOR 040

MONDAY EVENING, JUNE 20, 2000-2400

2000 Meeting of the Administrative Committee of IEEE AP-S

TUESDAY MORNING, JUNE 21, 0900-1215

AP-S 9	Measurement Facilities	120 121
AP-S 10	Numerical Techniques	JOR 041
AP-S 11	Reflectors, Feeds and Horns I	POL 161J
AP-S 12	Antenna Design III	QUA 370
IEMS 3	EM Theory II	JOR 040
0900	Tour of San Francisco	

TUESDAY AFTERNOON, JUNE 21, 1330-1650

AP-S 13	Near Field Probing and Measurements	120 121
AP-S 14	Adaptive Arrays	JOR 041
AP-S 15	Reflectors, Feeds and Horns II	POL 161J
AP-S 16	Joint Session:	JOR 040
IEMS 4	Antennas and the Environment	
AP-S 17	Rain and Random Media Effects	QUA 370

TUESDAY EVENING, JUNE 21, 1745-2200

1745	Wine Tasting	Paul Masson Winery,
1945	Dinner	Saratoga

WEDNESDAY MORNING, JUNE 22, 0900-1215

IEEE AP-S URSI IEMS USNC/URSI	Combined Session: In Memoriam of Professor Samuel Silver, 1915-1976	Music Building Dinkelspiel Auditorium
0900	Tour of San Juan Bautista Mission	

WEDNESDAY AFTERNOON, JUNE 22, 1330-1650

IEMS 5 B-1	Joint Session: Optics	JOR 040
AP-S 18	Reflectors, Feeds and Horns III	POL 161J
AP-S 19 B-3	Joint Session: Surface Effects on EM Waves	JOR 041
AP-S 20 B-2	Joint Session: Transients, SEM and Identification	380 380Y
E-1	Man-Made Radio Noise and Interference	JOR 050
F-1	Clear-Air Doppler Studies of the Troposphere and Ionosphere	QUA 370
F-2	Radio Oceanography	120 121
G-1	Ionospheric Mapping I	MCC 134

WEDNESDAY EVENING, JUNE 22, 1830-2400

1830	Reception, Cash Bar	Four Seas Restaurant,
1930	Banquet, Speaker Russell Targ: "ESP - Fact or Fantasy"	San Francisco

THURSDAY MORNING, JUNE 23, 0900-1215

		Bldg Rm
IEMS 6	Inverse Scattering and Remote Sensing	JOR 041
IEMS 7	Numerical Techniques I	JOR 040
B-4	EM Theory	POL 161J
C-1	Multiple-Access Satellite Communications Systems	380 380Y
F-3	Remote Sensing	QUA 370
F-4	Earth-Space Propagation Above 10 GHz	120 121
G-2	Ionospheric Mapping II	MCC 134
H-1	Theory of Waves and Antennas in Plasmas	JOR 050
0900	Tour of U C Berkeley Campus	

THURSDAY AFTERNOON, JUNE 23, 1400-1720

IEMS 8	Random Media	JOR 041
IEMS 9	Numerical Techniques II	JOR 040
B-5	Scattering and Shielding	POL 161J
C-2	Signal Processing	380 380Y
E-2	Natural Radio Noise	JOR 050
F-5	Radio Meteorology	120 121
F-6	Radio Oceanography, Wave Propagation and Remote Sensing	QUA 370
G-3	ELF to VLF Propagation and Probing I	MCC 134

THURSDAY EVENING, JUNE 23, 1730-2400

1730	USNC/URSI Commission B Business Meeting
1730	USNC/URSI Commission C Business Meeting
1730	USNC/URSI Commission E Business Meeting
1730	USNC/URSI Commission F Business Meeting
1730	USNC/URSI Commission G Business Meeting
2000	USNC/URSI Commission H Business Meeting

FRIDAY MORNING, JUNE 24, 0900-1215

IEMS 10	Antennas and Arrays	JOR 041
IEMS 11	HF Scattering	JOR 040
B-6	Numerical Methods	POL 161J
C-3	Frequency Stability and its Applications to Telecommunication and Time Service Systems	380 380Y
F-7	Scattering of Radio Waves, Theory and Experiment	120 121
G-4	ELF to VLF Propagation and Probing II	MCC 134
G-5 H-2	Joint Session: Wave Phenomena in Ionosphere and Magnetosphere	JOR 050

FRIDAY AFTERNOON, JUNE 24, 1400-1715

IEMS 12	Transients and Singularities	JOR 041
IEMS 13	Scattering	JOR 040
B-7	Antennas	POL 161J
C-4	Timing and Carrier Phase Recovery in Data Communication	380 380Y
F-8	Theoretical and Experimental Studies of Radio Propagation Problems	120 121
G-6	Radio Effects of Ionospheric Waves and Irregularities	MCC 134
G-7	Probing of the High Latitude Ionosphere and Magnetosphere	QUA 370
H-3	Waves in Plasmas	JOR 050

- - - - - - - - - - - - -

Building Abbreviations:

JOR	Jordan
MCC	McCullough
POL	Political Science
QUA	Quadrangle

United States National Committee

INTERNATIONAL UNION OF RADIO SCIENCE

PROGRAM AND ABSTRACTS

1977 Meeting

June 22-24

Held Jointly with the

URSI SYMPOSIUM ON ELECTROMAGNETIC WAVE THEORY

and

ANTENNAS AND PROPAGATION SOCIETY

INSTITUTE OF ELECTRICAL AND ELECTRONICS ENGINEERS

INTERNATIONAL SYMPOSIUM

Stanford, California

NOTE

Programs and Abstracts of the USNC-URSI Meetings are available from:

USNC-URSI
National Academy of Sciences
2101 Constitution Avenue, N.W.
Washington, D.C. 20418

at $2.00 for meetings prior to 1970, $3.00 for 1971 - 1975 meetings, and $5.00 for the 1976 meeting, and $6.00 for the 1977 meeting. The full papers are not published in any collected format, and requests for them should be addressed to the authors who may have them published on their own initiative. Please note that these meetings are national and are not organized by international URSI, nor are these programs available for the international Secretariat.

WELCOME

TO

SAN FRANCISCO

The steering committee of the 1977 APS-URSI Symposium welcomes you to San Francisco and the campus of Stanford University.

The Technical Program Committee headed by Professor Kenneth K. Mei has worked tirelessly to provide you with an outstanding collection of papers describing the latest advances in the field of electromagnetics. We hope that you will find your visit here professionally stimulating and rewarding.

San Francisco is the cultural and financial center of the western United States. It abounds in museums, art galleries, opera, ballet, theatre, restaurants, sports and entertainment of all kinds. We hope that you will find the time to sample and savor this galaxy of attractions. To this end, Dr. Tony Jennetti, Chairman of the Arrangements Committee, has planned two special events for you. California is the wine capital of the United States. On Tuesday evening we will visit the famous Paul Masson Winery to taste their wines and enjoy an outdoor steak barbecue dinner. San Francisco boasts the largest Chinese settlement in the United States. On Wednesday evening we will travel to romantic and enchanting Chinatown for a magnificent Chinese banquet at the Four Seas Restaurant.

Finally, I wish to thank all those who helped to make this Symposium the grand event that it is: the committeemen, the speakers, the session chairmen, Stanford University and our Industry supporters. We are all volunteers. No one is paid for his services. If you find the opportunity, take a minute to thank these hard working members personally for their efforts. For without them, there would be no Symposium.

John B. Damonte

John B. Damonte
General Chairman
Steering Committee

STEERING COMMITTEE

John B. Damonte, General Chairman
Fred M. Tesche, S.F. APS Chapter Chairman
Tom N.C. Wang, S.F. APS Chapter Vice-Chairman

Local Arrangements

Tony G. Jennetti, Chairman
Marvin Wahl, Vice-Chairman
Herbert Greenman C.A. Chuang
Donald Rucker

Finance

Wilbert H. Chang, Chairman
Bruce A. Fox

Digest

Allen E. Smoll, Chairman
Herman W. Bilenko

Publicity

Claes T. Elfving

Professional Listings

Harry Eustace Ron Rose

Registration

John D. Bruce, Chairman
Richard C. Davis

Ladies Activities

Cleone J. Damonte, Chairman
Fay Chang Mary Jane Jennetti
Jeanne Elam Wennie Mei
Nonnie Elfving Sabrina Wang

Technical Program

Kenneth K. Mei

URSI-IEMS	APS	URSI-USNC
Frederick M. Tesche	Edward K. Miller	Frederick W. Crawford
Thomas B.A. Senior	Andy J. Poggio	
Leopold B. Felsen	Tom K. Liu	
	R. Jeff Lytle	

IN MEMORY OF

Professor Samuel Silver, born in Philadelphia, Pennsylvania(USA) on February 25, 1915, died on November 5, 1976, in Walnut Creek near Berkeley, California (USA). He is survived by his wife, Marjorie Silver, a son Daniel Silver, a daughter Deborah Brewer, both of Maryland (USA), and six grand-children.

Professor Silver's affiliation with URSI began after World War II when, in 1950, he became a member of the USA National Committee. He served as Chairman of USA Commission 6 from 1950-1954 and thereafter as Secretary (1957-1963) and Vice-Chairman (1963-1966) of the USA National Committee. At the same time, he held positions within the URSI International Organization: Chairman of Commission 6 (1952-1957), Vice President (1963-1966) and President (1966-1969). He also was Chairman of the Committee on Space Radio Relays and Committee on Space Research (COSPAR)(1957-1966), and URSI representative to the Executive Councils of COSPAR and ICSU (International Council of Scientific Unions). He was a delegate to every General Assembly of URSI since 1950, and was elected permanent Honorary President of URSI at the Warsaw General Assembly in 1973.

While his broad scientific interests related to the work of several of the URSI Commissions, Professor Silver's closest contacts remained with Commission 6. He was a major participant in the conception and organization of the first International Electromagnetic Wave Theory Symposium at McGill University, Montreal, Canada, in 1953. The outstanding success of this symposium has led to a regular triennial series of symposia under this heading, which constitute the most important international forum on electromagnetic theory and its impact on other disciplines. As Chairman of Commission 6, Silver stressed the importance of broadening the scope of its activities and of addressing problems which are of concern to other commissions. His forward looking view of the role of Commission 6, as well as a tracing of historical events leading to its formation in 1950, are contained in Silver's report Radio Waves and Circuits, Vol. 6 of the Proceedings of the XIIIth General Assembly of URSI, Elsevier Publishing Company (1960).

Professor Silver's scientific orientation ranged from theory to application, with strong emphasis on the latter. A physicist by academic training, with B.A. and M.A. degrees from Temple University, Philadelphia, Pennsylvania (USA) and the Ph.D. degree from the Massachusetts Institute of Technology (MIT) in 1940, he soon thereafter bridged the gap with engineering by becoming involved from 1943-1946 in microwave antenna problems at the MIT Radiation Laboratory. The book Microwave Antenna Theory and Design, Vol. 12, MIT Radiation Laboratory Series (1949), for

which he served as Editor and major contributor, became the foundation for modern microwave antenna research and development and still is a standard reference text. Silver's own perceptions of his scientific interests and activities are contained in a fascinating lecture delivered on the occasion of the bestowal upon him of the second John T. Bolljahn Memorial Award (the lecture is reprinted in IEEE Transactions on Antennas and Propagation, May 1972). Apart from the clarity with which the various scientific endeavors are described there, and which demonstrates his qualities as an outstanding teacher, the reader cannot fail to note the thoughtful attribution of credit to others, especially graduate students, who participated in the work.

After leaving the MIT Radiation Laboratory, Professor Silver joined the faculty of the Department of Electrical Engineering, University of California, Berkeley, where in 1950 he was made Professor of Electrical Engineering, and a few years later Professor of Engineering Science. At the University of California, Berkeley, he developed a research program on microwave antennas and applied electromagnetic theory and related areas of microwave electronics. He organized the Electronics Research Laboratory of the Department of Electrical Engineering, of which he became Director in 1956. In 1960 he was appointed to the post of Director of the Space Sciences Laboratory and given the task of developing a campus-wide program of space research and a facility to serve as a center for faculty/graduate student work in the space sciences. He was a Fellow of the Institute of Electrical and Electronics Engineers (IEEE), the American Geophysical Union and the American Physical Society, a member of the American Meteorological Society, and the recipient of Guggenheim Fellowship Awards in 1953 for his work on scattering and diffraction of electromagnetic waves, and in 1960 for his research in physics of the upper atmosphere. He received an honorary degree of D.Sc. in 1963, and a Distinguished Alumnus Award in 1964, from his alma mater, Temple University. He was elected to the U.S. National Academy of Engineering in 1968 and as already noted, was the second recipient of the John T. Bolljahn Memorial Award.

While his scientific accomplishments and his dedication to his profession earned Professor Silver the admiration and respect of his peers, those who knew him well loved him for his human qualities. He was uncompromising in his quest for excellence and in upholding what he perceived to be basic principles of integrity and conduct within and outside the scientific sphere. He was truly an educator, freely giving advice and counsel. He was modest, unassuming and gentle when dealing with people but impatient with those whom he thought pompous or hypocritical. He had a highly developed sense of humor and would relate a good joke with relish. He was proud of his ethic and religious heritage as a Jew and even included in his curriculum vitae the sources of his pre-college religious education. He was compassionate of the human condition but realistic about the difficulties in effecting a change. To many who knew him, he was a true friend. He will be sorely missed.

DESCRIPTION OF

INTERNATIONAL UNION OF RADIO SCIENCE

The International Union of Radio Science is one of 17 world scientific unions organized under the International Council of Scientific Unions (ICSU). It is commonly designated as URSI (from its French name, Union Radio Scientifique Internationale). Its aims are (1) to promote the scientific study of radio communications, (2) to aid and organize radio research requiring cooperation on an international scale and to encourage the discussion and publication of the results, (3) to facilitate agreement upon common methods of measurement and the standardization of measuring instruments, and (4) to simulate and to coordinate studies of the scientific aspects of telecommunications using electromagnetic waves, guided and unguided. The international Union itself is an organizational framework to aid in promoting these objectives. The actual technical work if largely done by the National Committees in the various countries.

The officers of the International Union are:

President:	J. Voge (France)
Immediate Past President:	W.J.G. Beynon (UK)
Vice Presidents:	W.N. Christiansen (Australia) W.E. Gordon (USA) V.V. Migulin (USSR) F.L.H.M. Stumpers (Netherlands)
Secretary General:	C.M. Minnis (Belgium)
Honorary Presidents:	B. Decaux (France) W. Dieminger (West Germany) J.A. Ratcliffe (UK) R. L. Smith-Rose (UK)

The Secretary's office and the headquarters of the organization are located at 7 Place Emile Danco, 1180 Brussels, Belgium. The Union is supported by contributions (dues) from 35 member countries. Additional funds for symposia and other scientific activities of the Union are provided by ICSU from contributions received for this purpose from UNESCO.

The International Union, as of the XVIII General Assembly held in Lima, Peru, August 1975, has nine bodies called Commissions for centralizing studies in the principal technical fields. The names of the Commissions and the chairmen to follow.

A. Electromagnetic Metrology
Altschuler (USA)

B. Fields and Waves
van Bladel (Belgium)

C. Signals and Systems
Picinbono (France)

D. Physical Electronics
Smolinski (Poland)

E. Interference Environment
Likhter (USSR)

F. Wave Phenomena in Nonionized Media
Eklund (Sweden)

G. Ionospheric Radio
King (United Kingdom)

H. Waves in Plasmas
Gendrin (France)

J. Radio Astronomy
Westerhout (USA)

Every three years, the International Union holds a meeting called the General Assembly. The next General Assembly, the XIX, will be held in Helsinki, Finland in August 1978. The Secretariat prepares and distributes the Proceedings of these General Assemblies. The International Union arranges international symposia on specific subjects pertaining to the work of one Commission or to several Commissions. The International Union also cooperates with other Unions in international symposia on subjects of joint interest.

Radio is unique among the fields of scientific work in having a specific adaptability to large-scale international research programs, for many of the phenomena that must be studied are worldwide in extent and yet are in a measure subject to control by experimenters. Exploration of space and the extension of scientific observations to the space environment is dependent on radio for its communication link and at the same time expands the scope of radio research. One of its branches, radio astronomy, involves cosmos-wide phenomena. URSI has in all this a distinct field of usefulness in furnishing a meeting ground for the numerous workers in the manifold aspects of radio research; its meetings and committee activities furnish valuable means of promoting research through exchange of ideas.

U.S. National Committee
for the
International Union of Radio Science

MEMBERSHIP

Officers and Editor

Chairman	*Dr. John V. Evans
Vice-Chairman	*Dr. C. Gordon Little
Secretary	*Dr. James R. Wait
Editor	Dr. Thomas B.A. Senior

Members from National Societies

AGU	Dr. Alexander J. Dessler
IEEE	Dr. Ernst Weber

Liaison Representatives from Goverment Agencies

OTP	Mr. S.E. Probst
NSF	Dr. R. Marcus Price
DOC	Mr. Alan H. Shapley
NASA	Dr. Erwin R. Schmerling
FCC	Mr. Harry Fine
DOD	Mr. Emil Paroulek
Army	Mr. A. W. Anderson
Navy	Dr. Alan H. Schooley
Air Force	Dr. A. C. Schell

Members-at-Large (twelve) (Term expires December 31 of year indicated)

1977

Mr. Jack W. Herbstreit - E, F g
Dr. Curtis C. Johnson - B u
Prof. V.H. Rumsey - B, J u
Prof. John M. Wozencraft - B, C u

1978

Dr. David Atlas - F np
Dr. Jack K. Wolf - B, C u
Dr. M.K. Barnoski - i

---

*-Members of Executive Committee (the USNC Executive Committee consists of the Chairman, Vice-Chairman, Secretary and Immediate Past Chairman).

Key:
1. Capital letters designate the commissions of which the individuals are members.

2. Small letters designate employment of individuals:
g (government), i (industry), np (nonprofit) and u (university).

Ex-Officio Members

a. Immediate Past Chairman of USNC-URSI *Dr. Francis S. Johnson

b. Chairmen of the USNC-URSI Commissions

Commission A	Dr. George E. Schafer
Commission B	Dr. Thomas A. Senior
Commission C	Dr. William F. Utlaut
Commission D	(Vacant)
Commission E	Mr. George H. Hagn
Commission F	Dr. A.H. LaGrone
Commission G	Dr. Thomas E. VanZandt
Commission H	Dr. Frederick W. Crawford
Commission J	Dr. K.I. Kellerman

c. Officers of URSI resident in the United States

Vice President	*Prof. William E. Gordon

d. Chairmen and Vice-Chairmen of Commissions of URSI resident in the United States

Chairman of Commission A	Dr. Helmut M. Altschuler
Chairman of Commission J	Prof. Gart Westerhout
Vice-Chairman of Commission B	Prof. Leopold B. Felsen
Vice-Chairman of Commission E	Mr. George H. Hagn
Vice-Chairman of Commission F	Prof. Alan T. Waterman
Vice-Chairman of Commission H	Dr. Frederick W. Crawford

e. Foreign Secretary of the U.S. National Academy of Sciences — Dr. George S. Mammond

f. Chairman, Officer of Physical Sciences-NRC — Dr. D. Allan Bromley

Honorary Members

Dr. Harold H. Beverage
Prof. Arthur H. Waynick

*Members of Executive Committee

Memorial Session for PROFESSOR SAMUEL SILVER, 1915-1976

Combined Session (URSI IEMS, IEEE APS, USNC/URSI)

Wednesday, June 22

Chairman: J.G. Van Bladel
Laboratorium voor Electromagnetisme
en Acustica
Ghent, Belgium

OPTICS

Commission B - Session 1
(Joint with IEMS Session 5)

Wednesday p.m., June 22

Chairman: L.B. Felsen
Polytechnic Institute of New York
Brooklyn, New York, USA

TRANSIENTS, SEM, AND IDENTIFICATION

Commission B - Session 2
(Joint with IEEE APS Session 20)

Wednesday p.m., June 22

Chairman: M.B. Van Blaricum
MRC
Santa Barbara, California

SURFACE EFFECTS ON EM WAVES

Commission B - Session 3
(Joint with IEEE APS Session 19)

Wednesday p.m., June 22

Chairman: K. Casey
Kansas State University
Manhattan, Kansas

EM THEORY

Commission B - Session 4

Thursday a.m., June 23

Chairman: R.E. Kleinman
University of Delaware
Newark, Delaware

SCATTERING AND SHIELDING

Commission B - Session 5

Thursday p.m., June 23

Chairman: D.R. Wilton
University of Mississippi
Oxford, Mississippi

NUMERICAL METHODS

Commission B - Session 6

Friday a.m., June 24

Chairman: E. K. Miller
Lawrence Livermore Laboratory
Livermore, California

ANTENNAS

Commission B - Session 7

Friday p.m., June 24

Chairman: G.A. Thiele
Ohio State University
Columbus, Ohio

MULTIPLE-ACCESS SATELLITE COMMUNICATIONS SYSTEMS

Commission C - Session 1

Thursday a.m., June 23

Chairman: J. Aein
Institute for Defense Analyses

SIGNAL PROCESSING

Commission C - Session 2

Thursday p.m., June 23

Chairman: B.D. Steinberg
University of Pennsylvania

FREQUENCY STABILITY AND ITS APPLICATIONS TO TELECOMMUNICATION AND TIME SERVICE SYSTEMS

Commission C - Session 3

Friday a.m., June 24

Chairman: W.C. Lindsey
University of Southern California

TIMING AND CARRIER PHASE
RECOVERY IN DATA COMMUNICATION

Commission C - Session 4 (Invited Session)

Friday p.m., June 24

Chairman: L.E. Franks
University of Massachusetts

MAN-MADE RADIO NOISE AND INTERFERENCE

Commission E - Session 1

Wednesday p.m., June 22

Chairman: George Hagn
Stanford Research Institute
Washington, D.C.

NATURAL RADIO NOISE

Commission E - Session 2

Thursday p.m., June 23

Chairman: G.H. Price
Stanford Research Institute
Menlo Park, CA

CLEAR-AIR DOPPLER STUDIES OF THE TROPOSPHERE AND STRATOSPHERE

Commission F - Session 1

Wednesday p.m., June 22

Chairman: Dr. Thomas E. VanZandt
Aeronomy Laboratory, NOAA
Boulder, CO

RADIO OCEANOGRAPHY

Commission F - Session 2

Wednesday p.m., June 22

Chairman: K.R. Carver
Physical Science Laboratory
New Mexico State University

REMOTE SENSING

Commission F - Session 3

Thursday a.m., June 24

Chairman: Dr. A. Fung
Center for Research, Inc.
Lawrence, Kansas

EARTH-SPACE PROPAGATION ABOVE 10 GHZ

Commission F - Session 4

Thursday a.m., June 23

Chairman: Dr. D.C. Cox
Bell Telephone Labs

RADIO METEOROLOGY

Commission F, Session 5

Thursday p.m., June 23

Chairman: A. T. Waterman
Stanford University

RADIO OCEANOGRAPHY, WAVE PROPAGATION AND REMOTE SENSING

Commission F, Session 6

Thursday p.m., June 23

Chairman: R. H. Stewart
Scripps Institute of Oceanography
La Jolla, California

SCATTERING OF RADIO WAVES,
THEORY AND EXPERIMENT

Commission F, Session 7

Friday a.m., June 24

Chairman: W. Vogel
Electrical Engineering Research Lab
The University of Texas at Austin

THEORETICAL AND EXPERIMENTAL STUDIES
OF RADIO PROPAGATION PROBLEMS

Commission F, Session 8

Friday, p.m. June 24

Chairman: C. R. Beard
Naval Research Laboratories
Washingron, D.C.

IONOSPHERIC MAPPING I

Commission G, Session 1

Wednesday p.m., June 22

Chairman: C. Rush
Air Force Geophysics Laboratory
Bedford, Massachusetts

IONOSPHERIC MAPPING II

Commission G, Session 2

Thursday a.m., June 23

Chairman: C. Rush
Air Force Geophysics Laboratory
Bedford, Massachusetts

ELF TO VHF PROPAGATION AND PROBING I

Commission G, Session 3

Thursday p.m., June 23

Chairman: O. G. Villard, Jr.
Stanford Research Institute

ELF TO VLF PROPAGATION AND PROBING II

Commission G - Session 4

Friday a.m., June 24

Chairman: A. J. Ferraro
Pennsylvania State University

WAVE PHENOMENA IN IONOSPHERE AND MAGNETOSPHERE

Commission G - Session 5
Commission H - Session 2

Friday, June 24

Chairman: R. A. Helliwell
Radioscience Laboratory, Stanford University

RADIO EFFECTS OF IONOSPHERIC WAVES AND IRREGULARITIES

Commission G - Session 6

Friday, June 24

Chairman: T. Croft
Stanford Research Institute

PROBING OF THE HIGH LATITUDE IONOSPHERE AND MAGNETOSPHERE

Commission G - Session 7

Friday, June 24

Chairman: M. Baran
Stanford Research Institute

THEORY OF WAVES AND ANTENNAS IN PLASMAS

Commission H - Session 1

Thursday, June 23

Chairman: T. N. C. Wang
Stanford Research Institute

WAVES IN PLASMAS

Commission H - Session 3

Friday, June 24

Chairman: F. W. Crawford
Institute for Plasma Research
Stanford University

PROPAGATION IN THE DIPOLE-MODE ALONG METAL WAVEGUIDE STRUCTURES OF CIRCULAR CROSS-SECTION.

Harold M.Barlow
Department of Electronic & Electrical Engineering,
University College, London, United Kingdom.

The HE_{11} dipole-mode propagated along a dielectric rod or tube is well known;[1] it is a 'slow' wave not subject to cut-off and has found application both in the microwave and optical parts of the spectrum.

An alternative form of waveguide for use at the lower frequencies in the support of this wave, is a cylindrical grid of wires running parallel to one another along the length of the waveguide and separated by dielectric. Fig.1.(a). The essential requirement is a structure capable of energy storage and one that presents at its cylindrical surface, inductive impedance to longitudinal current associated with capacitive impedance to circumferential current. Both the dielectric and metal waveguides described possess characteristics of the kind required but the wire-grid structure exhibits a specially interesting and important feature namely, falling axial attenuation as the number of wires forming the grid is increased and this simultaneously with rising radial attenuation. Fig.1.(b). The penalty of increasing the number of wires lies in a progressive decrease in power-carrying capacity, which of course falls to zero when adjacent wires ultimately touch one another. In a practical multi-wire arrangement e.g. 16 copper wires, the decay of the field in the radial direction at 2 G.Hz., may be as much as 10 Nepers/m. with corresponding axial attenuation of only about 2×10^{-3} Nepers/m.

The disadvantage of any single-surface waveguide is that it can never be completely screened and an important consideration in this work is therefore, the effect of enclosing the structure in a continuous coaxial metal sheath. Fig.2.(a). It will be recalled that when the circular 'slow' surface-wave is enclosed, the familiar coaxial T.E.M. mode is obtained.

Starting from the dipole wave-equation describing behaviour in an annular dielectric-filled space between two coaxial surfaces of defined impedances to axial and circumferential currents,[2] computations have been made at 2 G.Hz. for a wire-grid type of inner surface ranging in radii r_1 from 0.5 cm. upwards, associated with a continuous smooth metal outer of fixed radius $r_2 = 4$ cms. Thus, the surface impedances, looking towards the axis of the guide are;-

for the inner $Z_{x_1} = (1+j)R$ and $Z_{\theta_1} = (R-jX_{\theta_1})$, while
for the outer $Z_{x_2} = Z_{\theta_2} = -(1+j)R$ where $R = \sqrt{\frac{\omega\mu}{2\nabla}}$ and ∇ is the conductivity of the metal, assumed to be the same throughout.

Having defined the surface impedances, X_{θ_1} being taken as a nominal 1000 Ohms, the calculations from real and imaginary parts of the wave-equation can conveniently be made in terms of (a/b) and (b) where the radial propagation constant $u = (a-jb)$. For a structure in which the dielectric is loss-less we have $ab = \alpha\beta$, α being the corresponding axial attenuation and β the axial phase-change, a quantity that remains substantially constant. The results are shown in Fig.2.(b).
To satisfy the requirements (a/b) was found to be just a little greater than $(1+\sqrt{2})$, the figure that characterises propagation in the circular mode between two smooth coaxial metal surfaces.[3] There is thus, a radical change from the situation found in the case of the unscreened dipole-mode when supported by a similar wire-grid structure for which (a/b) was found to be of the order of 200 or 300.

The outer screen when added, therefore tends to dominate the field distribution and therein lies the importance of the inner for the support of a significant dipole-mode. The wire-grid structure, with the possibility of a strong electric field across its diameter, performs better as an energy-storage structure than a simple dielectric rod. Moreover, when using a grid of parallel wires Z_{x_i} acquires a slightly increased inductive reactance while X_{θ_i} becomes finite, producing a value of (a/b) some 10^{-2} % above the ($1+\sqrt{2}$) figure for the screened circular mode. The values of α , computed as they were for (a/b) close to 2.4142 , were not significantly affected either by small changes in (a/b) or by the corresponding X_{θ_i} quantity. At the same time X_{θ_i} proved to be very dependent on the precise value required for (a/b).

The presence of the outer metal screen makes possible 'fast' waves if the cross-sectional dimensions are sufficient. In particular, the septum-mode may make its appearance when semi-circumferential half-wave resonance is permitted, the approximate cut-off wavelength of this mode being $\lambda_c = \pi (r_1 + r_2)$. Fig.2.(a).

A prominent feature of the α curve in Fig.2.(b), is what appears to be shunt resonance behaviour in the expected septum-mode region and this leads to a steep rise in transmission losses. However, for the most part, the attenuation of the circular 'slow' wave mode (coaxial T.E.M.), as shown by the dotted V curve in Fig.2.(b), remains comparatively high. The field of the dipole-mode necessarily penetrates to the axis of the inner wire-grid structure while, in the case of the circular mode the field cannot go beyond the surface of the inner and power transmission is then confined to the annular space between the two surfaces.

Employing suitable parameters for the wire-grid structure of the inner, incorporating some solid dielectric for support of the wires and incidentally thereby accentuating electric field-strength capability, it seems likely that a practical screened dipole-mode cable of comparatively small loss, can be developed.

Acknowledgments.

It is a pleasure to acknowledge the contribution made by Prof. M.Nouri of Arya-Mehr University, Tehran, to the experimental results recorded in Fig.1.(b)., and the support given to the work by the U.K. Ministry of Defence.

References.

(1) Kikuchi H. & Yamashita E.,'Theory of dielectric waveguides and some experiments at 50 G.Hz.', Symposium on millimeter waves, Polytechnic Institute of Brooklyn, New York, 1959, p.p. 619-638.

(2) Barlow H.M., 'Screened surface-waves of the dipole-family in a coaxial waveguide', J.Phys.D.,1972,Vol.5, p.p.1049-1062.

(3) Barlow H.M., 'Screened and unscreened axially-cylindrical surface-waves', J.Phys.D., 1971,Vol.4.,p.p.372-380.

Fig.1.(a).
Unscreened cylindrical wire-grid structure.

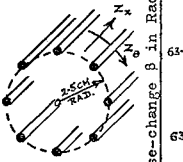

Measured propagation constants at 3 G.Hz.
Fig.1.(b).

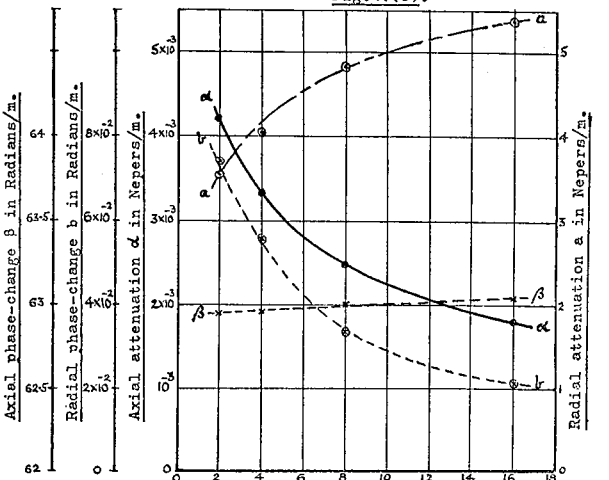

Fig.2.(a).
Screened cylindrical wire-grid structure.

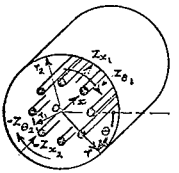

Approx. E field.

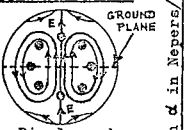

Dipole-mode.

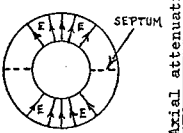

Septum-mode.

Calculated attenuation of screened waveguide at 2 G.Hz.
Fig.2.(b).

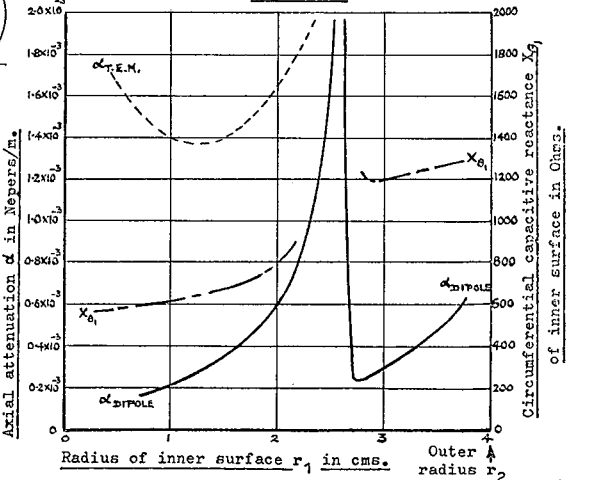

Calculations for:- f=2 G.Hz., r_2= 4cms., σ=5.778 X 10^{-2} mhy.
Z_{x_1} =(1+j)R , Z_{θ_1} =R-jX_{θ_1} , Z_{x_2} = Z_{θ_2} = -(1+j)R
where R = 1.169 X 10^{-2} Ohms.

Combined Session, 0940, Wednesday, June 22

WAVEGUIDES FOR INTEGRATED OPTICS: COMPARISON OF ANALYSIS METHODS, AND NEW PHYSICAL EFFECTS

S. T. Peng and A. A. Oliner
Polytechnic Institute of New York
Brooklyn, New York

The methods of analysis which have so far been used to determine the propagation characteristics of waveguiding structures proposed for integrated optical circuits are relatively elementary and crude. It is generally believed that these simple methods are sufficient, and under some circumstances this belief is justified. However, more careful considerations indicate that for certain structures, and for certain classes of modes on all structures, additional sophistication, even if still elementary, is required. In fact, these additional simple considerations have shown that under appropriate circumstances new physical effects such as leakage and resonance are present; these effects are completely undetected when the simpler analysis methods are employed.

This paper first presents a comparison of the analysis methods which have appeared in the literature, and indicates their basic approaches and limitations in the context of a rigorous phrasing. It then shows the ways in which simple improvements in accuracy can be achieved easily, and presents two examples for which these simple improvements demonstrate important qualitative behavior effects which the simpler analyses miss entirely.

The waveguides treated here confine the fields both vertically and horizontally; planar guiding structures which confine the field in the vertical direction only can of course be analyzed rigorously in a trivially-simple fashion. Two well-known examples of the class of waveguides under consideration here are shown in Fig. 1.

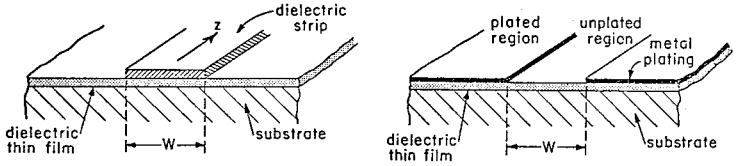

THE STRIP WAVEGUIDE THE SLOT WAVEGUIDE

Fig. 1. Two well-known waveguides for integrated optics.

The thicknesses of the film and the other coatings are such that only one TE and one TM mode can be supported in each of the constituent regions at the frequency of operation. (The final wave guided in the longitudinal (z) direction is a hybrid mode; the terms TE and TM used hereafter refer to the basic surface waves in each constituent region.) The simple theories in the literature assume that, due to the polarization of the exciting mechanism, only the TE or the TM mode type need be considered in the analysis. Although transmission line phrasings are usually not employed, it is instructive to use here the transverse equivalent network shown in Fig. 2 to characterize the nature of the approximations currently employed. Choosing the strip waveguide, for example, for a basically TE type mode, the transmission lines represent separately the TE modes in the

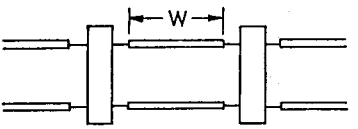

Fig. 2. Transverse equivalent network assuming only one propagating mode in each constituent region.

inner and outer regions. The boxes in Fig. 2 represent the step discontinuity formed by the junction between the loaded and unloaded regions. In an almost rigorous phrasing, the boxes would contain contributions from any discrete modes and from the continuous spectrum. (A rigorous phrasing would also require the coupling between the discontinuities.) The properties of the guided modes are then found from the resonances of the transverse equivalent network.

One approximate method, which has been called the "effective dielectric constant" method, dispenses with the boxes altogether, so that the transmission lines connect directly with each other. This method thus neglects any contributions from the discrete TM modes in each region and from the continuous spectrum (which is purely reactive here). It has been applied to the strip waveguide [1], to some types of millimeter waveguides [2, 3, 4], and to thin-film semiconductor lasers [5].

Another approximate method, which is only slightly different from the "effective dielectric constant" method, is a modification of an approximate procedure proposed by Marcatili [6] for structures in which the film is absent. In this method, the outer transmission lines represent some fictitious composite structure rather than the actual one, and the continuous spectrum and discrete TM modes are again neglected. This method was applied to strip waveguides [7, 8] and to slot waveguides [9].

The application of the modified-Marcatili method to slot waveguides (see Fig. 1) yielded reasonably good results for the mode or polarization which is basically TE (called the E^x mode by Marcatili [6]), but was inadequate for the basically TM mode (Marcatili's E^y mode). This difficulty was pointed out by Oliner and Peng [10, 11], who showed that for the latter polarization another mode, the basic plasmon mode, must be included in the metal-plated regions. The resulting transverse equivalent network (see Fig. 3) must now contain

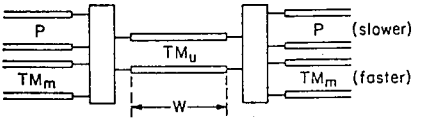

Fig. 3. Transverse equivalent network for the slot waveguide taking the plasmon (P) mode into account.

another transmission line in the outer (plated) regions to accommodate the plasmon (P) mode. The terms TM_u and TM_m signify respectively the TM modes in the uncoated and metal-coated regions. It is no longer possible now to neglect the boxes because coupling among the three transverse modes must occur. Oliner and Peng employed overlap integrals to determine the coupling quantitatively.

Since the basic plasmon (P) mode is slower than the TM_u mode, the guided wave is no longer purely bound, as was previously thought, but it leaks transversely. The resulting attenuation constant for the guided wave thus increases substantially; for a silver plating, the increase is more than an order of magnitude.

It is also found that the wave can be guided over a larger range of film thicknesses than previously thought.

The next improvement in the approximation is to include the other discrete modes in the boxes. Pictorially, additional transmission lines are exhibited explicitly in the transverse equivalent network, and they are then coupled to the previous ones by the boxes at the step junctions. When the wave polarization is basically TE, the coupling with TM waves at the junctions produces only small numerical changes in the guided wave properties. For basically TM wave polarization, however, under appropriate but common conditions, interesting new physical effects occur. The nature of the coupling at a step junction is shown in Fig. 4, where it can be seen that the TE component excited in the

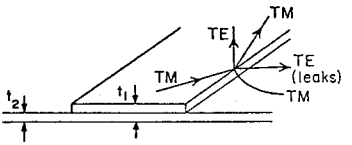

Fig. 4. TE-TM coupling at a step junction in the "TM" case, showing leakage.

outer regions is not evanescent; as a result, the guided mode becomes a leaky wave. The TE component in the strip region is excited at an angle closer to the normal than the TM component; this feature results in resonance effects at certain strip widths.

In the talk the nature of the coupling will be discussed further and numerical data in the form of curves will be presented for both the strip and slot waveguides which will show that these effects are quantitatively important in practical situations.

REFERENCES

1. V. Ramaswamy, Bell Syst. Tech. J., 53, 697-704, Apr. 1974.
2. P. P. Toulios and R.M. Knox, Wescon, Los Angeles, Aug. 1970.
3. W. McLevige, T. Itoh and R. Mittra, IEEE Trans. MTT-23, 788-794, Oct. 1975.
4. T. Itoh, IEEE Trans. MTT-24, 821-827, Nov. 1976.
5. T. Rozzi and T. Itoh, Proc. European Micr. Conf., 495-498, Rome, Italy, Sept. 1976.
6. E.A.J. Marcatili, Bell Syst. Tech. J., 48, 2071-2102, Sept. 1969.
7. H. Furuta, H. Noda and A. Ihaya, Appl. Opt., 13, 322-326, Feb. 1974.
8. N. Uchida, Appl. Opt., 15, 179-182, Jan. 1976.
9. Y. Yamamoto, T. Kamiya and H. Yanai, Appl. Opt., 14, 322-326, Feb. 1975.
10. A.A. Oliner and S.T. Peng, Topical Mtg. on Integ. Opt., Salt Lake City, Jan. 1976.
11. A.A. Oliner and S.T. Peng, Proc. European Micr. Conf., 499-503, Rome, Italy, Sept. 1976.

ACKNOWLEDGMENT

This research was supported by the Joint Services Electronics Program under Contract No. F44620-74-C-0056.

SYNTHESIS OF OFFSET DUAL SHAPED REFLECTORS WITH ARBITRARY CONTROL OF PHASE AND AMPLITUDE*

Victor Galindo-Israel and Raj Mittra, Consultant
Jet Propulsion Laboratory, Cal. Tech.,
Pasadena, CA 91103

The problem of synthesizing dual reflector antennas to achieve simultaneous control of the amplitude and phase of the radiating aperture of the main reflector is of great practical interest. Although a geometrical-optical solution to the synthesis problem was published as early as 1964 [1] for the case of dual rotationally symmetric reflectors, the generalization to the offset case, the subject of discussion of this paper, has not yet been reported. Mitzuguchi and Yokoi [2] recently derived a general set of equations relating the two surfaces satisfying Snell's Law (see figure 1) and the phase constraint in the aperture. However they concluded that simultaneous control of the aperture amplitude, imposed via the imposition of the energy condition, was not generally possible, and consequently they restricted themselves to solutions achieving 'phase only' synthesis of the main reflector aperture with limited amplitude control.

In an earlier paper, Kinber [3] had investigated the general problem of dual reflector antenna synthesis and had claimed that although a solution to the problem did exist for the two-dimensional (axially symmetric) case, it did not necessarily exist for the three-dimensional problem, e.g., the offset geometry.

In this contribution the authors demonstrate that an approximate general solution to the simultaneous amplitude and phase specification problem is indeed possible and present a systematic non-iterative approach for deriving the profiles of the two reflector surfaces by simultaneously imposing the geometrical-optical phase condition and the energy constraint governing the amplitude distribution. These conditions lead to two non-linear coupled differential equations which are readily integrated by standard numerical techniques. The application of the method is demonstrated by an example for which numerically generated surface profiles for the two reflectors are presented.

We commence with the premise that the two reflectors do exist and are described by:

$$z = z(\rho, \psi) \quad \text{and} \quad r = r(\theta, \phi) \tag{1}$$

for the main and subreflectors (see figure 1). Since the reflectors do exist, the partial derivatives at points on the reflectors connected by a common ray trajectory are found from

*This research was performed by J. P. L., California Institute of Technology, and was sponsored by NASA under Contract No. NAS7-100.

$$z_\rho = z_\rho(z, r/\rho, \psi; \theta, \phi), \quad z_\psi = z_\psi(z, r/\rho, \psi; \theta, \phi) \tag{3a}$$

$$r_\theta = r_\theta(z, r/\rho, \psi; \theta, \phi), \quad r_\phi = r_\phi(z, r/\rho, \psi; \theta, \phi) \tag{3b}$$

where the deviatives $z_\rho \equiv \partial z/\partial\rho$ represent Snell's law on the reflector surfaces as for example given by Mitzuguchi and Yokoi [2] . We recognize (z, r) as dependent and $(\rho, \psi; \theta, \phi)$ as independent variables.

Since the reflectors exist, the <u>total</u> differentials also exist:

$$\left.\begin{aligned} &dz = z_\rho d\rho + z_\psi d\psi; \; dr = r_\theta d\theta + r_\phi d\phi \\ &\text{where} \\ &z_{\rho\psi} = z_{\psi\rho} \text{ and } r_{\theta\phi} = r_{\phi\theta}. \end{aligned}\right\} \tag{4}$$

The objective is to integrate (4) with appropriate constraints. Equation (4) is presently <u>under-constrained</u>.

A significant constraint to be imposed is the <u>energy conservation</u> constraint

$$V_c \; V(\rho, \psi) \; \rho d\rho d\psi = N(\theta, \phi) \sin\theta d\theta d\phi \tag{5}$$

where $V_c \; V(\rho, \psi)$ is the projected aperture amplitude distribution and $N(\theta, \phi)$ is the feed amplitude pattern. Phase patterns are implicit in (3a) and (3b).

Although a more general approach to integrate (4) under constraint (5) has been developed by the authors, we will demonstrate the following approach which will be shown to be sufficiently general to transform any $N(\theta, \phi)$ into any prescribed $V(\rho, \psi)$ within prescribed circular boundaries. We look for solutions satisfying the condition

$$\psi = \psi(\phi) \text{ and } d\psi = \psi_\phi d\phi, \tag{6}$$

a slight generalization of a suggestion of Mitzugutchi and Yokoi. Thus (5) becomes

$$V_c \; V(\rho, \psi)\rho\left[\rho_\phi \psi_\phi \left(\frac{d\phi}{d\theta}\right) + \rho_\theta \psi_\phi\right] d\theta d\phi = N \sin\theta d\theta d\phi. \tag{7}$$

We now choose a <u>path</u> of integration in the (θ, ϕ) plane of the general character

$$\alpha(\theta, \phi) \; d\theta + \beta(\theta, \alpha) d\phi \tag{8}$$

that starts at a <u>single point</u> or <u>initial</u> condition of the problem

$$P_o \equiv (z_o, r_o/\rho_o, \psi_o; \theta_o, \phi_o) \tag{9}$$

implicit in (3). Paths of the type

$$d\phi = 0 \quad \text{or} \quad d\theta = 0 \tag{10}$$

and combinations thereof are most useful. For the type of path, $d\phi = 0$, we find from (7) that

$$\psi_\phi V_c \int_{\rho_o}^{\rho} V(\rho, \psi)\rho d\rho = \int_{\theta_o}^{\theta} N(\theta, \phi) \sin\theta \, d\theta \tag{11}$$

which leads to the value of V_c when $(\rho, \theta) \equiv (\rho_m, \theta_m)$ — the projected reflector peripheries. Equation (11) also leads to definition of the function ψ_ϕ and $\psi(\phi)$ with the use of the initial condition (9). Most important, (11) also leads to the definition of

$$\rho = \rho(\theta, \phi), \tag{12}$$

which permits (4), the differential equation, to be placed in first order nonlinear ordinary form:

$$dz = z_\rho \rho_\theta d\theta \ , \quad dr = r_\theta d\theta \ . \tag{13}$$

A choice of path of integration, $d\theta = 0$, similarly leads to

$$dz = (z_\rho \rho_\phi + z_\psi \psi_\phi) \, d\phi, \quad dr = r_\phi d\phi. \tag{14}$$

Equations (13) and (14) are readily integrable, and an example is presented for both cases on the same dual reflector pair. We illustrate solutions for the case

$$V(\rho, \psi) = 1 \text{ and } N(\theta, \phi) = \cos^{45}\theta, \tag{15}$$

the uniform phase and amplitude case, where $N(\theta)$ is chosen for a -3db taper at the edge of the subreflector. In figure 2, results are presented for radial paths of integration $d\phi = 0$. In figure 3, results are presented for circumferential paths of integration, $d\theta = 0$.

Some of the generalizations possible to the solutions of (4) by methods similar to that outlined herein are a more relaxed control of the periphery $\rho_m(\phi)$ and $\theta_m(\phi)$, and the ability to take a non-ϕ symmetric primary pattern $N(\theta, \phi)$ into a ψ-symmetric projected aperture distribution $V(\rho, \psi) = V(\rho)$. Also the feed phase function $\Psi(\theta, \phi)$, see [2], and the aperture phase function $\Gamma(\rho, \psi)$ are arbitrarily controllable.

References

1. Galindo, V., "Design of Dual Reflector Antennas with Arbitrary Phase and Amplitude Distributions," IEEE Trans. on AP, July 1964.

2. Mitzugutchi, Y. and Yokoi, H., "On Surface of Offset Type Dual Reflector Antenna," IECE, Vol 58-B, No. 2, 1975.
3. Kinber, B. Ye, "On Two Reflector Antennas," Radio Eng. Electron. Phys., Vol. 6, June 1962.

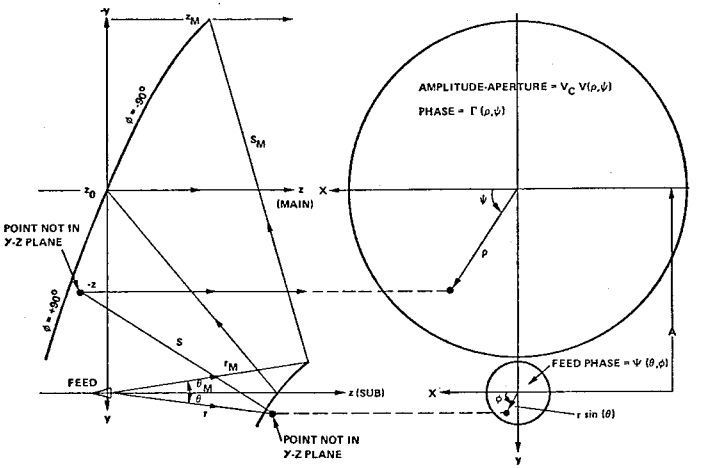

FIGURE 1. DUAL REFLECTOR GEOMETRY

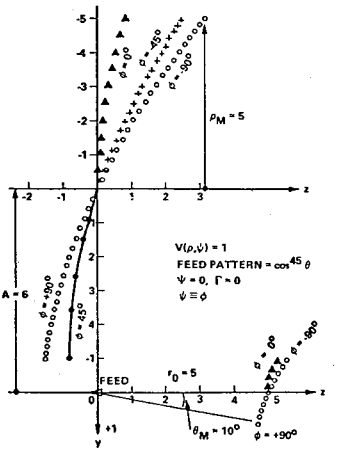

FIGURE 2. RADIAL PROFILES FOR UNIFORM PHASE-AMPLITUDE APERTURE

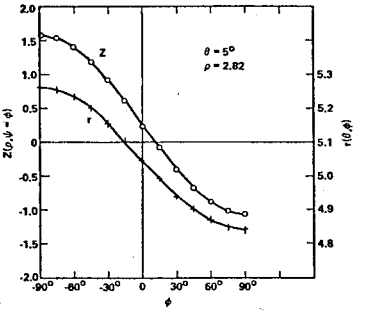

FIGURE 3. CIRCUMFERENTIAL PROFILES FOR UNIFORM PHASE-AMPLITUDE (SEE FIG. 2)

Combined Session, 1100, Wednesday, June 22

REMOTE SENSING -- THE OTHER SIDE OF THE COIN

C. Gordon Little
Wave Propagation Laboratory
Environmental Research Laboratories
National Oceanic and Atmospheric Administration
Boulder, Colorado 80302

Introduction

Propagation measurements in the lower atmosphere tend to be conducted by two largely separate groups of workers -- those telecommunicators who need quantitative information on the propagation limitations and capabilities of the medium for telecommunication purposes, and those atmospheric scientists who use observations of atmospheric propagation to derive information on the medium itself. These two activities can be thought of as being at the two sides of a single coin -- the coin being the interaction of electromagnetic waves with the atmosphere. It is unfortunate that the two groups are so separate, for often results obtained for one purpose can have direct relevance to "the other side of the coin." In recent years, there has been considerable progress on the remote sensing side of the coin; it is the purpose of this paper to summarize this progress and discuss its implications to local weather services.

Ground-Based Remote Sensing of the Lower Atmosphere

Before discussing the current status of ground-based remote sensing of the atmosphere, it may be appropriate to list the potential advantages of remote sensors. These include the fact that the data are conceptually available:

in 1, 2, or 3 spatial dimensions,

without the use of towers, balloons, or aircraft,

with excellent continuity in space and time,

with excellent resolution in space and time,

over a wide range of parameters,

as spatial averages,

using systems which may be readily automated.

Any one of these advantages might justify the development of a particular sensor; the combination of advantages in certain cases provides an overwhelming justification for the development and use of new remote sensors.

The present status of ground-based remote sensing of the primary meteorological variables of wind, temperature, and humidity is summarized in Table I. Because of the three-dimensional nature of the atmosphere, it is appropriate to differentiate between three levels of capability (a) measuring only the surface value of some parameter, (b) the ability to measure the mean vertical

profile, and (c) the ability to measure the parameter as a function of position in three-dimensional space. Since each parameter typically exhibits small random fluctuations in time and space, we need to be concerned with the ability to measure not only the mean value, but also its small-scale variability. This variability is usually expressed in terms of its structure constant, which may be thought of as the root-mean-square difference between simultaneous values of the parameter at two points unit distance apart. Again, the structure constant may be measured only at the surface, or as vertical profiles, or as full three-dimensional fields.

The vertical fluxes of momentum, heat, and water vapor are of great importance to meteorology. These result primarily from the covariance of the turbulent components of vertical velocity with horizontal velocity, temperature, and humidity respectively. Once again, these vertical fluxes can be measured just at the surface, or as vertical profiles, or as full three-dimensional fields.

In Table I, a number is used to denote which research concepts have exhibited the ability to make that particular measurement. In general, however, operational hardware suitable for routine use is not yet available. The oral version of this paper will include slides illustrating the capabilities of active or passive radio systems to measure profiles of wind, temperature, and humidity.

We see from Table I that, in the research mode, it is possible to measure vertical profiles of wind, temperature, and humidity. Progress has been especially complete in the case of wind measurements, where three-dimensional measurements of mean wind and turbulence have been reported, and three-dimensional measurements of momentum flux for spatial scales larger than the pulse volumes are implicit in the Doppler data. At the moment, these capabilities do not exist in all weather conditions, though the recent demonstration of clear air microwave and infra-red Doppler radar capabilities makes wind measurement feasible in essentially all weather conditions. The passive microwave radiometric measurement of temperature and water vapor profiles has recently been demonstrated to be valid under cloudy as well as clear sky conditions, but is not likely to be applicable in rain.

In Table II, the status of remote sensing of precipitation, and of cloud and aerosol particles is indicated. Here the most important parameters to be measured are the three-dimensional distribution of the particles, and their size distributions; in the case of clouds and precipitation, the water-or-ice phase identification is important; for precipitation, the precipitation rate is also meteorologically important.

Remote Sensing -- A Complementary Approach to Short-Term Local Weather Forecasting

The above status report indicates that continuous information on the precipitation field, the cloud field, and the velocity field, around an observing site could be provided by using a combination of sensitive microwave and infrared Doppler radar systems. Operational ranges could range from a few tens of kilometers in clear air, to greater than 100 kilometers in precipitation. In addition (but not during rain), temperature and humidity profiles could be monitored using a multi-wavelength microwave radiometer system; the same system could also monitor integrated liquid water content.

Since virtually all changes in weather can be well described in terms of the observed changes in the wind, cloud, and precipitation fields, this immediately suggests that remote sensors could be used to continuously and automatically observe the state of the atmosphere over an urban area out to ranges of perhaps 100 kms. Recent progress in data processing and display further suggest that it would be possible to prepare, and disseminate in essentially real time, (using a dedicated TV channel) "nowcasts" or maps of the present state of the atmosphere over the area. Simple extrapolation techniques, incorporating the effects of the advection and trends observed in the remote sensing data, could then be used to prepare and issue short-term extrapolations or forecasts of local weather conditions for the next two or three hours.

Longer term (3-12 hour) forecasts would require meteorological data from outside the 200 km diameter circle. Fortunately, these are available from two sources -- geostationary satellites, and the numerical forecasts of the National Weather Service's National Meteorological Center. These data, plus the continuously available remote sensing data, could be used in local mesoscale numerical models to prepare detailed local weather forecasts for the 3-12 hour time frame. These local weather forecasts could be much more accurate and detailed than the present NWS forecasts, primarily because the local numerical models could take into account local topography and other surface features which are on too small a scale to be incorporated in the continental-scale NWS models.

A program to establish a prototype regional observing and forecasting service (PROFS) based in large part on the above considerations is now being discussed within the Department of Commerce. If successfully implemented, it could have major impact within the U.S. on short-term, local weather services, through widespread use of atmospheric remote sensing.

TABLE I. STATUS OF REMOTE SENSING OF PRIMARY METEOROLOGICAL VARIABLES

Type of Measurement	Wind	Temperature	Humidity
Surface Values			
Mean	1	5	9
Structure constant	-	1	-
Vertical flux	-	1	-
Vertical Profiles			
Mean	2,3,4	6,7	6,9
Structure constant	2,4	8	-
Vertical flux	2	-	-
3-D Field			
Mean	2	-	-
Structure constant	2	-	-
Vertical flux	-	-	-

Measurement System Code

1 Optical scintillation
2 Doppler radar
3 Doppler lidar (infra-red)
4 Acoustic Doppler
5 Optical time-of-flight
6 Multi-channel microwave radiometry
7 Hybrid radar-acoustic system
8 Monostatic acoustic sounder
9 Differential absorption lidar

TABLE II. STATUS OF REMOTE MEASUREMENT OF HYDROMETEORS AND AEROSOL

Type of Measurement	Cloud Particles	Precipitation	Aerosol
Vertical line integral	1	1	2
3-D distribution	3	4	5
Particle size distribution	-	-	-
Phase identification	6	6	-
Precipitation rate	-	3,7	-

Measurement System Code

1 Multi-channel radiometer can measure integrated liquid water
2 Lidar
3 Short wavelength radar
4 Radar
5 Lidar
6 Polarized lidar
7 Optical scintillation

Combined Session, 1130, Wednesday, June 22

OBSERVATIONS WITH INCOHERENT SCATTER RADAR OF IONOSPHERIC MODIFICATION IN THE AURORAL ZONE DURING PARTICLE PRECIPITATION AND JOULE HEATING EVENTS

J. D. Kelly and V. B. Wickwar
Radio Physics Laboratory, Stanford Research Institute
Menlo Park, California 94025, U.S.A.

The auroral zone ionosphere is both very interesting and confusing due to the wide variety of often interrelated phenomena that occur there. In addition to the factors affecting the midlatitude ionosphere, the auroral zone ionosphere is caught in the middle of other complex interactions involving the magnetosphere, ionosphere and thermosphere. As a result, the ionospheric layers with which we are familiar from midlatitudes are considerably modified. They are observed to appear, disappear or race by with a rapidity we are not used to. The electrons and ions become heated, the ion composition changes, and the layers themselves change shape.

The Chatanika Incoherent Scatter Radar has been operated by SRI near Fairbanks, Alaska, since 1971. It is a major instrument for studying the auroral zone ionosphere and placing what occurs there into the larger context of the magnetosphere and thermosphere. The radar signals backscattered from the ionospheric plasma can be used to determine the electron density distribution, the ion velocities, the ion and electron temperatures, and the proportion of molecular and atomic ions. Some of these data can also be applied to the magnetosphere to determine the convection electric fields and the spectral characteristics of the energetic electron precipitation. Thermospheric winds and temperatures can also be determined.

The magnetosphere has a significant effect on the auroral ionosphere because it supplies large amounts of energy from two sources: energetic electrons and convection electric fields. The first, energetic electrons, are the particles that cause the discrete visual auroras and much of the diffuse aurora. They also produce large E and F layers. The E layers typically have maximum densities between several times 10^5 and several times 10^6 electrons/cm^3. The peak altitudes range from 90 to 150 km, but are usually nearer 110 km. The F layers have maximum densities near 10^5 electrons/cm^{-3} and peak altitudes near 275 km. Like the visual auroras, the largest E layers exhibit great temporal and spatial variations. In addition, the energy brought into the ionosphere by these energetic auroral electrons is expended in heating the electrons (Figure 1) and neutrals.

The second energy source, convection electric fields, map down magnetic field lines into the ionosphere where they produce large perpendicular ion and electron drifts. These are typically 500 m/s, but can be as large as 2 km/s. As with particle precipitation, there is considerable temporal and spatial variation. While these fields are undoubtedly responsible for some of the motion of the visible auroras, they usually do not lead to visual effects. When combined with ionization in the E layer, F layer, or both, they give

rise to energy input to the ions and neutrals in the form of Joule or frictional heating (Figure 2), and the momentum input to the neutrals in the form of ion drag.

The amount of energy supplied to the upper atmosphere from these two magnetospheric sources is considerable. Typically each source produces a daily maximum of 20 to 30 ergs/cm^2 - s, but they can produce as much as 100 ergs/cm^2 - s. That these energies are significant is apparent when we realize that the input from the overhead sun in the same altitude region would be 3 ergs/cm^2 - s.

In addition to the major effects on density, velocity and temperature already described, we can determine more subtle changes that these energy inputs produce in the ionosphere. On short time scales, there is an increase in the altitude to which molecular ions dominate. Figure 3 shows a dramatic 50 km increase in this altitude during a Joule heating event. The resultant change in chemistry leads to a reduction in the F-region ionization, Figure 4. These changes are most likely explained in terms of an upwelling of the neutral gas and changing rate coefficients caused by the large relative ion-neutral velocities, increased temperatures, and perhaps even vibrational excitation. On longer time scales, there are also increases in the thermospheric temperature, which would affect the worldwide upper atmosphere circulation and hence both the neutral and ionized densities.

Thus, in addition to the ionospheric modification that is produced directly by the magnetospheric energy inputs, there are further significant changes in the ionosphere that are caused by more subtle interactions between the magnetosphere, ionosphere and thermosphere. These changes are more than curiosities of the auroral zone. Some of the resultant effects, such as upper atmospheric circulation and changes in the neutral composition, have worldwide manifestations. Furthermore, observation and understanding of these changes lead to an increased knowledge of these three regions and their interactions. Experimentally, the incoherent scatter radar is now providing much of the observational data needed to explore the complex processes that are manifested in the auroral zone ionosphere.

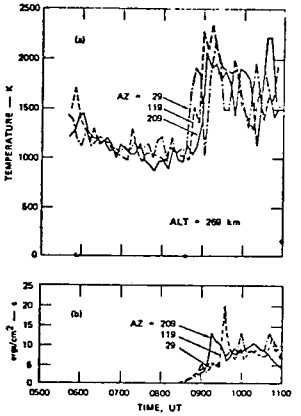

FIGURE 1 ELECTRON TEMPERATURE (a) AND ENERGY DEPOSITION FROM ENERGETIC PARTICLES (b) vs TIME FOR THREE DIFFERENT ANTENNA POSITIONS SHOWING ONSET OF AN AURORAL SUBSTORM. The data were taken during the night of 31 January 1976. SZA is always greater than 110°. (local time UT-10 hrs.)

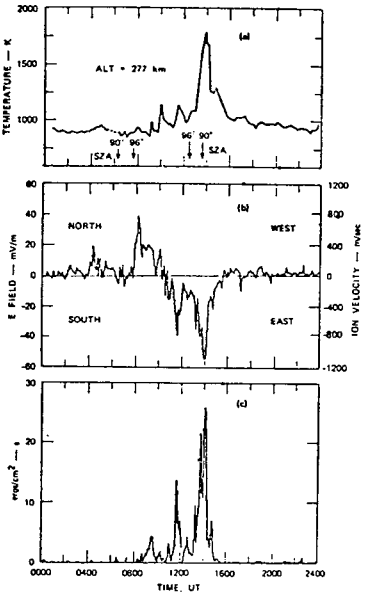

FIGURE 2 ION TEMPERATURE (a) AVERAGE NORTH-SOUTH ELECTRIC FIELD (b) AND ENERGY INPUT FROM JOULE HEATING (c) vs 24-HOURS IN 13 AUGUST 1975

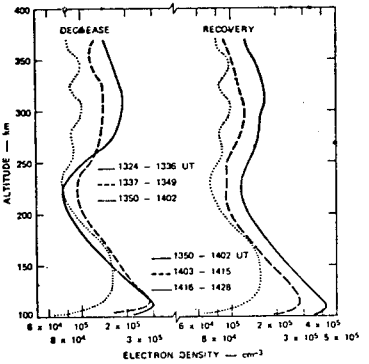

FIGURE 4 ELECTRON DENSITY PROFILES DURING THE JOULE HEATING EVENT ON 13 AUGUST 1975. The F-region density decreases during the event and then recovers as the heating subsides.

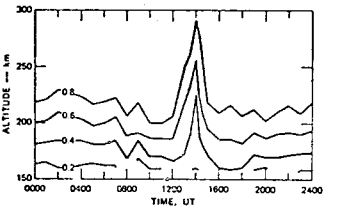

FIGURE 3 ION COMPOSITION. $[O^+]/[N_2]$, for 13 August 1975. The ion temperatures and the Joule heating are indicated in Figure 2.

SHORT WAVE PLASMA DIAGNOSTICS: INVERSE PROBLEM OF ELECTROMAGNETIC DIFFRACTION ON A CYLINDRICAL COLUMN

L.A.WAINSTEIN
Institute for Physical Problems of
the USSR Academy of Sciences, Moscow 117334

1. Introduction. The most interesting inverse diffraction problems are the short wave ones, because only short waves ($\lambda \ll \ell$) give us the possibility to resolve details with linear dimensions ℓ . There are several inverse problems (esp. in plasma diagnostics) solved on the basis of geometrical optics, but the real resolving power of the experimental installation can be determined only on the basis of wave theory.

The following problem is investigated. A narrow wave bundle is radiated by antenna 1, a directive antenna 2 receives this wave bundle after it is refracted, reflected, diffracted and attenuated by the cylindrical plasma column. In fig. 1 the line $11'$ is "the principal ray" of antenna 1, $22'$ - of antenna 2, both rays lie in the plane $z = 0$, φ_0 is the angle which $2'2$ makes with $1'1$, transmitted and received fields are concentrated near the plane $z = 0$, in this region $\varepsilon = \varepsilon(r)$, $\mathrm{Re}\,\varepsilon(r) < 1$, $0 \le \mathrm{Im}\,\varepsilon(r) \ll 1$, $\mu \equiv 1$; $\varepsilon(r) = 1$ for $r \gg \hat{r}$ where $\hat{r}$ is the radius of the plasma column. The amplitude and phase of the received signal are measured [1] during the motion of the column (or of the whole set-up), and we must calculate the unknown function $\varepsilon(r)$ using these experimental results.

2. Integral equations. The asymptotic solution of the scalar wave equation

$$\Delta U + k^2 \varepsilon(r) U = 0 \qquad \left(U \sim e^{-i\omega t},\ k = \frac{\omega}{c} = \frac{2\pi}{\lambda}\right) \tag{1}$$

for the three-dimensional problem stated above has the form [2]

$$f(\mu) = \int_{-\infty}^{\infty} K(\mu - \nu) e^{-i[\Phi(\nu) + \gamma\varphi_0]} d\nu. \tag{2}$$

Here $f(\mu)$ is a measured complex function (transmission coefficient, $f(\mu) \equiv 1$ if $\varepsilon(r) \equiv 1$ and $\varphi_0 = 0$), the kernel $K(\mu - \nu)$ $\left(\int_{-\infty}^{\infty} K(\mu - \nu)\, d\nu = 1\right)$ is the instrumental function that depends on the properties of antennae 1 and 2, $-\Phi(\nu)$ is the additional complex phase of the ray with the impact parameter ν (impact distance ν/k) due to the plasma column. The phase function $\Phi(\nu)$ is determined by the laws of complex geometrical optics. If we use parametric expressions

$$\varepsilon(r) = e^{-2E(\rho)}, \qquad kr = \rho e^{E(\rho)} \tag{3}$$

for the unknown function $\varepsilon(r)$, then we obtain an integral equation [3]

$$\Phi(\nu) = 2\int_{\nu}^{\hat{\rho}} \frac{E(\rho)\rho\, d\rho}{\sqrt{\rho^2 - \nu^2}}, \qquad \hat{\rho} = k\hat{r} \tag{4}$$

for the auxiliary function $E(\rho)$.

Other restrictions important for the validity of (2) are: 1) smoothness of the function $\varepsilon(z)$, $d\varepsilon/dz \ll k\varepsilon$, therefore the vector electromagnetic problem is reduced to the scalar equation (1) and the field is reflected only from the region where $Re\varepsilon(z) \leq C$; 2) the centre of the plasma column lies on the bisectrix of the angle $\pi - \varphi_0$ (fig.1), μ is the impact parameter of both rays $11'$ and $22'$; 3) both antennae 1 and 2 are far from the column, but only the inequalities $z_1 \gg \hat{z}$, $z_2 \gg \hat{z}$ must hold.

It is worth to mention that integral equations of the same type (2) and (4) are obtained in another inverse problem corresponding to "passive" diagnostics, when the thermal radiation of the plasma column is measured by an arbitrary antenna [4].

3. Comparison of the integral (2) with other solutions. The accuracy of the asymptotic solution (2) was verified in the following way: taking

$$\varepsilon(z) = 1 - \Theta e^{-\frac{z^2}{a^2}}, \quad K(\mu-\nu) = \sqrt{\frac{\zeta}{2\pi}}\, e^{-\frac{\zeta}{2}(\mu-\nu)^2}; \quad \Theta, a, \zeta \text{ are constants,} \qquad (5)$$

we can solve the corresponding two-dimensional diffraction problems for E- and H-polarisations exactly, i.e. numerically [5], and compare with (2). For $ka = 10 \div 20$ and $\varphi_0 = 0$ exact curves for both polarisations coincide and are in excellent agreement with (2). For $\varphi_0 = \pi/2$ and $\Theta > 1$ the results depend on polarisation (high frequency plasma resonance) and even the E-curve is in worse agreement with (2), see [2] and [5]. Therefore it is better to apply (2) in the case $\varphi_0 = 0$, when the principal rays $11'$ and $22'$ coincide; inverse problems can be solved only for transparent plasmas ($Re\varepsilon(z) > 0$, $Im\varepsilon(z) \ll 1$ everywhere).

The integral (2) gives reasonable results in the case of a thick conducting cylinder [2]. Taking $K(\mu-\nu) = \delta(\mu-\nu)$ we obtain the basic formula of ray diagnostics [3].

4. Virtual rays. The interpretation of (2) is possible on the basis of virtual rays [3] that play the role of diffracted and complex rays in the geometrical theory of diffraction. For instance, two points 1 and 2 in the plane $z = 0$ are connected with a continuous family of virtual rays ($-\infty < \nu < \infty$). In vacuum each ray consists of two rectilinear segments 11^* and 22^* and an arc 1^*2^* of the circle with radius ν/k (fig. 2); the generalisation for the plasma column is obvious. We get the ordinary rays of geometrical optics, when points 1^* and 2^* coincide. The integral (2) is taken over the whole family of virtual rays with a complex weight $K(\mu-\nu)$ depending on properties of antennae (their directivity, distances, etc); the factor $e^{-i\Phi(\nu)}$ depends on the plasma column and the factor $e^{-i\nu\varphi_0}$ on the mutual orientation of antennae.

5. How we solve our integral equations. Equations (2) and (4) have analytical solutions that are of little use because of their instability. A large amount of numerical work was performed: these equations were solved by various methods for several theoretical models and for real plasmas. Best results for equation (2) are obtained by the phase iteration method (operating with $Re\Phi(\nu)$ and $-\arg f(\mu)$) followed by the linear iterations; for narrow

wave bundles only few iterations (1 ÷ 3) are necessary to construct the complex phase function $\Phi(\nu)$ such that the calculated $f(\mu)$ agrees with measured $f(\mu)$ within experimental errors. Equation (4) is solved by the method of truncated series [6,7] .

Before all the instrumental function $K(\mu-\nu)$ must be found. This is done using a slot of width $2\nu_0/k$ instead of the plasma column, measuring the transmission coefficient $f(\mu)$ through the slot and solving the integral equation

$$f(\mu)=\frac{1}{2\nu_0}\int_{-\nu_0}^{\nu_0} K(\mu-\nu)\,d\nu \qquad (\varphi_0=0) \tag{6}$$

by iteration methods or by the method of truncated series.

References.

1. Э.А.Тищенко, В.Г.Зацепин. ЖЭТФ 68, №2, 547-561, 1975.
2. Л.А.Вайнштейн, Е.С.Биргер, Н.Б.Конюхова, Е.Л.Косарев, Г.П.Прудковский. Физика плазмы 2, №4, 658-671, 1976.
3. Л.А.Вайнштейн, Э.А.Тищенко. ЖТФ 46, №11, 2271-2279. 1976.
4. Э.А.Тищенко, Л.А.Вайнштейн. Физика плазмы 3, №1, 124-134, 1977.
5. Е.С.Биргер, Л.А.Вайнштейн, Н.Б.Конюхова. Журнал вычисл.математики и мат.физики. 16, №6, 1526-1538, 1976.
6. Л.А.Вайнштейн. Докл.АН СССР 204, №5, 1067-1070, 1972.
7. Е.Л.Косарев. Журнал вычисл.математики и мат.физики 13, №6, 1591-1595, 1973.

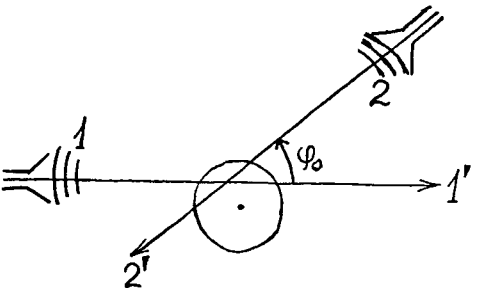

Fig.1

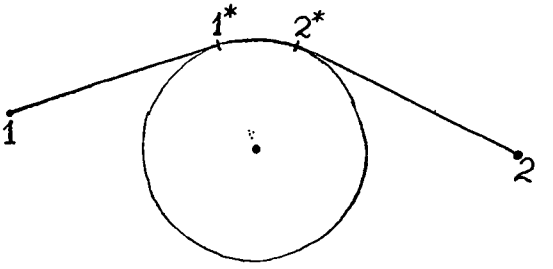

Fig.2

Commission B - Session 1

(Joint with IEMS Session 5)
Wednesday P.M. 1330 - 1650

OPTICS

Chairman: L. B. Felsen, Polytechnic Institute of New York

1. SCATTERING AND GUIDED WAVES IN OPTICAL DIELECTRIC WAVEGUIDES WITH RANDOM INHOMOGENEITIES: Y. Miyazaki, Department of Electrical Engineering and Electronics, Nagoya University, Chikusa-ku, Nagoya, Japan

Introduction

Propagation losses and pulse broadenings due to scattering and mode conversions in optical glass fibers are important factors for evaluation of repeater distances and channel capacities in optical communication systems.[1,2] Statistical properties of wave propagation in random media have been recently investigated by various authors[3-5], particularly, in the case of infinite space without boundaries. However, statistical properties of scattering and mode conversions of guided waves due to random inhomogeneities such as index fluctuations and irregular bends in optical fibers have not been clarified. Some approximate theories of scattering losses have been shown without evaluation of boundary effects at the circular boundary between core and cladding media and multiple scattering, by the author and others[6,7]. The purpose of this paper is to show scattering losses and statistical guided modes that yield pulse broadenings at an output, by using statistical Green's dyadics with boundary effects and multiple scatterings, for various correlation lengths of irregularities.

Statistical Fields in Fibers

In this paper optical fibers with random core index $\epsilon_1 = \epsilon_1^{(1)} + \epsilon_1^{(2)}$ where $\epsilon_1^{(2)}$ is a random function, and cladding index ϵ_2, and with irregular bends of radius $R(z)$ are studied. A curved waveguide in the space (X,Y,Z) can be transformed into a straight waveguide in the space (x,y,z) by mapping function $X+jZ=R(z)(1+x/R(z))e^{jz/R}$. Vector wave equations for the time harmonic field $\mathcal{E} = \begin{pmatrix} E_1 \\ E_2 \end{pmatrix}$ and sources $\mathcal{J} = \begin{pmatrix} J_1 \\ J_2 \end{pmatrix}$ represented in the space (x,y,z) are shown by operator formulation as follows, for the core Ω_1 and cladding Ω_2 region.

$$\mathcal{L}_o \mathcal{E} = \mathcal{J} + \mathcal{L}_\epsilon \mathcal{E} + \mathcal{L}_F \mathcal{E} \qquad (1)$$

The differential operator $\mathcal{L}_o$ is

$$\mathcal{L}_o = \begin{pmatrix} \nabla_{xyz} \times \nabla \times - \omega^2 \epsilon_1^{(1)}(r)\mu & 0 \\ 0 & \nabla_{xyz} \times \nabla \times - \omega^2 \epsilon_2(r)\mu \end{pmatrix}$$

The statistical operators $\mathcal{L}_\epsilon$ and $\mathcal{L}_F$ concerned with the index fluctuations and irregular bends are

$$\mathcal{L}_\epsilon = \begin{pmatrix} \omega^2 \epsilon_1^{(2)}\mu & 0 \\ 0 & 0 \end{pmatrix} \qquad \mathcal{L}_F = \begin{pmatrix} F_1 & 0 \\ 0 & F_2 \end{pmatrix}$$

The differntial vector operators F_i are given by the metrical coefficient $h = 1 + x/R(z)$.

The Green's oprator $\mathcal{G}$ corresponding to inverse operator $\mathcal{L}_o^{-1}$ is defined as

$$\mathcal{L}_o^{-1}\mathcal{J} = \mathcal{G}\mathcal{J} = \int \begin{pmatrix} \mathbb{G}_1^{(1)} & \mathbb{G}_2^{(1)} \\ \mathbb{G}_1^{(2)} & \mathbb{G}_2^{(2)} \end{pmatrix} \begin{pmatrix} J_1 \\ J_2 \end{pmatrix} \, dv$$

The statistical average of the field in the fiber, $\langle \mathcal{E} \rangle$, satisfys the following stochastic differential equation

$$\begin{aligned} &\left[\mathcal{L}_o - \langle \mathcal{L}_\epsilon + \mathcal{L}_F \rangle + \langle \mathcal{L}_F + \mathcal{L}_\epsilon \rangle \mathcal{L}_o^{-1} \langle \mathcal{L}_F + \mathcal{L}_\epsilon \rangle \right. \\ &\left. - \langle (\mathcal{L}_F + \mathcal{L}_\epsilon) \mathcal{L}_o^{-1} (\mathcal{L}_F + \mathcal{L}_\epsilon) \rangle \right] \langle \mathcal{E} \rangle = \langle \mathcal{J} \rangle \end{aligned} \qquad (2)$$

The inverse operator $\mathcal{L}_o^{-1}$ and Green's operator $\mathcal{G}$ are operators for the field in the straight fiber with the core index $\epsilon_1(\mathbf{r}) = \epsilon_1^{(0)}(\mathbf{r})$. The Green's dyadic $\mathbb{G}_1^{(1)}$ for the core field is written as a sum of fundamental Green's dyadic $\mathbb{G}_{10}^{(1)}$ and general Green's dyadic $\mathbb{G}_{11}^{(1)}$ shown by spectrum representations of Bessel and Hankel functions or confluent hypergeometric functions for the step index core or the graded index core, respectively. The fundamental Green's dyadic $\mathbb{G}_{10}^{(1)}$ can be written as

$$\mathbb{G}_{10}^{(1)} = \left(\mathbb{I} - \nabla \frac{1}{\omega^2 \epsilon_1^{(1)}(\mathbf{r}) \mu} \nabla' \right) G_o$$

where G_o is the solution of $(\nabla^2 + \omega^2 \epsilon(\mathbf{r}) \mu) G_o = -\delta(\mathbf{r} - \mathbf{r}')$. In the case of homogeneous cladding, $\mathbb{G}_1^{(2)}$ can be represented by Bessel and Hankel functions. Other Green's dyadics are shown in similar forms. Hence, the Green's operator $\mathcal{G}$ can be written as, when $\beta_1^2 = \omega^2 \mu \epsilon_1^{(1)}$ and $\mathcal{G}_o(\beta_1)\langle \mathcal{E} \rangle = \int \begin{pmatrix} 0 & 0 \\ 0 & \mathbb{I} G_o \end{pmatrix} \langle \mathcal{E} \rangle \, dv$,

$$\mathcal{G}(\beta_1)\langle \mathcal{E} \rangle = \mathcal{G}_o(\beta_1)\langle \mathcal{E} \rangle + \left\{ \mathcal{G}(\beta_1) - \mathcal{G}_o(\beta_1) \right\} \langle \mathcal{E} \rangle$$

When random functions $\epsilon_1^{(2)}$ and R(z) are statistically independent and the average of $\epsilon_1^{(2)}$ is zero, and the correlation of index fluctuations is $\langle \mathcal{L}_\epsilon \mathcal{L}_\epsilon \rangle = \langle \mathcal{L}_\epsilon^2 \rangle C_\epsilon(\mathbf{r} - \mathbf{r}')$, with the help of the mean value theorem for solutions of the wave equation, we obtain,

$$\left[\mathcal{L}_o - \mathbf{A} - \langle \mathcal{L}_F \rangle\right] \langle \mathcal{E} \rangle = \langle \mathcal{J} \rangle + \left[\langle \mathcal{L}_\epsilon \{\mathcal{G} - \mathcal{G}_o\} \mathcal{L}_\epsilon \rangle - \langle \mathcal{L}_F \mathcal{L}^{-1} \mathcal{L}_F \rangle \right] \langle \mathcal{E} \rangle \qquad (3)$$

where the matrix $\mathbf{A}$ is defined by $\mathbf{A} = \begin{pmatrix} A_{11} & 0 \\ 0 & 0 \end{pmatrix}$ and $A_{11} = \frac{j \langle \mathcal{L}_\epsilon^2 \rangle}{2\beta_1} \int_0^{P(\mathbf{r})} \left(e^{-2j\beta_1 \mathbf{r}'} - 1 \right) C_\epsilon(\mathbf{r}') \, d\mathbf{r}'$.

and the statistical bend operator is $\langle \mathcal{L}_F \rangle = -3 x^2 \langle \frac{1}{R^2} \rangle \frac{\partial^2}{\partial z^2} \begin{pmatrix} 1 & 0 \\ 0 & 1 \end{pmatrix}$ if $\langle \frac{1}{R} \rangle = 0$.

The function P(r) is equal to infinite if radius of the fiber is larger than the correlation length of index fluctuations.

From Green's operator $\hat{\mathcal{G}} = \hat{\mathcal{L}}^{-1} = (\mathcal{L}_o - \mathbf{A} - \langle \mathcal{L}_F \rangle)^{-1}$ the average field are obtained from eq.(3), and statistical eigen-functions $\hat{\Phi}_\nu$ of guided waves are approximately derived from the operator $\hat{\mathcal{L}}$ with the boundary condition. For straight optical fibers with random index fluctuations, Green's dyadics $\hat{\mathbb{G}}_{ij}$ and eigen functions $\hat{\Phi}_\nu$ can be obtained from $\mathbb{G}_{ij}$ and Φ_ν concerned with normal fibers by replacing β_1^2 with $\hat{\beta}_1^2 = \beta_1^2 + A_{11}$.

In the case of a step index fiber of radius a and core index ϵ_1, cladding index ϵ_2 with index fluctuations given by $C_\epsilon(\rho) = \exp(-\rho/\rho_t)$, the phase constants

$\hat{\beta}_{mnr}$ and attenuation constants $\hat{\alpha}_{mn}$ of statistical guided (m,n) modes having leaky properties due to inhomogeneities are asymptotically calculated as ,when $\langle \delta^2\epsilon \rangle \beta_1^4 = \langle (\mathcal{L}_\epsilon^2)_{11} \rangle$ and $\beta_2^2 = \omega^2 \epsilon_2 \mu$

$$\hat{\beta}_{mnr}^2 \cong \beta_1^2 + \frac{\beta_1^4 \langle \delta^2\epsilon \rangle \rho_t^2}{1+4(\beta_1\rho_t)^2} - \left(\frac{\lambda_{mn}}{a}\right)^2 e^{-\frac{2}{(\beta_1^2-\beta_2^2)a^2}} \qquad \hat{\alpha}_{mn} \cong \frac{\beta_1}{\hat{\beta}_{mnr}} \frac{\beta_1^4 \langle \delta^2\epsilon \rangle \rho_t^3}{1+4(\beta_1\rho_t)^2} \qquad (4)$$

where the parameters λ_{mn} are zeros of Bessel functions for hybrid modes.Fig.1 shows some numerical examples of propagation constants. Short or long correlation of fluctuations corresponds to Rayleigh or Mie scattering,respectively. Attenuations of higher modes are larger than those of lower modes. Statistical fields in graded index fibers can be similarly calculated.

Correlation functions of fields are shown by

$$\langle \mathcal{E}(x_1)\, \mathcal{E}^*(x_2) \rangle = \Big\{ 1 + \mathcal{G}(x_1)\, \mathcal{G}^*(x_2) \Big[\langle (\mathcal{L}_F + \mathcal{L}_\epsilon)(\mathcal{L}_F + \mathcal{L}_\epsilon) \rangle - \langle (\mathcal{L}_F + \mathcal{L}_\epsilon) \rangle \langle (\mathcal{L}_F + \mathcal{L}_\epsilon) \rangle \Big] \Big\} \langle \mathcal{E}(x_1) \rangle \langle \mathcal{E}^*(x_2) \rangle \qquad (5)$$

The transmitted power is $J = \sum \hat{b}_{mn}\, e^{-2\hat{\alpha}_{mn} z}$ where $\hat{b}_{mn}$ are constants. For incident HE_{11} modes transmission loss is 4.34 dB/km when $\beta = 10^7\,(m^{-1})$, $\sqrt{\langle \delta^2\epsilon \rangle} = 10^{-5}$ $V = \sqrt{\beta_1^2 - \beta_2^2}\, a = 2.5$ and $\rho_t = 0.2\,\mu m$.

With the help of correlation functions of eq.(5),pulses of partially coherent waves generated from LED and semiconductor lasers propagating in optical fibers with index fluctuations and microbendings can be evaluated by double Fourier integrals. It is shown that pulse broadenings are proportinal to square root of the fiber length when irregularities in the fibers lead strong mode mixing or for large dispersion of statistical eigenvalues $\hat{\alpha}_{mn}$.

References

(1) H.G.Unger,Proc. of 1973 European Microwave Conf. Brussels(1973)B.5.1.
(2) Y.Miyazaki, Arch.Elekt.Über. 28(1974) 160.
(3) J.B.Keller,Proc. of Sym.in Appl.Math. XVI (1964, Amer.Math.Soc.)145.
(4) N.V.Kampen,Physics Reports(Section C of Phys. Lett.)24 (1976)171.
(5) Y.Miyazaki, Japanese J. Appl.Phys. 13 (1974) 1238.
(6) D.Marcuse, Theory of Dielectric Optical Waveguides(1974 ,Academic Press)
(7) Y. Miyazaki, Trans.IECE,Japan ,57-C (1976)37.

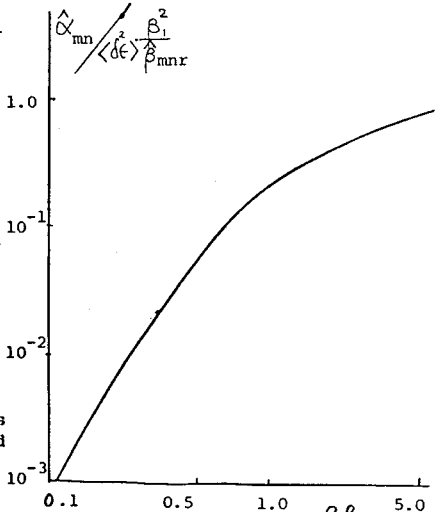

Fig.1
Attenuation constants of statistical guided modes.

2. ON THE MATCHING OF TWO OPTICAL WAVEGUIDES: Dr. Benjamin Rulf*, Division of Electrical Engineering, National Research Council of Canada, Ottawa, Ontario, Canada, K1A 0R8

When two dielectric waveguides are brought together end to end, perfect matching can be achieved only when the guides are identical in their geometric and material properties, and their axes perfectly aligned. Discontinuities due to the difference in the geometric or material properties of the guides, or due to misalignment will result in transmission losses, through reflections and radiation from the discontinuity. If in either guide more than one mode can exist, then any mode that impinges on the discontinuity will excite all the other modes. One can construct a reflection matrix R and a transmission matrix T, whose elements are the ratios between the amplitudes of some incident mode and another reflected or transmitted mode respectively. Knowledge of these matrices for a given waveguide junction is obviously of great practical importance.

We consider the problem shown in Figure (1). We assume that the left hand slab ($x<0$) can support J discrete modes, while the right hand slab ($x>0$) can support K discrete modes at a given frequency.

The reflection matrix R is a square JxJ matrix whose element R_{ij} gives the ratio between the amplitude of the j^{th} reflected mode and the i^{th} incident mode. The transmission matrix T is a rectangular JxK matrix, whose element T_{ik} gives the ratio between the k^{th} transmitted and the i^{th} incident mode amplitudes. We consider modes travelling from $x = -\infty$ towards the origin as "incident", while modes that travel from the origin towards $x = \infty$ or $x = -\infty$ are "transmitted" or "reflected", respectively.

We can formulate the matching problem, and reduce it to a system of singular integral equations using the techniques of [1] [2]. All the elements of the reflection and transmission matrices can be computed in terms of solutions of these equations. These integral equations can usually not be solved in closed form for general discontinuities. It will be shown however that for small discontinuities (which is the case most often encountered in practice), approximate expressions for the matrix coefficients can be calculated in a systematic way.

---

* On leave of absence from Department of Mathematics, Tel Aviv University, Tel Aviv, Israel.

In order to avoid unessential complexities, we deal in this paper with scalar waves in a two dimensional dielectric slab geometry only. It seems reasonable, however, to assume that this technique can be generalized to deal with electromagnetic fields in circular fibers.

In the method that we present, we know the modes of each of the waveguides. There is no doubt that the method can be applied to homogeneous or step index circular fibers and to electromagnetic fields, since the modes for these cases can be found explicitly.

References

[1] Rulf, B. and Kedem, N. (1976), Surface Wave Diffraction by Means of Singular Integral Equation, J. Sound and Vibration 45(1), 15-28.

[2] Rulf, B. (1975), Discontinuity Radiation in Surface Waveguides, J. Opt. Soc. Am. 65(11), 1248-1252.

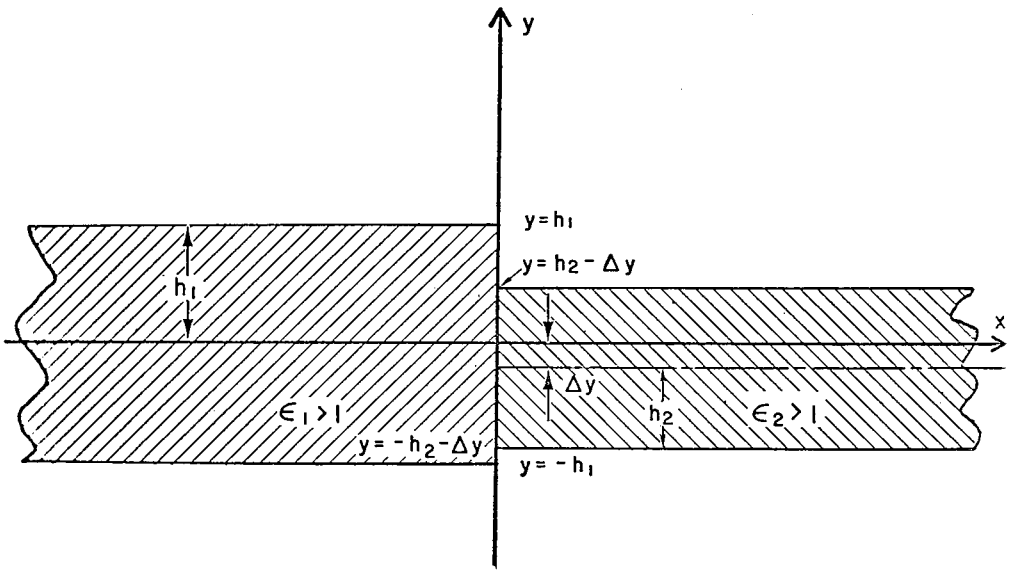

FIG. 1: A JUNCTION OF TWO DIELECTRIC SLAB GUIDES

3. FREE AND FORCED OSCILLATIONS OF A FABRY-PEROT RESONATOR WITH A UNIAXIAL DIELECTRIC SLAB: H. Blok, N. P. De Koo*, Department of Electrical Engineering, Delft University of Technology, Delft - 2208, The Netherlands

Summary

The analysis of (excited) forced oscillations and the analysis of free oscillations in an open resonator both are of considerable practical interest in quantum electronics. In the present paper we investigate a Fabry-Perot resonator in which a uniaxial dielectric slab is present. The theory can be considered as an extension of the one pertaining to an empty open resonator (BLOK [1]) and the one pertaining to an open resonator completely embedded in a uniaxial dielectric medium (BLOK and DE KOO [2]). In our approach the modes are considered to be free oscillations of the resonator. Due to the leaky character of an open resonator, its energy stored in a mode radiates away to infinity, and its characteristic frequency is complex, thus allowing for an exponentially decaying amplitude in time. In view of the complexity of the general problem of excitation of an open resonator with a slab, we confine ourselves to two simpler subproblems: (*i*) The analysis of *free* oscillations in a Fabry-Perot resonator with a uniaxial dielectric slab; (*ii*) The problem of the *excitation* of *forced* oscillations in an empty Fabry-Perot resonator. Both probems are formulated as electromagnetic boundary-value problems. In the first instance we are interested in the peculiarities of the behaviour of the resonator and therefore we investigate the two-dimensional configuration of the resonator consisting of two perfectly conducting strip mirrors. The optical axis of the uniaxial slab is chosen in the plane perpendicular to the direction of cylindricity. The vectorial electromagnetic problem can then be reduced to two separate scalar ones (corresponding with TE- and TM-polarization). Applying the modified Kirchhoff approximation [1] and an appropriate Green's functions technique, both problems are reduced to the solution of a system of two coupled integral equations of the Fredholm type (homogeneous in the case of free oscillations, inhomogeneous in the case of forced oscillations), in which the unknown field distributions on the mirrors occur as unknowns.

(*i*) *Free oscillations in an open resonator with an uniaxial dielectric slab.*

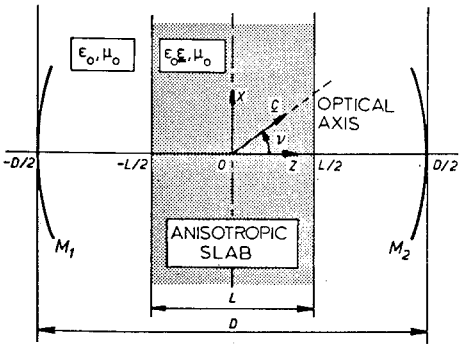

* Now at the Computing Centre, Delft University of Technology.

For TE-polarization the slab behaves as if it were isotropic. The special case of two parallel plane mirrors situated on the boundaries of an isotropic slab has been treated by FONG and LEE [3], using Vainshtein's method. ENOTO [4], SESHADRI [5] and ERMERT [6] have published on this subject. Our approach has to the knowledge of the authors never been presented before. For both polarizations the complex characteristic frequencies and the corresponding field distributions on the mirrors are computed numerically. In our method there are no restrictions as to either the shape of the mirrors or the anisotropy of the medium (if uniaxial). For various resonator configurations the influence of the orientation of the optical axis ν and of the ratio l/d is studied in detail. Numerical results are presented.

(ii) Excitation of forced oscillations in an empty Fabry-Perot resonator. The forced oscillations are excited by a spatially distributed source located in between the mirrors. Specifically, the excitation by a line source and by a plane current sheet are studied. In the latter case the driving current distribution is chosen such that the mirrors are illuminated by a gaussian beam. In view of the *complex source point method* (FELSEN [7]), the latter situation is identical with the excitation by a line source situated in an appropriately chosen complex source point. Several publications have been devoted to the

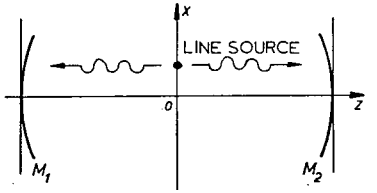

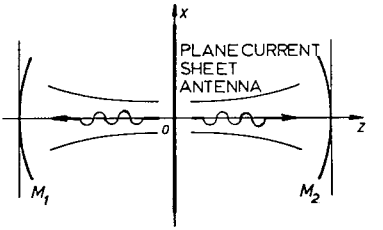

problem of the excitation of an open resonator [viz. 8,9,10,11,12]. In none of them our straightforward approach has been applied. In our approach there are no restrictions as to the shape of the mirrors. Numerical results will be presented for the two types of excitation for stable and unstable resonators with curved mirrors, for a resonator with plane mirrors and a resonator with flat-roof mirrors whose top angles vary up to 90 degrees.

References

[1] BLOK, H., *Diffraction theory of open resonators*, thesis,, Delft University of Technology. Lab. of electromagnetic research, 1970-7, pp.1-119, on request available; Alta Frequenza, 38, No. Speziale (1969) 305-311.

[2] BLOK, H., and N.P. DE KOO, 1974 URSI Symposium on electromagnetic wave theory, London 1974, Conference publication 114, pp.46-47; Appl. Phys. 7 (1975) 145-156.

[3] FONG, T.T. and S.W. LEE, IEEE Journ. Quant. Electr., QE-7 (1971) 1-11

[4] ENOTO, T., et al, Electr. Comm. Japan 54-B (1971) 70-77.

[5] SESHADRI, S.R., Proc. IEEE (1969) 1187-1188.

[6] ERMERT, H., A.E.Ü. 12 (1969) 631-632.

[7] OGURA, H., et al, Journ. Phys. Soc. Jap. 22 (1967) 1421-1433.

[8] VAINSHTEIN, L.A., Sov. Phys.-Tech.Phys. 9 (1965) 1197-1206.

[9] KATSENELENBAUM, B.Z. and A.N. SIVOV, Rad. eng. elect. phys. 12 (1967) 1101-1107.

[10] PASQUALETTI, F. and L. RONCHI, Appl. Opt. (1972) 1133-1142.

[11] FOX, A.G. and T.LI, IEEE Journ. Quant. Elect. QE-4 (1968) 460-465.

4. LEAKY-WAVE CHARACTERISTICS OF DIELECTRIC GRATINGS WITH ARBITRARY PROFILES:*
S. T. Peng, T. Tamir, K. C. Chang, Department of Electrical Engineering and Electrophysics, Polytechnic Institute of New York, Brooklyn, New York

Dielectric gratings play a principal role in many integrated-optics applications, such as beam couplers, distributed-feedback lasers, filters and other devices. The analysis and design of these gratings has therefore become of increasing importance, but rigorous solutions leading to exact results are few and they apply only to specialized grating profiles and/or need very elaborate and time-consuming computer programs; most other analytical treatments have involved approximate perturbation methods, which are restricted to shallow grooves [1]. By extending an improved perturbation procedure, which has already been shown to yield accurate results for beam couplers [2] and distributed-feedback lasers [3], we have determined general properties of gratings having arbitrary profiles and groove depths.

The periodic configuration considered here is shown in Fig. 1(a), where it is assumed that a grating of thickness t_p is present on a thin-film optical waveguide of thickness t_f, which is supported by a relatively thick substrate. While the grating grooves in Fig. 1(a) have an arbitrary asymmetric profile, a special case is described by the symmetric rectangular shape shown in Fig. 1(b). The main thrust of the present analytical approach is to view the grating region ($0 < z < t_g$) as a modification of a (basic) uniform layer having a (volume) average permittivity ϵ_g. The solution of every space-harmonic field of the waves supported by the grating can then be characterized by an equivalent transmission-line network (with respect to the transverse z direction) as shown in Fig. 2. Each one of the grating diffraction orders thus reduces to a simple, uncoupled and independent circuit, wherein the effect of mode coupling has been replaced by voltage $v_n(z)$ and current $j_n(z)$ sources, which are distributed inside the grating region only.

The equivalent network of Fig. 2 can be easily applied to any given excitation problem. Thus, the incident field may be a plane wave impinging obliquely on the grating (for scattering phenomena), a surface wave traveling longitudinally (for beam-coupling or filtering applications), or a standing wave along the grating (for distributed-feedback lasers). Each one of these situations is distinguised from the other only by different voltage and current sources. However, these sources are known in every case, and they are simply prescribed by the given incident field.

It has been recognized [1] that the single most important factor in the operation of most integrated-optics applications is the leakage parameter α, which characterizes leaky-wave fields of the form $f(z;\beta_o)\exp[(i\beta_o-\alpha)x-i\omega t]$. Here β_o is very closely equal to the propagation factor β_{sw} of the surface wave guided by the (basic) uniform configuration mentioned above. Thus, while examining also other grating characteristics, our study has focused on the dependence of α on the grating parameters, with special emphasis on rectangular, trapezoid, triangular and other typical grating profiles.

*Portions of this work have been supported by the U. S. Office of Naval Research, by the National Science Foundation and by the U. S. Joint Services Electronics Program.

An important aspect is that, out of all grating shapes, α is largest for a grating having a rectangular profile with $d=2d_1$. This particular grating has been therefore viewed here as a canonic configuration to which gratings with other shapes have been compared. As a function of the grating height t_g, the leakage α in canonic gratings varies as shown in Fig. 3. The behavior of α in the parabolic region (where α is proportional to t_g) and in the saturation region (where α undergoes oscillations of period $\Lambda/2$ about an average value α_∞), as well as other features, can all be explained in terms of the equivalent network of Fig. 2.

A particularly useful outcome of the approach presented here is the derivation of explicit expressions for α. As an example, for a canonic grating operating in a TE mode and with only the n=-1 space harmonic radiating, we get

$$\alpha_\infty \lambda = \frac{(\epsilon_f - N^2)\,(\epsilon_r - \epsilon_a)^2}{\pi N\,(\epsilon_f - \epsilon_g)\,(2N - \lambda/d)} \cdot \frac{d}{\beta_{-1}\,\lambda\,t_f}, \qquad (1)$$

where $N = \beta_{sw}\lambda/2\pi$ is an effective refractive index, λ is the wavelength in air, $\beta_{-1} \cong \beta_{sw} = 2\pi/\lambda$, ϵ_g is the average grating permittivity and all other ϵ_u ($u = a, r, f$ and s) are shown in Fig. 1. Results similar to Eq. (1) have been obtained for TM modes and for the parabolic region of Fig. 3. Furthermore, these results have been extended to cases for which leakage occurs in another ($n \neq -1$) harmonic or in a multiplicity of harmonics.

Gratings having other than rectangular shapes can be similarly treated provided their profile is symmetric with respect to a vertical axis. The results are then in the form of Eq. (1), multiplied by a form factor $\rho \leq 1$ which depends in a simple fashion on the grating profile. Asymmetric gratings, on the other hand, do not readily yield explicit expressions for α, but their analysis can nevertheless be easily carried out despite the absence of such simple expressions. A particularly interesting property of gratings having asymmetric profiles is that they can produce directional discrimination ("blazing") of an incident surface wave, which depends on whether incidence is from the right or left, respectively.

All of these aspects will be illustrated by specific examples and, in particular, the leakage properties of a grating will be discussed as the grating profile is changed progressively from a rectangular, through a trapezoid, to an asymmetric triangular shape. Such a procedure was found to be highly instrumental in establishing systematic design criteria for the fabrication of dielectric gratings for optical beam couplers having prescribed characteristics.

References

1. T. Tamir, "Beam and Waveguide Couplers", in Integrated Optics (Springer-Verlag, New York, 1975) p. 84; a detailed bibliography is included therein.

2. K. Handa, S. T. Peng and T. Tamir, "Improved Perturbation Analysis of Dielectric Gratings", Appl. Physics, vol. 5, pp. 325-328, and vol. 6, pp. 35-38; January and May 1975.

3. W. Streifer, D. R. Scifres and R. D. Burnham, "Analysis of Grating Coupled Radiation in GaAs: GaAlAs Lasers and Waveguides", IEEE J. Quant. Electronics, vol. QE-12, pp. 422-428 and 482-499; July and August 1976.

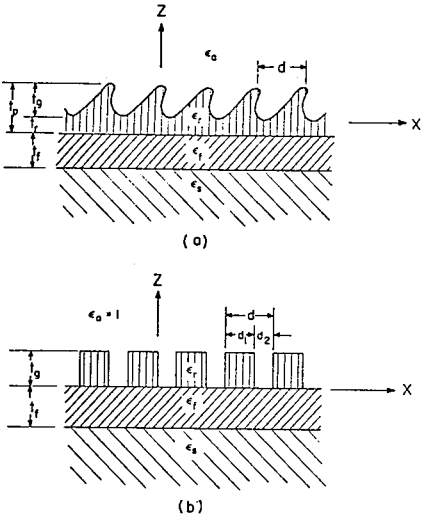

Fig. 1 Dielectric-grating configurations:
(a) General asymmetric profile;
(b) Rectangular profile.

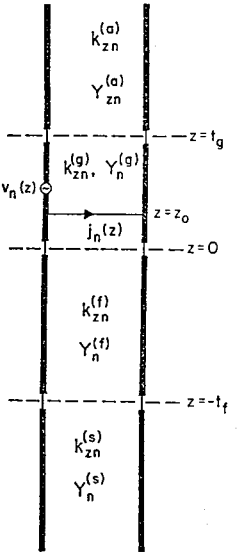

Fig. 2 Equivalent transverse network for dielectric gratings. For simplicity, $t_r = 0$ was assumed.

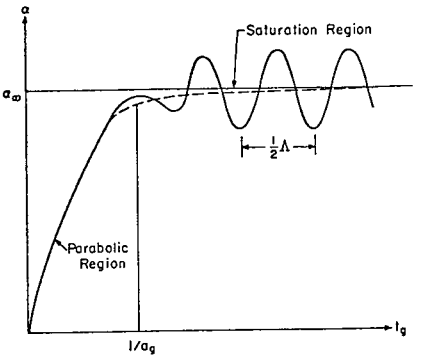

Fig. 3 Leakage α versus grating height t_g in a typical rectangular grating.

5. BEAM DISPLACEMENT OF A REFLECTED BEAM AT AN INTERFACE BETWEEN INHOMOGENEOUS MEDIUM AND FREE SPACE: S. Kozaki, H. Harada,
Department of Electrical Engineering, Gumma University, Kiryu 376, Japan

The geometry of the problem is illustrated in Fig.1. Gaussian beam is obliquely incident on the inhomogeneous medium, for which the permittivity decreases linearly as z increases. The permittivities for $z < 0$ and $z > d$ are constant. Reflected beam after it has propagated through the inhomogeneous medium is obtained. A beam center of the reflected beam, at which the beam amplitude has a maximum value, is shifted from optical axis y_r obtained by Fermat principle by an amount of several wave lengthes when the incident angle θ is equal to the critical angle θ_c. This effect is analogous to G.H.shift, whose displacement is always less than two wave lengthes.

In Fig.2 the beam displacement D/λ is plotted versus the gradient of the permittivity $b\lambda$ for parameters $a\lambda$, λ being wave length. The incident beam is assume to be represented by

$$E_x^i(y_i, 0) = e^{-(a\lambda)^2(y_i/\lambda)^2} \qquad (1)$$

Numerical examples have been obtained by means of numerical integration. The critical angle θ_c is defined by

$$\theta_c = \cos^{-1}\sqrt{bd} \qquad (2)$$

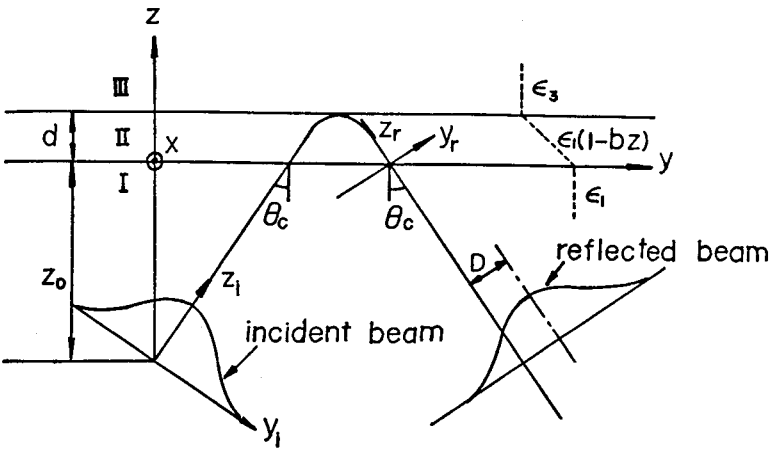

Fig. 1 Geometry of the problem

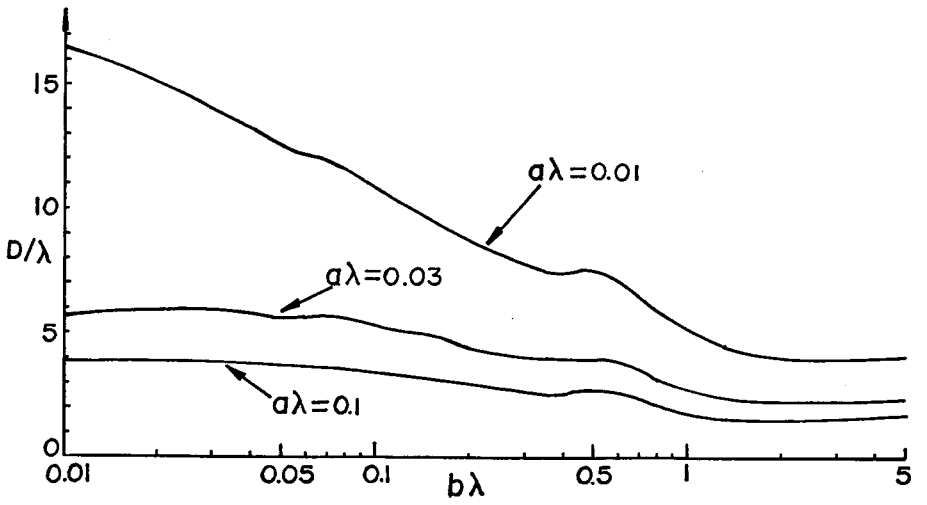

Fig. 2 Beam displacement of the reflected beam

6. THE DIFFRACTION OF GAUSSIAN BEAMS BY PERIODIC LAYERS: R. S. Chu, Communication Systems Division, GTE Sylvania Inc., Needham, Mass., J. A. Kong, Department of Electrical Engineering and Computer Science, Massachusetts Institute of Technology, Cambridge, Mass., and T. Tamir, Department of Electrical Engineering and Electrophysics, Polytechnic Institute of New York, Brooklyn, New York

The scattering of a Gaussian beam incident at or close to a Bragg angle on a periodic half space has been analyzed by Chu and Tamir[1]. Experiments carried out by Forshaw[2] with a thick holographic film verified their results by showing that (a) the diffracted beams are formed by depletion of energy away from the center of the original beam, and (b) the transmitted beams split at the exit plane of the film. Forshaw also measured the far-field patterns of the emerging beams and found their profiles via a Fourier transform of Chu and Tamir's field solution at the exit plane. The analytic results thus derived by Forshaw provide an extension of the half-space results, but they do not predict the observed ripples in the intensity of beams diffracted by a layer of finite thickness.

In this paper, we treat the diffraction of a Gaussian beam by a periodic layer and derive solutions for both the near and the far fields by integrating over an appropriate plane-wave spectrum. For this purpose, we examine a first-order coupled mode expression of the plane-wave solution and compare it with a highly accurate second-order formulation developed by Kong[3], who verified its validity and accuracy by means of a rigorous method. Our results show that, while the first-order approach is accurate for Gaussian beams scattered by layers with small periodic modulation, the second-order formulation must be used for strongly modulated media. The latter formulation can easily handle also asymmetric configurations involving a periodic layer which is bounded on its two sides by media having different dielectric constants. Computed results agree well with Forshaw's experimental observations and they account for

the ripples of the diffracted beam profiles. We also find that, in contrast to previous theoretical studies which assumed an incident plane-wave of infinite extent, complete conversion of energy into the Bragg field cannot generally occur in the case of bounded beams.

[1] R. S. Chu and T. Tamir, J. Opt. Soc. Am., 66, 220 and 1438 (1976).

[2] M. R. B. Forshaw, Opt. Commun., 12, 279 (1974).

[3] J. A. Kong, J. Opt. Soc. Am., 67, (1977).

7. BEAM PROPAGATION IN MULTIMODE FIBER GUIDES: C. Yeh, Electrical Sciences and Engineering Department, University of California at Los Angeles, Los Angeles, Calif.

The ability to predict the light propagation characteristics in various practical guiding structures is very important in optical fiber communications and in optical image transfer. In this presentation a numerical technique is described which is capable of providing useful data on the propagation characteristics of optical guiding structures whose index of refraction variation may be quite arbitrary. As a specific example, the problem of infinite or truncated Gaussian beam propagation in a radially inhomogeneous fiber with parabolic index profile is solved. The numerical results of the infinite Gaussian beam case are compared with exact analytical data and they are in complete agreement.

8. MICROBEND LOSSES IN MULTIMODE OPTICAL FIBERS: A. Q. Howard, Jr., Department of Electrical Engineering, The University of Arizona, Tucson, Arizona

Using the now well known isolated radiation loss formula for a simple bent section of optical fiber, the effect of a statistical distribution of microbends is calculated. This is done using the diffusion equation approximation to the coupled mode equation for power. The statistical content of the theory accounts for Poisson distributed initial points of bends where the bend arc length is uniformly distributed. The paramount analytical result of the paper is a Strum-Liouville eigenvalue matrix equation for the mode dependent attenuation constants. The theory has application to predicting mode coupling and the change in the polar angular distribution of the optical intensity due to longtitudinal step perturbations in the effective refractive index structure of the fiber.

Two theories are combined to predict the effects of the statististical distribution of microbends on multimode

optical fiber waveguides. These are (1) the rather elegant treatment of the isolated bend radiation loss (or three dimensional open wave-guides); and (2) the coupled mode theory resulting in the case of weak coupling in the mode diffusion equation. This problem if attacked in complete generally would be intractable. However since the microbend losses cannot be excessive if a lightwave fiber communication link is to be competitive with alternative systems, the losses are treated herein as perturbations. This allows the single bend loss result to be treated accurately in a comparatively simple manner when the bend radius of curvature is large compared to a wavelength. Also, if the single event distortion is small, and the density of bends is also small, the coupled mode equation can be characterized completely by the second order statistics of the distribution of bends.

Futhermore, in the case of multimode fibers considered herein, the fiber cross section, while being small compared to typical bend curvatures, is large compared to all wavelengths in the spectra of the communication signal. Hence optical notions of rays, asymptotic approximations to mode fields, and transverse field dependence are also advantageously used to simplify the theory.

It is shown that by introducing an appropriate set of expansion functions which satisfy the relevant boundary conditions, a real symmetric matrix eigenvalue problem results

which is suitable for numerical work. Numerical results for attenuation and power density distribution as a function of the statistics of the microbends are presented.

9. APPLICATION OF GEOMETRICAL OPTICS TO SCATTERING OF PLANE ELECTROMAGNETIC WAVES BY GRADED INDEX OPTICAL FIBRE: P. L. Chu, University of New South Wales, Australia

1. Introduction

The scattering of plane electromagnetic waves by an optical fibre may be studied in two approaches: (1) modal analysis and (2) geometrical optics or ray theory. For fibres with uniform refractive index, modal approach has been used by Farone and Kerker [1] and by Lundberg [2] to obtain the forward scattered pattern from which information about the fibre radius and refractive index was derived. The geometrical optics approach has been used by Presby [3] and others to obtain the backward scattered pattern from which information about the fibre can also be derived. For optical fibre with graded index profile, the problem is more difficult. Marcuse and Presby [4] obtained the backward scattered pattern by means of the perturbational modal analysis. The purpose of this paper is to present a geometrical optical solution to the plane wave scattering by a graded index optical fibre. In this paper, the ray path, its amplitude and phase and the wavefront of the scattered electromagnetic wave will be given. From these, the backward scattered patterns may be constructed.

2. Ray Path

Let $\underset{\sim}{x}(t,\alpha)$ be the vector position of the electromagnetic ray in the fibre. It is a function of two parameters α and t. α is the incident angle of the ray at fibre surface, and t is a quantity that increases with the ray and t=0 at incidence. If n is the refractive index of the fibre, then

$$\frac{d^2\underset{\sim}{x}}{dt^2} = \frac{1}{2}\nabla n^2 \qquad \text{——————(1)}$$

For graded-index optical fibre, its index profile is nearly parabolic but not exactly. We can represent it as:-

$$n^2 = n_2^2\left[1 - \Delta^2\left(\frac{r}{b}\right)^{2+\epsilon}\right] \qquad \text{——————(2)}$$

where $|\epsilon| \ll 1$ and b=radius of fibre

Substituting eq.(2) into eq.(1) and using rectangular coordinates (Fig.1), the resultant nonlinear ray differential equations may be solved by regarding ϵ as a converging parameter and by means of Lindsted method. The first order approximation is:

$$x(t) = \left[b\cos\alpha + \tfrac{1}{2}\epsilon A_1\cos\phi_1\right]\cos\Omega t - \left[b\cos(\alpha+\theta_1)\sqrt{\tfrac{1}{\Delta^2}-1} + \tfrac{1}{2}\epsilon A_1\sin\phi_1\right]\sin\Omega t \qquad \text{——————(3)}$$

$$y(t) = \left[b\sin\alpha + \tfrac{1}{2}\epsilon B_1\cos\Psi_1\right]\cos\Omega t - \left[b\sin(\alpha+\theta_1)\sqrt{\tfrac{1}{\Delta^2}-1} + \tfrac{1}{2}\epsilon B_1\sin\Psi_1\right]\sin\Omega t \qquad \text{——————(4)}$$

It can be shown that for purely parabolic fibre ($\epsilon = 0$), the ray path in the fibre is a part of an ellipse. Fig.2 shows the ray trajectories scattered by the fibre.

3. Ray Amplitude

From the ray path, the amplitude of the electric field along the ray may be obtained by solving the transport ray equation. The intensity of the emergent ray after it has traversed the fibre through refraction, reflection and refraction again is given by:

$$I = \frac{b}{r} I_i \cos\varphi_i \left[1 - \frac{\sin^2(\varphi_i - \theta_i)}{\sin^2(\varphi_i + \theta_i)} \right]^2 \frac{\sin^2(\varphi_i - \theta)}{\sin^2(\varphi_i + \theta)} \left| \frac{d\varphi_i}{d\Phi} \right| \qquad (5)$$

where

$$\frac{d\varphi_i}{d\Phi} = \frac{1}{2 - 4\frac{d\theta_i}{d\varphi_i} - 2\frac{d\sigma}{d\varphi_i}} \quad , \quad \frac{d\theta_i}{d\varphi_i} = \frac{\cos\varphi_i}{\sqrt{n_i^2 - \sin^2\varphi_i}}$$

$$\sigma = 2\left[\theta_i + \sin^{-1} \frac{\left(\frac{r_o}{b}\right)^2 - 2(1-\Delta^2)\sin^2\theta_i}{\left(\frac{r_o}{b}\right)^2 \sqrt{1-\Delta^2(1-\Delta^2)(1-\epsilon)\sin^2\theta_i}} - \sin^{-1} \frac{1 - 2(1-\Delta^2)\sin^2\theta_i}{\sqrt{1-\Delta^2(1-\Delta^2)(1-\epsilon)\sin^2\theta_i}} \right]$$

When

$$2\frac{d\theta_i}{d\varphi_i} + \frac{d\sigma}{d\varphi_i} - 1 = 0 \qquad (6)$$

the scattered ray intensity is infinite according to eq.(5). This result arises from the assumption that the emergent wavefront is Gaussian. It will be shown in Section 5 that the real wavefront in the region of maximum intensity is cubic with a cusp (Fig.2). The emergent angle of the ray that results from the solution of eq.(6) is called the rainbow angle.

4. Ray Phase

With a phase reference plane 1-1' as shown in Fig.1, the total phase of a typical ray that has undergone a refraction, a reflection and a refraction is given by:

$$\Psi = 2k_o b(1-\cos\varphi_i) + 4n_2 b k_o \sqrt{1-\Delta^2}\cos\theta_i - 2\Delta^2(2+\epsilon)k_o b\left\{ \left[\frac{1-\epsilon/2}{-2P^2} + \frac{\epsilon}{4}\left(\frac{y}{-2P^2} - \frac{2}{4P^4}\right) \right] \right.$$
$$\left. \sqrt{-P^2y^2 + y^2 - Q^2} + \left[\frac{\epsilon}{4}\left(\frac{3}{8P^4} - \frac{Q^2}{2P^2}\right) + \frac{1}{4P}(1-\epsilon/2) \right] \frac{(-)}{P} \sin^{-1} \frac{1 - 2P^2 y}{\sqrt{1-\Delta^2(1-\Delta^2)(1-\epsilon)\sin^2\theta_i}} \right\}_1^{(r_o/b)^2}$$

where $P = \Delta\sqrt{1-\epsilon}$, $Q = \sqrt{1-\Delta^2}\sin\theta_i$ (7)

5. Wavefront

For the purely parabolic index profile ($\epsilon = 0$), the emergent wavefront may be obtained by moving the coordinate system to x'y' centred at A (Fig.1), y' axis being parallel to the emergent rainbow ray. The wavefront is given by:-

$$y_f = \frac{1}{b^3 \cos^3\alpha_R} C x_f^3 \qquad (8)$$

where C is a complicated function of the incident angle α_R giving rise to the emergent rainbow ray. This equation shows that the wavefront near the rainbow angle is cubic with a cusp as shown in Fig.2. Therefore as the incident ray increases in its incident angle α from 90° to 180°, the emergent ray initially decreases in its emergent angle Φ until $\alpha = \alpha_R$ giving $\Phi = \Phi_R$, then Φ begins to increase again.

6. Backward-scattered Patterns

The backward-scattered pattern may be obtained in three ways: (1) By considering the interference between the two emergent parallel rays. There is also a third interferring parallel ray resulting from externally reflection by the fibre surface. Curve a of Fig.3 shows the backward-scattered pattern

obtained by this method. (2) Since the actual wavefront near the rainbow region is not Gaussian but is cusped as given by eq.(8), the scattered pattern in this region is accurately predicted by Airy's function Ai(x) in the following manner:-

$$E(\theta) = K\left[\frac{6\pi C\cos\theta}{\lambda b^3\cos^3\alpha_R}\right]^{-1/3} \pi\, Ai\left[-\left(\frac{6\pi C\cos\theta}{\lambda b^3\cos^3\alpha_R}\right)^{-1/3}\frac{2\pi\sin\theta}{\lambda}\right] \qquad (9)$$

Curve c of Fig.3 shows such a pattern. The fine structure is absent because the externally reflected ray is not taken into consideration. (3) The modal analysis using first order approximation gives pattern b in Fig.3. Comparisons of patterns a with b, and c with b shows that near the rainbow region, the interference of the two refracted rays dominates while near the axis region, the externally reflected ray and one of the refracted rays are important.

7. References

(1) W.A. Farone, M. Kerker "Light Scattering from Long Submicron Glass Cylinders at Normal Incidence" J. Optic. Soc. Amer. Vol.56, pp.481-487,1966

(2) J.L. Lundberg "Light Scattering from Large Fibers at Normal Incidence" J. Colloid & Interf. Sci. Vol.29, pp.565-583, March 1969

(3) H.M. Presby "Refractive index and diameter measurements of unclad optical fibres" J. Optc. Soc. Amer. Vol.64 pp.280-284, March 1974

(4) D. Marcuse, H.M. Presby "Light scattering from optical fibres with arbitrary refractive index distribution" J. Opt. Soc. Amer. 65, p.367-375

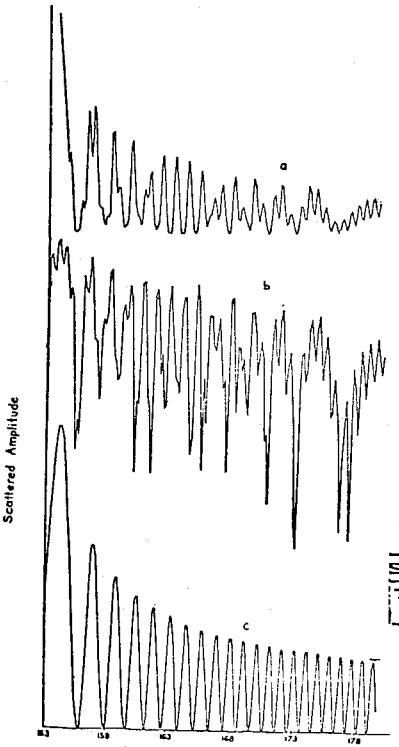

Fig 3. Backward-scattered Pattern

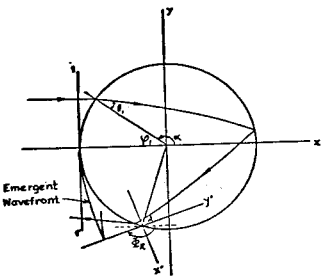

Fig.1 Plane Wave scattering by Graded Index Optical Fibre

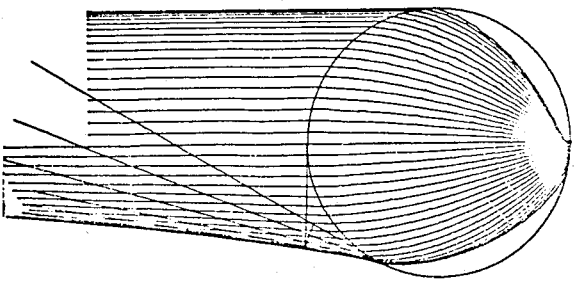

Fig 2. Ray trajectories

Commission B - Session 2

(Joint with IEEE AP-S Session 20)
Wednesday P.M. 1330 - 1650
TRANSIENTS, SEM AND IDENTIFICATION
Chairman: M. B. Van Blaricum, MRC, Santa Barbara, CA

1. TRANSIENT RADIATION FROM A SPHEROIDAL ANTENNA: G. Franceschetti, J. D. Kotulski, P. L. E. Uslenghi, Communications Laboratory, University of Illinois at Chicago Circle

The canonical problem of a prolate spheroidal metallic antenna excited at an equatorial gap by an azimuthally-independent step voltage is considered. Starting from the exact modal solution of the problem in the frequency domain, a Laplace inverse transform yields the solution in the time domain, according to the singularity expansion method. The result for a spherical antenna is obtained as a particular case [1].

The location of poles in the complex frequency plane is determined numerically as a function of eccentricity, from the limiting case of a spherical antenna to that of a thin cylindrical antenna. The particular cases of early-time and late-time behavior of the field are discussed and compared with known results [1,2,3]. Finally, the study is extended to an imperfectly conducting spheroidal antenna with a variable surface impedance [4]. This research was performed under Grant AFOSR-72-2263.

[1] G. Franceschetti, "A canonical problem in transient radiation - The spherical antenna," to be published.
[2] C.W. Harrison and R.W.P. King, IEEE Trans., AP-15, 301-302 (1967).
[3] R.W. Latham and K.S.H. Lee, Radio Science, 5, 715-723 (1970).
[4] N.G. Alexopoulos and P.L.E. Uslenghi, "Antennas on spheroids with a variable surface impedance," URSI Fall Meeting, Columbus, Ohio (September 1970).

2. SEM PARAMETERS OF A THIN CYLINDER ABOVE LOSSY GROUND: T. H. Shumpert, Auburn University, Auburn, Alabama, D. H. Herndon, Harris Electronics Inc., Melbourne, Florida

The Singularity Expansion Method (SEM) is employed to determine the transient response of a thin, finite-length, perfectly conducting cylindrical scatterer above a lossy ground plane of infinite extent. The effects of the lossy ground on the currents and charges induced on the scatterer are treated using Fresnel reflection coefficients as defined for complex frequencies. The SEM parameters of interest such as natural frequencies, natural modes, and coupling coefficients are determined numerically as a function of the scatterer-ground plane geometry and electrical characteristics of the ground. The SEM parameters are presented in the form of appropriate graphs and tables. In addition, these data are compared with previously obtained SEM data for the thin cylindrical scatterer in free space and the thin cylindrical scatterer above a perfectly conducting ground plane of infinite extent. Commonalities between these data and the resulting inferences for other scatterers near lossy ground are discussed.

3. A PROCEDURE FOR CONSTRUCTING SINGLE PORT EQUIVALENT CIRCUITS FOR ANTENNAS FROM THE SEM SOLUTION: B. K. Singaraju, Dikewood Industries Inc., C. E. Baum, Air Force Weapons Laboratory

In complex frequency plane there are various equivalent representations for an electromagnetic coupling problem. In the singularity expansion method (SEM) the response can be written in terms of the s plane singularities such as poles, branch cuts, etc. Circuit models can be constructed from the singularity expansion method representation which has the advantage of providing physical insight, computational convenience and low cost laboratory simulation among others. Although both open circuit and short circuit boundary value problems can be treated in this fashion, only short circuit boundary value problems will be treated here.

The short circuit boundary value problem is defined by setting any impedance loading the gap of the antenna/scatterer to be zero. The scattered field can be represented as an integral over the antenna plus the gap. Defining the short circuit natural frequencies, natural modes, admittance coupling coefficients the response can be expressed in terms of these SEM quantities. Using the pole admittances and voltage sources an equivalent circuit consisting of an equivalent voltage source and an admittance is constructed for each pole. This equivalent circuit can be constructed for each set of conjugate pole pairs. Entire function contributions are also included. As an example a thin linear dipole antenna equivalent circuit is constructed. The input admittance and the response are compared to the measured quantities.

4. TRANSIENT RESPONSE OF A WIRE BEHIND AN APERTURE PERFORATED CONDUCTING SCREEN DUE TO AN EMP EXCITATION: K. R. Umashankar, S. Singarayar, University of Mississippi, University, Mississippi

Recently attention is focused on the study of characterization and responses of objects in the vicinity and behind apertures perforated conducting screen. The scattering behavior of the objects are greatly affected due to the direct coupling to apertures in the screen. Earlier investigation of the finite length wire behind and parallel to the aperture, in the form of narrow slot, perforated conducting screen based on the formulation of the boundary value problem indicate strong coupling depending on slot-wire dimensions and the distance between them. Based on this study wherein one solves a set of coupled integro-differential equations, investigation is extended to derive some of the characteristics regarding transient scattering and time responses of the electric field in the narrow slot and electric current on the wire.

Two practical cases of interest are studied here; the first case involves the excitation of the wire behind a narrow slot perforated screen by an EMP and the second case treats the wire as an antenna with EMP excitation at the center. For such hybrid configurations, time responses of the electric current on the wire and the electric field in the narrow slot are derived through direct fourier transform of the results in the frequency domain.

The results of the transient characterization with the application of the Singularity Expansion Method are also presented where the coupling between the wire and the slot can be explained by means of pole trajectories in the complex plane as a function of orientation of the wire with respect to the slot.

Figures 1 and 2 are the representation results of the transient response by direct fourier transform.

Figure 1 gives the time response at the center of the wire behind a narrow slot perforated screen excited by a step plane wave incidence, normal to the slot at $t = 0$. Similarly Figure 2 gives the time response at the center of the antenna in the presence of a narrow slot perforated screen with an EMP excitation at the center of the antenna. The slot is in xy plane and oriented along the x axis with its center at the origin, while the thin wire is placed parallel to the screen and the angle β of the axis of the wire is measured with respect to y axis so that when $\beta = 0$, the wire is perpendicular to the screen. The location and orientation of the wire is specified with coordinates of the center of the wire (x_c, y_c, z_c) and angle β.

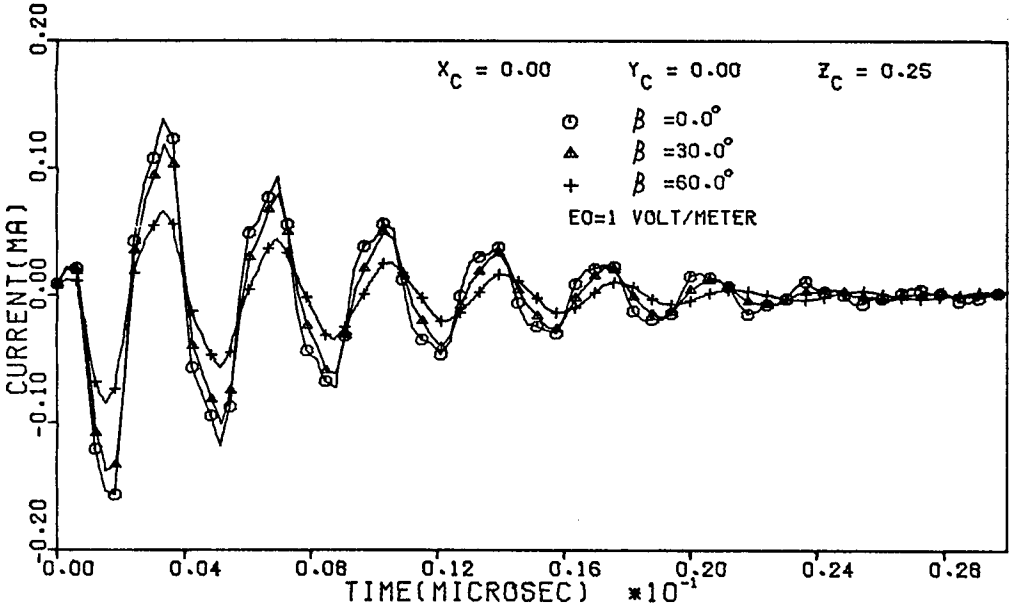

Fig. 1. Time Response of the Current at the Center of the Wire behind a Narrow Slot with Step Plane Wave Incidence (Slot: Length 0.5 m, Width 0.05 m; Wire: Length 0.5 m, Radius 0.001 m)

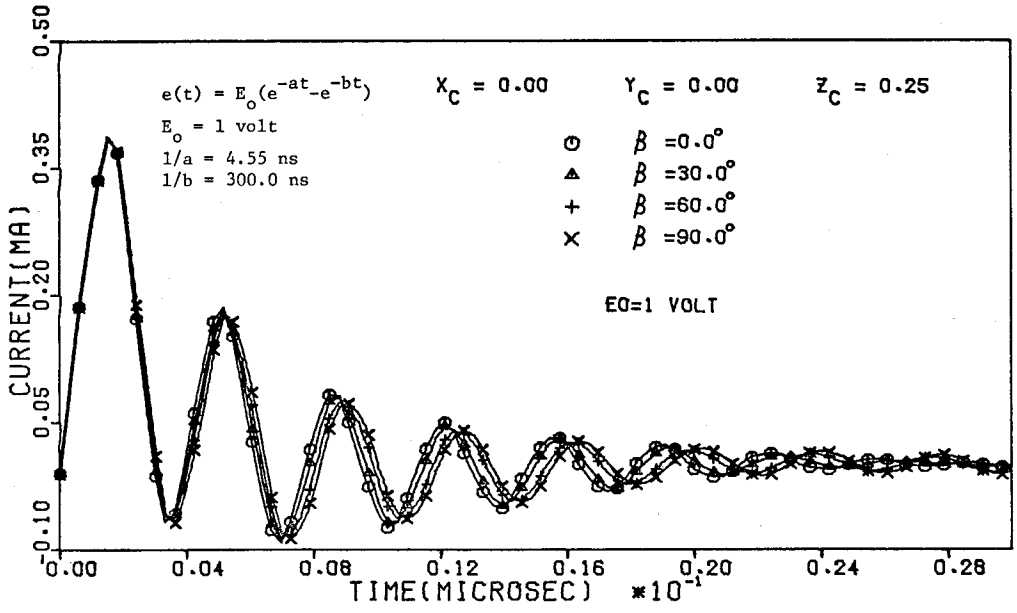

Fig. 2. Time Response of the Current at the Center of the Antenna in the Presence of a Narrow Slot with an EMP Excitation (Slot: Length 0.5 m, Width 0.05 m; Wire: Length 0.5 m, Radius 0.001 m)

5. A DISCRETE SAMPLING APPROACH TO THE INVERSE SCATTERING PROBLEM:
P. Jedrzejewski, Naval Air Development Center, H. Kritikos, Moore School of Electrical Engineering, University of Pennsylvania

INTRODUCTION

The category of problems termed inversed scattering seek to describe the properties of a remotely located body through a knowledge of scattering data. Analytic considerations require that the scattering data, in the form of the reflection coefficient, be known for all frequencies from $-\infty$ to $+\infty$. In practice it is feasible to take only a finite number of frequency readings. An approach is presented which bridges the gap between the analytical and the practical. Two methods are applied to data resulting from the frequency sampling of a hypothetical third order body, that is, a body whose scattering data results in a third order rational reflection coefficient. The resulting constructed reflection coefficients are used in conjunction with the Gelfand-Levitan equation and solved by Kay's method to arrive at an estimated expression for the potential arising from the constructed reflection coefficients to the actual potential of the hypothetical third order body.

SAMPLING CONSIDERATIONS

Due to the work of Kay [1] and Sims [2], it is reasonable to assume that the actual reflection coefficient of the hypothetical body being irradiated is given by a rational function of the form

$$(1) \qquad b(k) = \frac{b_o + b_1 k + b_2 k^2 + \ldots + b_m k^m}{a_o + a_1 k + a_2 k^2 + \ldots + a_n k^n}$$

where m and n are unknown and $n \geq m + 2$.

Sampling the reflection coefficient consists of transmitting a signal of known amplitude at the inhomogeneous dispersive media, measuring the amplitude and phase of the return and calculating the ratio of reflected to transmitted wave. At sampling frequencies of $k_1, k_2, \ldots, k_s$, where the k's are taken along the real axis, the numbers calculated will be the complex quantities $b(k_1), b(k_2), \ldots, b(k_s)$.

SIMPLE APPROXIMATIONS

Given the samples $b(k_1), b(k_2), \ldots, b(k_s)$ of the rational function b(k) a rational approximation

(5)

$$\hat{k}_1 = \frac{[-(k_o^2-(C_1^2+C_2^2+2aC_2))^2+4(2C_2+a)a(C_1^2+C_2^2)]^{1/2}-[k_o-(C_1^2+C_2^2+2aC_2)]i}{-2(2C_2+a)}$$

$$\hat{k}_2 = \frac{-[-(k_o^2-(C_1^2+C_2^2+2aC_2))^2+4(2C_2+a)a(C_1^2+C_2^2)]^{1/2}-[k_o^2-(C_1^2+C_2^2+2aCa)]i}{-2(2C_2+a)}$$

In the above k_o is the sampling frequency. As long as

$$k_o < [(C_1^2 + C_2^2 + 2aC_2) - [2a(2C_2 + a)(C_1^2 + C_2^2)]^{1/2}]^{1/2}$$

non-singular potentials result. These non-singular potentials approach the negative going slope of the corresponding third order potential when sampling frequency is increased. In addition, the peak of the actual potential and the reconstructed potential are approximately the same for all sampling frequencies. It is felt that properties like the latter, namely those which are invarient with sampling frequency, that are most important and should be emphasized in any future work in this area.

REFERENCES

[1] Kay, Irvin. The Inverse Scattering Problem, Institute of Mathematical Sciences, New York University, Report EM-74. New York: 1955.

[2] Sims, A. R. "Certain Aspects of the Inverse Scattering Problem," Journal of the Society of Industrial and Applied Mathematics, Vol 2., No. 4, pp. 183-205. December 1957.

[3] Kay, Irvin. "The Inverse Scattering Problem When the Reflection Coefficient is a Rational Function," Communications on Pure and Applied Mathmatics. Vol. XIII, pp. 371-393. 1960.

[4] Frost, P. A. and E. Y. Harper. "An Extended Padé Procedure for Constructing Global Approximations for Asympotic Expansions: An Explication with Examples," SIAM Reivew, Vol. 18, No. 1:62-91. January 1976.

6. EXACT SOLUTION TO AN INVERSE SCATTERING PROBLEM: Shimon Coen, Department of Electrical Engineering and Computer Sciences, University of California, Berkeley, Calif.

Introduction

For the medium shown in Fig. 1, Linlor and Jiracek [1] assumed lossless and non-dispersive dielectrics and then via Stratton analysis [2], presented a synthesis solution. This requires the minimum and maximum values of the reflection coefficient amplitude. The method proposed in this paper may be applied to lossy dielectrics, requires the reflection coefficient amplitude and phase, but only at three discrete, equally spaced frequencies. The problem may be stated as follows: given the reflection coefficient at three discrete equally spaced frequencies from a normally incident plane wave, find the complex dielectric constant of the layer and the half space and the thickness of the layer (see Fig. 1).

The Solution

The reflection coefficient P for this problem may be determined by solving the one-dimensional wave equation subject to the continuity of the tangential fields. The result is

$$P = \{-\xi + \eta e^{2jkh\sqrt{\varepsilon}}\}/\{1 - \xi\eta e^{2jkh\sqrt{\varepsilon}}\} \tag{1}$$

where $\xi = (\sqrt{\varepsilon}-1)/(\sqrt{\varepsilon}+1)$, $\eta = (\sqrt{\varepsilon}-\sqrt{\varepsilon_e})/(\sqrt{\varepsilon}+\sqrt{\varepsilon_e})$, k is the free space wave number, h is the height of the layer and ε and ε_e correspond to the complex dielectric constant of the layer and the half-space respectively. Equation (1) may be cast into a more convenient form, namely

$$\alpha = \eta e^{2jkh\sqrt{\varepsilon}}, \quad \alpha = (P+\xi)/(1+P\xi) \tag{2}$$

Note that by assuming that all the complex dielectric constants involved are not a function of frequency, then η is frequency independent. Now write Eq. (2) for three equally spaced frequencies

$$\alpha_i = \eta e^{2jk_i h\sqrt{\varepsilon}}, \quad i = 1,2,3 \tag{3}$$

where $k_3-k_2 \equiv \Delta \equiv k_2-k_1$ and Δ is arbitrary; this gives

$$\alpha_1/\alpha_2 = \alpha_2/\alpha_3 = e^{-2jh\sqrt{\varepsilon}\Delta} \tag{4}$$

for which the following is obtained

Research sponsored by the NASA-Ames Research Center contract NCA2-OR050-406.

$$\frac{(P_1+\xi)(P_3+\xi)}{(1+P_1\xi)(1+P_3\xi)} = \left(\frac{P_2+\xi}{1+P_2\xi}\right)^2 \tag{5}$$

where P_i corresponds to k_i.
With the following notation: $U_i = 1+P_i$, $V_i = P_i-1$ and $t = \sqrt{\epsilon}$ Eq. (5) may be cast into

$$\frac{(U_1t+V_1)(U_3t+V_3)}{(U_1t-V_1)(U_3t-V_3)} = \left(\frac{U_2t+V_2}{U_2t-V_2}\right)^2 \tag{6}$$

This equation may be now solved for t; the result is

$$\varepsilon = \frac{-(U_1V_3+V_1U_3)V_2^2+2V_1V_2V_3U_2}{(U_1V_3+V_1U_3)U_2^2-2U_1U_2U_3V_2} \tag{7}$$

Equation (7) states that the complex dielectric constrant of the layer is uniquely determined from the knowledge of the reflection coefficient at three discrete equally spaced frequencies.

The height of the layer may be now determined from Eq. (4); the result is

$$h = \log|\alpha_1/\alpha_2|/\{2\Delta \mathrm{Im}(\sqrt{\varepsilon})\} \tag{8}$$

where $\mathrm{Im}(\sqrt{\varepsilon})$ denotes the imaginary part of $\sqrt{\varepsilon}$. Note that the height obtained is unique provided that $\mathrm{Im}(\sqrt{\varepsilon}) \neq 0$.

Finally, the complex dielectric constant of the half space is obtained from Eq. (3); the result is

$$\varepsilon_e = \varepsilon\{(1-\alpha_1 e^{-2jk_1h\sqrt{\varepsilon}})/(1+\alpha_1 e^{-2jk_1h\sqrt{\varepsilon}})\}^2 \tag{9}$$

This completes the solution of the inverse scattering problem associated with the medium shown in Fig. 1.

Acknowledgement: Professor K. K. Mei suggested the problem.

References

[1] W. J. Linlor and G. R. Jiracek, "Electromagnetic reflection from multi-layered snow models," Journal of Glaciology, Vol. 14, No. 72, pp. 501-516, 1975.

[2] J. A. Stratton, Electromagnetic Theory: New York, McGraw-Hill Book Co. Inc., 1941.

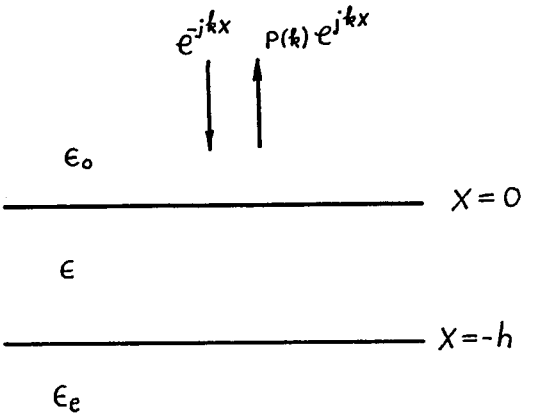

Fig. 1: A Three Layers Medium

7. IDENTIFICATION OF EM SPECTRUM BY KNOWN POLE SETS*: E. K. Miller, J. N. Brittingham, J. L. Willows, University of California, Lawrence Livermore Laboratory

In previous work[1] a numerical procedure was demonstrated that extracts the poles of an object from its EM spectrum. That procedure returns both physical and curve-fitting poles. This paper describes a method by which the curve-fitting poles can be separated from the physical poles. Also presented in this paper is an algorithm that uses stored pole sets of different known targets and an observed spectrum to identify an unknown target. This identification algorithm is a process differing from previous methods[2] since it is performed entirely in the frequency domain.

The procedure for separating the physical and curve-fitting poles is accomplished by using a band limited frequency window on the given spectral data and extracting the poles by the method presented in the previously described report.[1] The frequency window is then shifted by one sample interval and the data again processed for the poles. By plotting all the poles from the various runs on the same graph, the physical poles cluster together while the curve-fitting poles are more scattered, thus permitting them to be identified.

To demonstrate this sliding-window method, the backscattered spectrum of ship model 3 of Fig. 1 for the case of a 60° incident wave was calculated for a frequency range of 0.125 to 10 MHz at 0.125 MHz intervals. A frequency window 5 MHz wide was used for 10 successive pole calculations over the range 0.125 to 5 MHz, 0.250 to 5.125 MHz, etc. Figure 2 shows a cluster plot of the 10 different calculations. All poles in each run are represented by a single letter A through J. Note that the physical poles form clusters while the locations of the curve-fitting poles vary.

Using pole sets obtained in this way, the identification of an object from a set of stored (previously obtained) library poles can be accomplished totally in the frequency domain. This process begins by separating the spectrum of the unknown object into two sets of data, $F_M(\omega_q)$, $F_M(\omega_p)$ which interleave along the $j\omega$-axis. The stored pole sets are used to calculate a set of residue values R_n^L from the data by employing the equation

$$F_M(\omega_q) = \sum_{n=1}^{N} \frac{R_n^L}{j\omega_q - \alpha_n^L}; \quad q = 1,\ldots, N/2 \qquad (1)$$

*This work was supported in part by the Engineering Research Division of the Lawrence Livermore Laboratory's Electronics Engineering Department and in part by the Advanced Research Project Agency.

where α_n^L denotes the Lth set of library poles. The residues found from the solution of equation (1), along with the corresponding library pole set used to find them, are then used to calculate a predicted response on the ω-axis at the points ω_p by the expression

$$F_C^L(\omega_p) = \sum_{n=1}^{N} \frac{R_n^L}{j\omega_p - \alpha_n^L} \quad ; p = 1, \ldots, N/2$$

The normalized rms error between the actual response F_M and the calculated response F_C^L is then calculated and a correlation number between the stored poles set and the unknown object is obtained by computing

$$R_L = \frac{1}{1 + \epsilon_L}$$

where ϵ_L is the normalized rms error.

To demonstrate this procedure the poles of the three models shown in Figure 1 for an incidence angle of 60° were found and stored. Then the same three backscattered responses were used in the above identification process. The results of this numerical identification test is shown in Figure 3. Note that each set of poles does correlate best with backscattering data from the model for which it was derived.

REFERENCES

1. J. N. Brittingham, E. K. Miller, J. L. Willows, "The Derivation of Simple Poles in a Transfer Function from Real-Frequency Information, Part 2: Results from Real EM Data," Lawrence Livermore Laboratory, Report UCRL-51118, August 23, 1976.

2. D. C. Moffatt, and R. K. Mains, IEEE Trans. Antenna and Propagation, AP-23 (3), 358-367, 1975.

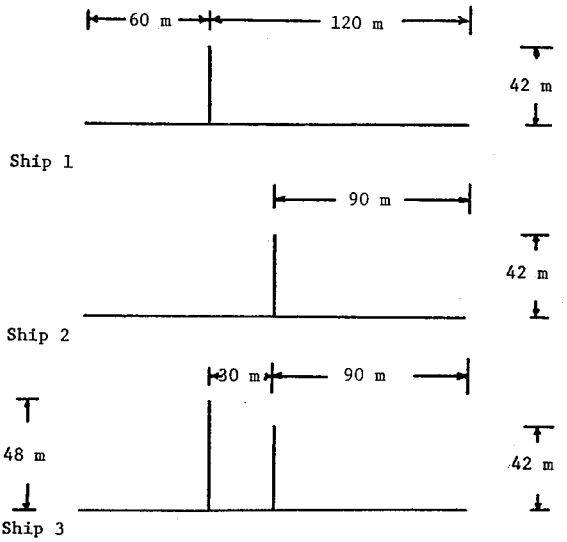

Figure 1. This figure presents three separate stick models of ships. All dimensions are in meters.

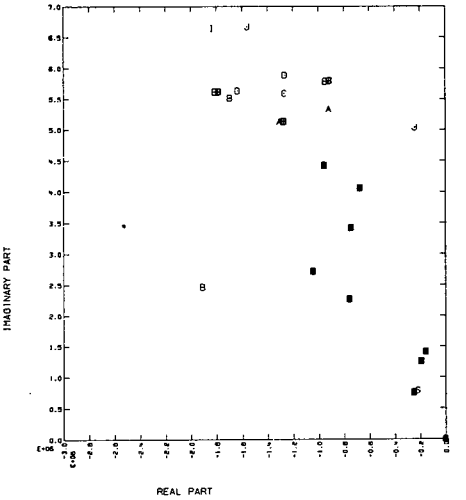

Figure 2. This is a cluster plot that demonstrates the results of using a sliding frequency window on data for ship model 3 of Figure 1 for the case of a 60° incident wave. The original spectrum was calculated for a frequency range of .125 to 10 MHz. A frequency window of 5 MHz wide was used for 10 successive pole calculations, each displaced by 0.125 MHz. The poles in each successive run are represented respectively by a single letter A through J.

Figure 3

A tabulation showing the correlation results for the three ship models of Figure 1 is presented here. The library poles were first extracted from the backscattered spectrum of each ship for the case of a 60° incident wave. The frequency domain correlation procedure was then applied to each of these spectra using the above poles.

x/i	1	2	3
1	1.000	0.329	0.637
2	0.316	1.000	0.701
3	0.523	0.536	1.000

8. CLASSIFICATION OF RADAR TARGETS BY MULTIFREQUENCY MEASUREMENTS*:

J. P. Toomey, C. L. Bennett, Sperry Research Center, Sudbury, Mass.

Since the launching of Sputnik I in 1957, there has been considerable interest in determining the shape and size of orbiting space vehicles using remote sensors such as radar [1]. The subject of this paper is the use of radar sites with a multifrequency capability in the space object classification problem. The basic technique developed during this study consists of comparing noisy multifrequency Radar Cross Section (RCS) measurements with stored data describing the RCS of assumed target shapes.

The contents of the signature library were obtained using the space-time integral equation method developed by Bennett [2]. This technique enables the calculation of the exact scattering response of conducting bodies at all frequencies including the difficult resonance region where the wavelength is of the order of the overall size of the target. The space-time integral equation method has been developed to a point where the scattering response of a large class of target shapes can be calculated. It has been used to compute the smoothed impulse response of smooth convex targets, targets with edges, thin wires, smooth convex bodies with wires attached, open thin surfaces, and cylinders with fins attached. In addition, this technique has been extended to the computation of the impulse response (entire frequency response) or smooth convex targets, targets with edges, rectangular plates and cylinders with fins attached. The applicability of the method is presently being increased further.

The targets assumed for this paper were a one-meter-diameter sphere, a prolate spheroid with diameter one meter and overall length two meters, and a sphere-capped cylinder with diameter 2/3 meters and an overall length of two meters. The circularly polarized radars were assumed to be the currently operational ALTAIR and TRADEX, which are collocated and simultaneously operate in the VHF, UHF, L, and S bands. The two lower frequencies lie in the resonance region of the targets.

Since the ALTAIR and TRADEX radars operate with circular polarization, only the circular polarization radar cross section is considered. This has the additional benefit of eliminating any explicit dependence of the radar cross section on the polarization vector orientation with respect to the target axis, thus enabling cost-effective classification processing. These radars transmit right-hand circular polarization (RHCP) and will see the sphere only in the left-hand circular polarization (LHCP) received channel. The numerical results given here apply to radars which transmit and receive opposite sense polarizations, but the classification software

*The work reported in this paper was supported by Air Force Contract No. F30602-76-C-0039.

is set up to handle dual receive polarizations (RHCP and LHCP) at multiple frequencies. With the circular polarization condition specified, the elements of linear polarization scattering matrix, computed from the space-time integral equation, can be used to calculate the radar cross section appropriate to these radars. The radar cross section (RCS) depends on radar carrier frequency and target aspect, which may be specified as the angle, ϕ, between the line of sight and the target axis. For example, consider the RCS seen by ALTAIR (VHF and UHF). An efficient way of displaying the dependence of the RCS on frequency and aspect is to plot $\sigma(f_1, \phi)$, the RCS at VHF, versus $\sigma(f_2, \phi)$, the RCS at UHF. The aspect variation then appears parametrically on these "frequency space trajectories." Figure 1 shows this plot (the RCS values are in dB relative to one square meter) for the three targets. Since the sphere RCS is independent of viewing angle, it appears as the point located at (-3.7, -2.0) dBSM. The RCS of the other targets is aspect dependent and the resulting curves show this dependence by indicating the aspect angle at various points on the trajectory. The frequency space trajectory (FST) for the sphere-capped cylinder is more complex than that for the prolate spheroid, as might be expected.

A noise-corrupted multifrequency UHF and VHF observation of the RCS of an orbiting vehicle can be represented by a point in the plane of Figure 1. The location of this point will depend on the shape and size of the target being illuminated, the apsect angle, and the polarization of the radars. Even under identical conditions (static target), however, the location of this point from pulse to pulse will fluctuate randomly about the true target RCS due to noise effects. The magnitude of these fluctuations will depend on range, RCS, and the parameters of the radar(s). In order to classify targets, a measure of closeness or distance between the noisy observations and the library RCS data represented in Figure 1 was developed. The classifier operates by choosing the frequency space trajectory which is closest to the observed data.

The classifier was developed from the principles of statistical decision theory which indicate that the likelihood function or probability density of the radar observations provides the best measure of closeness between the observed data and the stored signatures. This viewpoint required a statistical model of the effect of radar receiver noise on the RCS measurements made by radars. The resulting generalized likelihood classifier has several advantages over those described in previously published work [3, 4]. It requires modifications to only the data-processing portions of existing radars and therefore would be a relatively simple add-on to operational sites with a multifrequency capability. The classifier requires absolutely no prior information (statistical or deterministic) concerning target aspect or dynamical motion; aspect estimation is an automatic "by-product" of the operation of the classifier. This feature could be used to measure target motion or detect sudden changes in target attitude.

The classifier operates sequentially in time on the received radar data. No storage of radar data is required, but the decision

at a given time is dependent on all the data received up to and including that time. The decision statistic is updated after each observation is received. A measure of the confidence to be associated with the current decision is also computed. The classifier structure thus enables very early target classification depending on the desired decision confidence. The simulation studies done during this study show that only a small number of radar observations (at only two frequencies) during the early portion of the first pass of either stable or tumbling objects are required for essentially error-free shape classification. An additional attractive feature of this classification method is the capability to recognize that the target being tracked is not closely represented by any of the targets in the signature library. This target reject confidence measure will be described.

[1]. C. Brindley, "Target Recognition," Space/Aeronautics, June 1965, pp. 62-68.

[2]. C.L. Bennett, A.M. Auckenthaler, R.S. Smith and J.D. DeLorenzo, "Space-Time Integral Equation Approach to the Large Body Scattering Problem," Sperry Research Center, Sudbury, Mass., Final Report on Contract No. F30602-71-C-0162, May 1973.

[3]. A.A. Ksienski, Y. Lin, and L.J. White, "Low Frequency Approach to Target Identification," Proc. IEEE, Vol. 63, No. 12, December 1975, pp. 1651-1660.

[4]. W.B. Goggins, "Identification of Radar Targets by Pattern Recognition," Ph.D. Dissertation, Air Force Institute of Technology, Wright-Patterson AFB, Ohio, 1973.

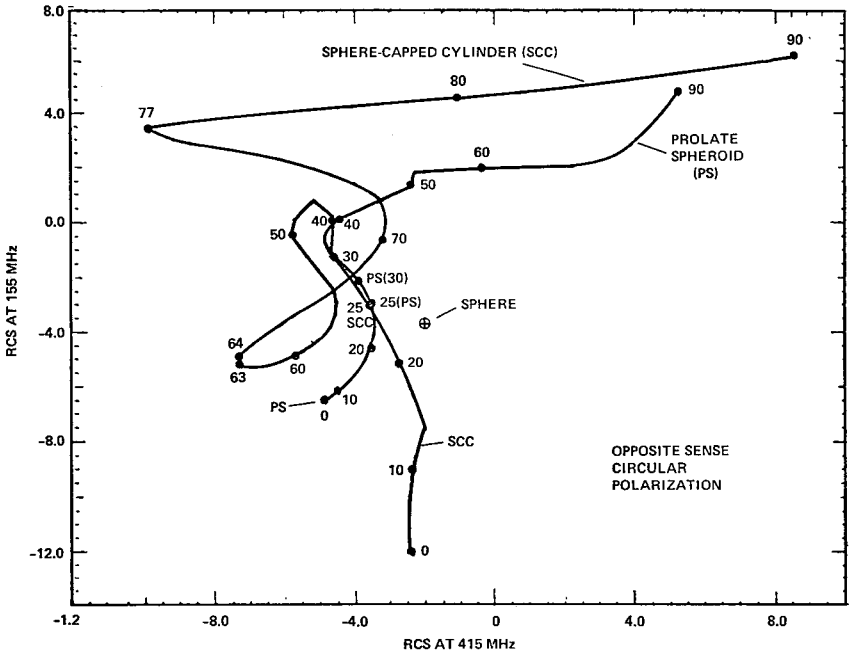

FIG. 1 Frequency Space Trajectories at VHF/UHF

9. SUBOPTIMAL SYSTEM APPROXIMATION/IDENTIFICATION BY COMPLEX EXPONENTIALS:

T. K. Sarkar, Rochester Institute of Technology, Rochester, New York,
J. Nebat, D. D. Weiner, Syracuse University, Syracuse, New York

1. Introduction

Prony's algorithm for deriving complex poles and residues for equispaced data samples [1] is quite straightforward. However, the Prony method does not yield an optimum set of poles and residues; nor does it give a measure of accuracy. Also the set of poles obtained by Prony's method depends on how the set of data points are chosen. Prony's method become quite complicated when the response to a system is given for an arbitrary input and for nonzero initial conditions. Furthermore, when the order of approximation is increased from n to n+1, the whole procedure must be repeated again. Reference [2] describes a procedure for obtaining the optimum exponents and the weighting constants needed to minimize the integrated square error (ε). Unfortunately this method requires a solution of nonlinear algebraic equations, and a linear iterative method. The method presented here is suboptimal. In this method [3] the poles are suboptimal. However, they appraoch the optimum poles [4] when the mean-squared error ε is made small. Having obtained the poles, the weighting constants are evaluated by a least square method.

2. Approximating a Signal by Exponentials

Let the signal x(t) be real for $t \geq 0$ and zero otherwise and be square integrable over $[0, T]$. Let the least-square approximation (minimizes the integrated square error) of x(t) be g(t) and of the form

$$g(t) = \sum_{i=1}^{n} A_i \exp(s_i t)$$

for $t \geq 0$, $\mathrm{Re}[s_i] < 0$, $s_i \neq s_k$ for $i \neq k$ and $A_i \neq 0$. A measure of approximation of x(t) is the non-negative number ε defined by $x(t) = g(t) + \varepsilon\, r(t)$, where r satisfies $\langle g,r \rangle = 0$ and $||g|| = ||r||$. If the function x(t) is integrated repeatedly n times, a set of n+1 functions are obtained, namely $x(t) = x_1(t)$, and $x_{k+1}(t) = \int_0^t x_k(\tau)d\tau$, for k=1,...,n. Also each function can be written as $x_k(t) = g_k(t) + \varepsilon\, r_k(t)$ where g_k and r_k are obtained by repeated integrations of $g = g_1$ and $r = r_1$, respectively. The set of functions $\{g_1,\ldots,g_{n+1}\}$ form an n order subspace S_n of a Euclidean space Ω of functions [3]. For $\varepsilon = 0$, x(t) is in S_n and the exact exponents can be determined from the n order polynomial equation $\sum_{i=1}^{n+1} \sqrt{\Delta_{ii}}\,\lambda^{n+1-i} = 0$ where the Δ_{ii} are the diagonal cofactor of the matrix $[G_{n+1}] = [g_{ij} = \langle g_i, g_j \rangle]$. Moreover it is necessary and sufficient for perfect

n approximation of g(t) that $|G_{n+1}| = 0$. So the calculation of the system exponents s_i, is reduced to finding the roots of a polynomial. For the general case (suboptimal case) when $\varepsilon \neq 0$, the positive square root of $\det [H_{n+1}]$ is the same order of magnitude as ε, i.e. $\sqrt{|H_{n+1}|} = \theta(\varepsilon)$ and the diagonal cofactors Δ'_{ii} of H_{n+1} are related to Δ_{ii} as

$$\sqrt{\Delta'_{ii}} = \sqrt{\Delta_{ii}} + .5\,\varepsilon\,\delta_{ii}/\sqrt{\Delta_{ii}} + \theta(\varepsilon^2)$$

where the matrix H_{n+1} is defined as $[h_{ij} = \langle x_i, x_j \rangle]$ and δ_{ii} are certain constants, which is dependent only on the function g. It can also be shown [3] that the suboptimal roots s'_i of the equation $\sum_{i=1}^{n+1} \sqrt{\Delta'_{ii}}\,\lambda'^{n-i+1} = 0$ are related to the optimum exponents s_i as $s'_i = s_i + \varepsilon \ell_i + \theta(\varepsilon^2)$, where ℓ_i are the appropriate constants. Once the suboptimal exponents are found, the weights A_i can be obtained by a least-square solution. Next section gives the solution procedure of a general case. The following result due to Gram is used to calculate ε. If $\{e_1,\ldots,e_n\}$ span an n-dimensional subspace S_n of an inner product space, then the least square approximant in S_n to a given $x \notin S_n$ is

$$g(t) = \frac{-1}{|G_n|} \begin{vmatrix} 0 & e_1 \cdots e_n \\ \langle e_1, x\rangle & \\ \vdots & [G_n] \\ \langle e_n, x\rangle & \end{vmatrix}$$

Where $G_n = [g_{ij} = \langle e_i, e_j \rangle]$ and $e_1,\ldots,e_n$ are the n exponents to approximate x(t) (i.e. $e_1 = \exp(s_1 t),\ldots$)

$$\varepsilon = \frac{\sqrt{\langle \varepsilon r,\ x-g\rangle}}{\|r\|} = \frac{\sqrt{\varepsilon\langle r, x\rangle}}{\|g\|} = \frac{1}{\|g\|\,|G_n|^{1/2}} \begin{vmatrix} \langle x,x\rangle & \langle e_1,x\rangle \cdots \langle e_n,x\rangle \\ \langle e_1,x\rangle & \\ \vdots & [G_n] \\ \langle e_n,x\rangle & \end{vmatrix}^{1/2}$$

An alternative expression for ε can also be obtained as

$$\varepsilon = \sqrt{[(\|x\|^2/\|g\|^2) - 1]}$$

3. Identification of System Poles and Residues to an Arbitrary Input

The problem is to find the system poles and the residues at the poles when the output y(t) of the system is known for a known input x(t). The impulse response h(t) is assumed of the form

$h(t) = \sum_{i=1}^{n} A_i \exp(s_i t)$ where h (t) is real valued and the poles are all distinct and has a negative real part. The restriction on the poles being distinct can be removed if the impulse response is chosen of the form

$h(t) = \sum_{i=1}^{q} \sum_{j=1}^{m_i} A_{ij}\, t^{j-1} \exp(s_i t)$ where $\sum_{i=1}^{q} m_i = n$. The input and the output time functions are integrated n times from t = 0 to t = T. For zero initial conditions the output can be expressed as

$y(T) = \sum_{i=1}^{n} A_i \exp(s_i T) \int_0^T \exp(-s_i \tau)\, x(\tau) d\tau$. Jain has shown [3] that the pencil set $y_1 - \lambda y_2,\ y_2 - \lambda y_3, \ldots, y_n - \lambda y_{n+1};\ x_2, x_3, \ldots, x_{n+1}$ is linearly dependent if and only if λ is one of the system poles s_i. The system poles are then obtained from the polynomial equation

$\sum_{i=1}^{n+1} Q_i\, \lambda^{n+1-i} = 0$ where Q_i are the positive square roots of the diagonal cofactors of a (2n+1) order Gram matrix G_{2n+1} defined by the set of functions $\{y_1, \ldots, y_{n+1};\ x_2, \ldots, x_{n+1}\}$. Absence of x_1 from the set implies that the procedure is valid for any non-zero input. The output y(t) can now be expressed as

$y(T) = \sum_{j=1}^{n} A_j P_j(T) \triangleq \sum_{j=1}^{n} A_j \exp(s_j T) \int_0^T \exp(-s_j \tau)\, x(\tau) d\tau$ The unknown constants A_j can be obtained from a least square procedure. The following n+1 equations can be set up as

$y_i(T) = \sum_{j=1}^{n} c_{ij} A_j, \qquad i = 1, \ldots, n+1$ where

$$c_{ij} = \begin{cases} P_j(T) & \text{for } i = 1 \\ \dfrac{P_j(T)}{(s_j)^{i-1}} - \sum_{m=1}^{i-1} \dfrac{x_{m+1}(T)}{(s_j)^{i-m}} & \text{for } i = 2, \ldots, n+1 \end{cases}$$

There are n+1 equations to solve for N unknowns. The initial output, $y_1(t)$ will be discarded since it is the noisiest measurement and use will be made only of the integrated outputs $y_2(T), \ldots, y_{n+1}(T)$.

The Integrated square error can be found as before.

Example

Input: expt (-2t) cos (t) Output: $0.5\,[\exp(-t) - \exp(-3t)]$

Data: 201 equispaced samples of a record of 3 seconds.
The true transfer function is

$$H(s) = \frac{1}{2\pi} \frac{(s - 2 - j)(s - 2 + j)}{(s + 1)(s + 2)(s + 3)}$$

A third order approximation was chosen and the result is:

$$H'(s) = \frac{.83319\ (s - 2.00099 - .998619j)(s - 2.00099 + .998619j)}{(s + .999979)(s + 1.99997)(s + 2.99949)}$$

4. Nonzero Initial State

When the initial state is not zero the output can be expressed as

$$y(T) = \sum_{i=1}^{n} \exp(s_i T) \left[a_i + A_i \int_0^T \exp(-s_i \tau)\, x(\tau) d\tau\right]$$ where a_i are related linearly to the initial state. For this case, it can be shown that the pencil set $\{y_1 - \lambda y_2, \ldots, y_n - \lambda y_{n+1}; x_2, \ldots, x_{n+1}; 1, t, \ldots t^{n-1}\}$ is linearly dependent if and only if λ is one of the system poles. The development is similar to that of the previous section except that the Gram matrix is now 3n+1 dimensionals as defined by the functions $\{y_1, \ldots, y_{n+1}; x_2, \ldots, x_{n+1}; 1, \ldots, t^{n-1}\}$.

5. Discussions

The suboptimal exponents determined noniteratively are $s_i' = s_i + \epsilon \ell_i$. Thus as the order of approximation n is increased, not only should the error decrease but the suboptimal approximation will approach the optimum. Furthermore, only n+1 new entries have to be computed for H_{n+1} when the order of approximation is increased from n to n+1, resulting in a considerable savings of time. Also, for direct computation of error a formula has been developed. The major disadvantage of this technique is to carry out the n-fold integrals. However, when the data is noisy the integrators in the above system can be replaced by FOF (First Order Filters) to enhance accuracy in the estimation procedure. The FOF has a transfer function of 1./(s+p). Secondly, realizability of FOF's are easier than ideal integrators. Thirdly, when the system poles are very close to each other the technique described in [3] becomes in error. However use of FOF in case of ideal integrators again will enhance the accuracy of this estimation procedure.

6. References

[1] M. L. Van Blaricum and R. Mittra, "A Technique for Extracting the Poles and Residues of a System Directly from its Transient Response," IEEE Trans. on Ant. and Propagat., Vol. AP-23, No. 6, November 1975.

[2] R. N. McDonough and W. H. Huggins, "Best Least-Squares Representation of Signals by Exponentials," IEEE Trans. on Automatic Control, Vol. AC-13, No. 4, August 1968.

[3] V. K. Jain, "Filter Analysis by Use of Pencil Functions: Part I," IEEE Trans. on Circuits and Systems, Vol. CAS-21, No. 5, September 1974.

[4] V. K. Jain, "Decoupled Method for Approximation of Signals by Exponentials," IEEE Trans. on Systems Science and Cybernetics, July 1970.

Commission B - Session 3

(Joint with IEEE AP-S Session 19)
Wednesday P.M. 1330 - 1630
SURFACE EFFECTS ON EM WAVES
Chairman: K. Casey, Kansas State University, Manhattan

1. SURFACE WAVES ON GENERALIZED YAGI ARRAYS: W. K. Kahn, George Washington University, Washington, D. C.

The dispersion characteristics and excitation coefficients for surface waves on uniform arrays of parasitic antennas are formulated in a way that exhibits their close connection with properties of the same antennas when used as a phased array. Analytical and numerical results are obtained for arrays of electric dipoles arbitrarily oriented with respect to the axis of the array.

The role of surface waves on Yagi arrays was clarified by Ehrenspeck and Poehler. Sengupta and Mailloux computed characteristics of surface waves on arrays of dipoles perpendicular to the array axis. This paper outlines a network formulation applicable to arrays of general elements. The surface wave characteristics are then found in terms of the active impedance of the array. In particular, the active reactance for phasing angles corresponding to a beam pointing into the "invisible region" of a closely spaced array is required.

The formulation is illustrated through application to an array of parasitic electric dipoles, the axis of the dipoles being inclined at any angle to the array axis. For such arrays an essentially closed form for the required active reactance has previously been given by Wasylkiwskyj and Kahn.

2. CAVITY RESONANCES AND MUTUAL COUPLING IN COLLECTOR ARRAYS: H. Steyskal, Polytechnic Institute of New York, Farmingdale, New York

Feed-through lens or dome antennas [1] present the problem of finding the mutual coupling between waveguides on the concave interior surface of the dome. Considering the dome as a lossless cavity (spherical or cylindrical) through which the waveguides are coupled allows an equivalent multiport network description. However, a complication with this approach are the many cavity resonances and large number of degenerate modes, since the cavity is large in wavelengths and is highly symmetric.

The scattering matrix for the network is obtained by matching the cavity and waveguide fields over the guide apertures and solving the resulting equation by the moment method. The matrix coefficients appear as the ratio of two determinants which by a series expansion can be brought into a form valid both at and off resonance.

A result obtained is the general condition that at a cavity resonance the total aperture field (for all waveguide apertures) must be orthogonal to the set of degenerate resonant cavity modes. This leads to zero coupling coefficients whenever the total number of aperture modes (for all waveguides) is less than or equal to the number of resonant modes.

[1] L. Schwartzman and J. Stangel: The Dome Antenna, Microwave Journal, Oct. 1975.

3. STUDIES OF METALLIC GRID SPATIAL FILTERS: R. J. Mailloux, Deputy for Electronic Technology (RADC), Hanscom AFB, Mass.

The use of several metallic grids arranged to achieve specified angular transmission factors is studied for the purpose of achieving antenna sidelobe suppression. In this analytical study each metallic grid is an infinite periodic array of infinitely long, zero thickness, perfectly conducting strips of width A_n (for the n'th grid). The inter-grid distance is variable but all grids have the same cell period.

Subject to the assumption of a unidirectional current, this analysis considers the arraying of N - such grids and presents computations describing the spatial filtering characteristics and mutual interaction between grids and transmission of normal and cross polarized fields for plane wave incidence.

4. EQUIVALENT SHEET IMPEDANCE OF A BONDED-MESH SCREEN ON AN ANISOTROPIC HALF-SPACE: K. F. Casey, Department of Electrical Engineering, Kansas State University, Manhattan, Kansas

Certain types of advanced composite laminates can be modeled as uniaxially anisotropic dielectrics whose optic axes are oriented normal to the laminate boundaries. In order to improve the electromagnetic shielding effectiveness of panels made of these materials, a bonded wire-mesh screen is often bonded to one surface. Since the reactive field carried by the screen is attenuated in a distance small in comparison to the panel thickness, the screen itself can be characterized by considering it to lie on an anisotropic dielectric half-space.

By incorporating appropriate charge continuity and current discontinuity conditions in the space-harmonic expansions for the currents in the screen wires, a rapidly convergent numerical solution can be obtained for these currents and thus for the equivalent sheet impedance of the screen. When the wavelength is much larger than the mesh period, the equivalent sheet impedance of the screen can be expressed as

$$\bar{\bar{Z}}_s = Z_w a \bar{\bar{I}} + \left(\frac{sa}{c}\right) \frac{\eta_o}{2\pi} \ln\left[1-e^{-2\pi r/a}\right]^{-1} \left[\bar{\bar{I}} - \left(\frac{c}{s}\right)^2 \frac{\nabla_s \nabla_s}{1 + \sqrt{\epsilon_{\ell r} \epsilon_{tr}}}\right]$$

in which a is the mesh period and r is the wire radius; Z_w is the wire impedance per unit length, s is the Laplace variable $\sigma + j\omega$, $c = 1/\sqrt{\mu_o \epsilon_o}$, and $\eta_o = \sqrt{\mu_o/\epsilon_o}$; $\bar{\bar{I}}$ is the identity operator and ∇_s the "surface" del operator and $\epsilon_{\ell r}$ and ϵ_{tr} denote the relative permittivities of the anisotropic medium in the directions normal and parallel to the boundary.

5. SCATTERING OF SURFACE WAVE BY A METALLIC STRIP ON A REACTIVE SURFACE:
T. Yoneyama, S. Nishida, Institute of Electrical Communication, Tohoku University, Sendai 980, Japan

A two dimensional scattering of surface wave by a metallic strip placed on a reactive surface is analyzed by means of a function theoretic technique. The geometry of the problem to be considered here is shown in Fig.1. The incident field is a TM surface wave travelling in the x-direction and guided by the reactive surface in the plane y=0. The surface has normalized reactance X_0 for $x<0$ and $x>\ell$ and zero reactance for $0<x<\ell$ which characterizes the metallic strip. The nonvanishing reactance is assumed to be positive and real. Our concern is to find reflection and transmission coefficients of the surface wave.

The problem is the so-called three parts mixed boundary value problem and can be formulated in terms of a simultaneous system of integral equations[1]. Jones's method of approximation is useful to solve the equations when ℓ is large compared to the wavelength [2], but no method is available for a small value of ℓ. In this summary, we describe a method of approximation for handling the integral equations regardless of a value of ℓ.

The simultaneous system of integral equations as given in literature[1] can be rewritten as follows:

$$\frac{G_n(\beta)}{K_-(\beta)} + P_1(\beta) + \varepsilon_n R_2(\beta) + A_n P_2(\beta) + \varepsilon_n A_n R_1(\beta) + \frac{\varepsilon_n}{j2\pi}\int_{\Gamma_-} \frac{K_+(\zeta)\, e^{-j\zeta\ell}}{\zeta+\beta}\, G_n(\zeta)\, d\zeta = 0, \qquad n=1,\ 2, \tag{1}$$

where

$$\varepsilon_n = \begin{cases} 1, & n=1 \\ -1, & n=2 \end{cases} \tag{2}$$

Diffinitions of the relevant functions can be found elsewhere[1] and the contour of integration Γ_- is taken along the branch cut of the function $K_+(\zeta)$ in the lower half complex plane. The parameter A_n is given by

$$A_n = R + \varepsilon_n T \exp(-j\beta_0\ell), \tag{3}$$

where R and T are the reflection and transmission coefficients of the surface wave to be determined and β_0 is the propagation constant of the surface wave. Hence, if the parameter A_n is found, calculation of the reflection and transmission coefficients is straightforward. In eq.(1), the function $G(\beta)$ is unknown, but analytic in the lower half plane and has no pole in the whole complex plane.

We can treat eq.(1) by a kind of iteration method and determine

A_n by invoking to the functional property of $G(\beta)$ as stated above. Prior to numerical computation, we must examine convergence of the iteration scheme, but this is difficult to be done analytically. We can infer numerically that the convergence of the iteration procedure is guaranteed for almost all cases of practical interest.

Solutions of the zeroth order approximation and of the first order approximation are found and the corresponding reflection and transmission coefficients are plotted in Figs.2 and 3. Both the approximations yield the results which are in a good agreement with each other for all values of ℓ. Therefore, we may say that the zeroth order approximation of the integral equations is sufficient for quick estimation of the reflection and transmission coefficients of the surface wave.

The technique described here may be applied to other three parts mixed boundary value problem, if the main concern of calculation is to find the reflection and transmission coefficients of the guided wave.

REFERENCES

[1] B. Noble, "The Wiener-Hopf Technique," Pergamon, New York (1958), Chap.V, pp.196-202.

[2] D. S. Jones, "Diffraction by a Wave-Guide of Finite Length," Proc. Camb. Philos. Soc., 48, pp.118-134(1952).

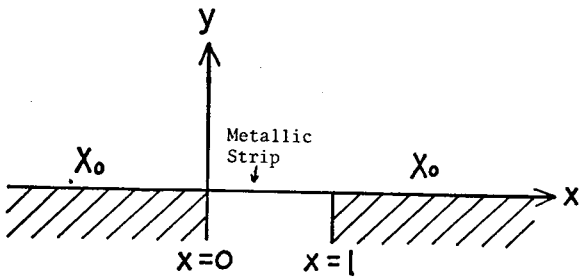

Fig.1 Geometry of the problem

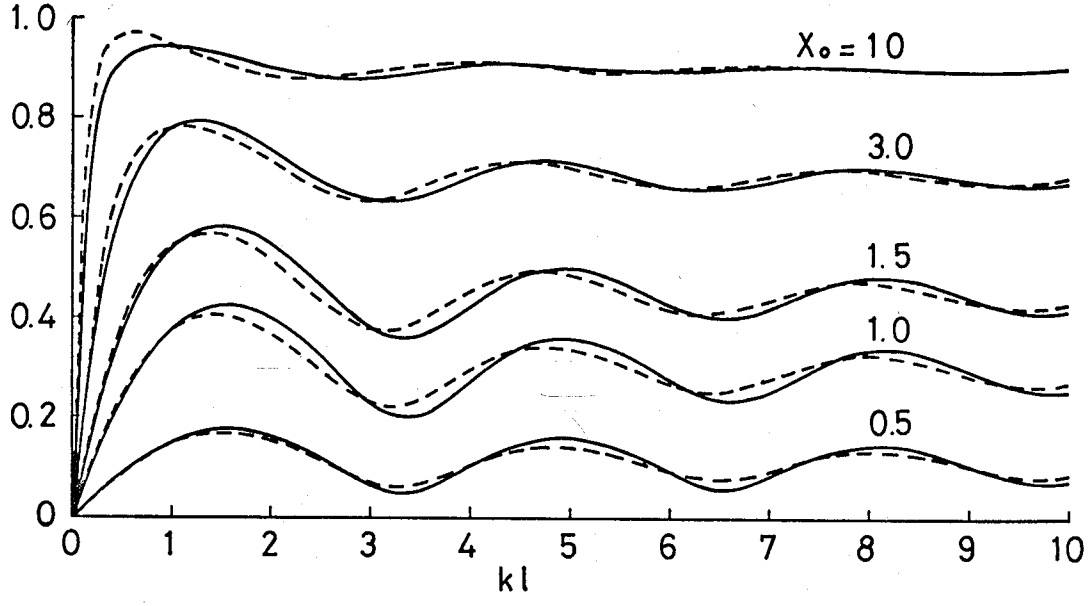

Fig.2 Magnitude of Reflection Coefficient versus Dimensionless Width of the Metallic Strip.
———— Zeroth Order, --------- First Order.

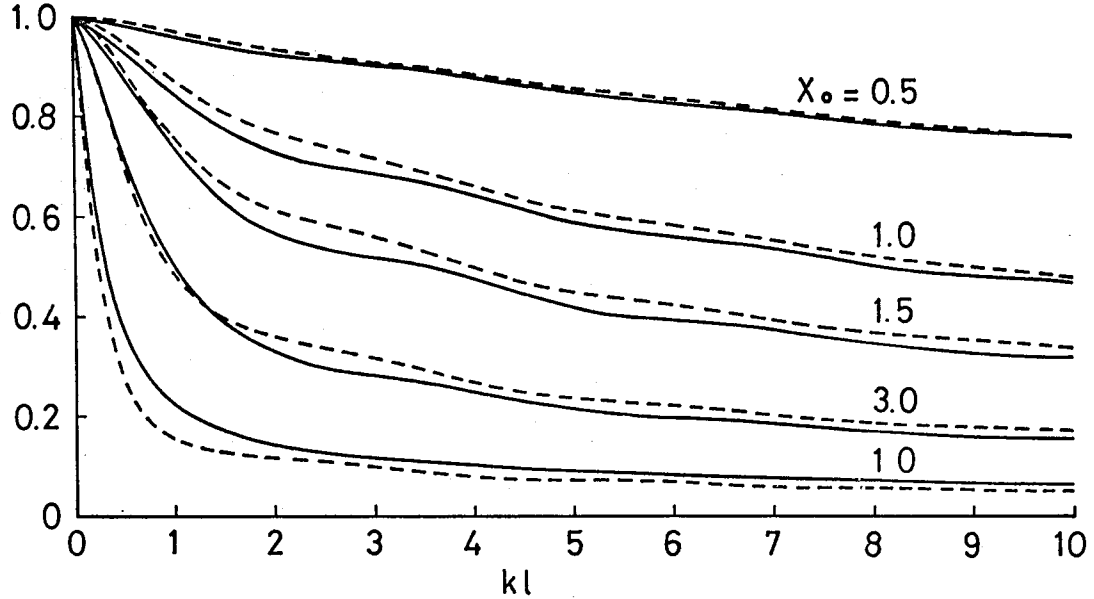

Fig.3 Magnitude of Transmission Coefficient versus Dimensionless Width of the Metallic Strip.
———— Zeroth Order, -------- First Order.

6. INTERFERENCE-FREE CONDUCTING SURFACES: E. V. Jull, J. W. Heath,
Department of Electrical Engineering, The University of British Columbia

Reflection gratings with a period $d = \lambda/(2 \sin\theta_i)$ scatter only two spectral orders in the angular range $19.5° < \theta_i < 90°$, where θ_i is the angle of incidence from the normal and λ is the wavelength (see Fig. 1). The corrugation depth h can be chosen to eliminate specular reflection, leaving only backscatter. This has already been shown for the grating profiles of Fig. 1. Here it is further investigated and the applications, in particular, of the rectangular-groove surface [1], to the reduction of electromagnetic interference from buildings and to the design of surfaces for maximum backscatter is discussed.

While different grating profiles may be used to eliminate specular reflection some have inherent limitations. Right angle triangular grooves, for example, are effective for only TM polarization (magnetic field parallel to the grooves). Sinusoidal and comb corrugations can be effective for both TM and TE (electric field parallel to the grooves) but not, in general, both simultaneously. The comb grating, for example, can eliminate specular reflection for arbitrary polarization only when $\theta_i = 59.4°$ ($d = 0.58\lambda$, $h = 0.56\lambda$). The rectangular groove grating possesses an extra variable in its aspect ratio a/d and can be made to backscatter all arbitrarily polarized energy incident in the angular range $19.5° < \theta_i < 59.4°$ [1,2,3]. For larger angles θ_i this effect can, in principle, also be achieved, but with inconveniently deep rectangular grooves. For smaller angles more than two spectral orders are scattered by corrugations with spacing $d = \lambda/(2 \sin\theta_i)$.

Within this angular range, however, elimination of specular reflection or perfect blazing for both polarizations can be amply demonstrated. Fig. 2 shows numerical and experimental results for a surface designed for this effect at $\theta_i = 45$. The numerical values are for plane wave incidence on an infinite surface of perfect conductivity. Experimental values are for 44 corrugations in a $31\lambda \times 13\lambda$ brass plate illuminated at $\lambda = 8.6$ mm. Identical transmitting and receiving horns were used at a range of 1.4 m. from the plate. Similar near perfect blazing for both polarizations and similar close agreement with predicted performance has also been demonstrated at $\theta_i = 54.5°$, 50° and 30° on plates of equal size with numbers of grooves ranging from 50 to 31. The surface tolerances required were relatively easy to achieve for the larger aspect ratios but less easy for small aspect ratios.

Interfering reflections from buildings usually occur for near grazing incidence so with the methods described here only a single polarization can be eliminated or reduced. The particular application considered is instrument landing system (ILS) interference from large hangars near airport runways. The hangar surfaces are metal and at an ILS frequency of 110 MHz about $30\lambda \times 12\lambda$. Horizontal polarization is used. The technique seems particularly applicable here and designs for fin corrugations [4,5] (wire screens) on existing hangars have been prepared. The grooves required are particularly shallow for near grazing incidence with TM polarization. Very shallow rectangular grooves formed with aluminum sandwich panels would be very appropriate for new buildings. Such surfaces with periods $d = \lambda/(\sin\theta_i)$ can also be effective; for near grazing

incidence, say $\theta_i = 80°$, the required depth h = 0.09 d with an aspect ratio of a/d = 0.333. The required number of corrugations is presently being investigated.

References

1. A. Hessel, J. Schmoys and D.Y. Tseng, "Bragg-angle blazing of diffraction gratings", J. Opt. Soc. Am., 65, 380-384 (1975).

2. J.L. Roumiguieres, D. Maystre and R. Petit, "On the efficiencies of rectangular-groove gratings", J. Opt. Soc. Am., 66, 772-775 (1976).

3. E.V. Jull, J.W. Heath and G.R. Ebbeson, "Gratings that diffract all incident energy", J. Opt. Soc. Am., 67, (in press).

4. G.R. Ebbeson, "TM-polarized electromagnetic scattering from fin-corrugated periodic surfaces", J. Opt. Soc. Am., 66, 1363-1367, (1976).

5. E.V. Jull and G.R. Ebbeson, "The reduction of interference from large reflecting surfaces", IEEE Trans. AP-25, (in press).

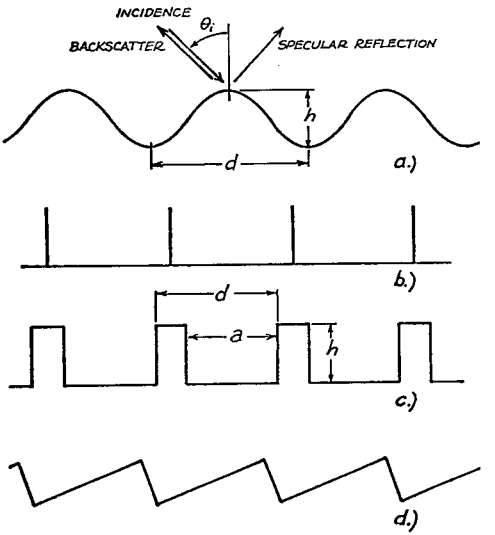

Fig. 1 Surface profiles: a) sinusoidal b) comb c) rectangular d) right angle triangular

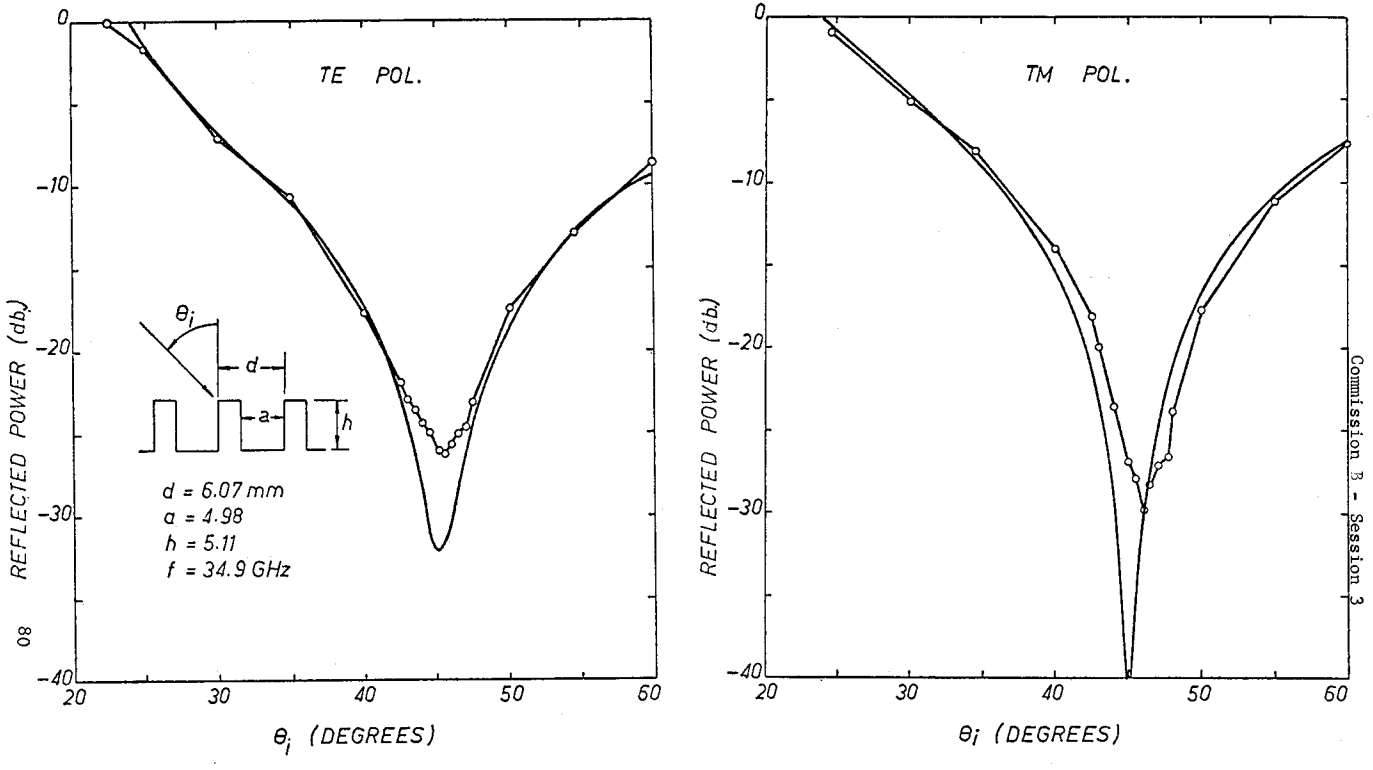

Fig. 2 Reduction of specular reflection from a rectangular groove surface blazed for $\theta_1 = 45°$ ——— calculated. ——o——o—— measured for 44 grooves at $\lambda = 8.6$ mm.

7. FREQUENCY SELECTIVE SURFACES: T. W. Leonard, L. R. Young, Harris Corporation, Electronic Systems Division, Melbourne, Florida

Frequency selective surfaces (FSS) have applications in antennas covering several frequency bands simultaneously. These surfaces are usually used between a reflector antenna and its focal point to almost completely reflect one frequency band to another focal point, and to pass another frequency band with low loss. Most applications of the FSS have been with two frequency bands separated by several octaves and at angles of incidence less than about 45°. A simple array of resonant crossed-dipoles is usually used for such applications. When more complex responses are required, an array of crossed-dipoles is not sufficient. By using multiple layers of capacitive sheets (an array of thin conducting rectangles), a wide variety of reflectance and transmittance responses may be obtained and easily predicted analytically. An FSS of this design can be used to diplex two or more bands closely spaced in frequency with equal E and H cut-offs and low cross-polarization, over angles of incidence over 65° from normal incidence.

Consider an antenna required to operate simultaneously over the five frequency bands shown in Figure 1. The total bandwidth (2.7 to 16 GHz) is too large to be covered by a single high efficiency feed. However, it is conceivable that two high-efficiency broadband feeds could be used, one covering the two low bands, and another covering the three high bands. The particular application in this case is an offset parabolic reflector. By placing the FSS at the position indicated in Figure 2, the frequency bands can be diplexed to the proper feed with low loss. The FSS giving the response of Figure 1 is made of four sheets of copper clad mylar etched to form a grid of rectangles. This type of sheet is essentially a lumped element capacitor, so long as the period of the grid is small in terms of wavelength. The reflectance and transmittance of single sheets of capacitive strips and grids are given in the references (1,2,3). The effect of using several of these sheets separated by low dielectric constant polystyrene foam is identical to placing capacitors along a transmission line. The response of several sheets is easily calculated by writing an S-parameter matrix for each sheet, converting these to T-parameter matrices taking into account the spacing between sheets, multiplying the T-parameter matrices together, and converting the

resulting matrix back to an S-parameter matrix. This procedure yields the calculated values appearing in Figure 1.

For angles other than normal incidence, Saleh and Simplak[4] suggested stretching the squares to rectangles so that the projected area appears as a square from the direction of the incident wave. However, to obtain equal E and H plane responses, the gap between the rectangles should also be widened so that the grid appears perfectly symmetric from the vantage point, as shown in Figure 3[5]. For a multi-layer FSS, the spacing between sheets should be increased as $1/\cos\theta$, where θ is the incidence angle, for equal E and H plane responses. The measured E and H plane cut-offs are virtually identical for angles as large as 65^{o} from normal incidence. If the maximum dimension of the rectangles should become approximately $\lambda/2$, the response will begin to break up, but this problem can be eliminated by simply halving the size of the rectangles and placing two sheets back-to-back (for this case, alignment of the sheets is critical). Because the sheet appears symmetric, it generates low cross-polarized components (>25 dB down for the FSS of Figure 1 at angles of incidence $>40^{o}$). Figure 4 shows an FSS designed for the Advanced Microwave Radiometer Feed System developed on NASA contract NAS5-22889. This FSS is designed for a spherical incident wave similar to the configuration in Figure 2, so the squares are stretched to rectangles in two directions towards the reflector edges, as shown in Figure 5. Preliminary far field patterns indicate losses less than 0.75 dB at the four lower frequency bands shown in Figure 1. Final test data will be presented.

For more complicated responses, more sheets may be added, but the phase shift of the FSS changes rapidly when sharper cut-offs and more sheets are used. Inductive sheets can also be used to obtain varied responses. By putting an inductive and a capacitive sheet back-to-back, parallel resonant band-pass filters have been constructed.

References

1. N. Marcuvitz, Waveguide Handbook, Mit Rad. Lab., Vol. 10, 1951; p. 280-285.

2. J. A. Arnaud and F. A. Pelow, "Resonant-Grid Quasi-Optical Diplexers", BSTJ, Vol. 54, No. 2, Feb. 1975, p. 263-283.

3. I. Anderson, "On the Theory of Self-Resonant Grids", BSJT, Vol. 54, No. 10, Dec. 1975; p. 1725-1731.

References (Continued)

4. A. A. M. Saleh and R. A. Semplak, "A Quasi-Optical Polarization Independent Diplexer for Use in the Beam Feed System of Millimeter Wave Antennas", IEEE Trans. Ant. Prop., Vol. AP-24, Nov. 1976; p. 780-785.

5. L. R. Young and W. P. Blackwood, Microwave Radiometer Antenna Feed System, Design Study Report for Goddard Space Flight Center, Contract NAS5-22889 August 1976; p. 4-4.

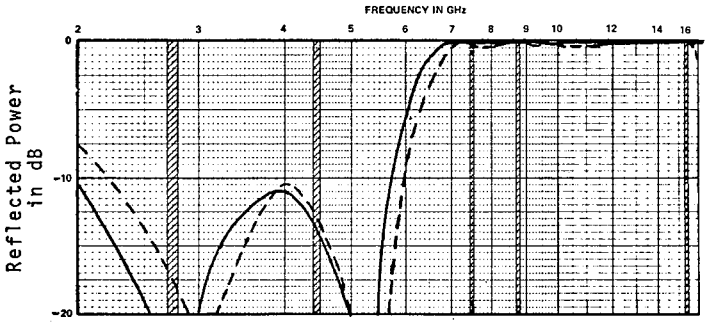

Figure 1 - Four layer FSS response and desired oeprating bands (shaded). ____ Measured at 26.5° incidence angle, --- calculated. The E and H plane responses are virtually identical. The sheets were spaced 0.425 inches apart.

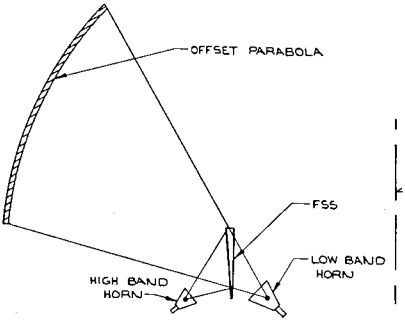

Figure 2 - Offset reflector geometry showing position of the FSS.

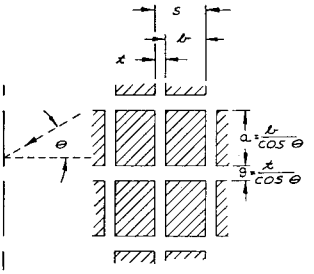

Figure 3 - Rectangle geometry for equal E and H plane responses.

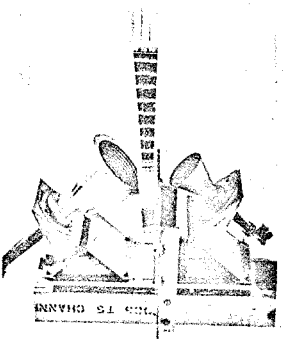

Figure 4 - The FSS for the Advanced Microwave Radiometer Feed System.

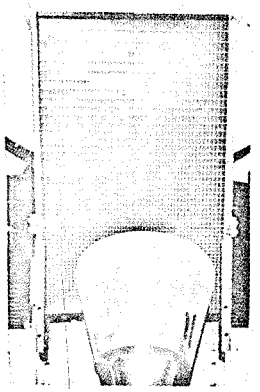

Figure 5 - The copper grid is stretched in two dimensions for illumination by a spherical wave front.

8. ANALYSIS OF FREQUENCY SELECTIVE SURFACES PRINTED ON DIELECTRIC SHEET:
V. D. Agrawal, W. A. Imbriale, TRW Defense and Space Systems Group, Redondo Beach, Calif.

INTRODUCTION

Frequency selective surfaces have found widespread applications in microwave antennas [1] and optics [2]. For circular polarization, one popular design is a planar array of crossed dipoles. This array becomes reflective near the dipole resonance frequency and is almost transparent at lower frequencies. In practice, these surfaces are often constructed by printing metal dipoles on a supporting dielectric sheet. The exact reflection and transmission characteristics, therefore, depend upon the length, width and spacing of dipoles, and the dielectric constant and thickness of the sheet. With so many parameters to control in a design, it is desirable to have an analytical solution. This paper describes the application of Floquet mode theory to frequency selective surfaces of crossed dipoles printed on a dielectric sheet.

ANALYSIS

Our analysis closely follows those of Chen [3] and Montgomery [4]. The surface, whose geometry is shown in Figure 1, is assumed to be infinite in the xy-plane. Several general cases have been considered by Chen [5] in an unpublished work. Periodicity allows us to expand the fields in terms of Floquet modes. The incident field is also represented as a series of these modes. Upon matching the boundary conditions at z = 0 and z = T, an integral equation in the unknown dipole current, $\vec{J}(x,y)$, is obtained. We next approximate the dipole current by orthonormal functions, $\vec{h}_n(x,y)$:

$$\vec{J}(x,y) = \sum_{n=1}^{N} c_n \vec{h}_n(x,y) \quad . \tag{1}$$

Now the integral equation reduces to a linear system of equations which can be readily solved for the coefficients, c_n. Once this is done, the final expressions for reflection and transmission coefficients follow easily. Omitting the details [4], the reflection coefficient can be written as,

$$R_m(\theta) = R_m^D(\theta) - \frac{1}{d^2 \, n_{m00}^{eq}} \sum_{n=1}^{N} c_n \vec{g}_n(\theta) . \vec{\kappa}_{m00} \tag{2}$$

where $\vec{g}_n(\theta) = \int \vec{h}_n(x,y) \exp(j\vec{k}_{00} . \vec{r}) \, dx \, dy$

the integral being performed over the surface of a cross dipole. Plane of reflection is the xy-plane and θ is the angle of incidence. Expressions for the TM and TE waves, as shown in Figure 1(A),

correspond to m = 1 and 2, respectively. $R_m^D(\theta)$ is the reflection coefficient of dielectric sheet and η_{m00}^{eq} is a complex addmittance; expressions for these may be found in [4]. Other quantities are defined below:

$$d = \text{Array spacing}$$

$$\vec{r} = x\hat{x} + y\hat{y}$$

$$\vec{k}_{pq} = \left(\frac{2\pi}{\lambda_0}\sin\theta + \frac{\sqrt{2}\pi p}{d}\right)\hat{x} + \left(\frac{\sqrt{2}\pi p}{d} + \frac{2\sqrt{2}\pi q}{d}\right)\hat{y}, p,q = 0,\pm1,\pm2\ldots$$

$$\vec{\kappa}_{1pq} = \vec{k}_{pq}/|\vec{k}_{pq}|,\ \vec{\kappa}_{2pq} = \hat{z} \times \vec{\kappa}_{1pq}.$$

Equation (2) considers only the zero-order Floquet mode (p = q = 0) since in a suitable design by using a small array spacing, the higher order Floquet modes, which correspond to the grating lobes, are made evanescent and hence they do not contribute to the far field. However, in the computation of c_n, higher order modes must be included since they are necessary for satisfying the boundary conditions. Expression for transmission coefficient is obtained in an identical manner [4]. Since the problem is solved for two orthogonal linear polarizations, any arbitrary polarization can also be treated.

NUMERICAL COMPUTATION

A computer program was written for calculating the reflection coefficient, using a Fourier expansion in Eq. (1). Computed reflection coefficient for L = 0.97cm, d = 0.92cm, and W = 40mil, is shown in Figure 2. Figure 2(A) assumes an absence of the dielectric (ε_r=1, T=0) and Fig. 2(B) is with a sheet of dielectric constant, ε_r = 4.25, and thickness, T = 5mil. It was found that a three-term expansion of current on each dipole was sufficient. Thus for the cross dipole at origin, we have

$$\vec{h}_1 = \hat{y}\sqrt{\frac{2}{WL}}\cos(\pi y/L),\ \vec{h}_2 = \hat{y}\sqrt{\frac{2}{WL}}\sin(2\pi y/L),\ \vec{h}_3 = \hat{y}\sqrt{\frac{2}{WL}}\cos(3\pi y/L)$$

$$\vec{h}_4 = \hat{x}\sqrt{\frac{2}{WL}}\cos(\pi x/L),\ \vec{h}_5 = \hat{x}\sqrt{\frac{2}{WL}}\sin(2\pi x/L),\ \vec{h}_6 = \hat{x}\sqrt{\frac{2}{WL}}\cos(3\pi x/L)$$

In addition, Floquet modes $|p|, |q| \leq 2$ were sufficient for a numerical convergence. A major influence of the dielectric sheet appears to be in lowering the resonance frequency at which the surface becomes a perfect reflector.

EXPERIMENTAL RESULTS AND DISCUSSION

An experimental frequency selective surface, as shown in Figure 1(B), was constructed by printing copper dipoles on a kapton sheet ($\varepsilon_r \approx 4.25$). Results of measurements, whose details may be found elsewhere [6], are given in Figure 2(C) and show a close agreement with the theoretical results of Figure 2(B). There is, however, a slight difference in the resonance frequency which may be attributed to the fact that the dipoles in the experimental surface had rounded ends, effectively making them a little longer. Also, the dielectric constant of the sheet at 10-18 GHz band was

only approximately known.

CONCLUSION

The Floquet mode theory as applied above is shown to predict the performance of a practical frequency selective surface. The importance of this analysis lies in the fact that even a thin dielectric sheet (5mil in Figure 2) has a significant effect on the performance.

REFERENCES

[1] V. D. Agrawal and W. A. Imbriale, "Experimental and Theoretical Design of a Dichroic Surface for a Spacecraft Antenna," Int. AP-S Symp., Amherst, Mass., October 1976.

[2] J. A. Arnaud and F. A. Pelow, "Resonant-Grid Quasi-Optical Diplexers," B.S.T.J., Vol. 54, pp. 263-283, February 1975.

[3] C. C. Chen, "Scattering by a Two-Dimensional Periodic Array of Conducting Plates," Trans. IEEE Ant. Prop., Vol. AP-18, pp. 660-665, September 1970.

[4] J. P. Montgomery, "Scattering by an Infinite Periodic Array of Thin Conductors on a Dielectric Sheet," Trans. IEEE Ant. Prop., Vol. AP-23, pp. 70-75, January 1975.

[5] C. C. Chen, Private communication.

[6] V. D. Agrawal and W. A. Imbriale, "Dichroic Subreflector," IR&D Final Report No. 76-7323.A.4-72, TRW Defense & Space Systems Group, Redondo Beach, Ca., September 1976.

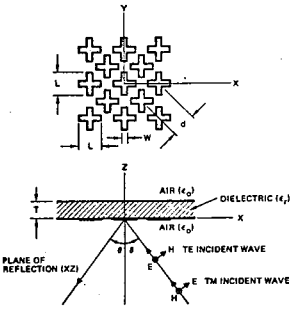

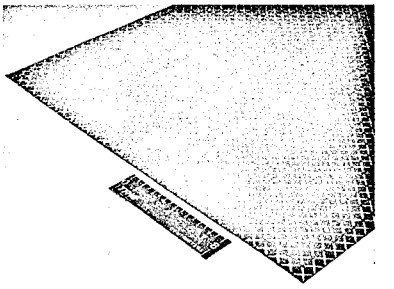

FIG. 1(A) GEOMETRY OF REFLECTION FIG. 1(B) EXPERIMENTAL SURFACE

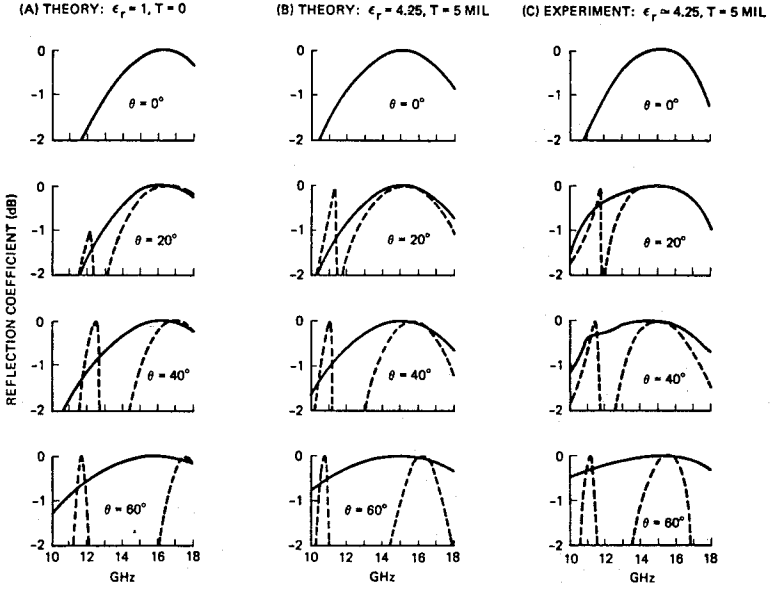

FIG. 2 COMPUTED AND MEASURED REFLECTION COEFFICIENT
L = 0.97cm, d = 0.92cm, W = 40mil, — TE, --- TM

Commission E - Session 1

Wednesday P.M. 1330 - 1630
MAN-MADE RADIO NOISE AND INTERFERENCE
Chairman: George Hagn, Stanford Research Institue, Washington D.C.

1. LARGE AMPLITUDE ULF ELECTROMAGNETIC FIELDS FROM BART: A.C. Fraser-Smith and D.B. Coates, Radioscience Laboratory, Stanford Electronics Laboratories, Stanford University, Stanford, California 94305

Starting in 1973, persistent large-amplitude magnetic signals began to be observed in recordings of ultra-low-frequency (ULF; frequencies less than 5 Hz) geomagnetic field fluctuations made on the Stanford campus. The energy of these ULF signals is concentrated predominantly at frequencies below about 0.3 Hz and the signals are observed with greatest amplitude during daylight hours (although they occur continuously throughout the 20 hr. interval 0500-0100 LT). With the exception of a few weeks before Christmas, when they are also observed on Saturday, the signals appear only on weekdays. The amplitude of these obviously man-made signals has increased since 1973 and has now reached a level at Stanford that is about ten times greater than the normal natural background level of geomagnetic activity, i.e., it is comparable to the level observed during great geomagnetic storms. ULF magnetic field measurements at additional locations away from the Stanford campus have enabled us to identify the San Francisco Bay Area Rapid Transit (BART) system as the source of these magnetic fields. Power for the BART trains is provided by a 1000 V DC third rail and it appears that the entire system constitutes a large ULF "antenna." Similar systems planned or already in operation in other parts of the U.S. (e.g., the Washington, D.C., Metro) will probably also produce similar large-amplitude ULF electromagnetic fields.

2. SPECTRAL PROPERTIES OF MAN-MADE RADIO NOISE: W.R. Vincent, EMTEL Division, DEVELCO, INC., Sunnyvale, CA 94086

Man-made radio noise in the HF, VHF, and UHF parts of the radio spectrum have been observed over a period of several years with a scanning receiver and a 3-axis CRT display. The 3-axis views (axis of frequency, time, and amplitude) of noise structure have been used to identify and classify several categories of man-made noise, and many 3-axis views have been associated with sources such as auto ignition noise, power-line noise, high power SCR radiation, industrial machines and processes, rapid transit systems and natural atmospheric noise. Most noise signatures have been found to be relatively narrow in spectral bandwidth, suggesting that wide bandwidth models for man-made noise apply only to limited situations.

3. ON PARAMETERS AND STANDARDS FOR ELECTROMAGNETIC INTERFERENCE MEASUREMENTS: C.P. Tou, Department of Electrical Engineering, Nova Scotia Technical College, Halifax, Nova Scotia, Canada

The control of electromagnetic interference (EMI) and the achievement of electromagnetic compatibility (EMC) cannot be successful without establishing adequate interference specification limits and practical data base for predicting the performance of communication systems. Again, meaningful specification limits and data base cannot be established unless measurement parameters, measurement methods, and instrumentation for the measurement are standardized. However, EMI occurs in various forms which are generally difficult to specify and measure. It has been a very difficult area to achieve standardization due to these technical considerations and due to different concerns of many interest groups.

The measurement of EMI may be carried out using one of the following approaches: (a) frequency domain, (b) time domain, or (c) amplitude domain, depending on the nature of the interference. Which parameters of EMI should be measured, i.e. peak value, quasi-peak value, average value, rms value, or amplitude probability distribution (APD), depends upon the objectives of the measurement and the characteristics of the interference. Different objectives require measurement of different parameters.

This paper deals with the rationale of establishing interference specification limits and parameters for measurements based on the results of a study of EMI problems carried out for the Department of Communications of Canada. In this study it has been shown that radio standards and specification limits for intentional emitters should be set based on frequency segment, type of modulation, type of service, background noise level, and technical considerations. On the other hand, specification limits for incidental emissions should be set based on frequency segment, type of noise, and technical considerations, but not on types of devices or systems.

It is believed that the results of the study should be of interest to those involved in the control of interference environments, in EMC work, and in the writing of standards for the measurement of electromagnetic interference.

4. STANDARD METHODS OF MEASUREMENT FOR IMPULSIVE RADIO NOISE: Neal H. Shepherd, Mobile Radio Products Department, General Electric Company, Lynchburg, Virginia

The peak method was the first developed for the measurement of impulsive radio noise. Although the peak method remains as a standard for a number of trade and governmental organizations, others believe that the impulse rate of noise has a significant influence on interference and should be included as part of noise measurement standards.

The quasi-peak method of measurement was thus developed based on subjective approach to the development of RC time constant circuits. At least five standard meter responses have been developed as the result of experiments operating independently.

In spite of claims by proponents of both the peak and quasi-peak methods of measuring impulsive noise, most communicators recognized a need for an improved method. The noise amplitude distribution (NAD) was developed as the first improved method for determining degradation of receiver performance.

This paper describes a standard, prepared by the IEC, for the measurement of impulsive noise immunity and the NAD overlay method for determining degradation of performance of receivers due to impulsive type noise.

5. DEGRADING EFFECTS OF IGNITION NOISE: Jules Deitz, Federal Communications Commission

In recent years, some attention has been directed to the degrading effects of automotive ignition radiation on the reception of land mobile signals. Other radio services are also susceptible. However, quality of reception in the land mobile service is particularly susceptible to this source of degradation because mobile units are often in close proximity to groups of motor vehicles.

The adequacy of the present automobile industry voluntary standards for suppression of ignition radiation has been examined and the results have been widely circulated for comment. See FCC Docket No. 20654.

There appears to be several viewpoints and some of them have generated specific issues:

1. The automobile industry appears to feel secure in their view that the SAE J551 (d) voluntary standard is adequate to "minimize serious interference to radio communications". This gives rise to several questions such as (a) What does "minimize" mean? (b) What does "serious" mean? What is the significance of the interference caused by a single vehicle in judging the cumulative effect of many vehicles as is commonly experienced in real life traffic patterns?

2. Since considerable degradation is found in real life situations, why? (a) Is it because vehicle owners rip out the suppression fixes built in at the factory? (b) If the fixes are ripped out, why are they ripped out?

3. If, like motherhood, improvement in ignition radiation suppression is certainly worthwhile, why then the impasse? (a) Is it because the automotive industry cannot agree that there is a need? (b) Or is it because there is a dearth of ideas on how to do better? (c) Or is it all a matter of cost feasibility?

These are key questions that need answers if a true understanding is ever to come to pass. There is no need to go into the history of SAE and CISPR. All the past is well documented and shows substantial effort over a long period of time. However, conditions keep changing and the time for reevaluation is now. Today, there are many millions of susceptible mobile receivers - not thousands.

Apparently there is not yet universal acceptance that the paramount question is: Who can do a better job in the suppression of ignition radiation, keeping in mind cost feasibility? In order to assist in legitimizing this question there is a current effort to further investigate item 2(a), above. The results of this effort will be reported at the Symposium in June. The comments submitted in Docket 20654 will also be reviewed.

6. TELEVISION RECEIVER SUSCEPTIBILITY TO BROADBAND NOISE: John A. Malack, IBM Corporation, Endicott, NY 13760

Television receivers are designed to respond to intelligence bearing rf signals of specified characteristics and levels to provide for satisfactory viewing. Incidental to the desired signals, there may also be noise signals present to subjectively compromise the quality of the received picture.

This paper discusses the interference relationship in the video response of commercial TV receivers due to periodic broadband noise of various pulse repetition rates for a FCC Grade A TV signal. TV broadband susceptibility levels are presented for the VHF TV service in terms of peak and CISPR quasi-peak detector instrumentations. The basic effects of background lighting, observer viewing distance, and type of receiver (color or black and white) are also presented.

The results may be used to derive TV protection ratios for broadband noise in the development of radiated noise limits to protect the TV service.

Commission F - Session 1

Wednesday P.M. 1330 - 1630
CLEAR-AIR DOPPLER RADAR STUDIES OF THE TROPOSPHERE AND STRATOSPHERE
Chairman: Dr. Thomas E. VanZandt, Aeronomy Laboratory, NOAA, Boulder, Colo.

1. TROPOPAUSE MEASUREMENTS USING FORWARD-SCATTER CW RADAR: W.P. Birkemeier and K.S. Gage*, University of Wisconsin, Madison, WI 63706
*Present affiliation: NOAA/ERL, Aeronomy Laboratory, Boulder, CO 80302

The results of a high altitude probing experiment are presented which demonstrate the capability of measuring atmospheric stability at tropopause altitudes using a 1 GHz bistatic CW radar system. Vertical profiles of the potential temperature gradient measured by radiosondes launched under the common volume of the radar systems are well correlated with profiles of received power from radar data taken nearly simultaneously. The tropopause can be located within a few hundred meters and its stability structure can be observed as it evolves.

2. MEASUREMENTS OF STRATOSPHERIC DYNAMICS:
D. A. Fleisch and W. E. Gordon, Rice University, Houston, TX 77001

Doppler radar wind measurements over the Jicamarca Radio Observatory are interpreted as the three vector components of the stratospheric wind and its fluctuations. Observations are available for a continuous 48-hour period in early January 1977 for the 12-39 kilometer altitude range. The data have resolutions of 3 km in height, 1/4 second in time, and better than 20 cm/sec in line-of-sight speed. The vector components are derived from three beams: one is pointed in the vertical, the others are pointed ~ 3.5 degrees off-vertical in the west and south directions. The paper discusses the observed wind profiles, mixing parameters, and the scattering mechanism.

3. ATMOSPHERIC ECHOES BETWEEN 30 AND 60 KM WITH THE JICAMARCA RADAR:
B.B. Balsley, NOAA, Boulder, CO 80302, D. T. Farley and C. La Hoze Cornell University, Ithaca, NY 14853, and R. F. Woodman, Max Planck, Institute for Aeronomy, Lindau, German Federal Republic

The 30-60 km height range of the tropical atmosphere has been shown to be all but inaccessible to high powered, ultrasensitive radar systems (Woodman and Guillen, 1974) [1]. The present contribution examines this region with somewhat more sensitive techniques in an attempt to better delineate the boundaries of inaccessibility.

[1] R. F. Woodman and A. Guillen, J. Atmos. Sci. 31, 2, 493-505, March 1974.

4. STRATOSPHERIC INVESTIGATIONS AT ARECIBO, PUERTO RICO: B.B. Balsley, NOAA/ERL, Aeronomy Laboratory, Boulder, CO 80302, D. T. Farley, Cornell University, Ithaca, NY 14853, and R. M. Harper, Arecibo Observatory, PR 00612

The high powered radar at the Arecibo Radio Observatory has been used in recent months to examine clear air echoes in the stratosphere. Spectral data from these experiments are discussed in detail. Advantages and limitations of the Arecibo radar as a tool for examining the lower atmosphere are outlined and the potential for future studies is discussed.

5. APPLICATION OF THE CHATANIKA RADAR FOR ARCTIC WIND MEASUREMENTS: N. Cianos and M. Baron, Stanford Research Institute, Menlo Park, CA 94025, B. B. Balsley, NOAA/ERL, Aeronomy Laboratory, Boulder, CO 80302, and D. T. Farley, Cornell University, Ithaca, NY 14853

Results of a recent series of experiments at the Chatanika, Alaska, radar facility show that the radar has great promise as a tool for investigating neutral atmosphere dynamics in the height range 2-25 km. Excellent agreement is obtained between radar-derived wind profiles and concurrent profiles obtained by conventional rawinsonde techniques. Additional data indicate that the radar can also measure vertical winds, turbulence parameters, and neutral atmospheric structure on scales of a few km.

6. SOUNDING OF THE LOWER ATMOSPHERE WITH A PORTABLE, 50 MHz, COHERENT RADAR: W. L. Ecklund and D. A. Carter, NOAA, Boulder, CO 80302

During October 1976 a portable 50 MHz Doppler radar system was temporarily installed at Poker Flat, Alaska. One purpose of this installation was to test the feasibility of using a portable radar to observe refractive index fluctuations in the troposphere and lower stratosphere. The Poker Flat radar used a simple, inexpensive 5000 m^2 array of 640 coaxial-collinear dipoles. In this experiment the antenna beam was fixed at 143° azimuth and 65° elevation. The half-power beamwidth was 2° in azimuth and 4° in elevation. The portable transmitter had a peak pulse power of 15 kW and was used to generate 5 or 10 μs pulses at repetition rates of 2 to 8 kHz. An on-line minicomputer was used to coherently integrate the returned signals and to perform the spectral analysis and spectral averaging. Even though the system sensitivity was degraded rather severely by suspected narrow-band interference during the experimental period, observations could usually be made to 8 km altitude using 5 μs pulses. On several days wind data were obtained from balloons launched at Poker Flat, and a comparison with concurrent velocities derived from the 50 MHz radar shows good agreement.

7. SPATIAL AND TEMPORAL VARIATIONS OF REFLECTIVITY MEASURED BY THE SUNSET RADAR: J. L. Green, T. E. VanZandt, J. M. Warnock, and W. L. Clark, NOAA, Boulder, CO 80302

The Sunset VHF Radar, located near Boulder, Colorado is a large Doppler radar that is used to study winds, waves and turbulence in the clear air of the troposphere and lower stratosphere. Variations of radar reflectivity have been observed with height resolutions as small as 150 m and time resolutions as low as 2 seconds. Variations of reflectivity at a fixed height as large as a factor of four in three minutes or a factor of 25 in five hours have been observed. The spatial and temporal structure of the reflectivity and its implications for turbulent structure will be discussed.

8. COMPARISON OF CALCULATED AND OBSERVED CLEAR AIR ATMOSPHERIC REFLECTIVITY: K. S. Gage, NOAA/ERL, Aeronomy Laboratory, Boulder, CO 80302

A theory has been developed to related clear air reflectivity (or alternatively, C_n^2) to measurable mean atmospheric fields of humidity, temperature and wind. This theory builds upon the work of Tatarski and takes into account the effect of the intermittent layered structure of small-scale inertial subrange turbulence in the stably stratified atmosphere. Wind gradients are used to evaluate the probability of a layer being turbulent (or alternatively, the fraction of a volume of the atmosphere which is turbulent). Vertical profiles of C_n^2 calculated according to the theory using ordinary rawinsonde data are in good agreement with nearly simultaneous radar observations. Comparisons will be presented utilizing the 40 MHz Sunset Radar near Boulder, Colorado, the 1295 MHz Chatanika Radar, and a portable 50 MHz radar, both near Fairbanks, Alaska.

Since the modified theory successfully predicts the magnitude of C_n^2 and its height variation for these radars, it is concluded that the stably stratified atmosphere is intermittently turbulent and that turbulent regions do satisfy the Kolmogoroff inertial subrange model at least over the length scales ranging from 10 centimeters to a few meters. These radars can therefore be used to study the structure and dynamics of atmospheric turbulence.

Commission F - Session 2

Wednesday P.M. 1330 - 1650
RADIO OCEANOGRAPHY
Chairman: K.R. Carver, Physical Science Lab., New Mexico State University

1. MODULATION OF COHERENT MICROWAVE BACKSCATTER BY SHOALING WAVES: W. J. Plant, W. C. Keller, and J. W. Wright, Ocean Sciences Division, Naval Research Laboratory, Washington, D.C. 20375

The orbital speed of long waves and the modulation of short, wind-generated waves by the long waves was obtained from the frequency and amplitude modulations, respectively, of the back-scattered signal of a coherent, CW, 9.375 GHz radar operated from the end of a pier on the Outer Banks of North Carolina. Modulations anomalously large compared to those predicted by the relaxation-time model (Keller and Wright, 1975) were observed in a restricted range of windspeeds near the shallow water wave speed. The model otherwise satisfactorily accounted for the measurements. The phase of the modulation places the maximum amplitude of the short waves near, and generally leeward of, the crests of the long waves for wind speeds up to 8 m sec^{-1}, the highest encountered in the experiment.

2. RADIOMETRIC SIGNATURE OF OCEAN FOAM AT MICROWAVE FREQUENCIES: Lawrence A. Klein, Joint Institute for Advancement of Flight Sciences, The George Washington University, NASA Langley Research Center, Hampton, VA

Experimental results are presented showing the measured increase in brightness temperature which occurs when foam is generated on the surface of salt water solutions. An increase in brightness temperature with increasing foam coverage is observed at C-, X-, and K-band microwave frequencies. The increase in temperature is more pronounced at horizontal polarization than at vertical. At 90% foam coverage, the X-band data show an increase in brightness temperature of approximately 150 K at a 10 degree viewing angle, as compared with the no foam case, and 60 K at a 60 degree viewing angle for vertical polarization. With the antenna horizontally polarized, the increase in brightness temperature is 160 K and 110 K for the corresponding conditions. These results indicate that foam has an emissivity of about 0.8 - 0.9. At 20% foam coverage, the increase in brightness temperature is 30 K at the 10 degree viewing angle and 20 K at 60 degrees for vertical polarization. The horizontally polarized results show an increase of 60 K at 10 degrees and 40 K at 60 degrees viewing angle.

3. A MONTE CARLO SIMULATION OF OCEAN WAVE SENSING USING A SHORT PULSE RADAR: D. M. LeVine, Goddard Space Flight Center, L. D. Davisson, University of Maryland, and R. L. Kutz, Goddard Space Flight Center

A Monte Carlo simulation has been developed for the scattering of short pulses from stochastic surfaces; and the simulation is currently being used to study the ocean wave sensing potential of a radar which scatters short pulses at small off-nadir angles. In the simulation a power spectrum for the surface heights is assumed to create a random surface and the signal scattered back to the radar is computed for each realization of the surface

using a physical optics analysis which takes wavefront curvature and finite radar-to-surface distance into account. It has been shown, using a Pierson-Moskovitz spectrum), an observation which is supported by experiments. Analysis suggests that at small nadir angles, wave information is also contained in the spectrum of scattered power, and the simulation is being used to verify this hypothesis.

4. REMOTE SENSING OF TWO-SCALE OCEAN WAVE SYSTEMS USING A DUAL-FREQUENCY RADAR: D. L. Schuler, Naval Research Laboratory

The modulation of 1.5 centimeter waves induced by 2 to 15 meter gravity waves has been observed using a coherent, dual-frequency X-band radar. This modulation appears as a narrow, Doppler-shifted, resonance peak in the product power spectrum of the backscattered returns. The dispersion relation (for both deep and shallow water) of the modulation pattern matches that of gravity waves. Modulation amplitude spectra have been experimentally obtained which, after sufficient averaging, closely resemble directional gravity wave spectra simultaneously obtained from capacitance wave probe and Sea Photo Analysis measurements. Stepped frequency modulation spectra have been completed in much shorter time periods. The presence of almost stationary sea/wind conditions for these rapidly acquired spectra reduces the necessity for averaging to a minimum. Strong modulations have been measured over a wide range of grazing angles and azimuth angles off of the wind direction. The radar is simultaneously able to measure gravity waves propagating upwind or downwind and is capable of measuring small surface currents superimposed on the gravity wave motion.

Gravity-capillary wave interactions may be studied because of the radar's unique ability to measure the Doppler spectrum of both gravity and capillary waves from the same data. In fact, the maximum modulation peak/background ratios were obtained by selective filtering out the Doppler returns from all but the fastest scatterers. In our low angle studies, these fast scatterers corresponded to strained capillary waves bound near the gravity wave crests. Most features of the experimental data have been interpreted in terms of composite surface scattering theory and the straining of wind-generated waves.

Preliminary results of studies using a dual-frequency, pulsed, L-band radar which senses longer waves through Bragg resonance with short-gravity waves will also be presented.

5. SYNTHETIC APERTURE HF OBSERVATIONS OF FETCH-LIMITED 7 SECOND OCEAN WAVES: Calvin C. Teague, Center for Radar Astronomy, Stanford University

During the first four months of 1976, an experiment was performed at Galveston, Texas, by workers from Stanford University and Scripps Institution of Oceanography in which the directional growth of 7-second ocean surface waves under fetch-limited conditions was measured with HF resonant scatter techniques. Most of the data were obtained just

after polar frontal passages, when the wind was offshore from the north, nearly perpendicular to the long, straight coastline which extends for several hundred kilometers. The growth of wave energy with distance was nearly exponential over about 2.5 orders of magnitude, with observed rates of 0.9%/ocean wavelength (0.50 dB/km) and 1.3%/ocean wavelength (0.73 dB/km) for wind speeds of roughly 9 and 12 m/s, respectively. The growth rate was independent of wave propagation direction out to ±45° from the wind, provided that the distance measure was taken as the projection of the distance the ocean waves had traveled on the direction of the wind. Some evidence of overshoot, by a factor of 3, was seen on one occasion. Evidence was also seen of damping of previously-existing waves by a newly-opposing wind immediately following a frontal passage, and of the growth with distance of waves traveling in opposition to a steady wind.

6. THE THIRD ORDER HYDRODYNAMIC CONTRIBUTION TO THE HF RADAR SEA-ECHO DOPPLER SPECTRUM: B. J. Lipa, Center for Radar Astronomy and D. E. Barrick, NOAA/ERL, Wave Propagation Laboratory

Expressions have been published relating the average HF radar sea-echo Doppler spectrum to the ocean wave-height directional spectrum. Based upon these equations, techniques have been developed for inverting the second-order integral equation for the Doppler continuum, normalized to the discrete first-order Doppler peaks. These inversion techniques, which provide many important features of the waveheight directional spectrum, are undergoing both theoretical and experimental evaluation. Critical to the success of these techniques is the assumption that third-order sea echo is negligible in the regions of the Doppler spectrum used in the inversion process.

To test this assumption, a theoretical expression was derived for the hydrodynamic contribution to the continuous third-order Doppler spectrum. Preliminary sea-echo predictions were obtained by using a colinear, unidirectional Phillips model for the ocean spectrum. These results show that the third-order sea echo can dominate the second-order portion for higher sea states and/or radar frequencies (i) in the region near the carrier frequency, (ii) in the gap between the second-order and first-order spectral peaks, and (iii) for large values of Doppler shift. Hence caution should be used in applying second-order inversion to these portions of the sea-echo Doppler spectrum.

7. USE OF THREE AND FOUR-ELEMENT DIRECTION-FINDING ANTENNA ARRAYS IN COASTAL HF RADAR OCEANOGRAPHY: B. L. Weber and D. E. Barrick, NOAA/ERL Wave Propagation Laboratory

A unique HF receiving antenna system has been devised and tested which can determine the azimuthal direction of arrival of sea echo with only a small number of closely spaced elements. Implicit in the operation of this "direction-finding" system

is the assumption that sea echo having the same Doppler shift will not originate from a large number of different angles. In particular, we have employed (i) a three-element colinear array with $\lambda/4$ spacing which can resolve two signals (amid noise) from 180°, and (ii) a four-element square array which can resolve two signals (amid noise) unambiguously from 360°. These arrays have been used to relate first-order sea echo to underlying surface currents and map these currents in coastal waters.

Closed-form solutions are presented for the two signal amplitudes, phases, and directions of arrival as determined from the complex voltages measured simultaneously at each of the three (and four) receiving antennas. Simulations of angular extraction accuracy show that for sea echo, this accuracy depends upon the actual signal direction of arrival (with respect to the array orientation) and to the signal-to-noise ratio. Finally results of actual radar operations indicate that azimuthal angular errors are typically less than 2°.

8. MAPPING NEAR-SURFACE COASTAL CURRENTS WITH A TRANSPORTABLE HF RADAR SYSTEM: D.E. Barrick and M. W. Evans, NOAA/ERL/Wave Propagation Laboratory

A low-powered coastal HF radar system consisting of two auto-transportable units separated by ~40 km has been constructed and successfully demonstrated for real-time measurement of near-surface ocean currents. Operating at ~25 MHz, the concept employs the first-order sea-echo Doppler spectrum backscattered from 6 m long ocean waves. By knowing the expected Doppler shift produced by waves of this length, any additional shift is directly attributable to underlying currents transporting the waves. Thus the Doppler shift is directly related to the current velocity radial to the radar from the scattering patch. The range to the scattering patch is determined by time-gating the echo signal; its azimuthal angle of arrival is ascertained over 180° of space by employing three simple colinear receiving antennas 1/4 -wavelength apart.

Examples are shown of radar-deduced current maps produced on-site after 15 minutes of radar operation. Complete current vectors are shown (as obtained from two-site data) at a grid of points 3x3 km apart, to a distance ~70 km from shore. Signal thresholding and temporal averaging are used to eliminate much of the error due to noise, second-order scatter, and sea-echo random fluctuation; spatial averaging or filtering is not employed, however, meaning that each grid-point vector is an independent observation. Integration of the hydrodynamic equation of continuity improves the accuracy in regions where signal resolution is poor. This remote-sensing system shows considerable promise as a research and/or operational tool in coastal physical ocenography.

9. A ONE DIMENSIONAL COMPOSITE SURFACE DESIGNED TO SIMULATE OCEAN SCATTERING: W. H. Peake and H. H. Porter, ElectroScience Laboratory, The Ohio State University

In order to design and test microwave systems where the antenna is near the ocean surface, it is often desirable to make model measurements. However, direct modelling of the ocean is impractical, and in-situ measurements expensive and hard to control. This paper describes an inexpensive one dimensional (cylindrical) surface of commercial corrugated roofing designed to simulate ocean backscatter according to the composite model. Backscatter at large angles of incidence (the Bragg component) is generated by a small scale trapezoidal profile of 20 cm wavelength which gives 5 Bragg angles at 3 GHz. Backscatter near normal incidence (the specular component) is generated by forming the profile into a large scale sine wave of 125 cm wavelength and 10^{o} rms slope.

The backscattering from this doubly periodic cylindrical surface, when illuminated by a conical beam antenna, was calculated by physical optics (specular component) by perturbation theory (Bragg component) and by a modified moment method (both components). The dependence of the calculated backscatter on incidence angle, polarization and frequency was found to be in good agreement with measurements.

Commission G - Session 1

Wednesday P.M. 1330 - 1630
IONOSPHERIC MAPPING I
Chairman: C. Rush, Air Force Geophysics Laboratory, Bedford, Mass.

1. FOUR DIMENSIONAL IONOSPHERE MODEL: T. W. Flattery and G. R. Davenport, U. S. A. F.

The Air Weather Service has developed a model of the ionosphere for operational purposes which is capable of ingesting all available current and proposed ionospheric data sources. This mathematical representation of the ionosphere specifies plasma frequency as a function of latitude, longitude, altitude, and time, using a spectral analysis technique. Four empirical orthogonal functions based upon incoherent backscatter radar observations from Millstone Hill, Massachusetts, represent plasma frequency profiles from 95 to 2000 km. Electron density profiles, foF2, height of the maximum electron density, total electron content, or any other useful parameter of interest, can be readily extracted from the array of expansion coefficients generated by the model. Some insight into the development of the model and some results of testing against extreme input data sets are discussed.

2. A HIGH LATITUDE EMPIRICAL MODEL OF SCINTILLATION EXCURSIONS - PHASE I: J. Aarons, Air Force Geophysics Laboratory, Hanscom AFB, and E. Martin, Emmanuel College

Using observations of scintillations of VHF beacons from synchronous satellites, a high latitude model of scintillation excursions is being developed. Several years of continuous records of ATS-3 amplitude recordings taken at Narssarssuaq, Greenland, Goose Bay, Labrador, and Sagamore Hill, Massachusetts, were reduced. This data base consists of values of 15-min. scintillation excursions in dB at 137 MHz. Equations were developed which yield scintillations at this frequency as a function of local time, magnetic index, solar flux, and month of the year. The concept is, given solar flux and magnetic index, to predict at sub-auroral and auroral latitudes scintillation excursion. The equations developed have been checked with one additional set of observations and are being checked with other data.

The frequency dependence conversion and geometrical corrections are being developed and will form Phase II of the model. Frequency dependence problems include utilizing strong and weakly scattered data; geometrical problems include determination of elongation properties of the high latitude ionosphere as well as height and thickness parameters.

3. ADAPTIVE MODELING OF IONOSPHERIC EFFECTS OVER THE FIELD OF VIEW OF RADAR AND NAVIGATION SYSTEMS USING TRANSIT SATELLITE MEASUREMENTS: R.S. Allen, Air Force Geophysics Laboratory, Hanscom AFB, D.D. DuLong, Regis College, G.K. Hartmann, Insitut fur Aeronomie, Lindau/Hartz FRG, and R. Leitinger, University of Graz, Austria

Precision UHF navigation and radar systems require correction for errors caused by the ionosphere. A first order correction over the entire field of view may be realized by using maps of the monthly median of the pertinent ionospheric effects. These maps can be calculated off line using model algorithms based on available climatologies of the ionosphere. They are capable of providing a residual error of about 20 to 25 percent of the monthly median effect.

A further reduction by a factor 3 to 10 may be obtained by adapting and correcting the median prediction of the ionospheric effect using real time local measurements, in this case total electron content along the slant path to TRANSIT (Navy Navigation Satellite System).

A study of sequential TRANSIT passes demonstrates that the effects from the mid-latitude electron density trough, and some large local features persist for several hours. The error of prediction using the adapted maps during the time between TRANSIT passes is reduced by a significant factor.

For UHF systems this technique appears capable of reducing the monthly r.m.s. error to below 50 feet.

4. SOME UNUSUAL CHARACTERISTICS OF THE F_2 LAYER TOPSIDE MORPHOLOGY SUGGESTED BY THE ATS6 BEACON MEASUREMENTS: D.B. Odom, A.H. Katz and T.I.S. Boak, III, Raytheon Company

A comparison is made between the ATS6 radio beacon electron content measurements and a three-dimensional model which describes the morphology of the top and bottom-sides of the median ionosphere. Earlier comparisons of the observed and predicted characteristics of the median ionosphere showed an agreement between the model predictions and the observations of the height and density of the F_2 layer maximum as well as the F_2 layer bottomside scale height. These comparisons indicated, however, that the predicted values of total electron were systematically low. The rationale most often advanced for this discrepancy was that the "shape factor" used to model the topside of the ionosphere was in error. To test this hypothesis, a comparison with the shape factor obtained from the ATS6 data was made. The observed shape factor was accurately predicted by the model for the three months

of data which were analyzed. However, a comparison between the predicted and observed values of total electron content for this period again showed the predicted values to be low. The unusual characteristics of the F_2 layer topside morphology which are suggested by this comparison with the ATS6 data are described.

5. EXPERIMENTAL EVALUATION OF ADAPTIVE IONOSPHERIC RANGE ERROR CORRECTION IN HIGH ACCURACY RADARS: D.D. Dulong, Regis College, R.S. Allen, Air Force Geophysics Laboratory, Hanscom Air Force Base, M.D. Grossi and A. H. Katz, Raytheon Company

An experimental evaluation has recently been performed of a novel procedure, developed by the authors, for the correction of radar range errors introduced by the ionosphere. This is a real-time adaptive scheme based on the combination of dispersive dual-frequency radar range measurements on available targets and of an ionospheric model constructed with climatological data and updated on a monthly basis. The data are from a precision L-band radar which operated from Spring 1976 to Spring 1977. The experimental verification has consisted of the following steps: a) updating the stored ionospheric model by means of dual-frequency range measurements performed on a target of opportunity at a certain time and in a certain direction; b) performing identical measurements on another target, at a later time and in another direction; c) Obtain the true range for this second target by subtracting from the apparent range the ionospheric error determined with the double-frequency approach; d) Obtain the true range by subtracting from the apparent range the ionospheric error estimated from the model after updating of Step 1 ; e) Compare the two values of true range. This experimental verification has shown that the method is effective in terms of reduction of the ionospheric range errors down to a few meters (in conditions of low solar flare activity) and is advantageous inasmuch as it minimizes the utilization of the radar resources for this scope.

6. CORRELATION DISTANCE OF MEAN DAYTIME TOTAL ELECTRON CONTENT: J.A. Klobuchar, Air Force Geophysics Laboratory, Hanscom AFB, J. Johanson, Emmanuel College

Using data from several northern latitude, western hemisphere stations the correlation coefficient, r, of local daytime, 10-16 hrs, mean TEC values taken near solar maximum, was compared for pairs of stations to determine the useful correlation distance. The winter season gives the highest values of r, while spring equinox values are generally lowest. For stations at nearly the same longitude, the latitude correlation distance, here defined as the station spacing where r=0.7, is approximately 2000 km. Northern mid-latitude stations within 10^{o} of the same geomagnetic latitude exhibit a longitude correlation distance of approximately 3000-4000 km., and up to 5000 km. in the winter season. Values of r for mean nighttime hours are generally much lower. The larger winter correlation distance is probably

due to predominant solar EUV control; whereas, the lower values in the other seasons are likely due to loss dominated processes controlled by the neutral wind, having a scale size of a few thousand kilometers. These results agree well with previous studies of the correlation distance of f0F2, and have applications in the required spacing of TEC monitoring stations for ionospheric time delay corrections for satellite ranging systems.

Commission B - Session 4

Thursday A.M. 0900 - 1155
EM THEORY
Chairman: R.E. Kleinman, University of Delaware, Newark, Delaware

1. ON DIFFRACTION SYNTHESIS OF DUAL REFLECTOR ANTENNAS: S. W. Lee*, R. Mittra*, V. Galindo-Israel**
*University of Illinois at Urbana, Consultants to JPL
**JPL, Pasadena, CA

In this paper we review and critically analyze a number of current approaches and introduce some new concepts for the diffraction synthesis of dual reflector antennas. The diffraction syntheses, it should be noted, often utilize geometrical optics synthesis (e.g., V. Galindo, U. C. Berkeley Electronics Rsch Lab Rept 64-22, 1964) as an 'initial' condition. The variety of available approaches may be classified under three general headings: (a) Field Matching Approach as introduced by Potter (Trans AP – No. 6, 1967); (b) Forward Scattering Method as developed by Daveau (Review Technique Thomson CSF, 1970); (c) Field Correlation Method as investigated by Wood (Electronics Letters, No. 11, 1970) and others. Potter's method, which is based essentially on an inverse scattering approach, requires infinite flexibility in the choice of the feed horn pattern and provides an analytical solution for the shape of the subreflector when the main reflector is a parabola. We first extend his approach for the more practical situation where the horn pattern is a priori specified and the objective is to derive an optimal design of the subreflector shape. Next, we turn to Daveau's method, which in contrast to that of Potter's 'inverse' approach, employs a linearized perturbation-iteration technique to successively solve for the subreflector and main reflector shapes. In this paper we extend Daveau's method by introducing a technique for simultaneously determining the dual shapes either by an extension of the inverse method a' la' Potter or the forward method a' la Daveau. In both methods we introduce the diffraction synthesis for feeds displaced from the nominal focus. In the last part of the paper we employ the reciprocity principle to derive Wood's field correlation integral in a more complete and exact form and examine precisely the approximations involved in this formula for the efficiency of a dual reflector antenna. New versions of the correlation formulas are derived which can be used efficiently to account for subreflector blockage. The relationship between the correlation and more direct diffraction syntheses methods is examined.

2. APPLICATION OF THE UNIFORM GTD TO THE DIFFRACTION AT EDGES ILLUMINATED BY TRANSITION REGION FIELDS: R. Tiberio*, R. G. Kouyoumjian**
*University of Florence
**Ohio State University, Columbus

In applying the uniform GTD, the interaction between a pair of nearby edges usually can be handled in a straightforward manner. However, if the point of diffraction on one edge lies on the shadow boundary of the other, the problem is complicated, because the field incident on the former edge has a rapid spatial variation and in addition it is not a ray-optical field. Although the former difficulty can be handled by introducing slope diffraction, the latter remains.

Recently there has been considerable interest in this type of problem [1,2]. The example studied consists of a pair of staggered, parallel half-planes illuminated so the second edge lies on the boundary of the first. It has been mentioned [2] that this example has not yet been successfully treated by the uniform GTD and its slope diffraction modification. In this paper it is shown that the shadow boundary field of the first edge can be decomposed into cylindrical waves whose diffraction can be determined by the uniform GTD. Superposition is then used to obtain a solution whose first two terms are in agreement with the correct asymptotic result. This procedure is also employed to treat the corresponding problem in the case of a thick edge; some interesting differences in the analysis arise in this case.

---

1. S. W. Lee and J. Boersma, J. Math. Phys., vol. 16, pp. 1746-1764, 1975.
2. Y. Rahmat-Samii, 1976 AP-S International Symposium, University of Massachusetts at Amherst.

3. ON THE DIFFRACTION OF EDGE EXCITED SURFACE RAYS: P.H. Pathak, R. G. Kouyoumjian, Ohio State University, Columbus

The excitation of surface rays by an edge in a two dimensional convex surface which is illuminated by an electric or magnetic line source is investigated in this paper. An asymptotic high frequency approximation for the edge, and edge excited surface diffracted ray fields is determined from the GTD solutions to the canonical problems of the diffraction by a wedge, and the radiation from a line source on a smooth convex cylinder. These ray field descriptions fail within the transition regions adjacent to the boundaries which are tangent to the convex surface. Thus, a uniform asymptotic result which remains valid within these transition regions is introduced, and outside the transition regions this result reduces to the edge and edge excited surface diffracted ray fields on the lit and shadow sides of the boundaries, respectively. Presently, this result is valid for a ray

incident on the edge which is not too close to grazing incidence on the convex surfaces. These results can be readily extended to treat the diffraction of an Elliot type mode excited on a curved impedance surface patch which covers a perfectly conducting convex cylinder. Numerical results are given for the diffraction by curved, perfectly conducting strips and the diffraction of Elliot type modes on a curved, impedance surface. These results are compared with calculations based on the moment method solution. The generalization of this method to include a rapidly varying field incident on the edge in the convex surface will be discussed.

4. COMPARISON OF EDGE-INDUCED AND SURFACE-INDUCED REFLECTION BOUNDARIES: M. Rahnavard, W.V.T. Rusch, University of Southern California, Los Angeles.

Conventional reflection boundaries are generated by truncating a reflecting surface so that the specular ray component abruptly ceases to exist beyond a certain point in space. Edge diffraction expressions which incorporate Fresnel integral transition functions in the vicinity of the reflection boundary can be used to characterize its features in terms of the geometric properties of the reflected wavefront. Of special interest is the gradient of the field magnitude at the boundary which provides an estimate of the diffracted energy in the shadow region.

Reflection boundaries can also be created by reversing the curvature of the reflecting surface. In such cases the wavefront of the reflected field becomes essentially cubic, and the reflected field can be characterized by the Airy function. Practical examples of such surfaces are the Galindo-Williams shapes for microwave antennas. A study has been carried out relating the characteristics of surface-induced reflection boundaries to the geometrical properties of the surface, and comparing these results to the more conventional edge-induced boundaries.

5. POYNTING THEOREM FOR MOVING DISPERSIVE MEDIA: H. C. Ko, C. W. Chuang, Ohio State University, Columbus

The law of energy conservation in the electrodynamics of moving media is derived. The medium is assumed to be isotropic, homogenous, lossless and frequency-dispersive in its own rest frame. It is shown that the total energy flux consists of two parts: the electromagnetic flux represented by the Poynting vector and the particle energy flux associated with the motion of the particles in the medium undergoing motion. The total energy flux is equal to the product of the total energy density and the group velocity. The direction of the energy flow is shown to coincide with the direction of the group velocity, but is distinct from that of the Poynting vector. The group velocity is shown to obey Einstein's velocity addition theorem rigorously. On the other hand, the energy velocity defined as the ratio of the Poynting vector and the energy density fails to obey the velocity addition theorem for moving dispersive media. The Poynting theorem for moving dispersive media is derived. The new formula disagrees with the result obtained by earlier investigators. The causes for the discrepancy are discussed. The result is applied to antenna radiation in moving dispersive media.

6. A FORMULATION FOR ELECTROMAGNETICS PROBLEMS USING DIRECT FIELD-SOURCE RELATIONS: D. F. Hanson*, P.E. Mayes**
*Iowa State University, Ames
**University of Illinois, Urbana

At present the most widely used formulations for electromagnetic field problems require vector and scalar potentials to relate the fields to the sources. Although direct field-source relationships have been known previously, they have not been widely used in establishing integral equations for electromagnetics. This paper presents a formulation for time- and frequency-domain electromagnetics scattering problems based on a direct relationship between the fields and sources. It is shown that if the fields and currents are treated as continuous linear functionals (Schwartz distributions), then doubts about interpretation of the differential and integral operators can be put aside. The formulation has been called "The Current Source-Function Technique" by one of the authors (P.E.M.). The analytical procedures required to solve the classical half-plane problem by this technique are given.

7. ANTENNA PATTERN INTERPOLATION: E. Mendelovicz, V. P. Cable, California State University, Northridge

Modern antenna characterization calls for measurements of patterns at many frequencies. The frequencies of interest can be strobed sequentially as the antenna is measured in a particular plane. This approach is considerably improved over methods predating the microwave frequency synthesizer. Nevertheless, when large numbers of frequencies are needed, this method still becomes tedious and slow. Tremendous amounts of data which are often stored also cause problems. Hence, a reliable pattern interpolation technique would be most useful since it might offer an acceptable trade-off between number of data points and pattern quality. Pattern interpolation has been tried previously without much success; e.g., it is particularly difficult to reproduce deep pattern nulls.

This paper will show some new results on interpolating and extrapolating electromagnetic radiation patterns. One method which is discussed is based on using a truncated Fourier series to reconstruct antenna patterns. This technique does not appear to be very promising however, since it is impossible to know the number of terms needed to give an acceptable reconstruction. Too few data points will lead to loss of energy in the estimated pattern while too many points will eventually tax the numerical limits of the computing machine. An optimum interpolation technique for reconstruction of bandlimited periodic functions is discussed. This technique appears to be much less sensitive to the number of terms needed to represent the pattern. Other suboptimum techniques which are easy to apply are evaluated based on this optimum result. These results show rather conclusively that improvements in efficiency of pattern measurements are possible.

8. A VECTOR DIAGRAM OF MAXWELL'S EQUATIONS: D. R. Wilton, University of Mississippi, University

A vector diagram of Maxwell's time-harmonic equations can be obtained simply by regarding the vector operator ∇ as a constant vector and examining the consequences thereof. If the medium is isotropic and there is no magnetic current, the diagram is essentially two-dimensional. All the common relationships between fields, sources, and potentials such as Maxwell's equations, the continuity equations, the various representations of fields in terms of potentials and the Helmholtz equations are either explicitly shown on the diagram or immediately obtainable by equating vector components. The arbitrariness of gauge conditions and the significance of both the Lorentz and Coulomb gauges is readily apparent. If an appropriate significance is attached to the "scalars" $(\nabla.\nabla)^{-1}$ and $(\nabla.\nabla + k^2)^{-1}$, the various integral relationships are also obtained. While no essentially new relationships are obtainable from the diagram, it does display the familiar relationships in an interesting graphical representation and can serve as a convenient reference. The representation is justified by transforming Maxwell's equations using the three-dimensional Fourier transform.

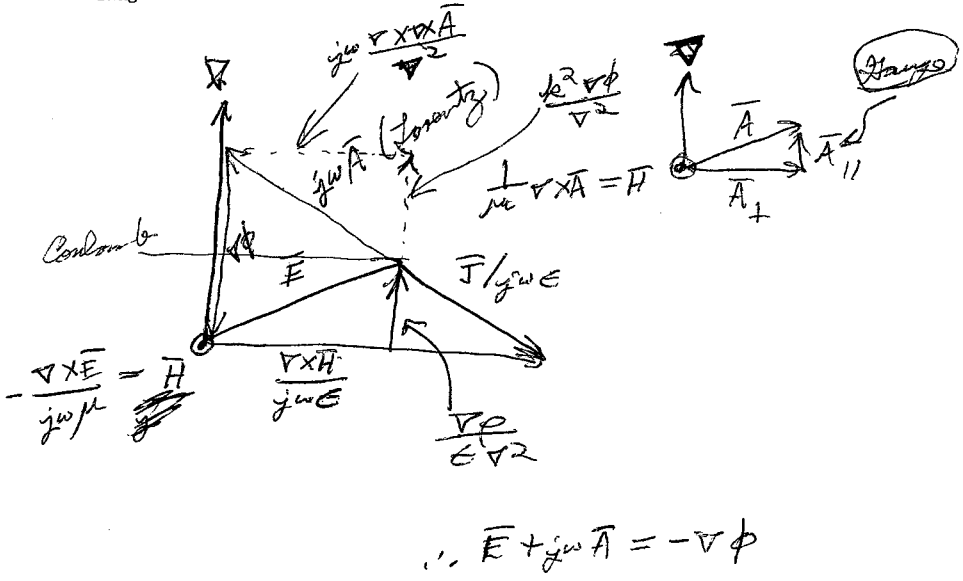

Commission C - Session 1

Thursday A.M. 0900 - 1140
MULTIPLE-ACCESS SATELLITE COMMUNICATIONS SYSTEMS
Chairman: J. Aein, Institute for Defense Analyses

1. ON CIRCUIT ALLOCATION FOR SATELLITE COMMUNICATION SYSTEMS: G. Gopinath, Bell Laboratories

We consider the mathematical theory of optimal allocation of a limited number of satellite circuits to different user classes. Classes are distinguished by:

a) request rate
b) holding time
c) bandwidth required
d) rate charged

Using a recently developed fully Markov model that assumes blocked circuit requests cleared we show for several canonical cases the structure of the optimal policy emphasizing the qualitative influence of a)-d) above. A cost weighted throughput criterion is used throughout. The optimal policy need not be myopic but has a state space characterization. We make comparisons of the optimal policy with i) a free access policy and ii) a policy of complete apriori assignment of circuits to classes. Asymptotic effects are also explored.

2. A PRIORITY-ORIENTED DEMAND-ASSIGNMENT (PODA) MULTIPLE-ACCESS PROTOCOL FOR BROADCAST PACKET SATELLITE COMMUNICATIONS: L. L. Lee, Linkabit Corporation

A Priority-Oriented Demand-Assignment Protocol for Time-Division Multiple-Access Broadcast Satellite Communications is presented. The satellite channel is dynamically divided into two subchannels with one for earth station reservations and the other for actual information transmission. The capacity of the information subchannel is assigned to the earth stations on a message basis according to the priority and the nature of the messages which are provided by the reservation requests. Messages with short acceptable delay or higher priority are given preferential treatment. The reservation requests are broadcast to all stations either through the reservation subchannel with the random multiple access technique of S-ALOHA, or by tagging the messages scheduled for transmission. The requests are then processed by all stations with an identical algorithm, thus achieving distributed channel assignment. It is shown that the procedure can be used to support stream-type traffic as well as block-type traffic, thus integrating the traditional role of circuit switching into a message switched communication protocol. It is also shown that distributed channel assignment performs well at normal channel error rates. Simulation results with hypothetical traffic statistics will be presented.

3. ADAPTIVE DAMA: L. Schuchman and J. Spilker, Stanford Telecommunications, Inc.

In this paper we discuss an extension of slotted Aloha in which each user transmits data in n continuous time intervals. When n=1 the system reduces to slotted Aloha while at the other extreme (n going to infinity) we have TDMA. The system is designed so that in acquiring a time slot, one time

slot is randomly selected from all non-busy time slots. When a time slot is acquired without overlap, it is reserved, for the acquiring user, for the next n-1 time frame.

Analytic results are presented which show the relationships between channel efficiency, message arrival rates and n.

The system concept of the "fair channel" is introduced. In this concept, the value of n is determined by the traffic so that when traffic is light n will be large, but when traffic increases the value of n will decrease. The paper also discusses options for implementing priorities.

4. CLOSED LOOP STABILITY CONTROLS IN RANDOM ACCESS SATCOM: M. Gerla, University of California at Los Angeles

In the family of random access satellite channel schemes for packet communications the simplest and probably the most studied scheme is the slotted ALOHA (S-ALOHA) scheme. In the S-ALOHA scheme the channel is divided into time slots, where each slot can be used to transmit a full size packet. Slots are not preassigned to stations; rather, each station at the beginning of a slot may start transmission if it has a packet to send. A conflict occurrs when two or more stations transmit in the same slot. To recover from conflicts, the packet is retransmitted after a random time. In general, both new transmissions and retransmissions are scheduled after a random time, using probability gates P(N) and P(R) respectively. The "gate" is defined to be the probability of sending a packet in the next slot.

It can be shown that S-ALOHA channels are intrinsically unstable. In fact, if transmission rates exceed some critical values, channel performance degrades and the channel is not operated cost-effectively. Once the system is driven into a degraded mode of operation, it will remain in such mode even if the peak traffic demands are removed.

For the above reasons it is necessary to introduce channel control mechanisms which adaptively adjust the gate values to the changing traffic pattern and provide for system recovery from degraded modes.

In this paper we present a novel approach to the control of S-ALOHA channels. The approach differs from previously proposed techniques in that: it is based on a closed loop control scheme; it does not require the capability of distinguishing between empty slots and collision slots; and it is capable of adjusting to permanent changes in traffic pattern.

Simulation results are presented to compare the performance of the closed loop algorithm to previous control algorithms.

5. A PROCESSING SATELLITE FOR PACKET COMMUNICATIONS: R. S. Davies, Ford Aerospace and Communications Corporation

The use of random packet transmissions (ALOHA) in a communication satellite is attractive because the need for network timing and control is virtually eliminated. However, the bandwidth utilization is low (less than 20%) and has led to the development of the slotted and reservation packet system concepts which do require timing and control at the user terminals.

As an alternative, suppose we design a system where inefficient bandwidth utilization could be tolerated. Due to limited frequency spectrum availability such a system would almost certainly have to operate the K_a-band (20-30 GHz) or above, and employ frequency reuse by the satellite. Frequency reuse is accomplished with a multibeam satellite antenna.

With many beams, it becomes desirable to demodulate the received data packets in the satellite and perform interbeam switching at baseband. An address word at the beginning of each packet would be decoded in the satellite to direct the packet to the desired downlink beam. If the downlink transmitter is in use, the packet is placed in a buffer storage, and transmitted later. Thus packet collisions on the downlink may be avoided and the data rate reduced to improve bandwidth utilization.

Rain attenuation in the uplink might be overcome by the development of a transmitting tube capable of delivering several kilowatts of power for a short period of time with low duty cycle.

A lower frequency band can be used for the downlink to circumvent the rain attenuation problem since we reduced the bandwidth requirements.

6. MUTUAL INTERFERENCE IN A SPREAD SPECTRUM MULTI-USER ENVIRONMENT: S.A. Musa, W. Wasylkiwskyj, Institute for Defense Analyses

This paper considers the mutual interference problem of several users employing the same spread spectrum technique in selected multiple user environments. The spread spectrum techniques consist of pseudo noise (PN), time division multiple access/PN, synchronous and asynchronous frequency hopping (FH). The environment consists of a desired transmitter-receiver pair located in an area where there are M interfering users situated according to either a bell-shaped distribution from the receiver or uniformly distributed along the perimeter of the communications area. The sensitivity of the communications performance (probability of bit error) of the desired link to the total number of interfering users which can be placed within the area is investigated for various parameters. The analysis shows that the mutual interference problem is less severe with users employing synchronous FH than with the other spread spectrum techniques. The comparison between asynchronous FH and PN is highly dependent on the relative location of interferers to the desired link and the time duty factor of the hopping. The penalties associated with synchronous operation in dense environments are also discussed.

Commission F - Session 3

Thursday A.M. 0900 - 1155
REMOTE SENSING
Chairman: Dr. A. Fung, Center for Research Inc., Lawrence, Kansas

1. INTERACTION OF ELECTROMAGNETIC AND ACOUSTIC WAVES IN A QUIESCENT ATMOSPHERE TO MEASURE TEMPERATURE AND HORIZONTAL WINDS: M. S. Frankel, N. Bhatnagar, and A. M. Peterson, Center for Radar Astronomy, Stanford University

The Radio Acoustic Sounding System (RASS) has thus far been used to remotely measure atmospheric temperature profiles. The basic concept behind RASS consists of Doppler tracking a high-intensity acoustic pulse with an RF (electromagnetic) radar. Measurement of the acoustic pulse propagation speed gives temperature as a function of altitude.

For acoustic pulses with carrier frequencies below a few kilohertz propagating (under typical atmospheric conditions) to altitudes of a few kilometers, turbulence has little effect on the strength of the received radio signal. Quiescent (mean) vertical winds and temperature gradients do not significantly affect the strength of the received signal level. Mean horizontal winds shift the focus of the reflected electromagnetic energy from its origin resulting in a decrease in received signal level when a monostatic RF system is used. The principle of specular reflection, however, can be utilized in a bistatic-radar configuration to remotely measure this wind component in addition to atmospheric temperature. Consistent with these theoretical predictions, a RASS operating at an acoustic frequency of 1 kHz and a radio frequency of 440 MHz (built at Stanford Research Institute) was able to provide both Doppler data and horizontal wind profiles for altitudes up to 1 km.

2. AN OPTIMUM METHOD FOR ESTIMATING MARINE ENVIRONMENTAL PARAMETERS USING RADIOMETRIC REMOTE SENSING SYSTEMS: Dr. M. M. Wisler and Dr. J. P. Hollinger, Space Science Division, Naval Research Laboratory

Microwave radiometry offers an attractive means of remotely sensing the physical properties of the earth's surface and atmosphere. This is a result of the variation of the emission, absorption, and reflection properties of matter with the observational parameters of frequency, polarization, and incidence angle. Since the microwave radiation from the earth is, in general, a complex function of the temperature, roughness, and physical composition of the surface as well as the absorption, emission, and scattering properties of the atmosphere, the principal problem in microwave radiometry is the quantitative determination of the environmental parameters from a limited set of noisy measurements of the microwave radiation. Because these measurements are, in general, not sufficient to specify the environmental

parameters without some prior knowledge and assumptions about the distribution of the parameters, most methods of determining these parameters involve the use of models which relate the parameters to the radiometer antenna temperatures. Within these models it is normal to either fix the physical parameters at known mean values or to allow them to vary between expected limits as the microwave brightness temperatures are calculated. The variation of these parameters between expected limits is then used to calculate how well they may be estimated by a specified set of measurements. Another factor, which is often overlooked but must be taken into consideration when a model is used to calculate how well parameters may be estimated, is the uncertainty of the physical relations which form the model equations. These are often the result of curves fitted to noisy experimental data, such as wind speed versus brightness, and are inherently uncertain. The spread of the experimental data used to determine them must be taken into account in error estimation. In this paper we present a method by which one may estimate remote sensing errors from three sources: the radiometer measurement errors, the statistical distributions of the environmental variables to be estimated, and the uncertainty of relations and assumptions used in modeling the radiometric properties of the environment. The mathematical development is given first, and then an example application of a five frequency radiometer system to the measurement of ocean surface and atmospheric parameters is described.

3. MICROWAVE RADIOMETRIC OBSERVATIONS OF THE MARINE BOUNDARY LAYER:
C. I. Beard and L. U. Martin, Naval Research Laboratory

Experiments by the Naval Research Laboratory (NRL) in 1975 demonstrated that 22-GHz microwave radiometers could detect, and localize in height, internal waves propagating on low-level temperature inversions at the upper boundary of the marine boundary layer. A second experiment in June 1976 examined the marine boundary layer in finer detail by using two narrow 3° beamwidth antennas whose beams could intersect at various altitudes. One result was the first detection and correlation between radiometers of short-period (2-3 minute) Kelvin-Helmholtz type waves. The presence of these waves was confirmed by the simultaneous detection by the Naval Electronics Laboratory Center's (NELC's) FM-CW radar and/or acoustic sounder which were used for comparison to the radiometer data. In addition, during relatively unchanging meteorological conditions, the radiometer traces would follow changes in the altitude of the inversion base with sensitivities between 17 and

50 m/°K. These results were unaffected by the presence or absence of stratus clouds. Using a "quiet" period to measure radiometer noise at $\pm$ 0.05°K, the average 25 m/°K sensitivity yields a resolution of approximately $\pm$ 1 meter, comparable to active sensors.

4. BEAM-PATTERN CHARACTERISTICS AND PRACTICAL ANTENNA-CUFF DESIGN FOR ECHOSONDE SYSTEMS: S. A. Adekola, NOAA/ERL/Wave Propagation Laboratory

The echosonde technique has proved to be a valuable method for remote-sensing of the structures and motions in the lower atmosphere. For example, this technique can be used for monitoring atmospheric conditions which aggravate air-pollution or for detecting wind shears which jeopardize aircraft safety near airports. These applications require directional antennas whose beam-patterns are formulated here in closed form integral-equations using either the Zernike polynomials or the generalized hypergeometric functions. Comparisons between theory and experiment are given. For sidelobe suppressions, an antenna shielding-cuff of height 1.8 m is necessary at 2-3 kHz giving a maximum operating range of about 760 m. For an increased operating range (e.g., 1.5 km), lower carrier-frequencies within 1-1.5 kHz are essential, with a larger antenna-cuff of about 2.4 m high. The larger antenna-size compensates for the higher noise-level at the lower frequencies by increasing the directivity and by further suppression of the sidelobes. Half-power beamwidth-variations between 6.6° and 9.8° are obtained within 1-1.5 kHz carrier-frequencies. Selection of antenna flare-angles between 15°-18° tend to give optimum sidelobe attenuations. Ground-level sidelobe attenuations of 50 to 60 dB are essential for minimizing external noise and also for minimizing the environmental impact of the sounder. Sidelobe rejections of 56.5 dB are obtained at 2 kHz frequency for the antenna-cuff of height 1.8 m.

5. A NEW REMOTE SENSING METHOD FOR ON-SITE PROFILE INVERSION IN SOIL MOISTURE PROBING: D. C. Chang and W. A. Bereuter, Electromagnetics Laboratory, University of Colorado

The task of this research is the development of an inverse scattering technique for the complex refractive index as a function of depth in top soil. One of the requirements is to process all data on site employing simple but sufficiently versatile schemes. The probing is based upon frequency scanning, starting at the high frequency end. Using the Ricatti equation for the reflection coefficient and a polynomial approximation for the logarithm of the refractive index, one obtains an asymptotic form for the surface reflection coefficient. This expression is valid over about one skindepth, and can be analytically inverted for the coefficients of the approximating polynomial. Upon lowering the frequency according to the next desired probing depth, and transforming the measured reflection numerically through the known first "layer" by a fourth order Runge-Kutta

routine with prespecified error-bound, one obtains the refractive index in the next layer. The layer thicknesses are adaptive to ensure versatility as well as speed. As a check or performance index the reflection coefficient due to the whole structure is recomputed. Aside from the usual resolution problem for the lower frequencies, it appears that the proposed method yield sufficiently accurate retrieval results. Practical numerical inversions will be presented.

6. ELECTROMAGNETIC TECHNIQUE OF MEASURING COAL LAYER THICKNESS: D. A. Ellerbruch and D. R. Belsher, Electromagnetics Division, National Bureau of Standards

An FM-CW microwave system was investigated for measuring coal layer thickness. Measurements were made in three different mines near Pittsburgh, Pennsylvania, near Fairview, West Virginia, and near Coffeen, Illinois. Microwave frequencies in the range 1-2 GHz were used to measure samples up to 55 cm thick. All samples were backed with a naturally occurring shale. Measurements were also made on coal and shale samples compounded in the laboratory at the Bureau of Mines Pittsburgh Mining and Safety Research Center near Bruceton, Pennsylvania.

The results indicate that layer thickness can be determined in most cases, although large anomalies may, in some cases, produce misleading results. Many anomalies that were detected with the FM-CW system were verified visually by drilling into the coal layer.

The dielectric constant of coal apparently varies significantly within a coal seam. It appears that this technique has the potential of measuring changes in the dielectric constant of a coal seam and providing an output that can be used for real-time corrections in layer thickness measurement.

This technique has great potential if fully developed. It would have significant impact in areas of energy, safety, and productivity.

7. PASSIVE MICROWAVE MAPPING OF ICE THICKNESS: J. J. Apinis and W. H. Peake, ElectroScience Laboratory, The Ohio State University

This paper presents the basic calculations from which the feasibility of a scanning microwave radiometer system for mapping the thickness of lake ice may be evaluated. An analytical model for the apparent brightness temperature as a function of ice thickness has been developed, and elaborated to include such variables as galactic and atmospheric noise, aspect angle, polarization, temperature gradient in the ice, and presence of transition layers such as snow, slush, and water, increased loss due

to air inclusions in the ice layer, and the presence of multiple ice thicknesses within the antenna footprint. It was found that brightness temperature measurements at six or seven frequencies in the range of 0.4 to 0.7 GHz were required to obtain unambiguous thickness estimates. A number of data processing methods were examined; a minimum-distance algorithm and a ternary brightness temperature quantization scheme were found to give accuracies of about 1 cm for ice thicknesses up to one meter. A brief system study of the effects of antenna beamwidth, scanning rate, receiver bandwidth, noise figure, and integration time showed that the receiver sensitivity requirements could be met with state-of-the art components. The radiometric system was found to fail for sea ice thickness measurement due to the very high losses of sea ice.

Commission F - Session 4

Thursday A.M. 0900 - 1200
EARTH-SPACE PROPAGATION ABOVE 10 GHz
Chairman: Dr. D. C. Cox, Bell Telephone Labs, Holmdel, N.J.

1. CTS 11.7 GHz BEACON ATTENUATION AND CROSS POLARIZATION MEASUREMENTS: JUNE 1976 TO MAY 1977*: W. J. Vogel and A. W. Straiton, Electrical Engineering Research Laboratory, The University of Texas at Austin

The nominally right hand circularly polarized 11.7 GHz beacon transmitter on the CTS satellite has been monitored at The University of Texas at Austin for the periods of its operation. A two channel receiver using a turnstile junction as feed was built. It's polarization is adjusted to give better than 45 dB isolation between the channel measuring the co-polarized signal and the one measuring the cross-polarized signal during clear air propagation. The signal levels in both channels were recorded for more than 300 days and used to determine attenuation to over 30 dB and cross-polarization isolation. Also measured was the rainrate.

Results of the data analysis are presented. They bear out the dependence of isolation on both attenuation and phase shift events in the path. While in the presence of rain isolation can be related reasonably well to attenuation, a substantial number of occurrences of phase shift events reduced isolation without any or little simultaneous fade or precipitation. Therefore it may be hazardous to estimate at 11.7 GHz isolation statistics from previously measured attenuation statistics, especially for isolation exceeding 25 dB.

*This research was supported by NASA Goddard Space Flight Center Contract NAS5-22576.

2. DEPOLARIZATION MEASUREMENTS USING THE COMSTAR SATELLITE: P. H. Wiley, C. W. Bostian, W. L. Stutzman, E. A. Manus, and R. E. Marshall, Virginia Polytechnic Institute and State University

The crowding of communications channels in the 4,6, and 8 GHz bands is forcing designers of earth-space communications systems into the region above 10 GHz. As the available bandwidth in this area of the spectrum is limited to atmospheric windows, there is increasing interest in using orthogonal polarization frequency sharing to realize double service from each assigned frequency.

The fundamental limitation of a system employing orthogonal polarization frequency sharing is depolarization caused by precipitation. Although depolarization is comparatively well understood for a ground path, measurements made with the CTS and COMSTAR satellites indicate that the observed depolarization and attenuation are not predictable from existing theory. Attenuations far in excess of expected values have been observed as well as significant depolarization during periods of relatively low attenuation. Initial data indicate that

1. Models based on ground depolarization are not directly applicable to earth-space propagation paths.

2. Attenuation and depolarization do not scale with frequency as expected.

3. For storms with the same ground rainfall rate there is a tremendous variation in the observed attenuation and depolarization.

The authors are currently monitoring the COMSTAR satellite at 19.04 and 28.56 GHz and the CTS satellite at 11.7 GHz. Recorded data includes all signal component amplitudes and relative phases, ground weather information, and integrated radar returns from the path. Simultaneous measurements at these three frequencies should provide sufficient information to develop a more reliable model for earth-space propagation.

3. ATTENUATION AND DEPOLARIZATION MEASUREMENTS AT CRAWFORD HILL USING THE COMSTAR BEACONS: H. W. Arnold, D. C. Cox and H. H. Hoffman, Bell Laboratories

Two receiving systems are in operation at Crawford Hill, New Jersey, for measuring earth-space propagation phenomena using 19 and 28 GHz beacons carried on the two COMSTAR communications satellites. One experiment, in operation since June 1976, collects 19 GHz attenuation data for two linear orthogonal polarizations using the satellite beacon at 128°W longitude. This experiment, using a 3.7m diameter receiving antenna, has a 45 dB clear-air signal-to-noise ratio. The second experiment, in operation since January 1977, collects attenuation, depolarization, and differential phase data at both 19 and 28 GHz using the beacon at 95°W longitude. This experiment uses a precision 7m diameter antenna, and in clear air has signal-to-noise ratio of 60 dB and polarization discrimination in excess of 35 dB.

This paper includes a brief description of the experiments using these two receiving systems and presents the distributions of precipitation-induced attenuation and differential attenuation observed over a continuous period of nearly one year. Observations will be described of events exhibiting significant depolarization at 19 and 28 GHz during periods of low signal attenuation (often < 1 dB). These events have been observed in association with both summer thunderstorms and winter storms where precipitation existed only as snow.

4. PRELIMINARY RESULTS IN TESTING SLANT PATH ATTENUATION PREDICTION METHODS USING RADAR AND THE 28 GHz COMSTAR BEACON: J. Goldhirsh, Applied Physics Laboratory, The John Hopkins University

Preliminary comparisons are made between directly measured rain fade levels at 28 GHz and predicted fades using radar. A system receiving the 28.56 GHz COMSTAR beacon signal is in operation at Wallops Island, Virginia, and fading due to rain is examined in both a case-by-case basis as well as statistically. A nearby high resolution S-band radar (0.4° beamwidth) measures simultaneously the rain reflectivity levels at adjacent range bins (150 m range resolution) along the propagation path. Assuming given drop size distributions, the reflectivity levels are related to attenuation coefficients at the corresponding range bins and the total path attenuation is evaluated as a function of time. These predicted levels are subsequently compared with the attenuation directly measured at the COMSTAR receiver.

5. SOME MEASUREMENT RESULTS OF RAIN ATTENUATION AND DEPOLARIZATION OF THE CTS SATELLITE BEACON SIGNAL: A. J. Rustako, Jr., Bell Laboratories

A measurement program is under way to determine attenuation and depolarization of the 12 GHz Communications Technology Satellite (CTS) beacon signal, due to rain and other atmospheric effects. A receiving system composed of a 20 ft. aperture horn reflector antenna and a two branch narrow band receiver continuously tracks and records the received signal envelope. The right-hand circular co-polarized beacon signal and the reverse sense cross-polarized due to atmospheric effects are measured.

The receiving system, located at Crawford Hill, Holmdel, N.J. is co-located with a 19 and 28 GHz COMSTAR beacon receiving system. The two paths are similar and show correlation in atmospheric propagation effects.

The CTS beacon measurement has been made since April 1976, providing approximately one year of data.

6. PRELIMINARY RESULTS OF THE 19/29 GHz COMSTAR BEACON MEASUREMENTS AT CLARKSBURG, MARYLAND: J. M. Harris, COMSAT Laboratories

The COMSTAR Centimeter Wave Beacons provide a continuous and stable source which uniquely allows the direct measurement of atmospheric induced attenuation, depolarization, and phase dispersion effects in the 19 and 29 GHz bands. Reliable reception of the COMSTAR I transmissions began at COMSAT Labs in mid July of 1976. The signals are received by a five meter dual polarized antenna system and a COMSAT Labs built receiver. Fade characteristics are measurable over a dynamic range of at least 30 dB.

This paper presents results of analysis performed to date on data collected during 1976. Examples of path-induced attenuation, degradation of clear weather Cross Polarization Discrimination, and differential phase and amplitude effects are given along with the cumulative fade statistics for the 19.04 GHz and the 28.56 GHz vertically polarized signals and the correlation analyses of 19 and 29 GHz fading levels. A comparison of radiometrically measured attenuation at 11.7 GHz with COMSTAR beacon attenuation data is made. Finally the wave-medium interaction describable by the available data will be discussed.

7. COMSTAR BEACON TRIAD IN FLORIDA: D. D. Tang, D. Davidson, GTE Laboratories, Waltham, Mass., V. Bloch, University of South Florida

In order to study 18/30 GHz downlink signal attenuation statistics and effects of diversity for regions with heavy rainfall rates, we designed, built and installed three COMSTAR 18/30 GHz beacon receivers in Tampa, Florida. The three stations are located on the vertices of a right triangle with orthogonal baselines. Distance between adjacent stations is about 12 Km. One station designated the main station will receive both the vertical and horizontal polarization of the 19.04 GHz beacon as well as the vertical polarization of the 28.56 GHz beacon. The two remote stations receive only the vertical polarization of the 19.04 GHz beacon for the study of diversity. All three stations are controlled by a programmable calculator located at the main station. Control and data acquisition of the remote stations are performed through data modem via telephone lines.

Design consideration of the three receivers and data acquisition equipment block diagrams will be discussed, and collected data will be presented.

8. COMSTAR OBSERVATIONS - A COMPARISON WITH RADIOMETRY: H. J. Bergmann and E. E. Muller, Bell Telephone Laboratories

Millimeter wave rain attenuation and diversity improvement statistics have been collected for the past several years by radiometric measurement at Bell Laboratories field stations near Denver, Chicago and Atlanta. The Beacon experimental package provided on the COMSTAR* satellites now permits the extension of these tests; combined beacon-radiometer observations are currently in progress at the latter two locations. This phase of the experimental program extends the dynamic measurement range, providing attenuation statistics with direct applicability towards 18/30 GHz satellite system design; it also provides data with which to compare radiometric observations with beacon attenuation measurements.

---

*The COMSTAR series of satellites is provided to the American Telephone and Telegraph Company for common carrier purposes by lease from the Comsat General Corporation.

This paper compares attenuation observations at several frequencies, on the basis of long-term averages as well as "instantaneous" values. The observed average attenuation ratio at 28.56 GHz and 19.04 GHz (≈2) is comparable to theoretic results. The "instantaneous" attenuation ratio, however, may depart very significantly from this average; this departure is a continuous function and will change significantly during short rain periods - thus suggesting a risk in indirect diversity improvement measurements.

Fade distribution statistics acquired from beacon measurements over an 8 month period are compared with longer-term radiometric results obtained at Atlanta and Chicago.

9. CTS BEACON RAIN ATTENUATION MEASUREMENTS: D. Davidson and O. G. Nackoney, GTE Laboratories

Propagation measurements using the 11.7GHz CTS beacon are being conducted by GTE Laboratories at Waltham, Mass. Measurements are made at a slant path angle of 23.5 degrees with a 3-meter, linear polarized, parabolic antenna. A phase-locked loop receiver coherently detects the received signal and continuously measures signal strength over a 20-dB dynamic range. A calculator-based measuring system collects data and computes daily attenuation exceedance statistics. The calculator is also used to automatically calibrate the receiver, re-acquire the signal during severe fades, and point the antenna. Meteorological data recorded at the site includes rain rate and wind velocity.

The paper will consist of a description of the terminal, followed by presentation of attenuation and related data measured since February 1977.

Commission G - Session 2

Thursday A.M. 0900 - 1105
IONOSPHERIC MAPPING II
Chairman: C. Rush, Air Force Geophysics Laboratory, Bedford, Mass.

1. PRACTICAL IMPLEMENTATION OF ADAPTIVE IONOSPHERIC RANGE ERROR CORRECTION FOR HIGH ACCURACY RADARS: A. H. Katz, T.I.S. Boak, III, and M. D. Grossi, Raytheon Company

The practical implementation of a radar's real-time adaptive scheme for ionospheric range error correction has confirmed that a hybrid hardware-software approach leads to an efficient utilization of radar resources. Specifically, an adaptive combination of dual-frequency measurements on targets of opportunity and an ionospheric model based on climatology represents a solution that minimizes the time that the radar must devote to ionospheric measurements for error correction. A stored model of the ionosphere can in fact provide the basic data for continuous range error correction, while the dual-frequency observations used to update the model can be made at times that are not at premium. For each hour of the day seven computer cards form the set of inputs required by the model and are valid for each day of one month. The first card specifies year, month, hour and an adjustable parameter C_0 that relates columnar electron content to range error. The other six cards define the dependence upon height, elevation and azimuth of the range error. The real-time dual-frequency update is used to adjust the parameter C_0. It can be shown that with this method the expected residual range errors are less than a few meters at L-band.

2. ACCURATE SPECIFICATION OF IONOSPHERIC ERRORS USING TRANSIT SATELLITE SIGNALS: N. M. Tomljanovich and L. W. Yoder, The MITRE Corporation

UHF radar accuracy is limited by ionospheric effects. Present correction procedures based on predictions from the monthly median behavior of the ionosphere are inadequate to account for the day to day variability which can be large and can at times exceed the desired accuracy.

A technique using Navy Navigation Satellite System (TRANSIT) signals in near-real time to determine the actual day to day behavior of the ionosphere has been developed. An analysis using real measurements has been conducted to establish the accuracy of the total electron content (TEC) information determined from TRANSIT signals. Results of our investigation showing a factor of 4 improvement over monthly predictions are presented.

A system using this TEC measurement technique, augmented by climatological predictions, is presently being developed to provide near-real time ionospheric correction over an entire radar coverage.

3. SPATIAL CORRELATION OF TRANSIONOSPHERIC SIGNAL TIME-DELAY: H. Soicher, Communications/ADP Laboratory, US Army Electronics Command

The requirement for high precision accuracy in radar detection, in earth-satellite orbit determination, and in satellite navigation systems necessitates that the signal data used be corrected for the errors imposed by the ionosphere. Time delay, or equivalently range errors are always encountered in transionospheric measurements because the electromagnetic propagation velocity in the medium is slightly less than the free space velocity. For frequencies at VHF and above, the excess time delay is inversely proportional to the square of the frequency and is directly proportional to the integrated electron density along the propagation path (i.e., total electron content $\equiv$ TEC). Thus, if TEC is measured or is accurately predicted, a perfect correction to ranging can be performed. For improved accuracy, prediction techniques should be supported by periodic (preferably real time) updating of data at specified locations. The question arises as to the extent of the geographic area surrounding a station with real-time TEC determination capabilities, within which TEC values could be interpolated within accepted accuracy.

To this end, an investigation designed to determine the correlation between TEC values at Fort Monmouth, NJ (40.18^{o}N, 74.06^{o}W) and Richmond, Florida (25.60^{o}N, 80.40^{o}W) was undertaken. Beacon transmissions aboard the geostationary Application Technology Satellite ATS-6 were used to determine the TEC at the two stations by means of the Faraday rotation technique. Correlation analysis was performed for monthly and daily intervals during the equinoctical and winter periods.

4. CORRECTION TO THE IONOSPHERIC TOTAL ELECTRON CONTENT DATA FOR THE NON-ZERO INCLINATION OF GEOSTATIONARY SATELLITES: Y. N. Huang, Telecommunication Laboratories, M.O.C., Republic of China

In calculating TEC value from the observed Faraday rotation angle of the VHF beacon signal transmitted from geostationary satellites, the Faraday factor M and the angle α between the spin axis of the satellite and the prime vertical of the observer have been assumed to be diurnally constant by most workers. According to SPACEWARN BULLETINE, the inclination of most geostationary satellites is non-zero. This non-zero inclination makes M and α to vary diurnally and may induce errors in observed TEC values if M and α were taken to be diurnally constant as were done by most workers in the past. Using TEC data obtained at Lunping (25.00^{o}N; 121.17^{o}E) by receiving 136.44 MHz signal from INTELSAT 2F3 geostationary satellite which had an inclination of

about 7^{o}, the author has estimated the possible errors caused by the non-zero inclination of the satellite, and obatined the following results. (a) The absolute error caused by the non-zero inclination of the satellite is small during nighttime when TEC is small and large during daytime when TEC is large. Seasonally, the error is larger in winter and equinoctical months than in summer months. (b) The maximum relative error amounts to about 20% without any significant seasonal difference. However, the phase of the diurnal pattern varies from month to month because of the gradual phase variation of the diurnal locus in subsatellite point. (c) Most of the TEC data obtained by TEC stations might have not made corrections for the non-zero inclination effect. Since the error is so large that the careless usage of these data may lead to faulse results. (d) The diurnal patterns of absolute and relative errors change so rapidly in a month that it seems necessary to renew the diurnal M and α curves every day or at least every week in order to obtain more reliable and exact TEC data.

5. MULTIDISCIPLINARY EVENT-ORIENTED DATA COLLECTION FOR 30 APRIL 1976: R. O. Conkright and D. B. Bucknam, World Data Center A for Solar-Terrestrial Physics

A multidisciplinary collection of data relevant to the ground level solar cosmic ray event of 30 April 1976 is presented. This date choice was made from within the Study of Travelling Interplanetary Phenomena Interval II. Ionospheric data such as f-plots, N(h) profiles and riometer events are included. This is a sample collection to illustrate a new service being initiated by World Data Center A for Solar-Terrestrial Physics at cost of reproduction. Event-oriented data collections for specific time periods have a particular value, especially for multidisciplinary investigations. World Data Center A for Solar-Terrestrial Physics has, from time to time over the years, published detailed data collections for specific events in the UAG Report series. The World Data Center A for Solar-Terrestrial Physics now offers to make available to any researcher its capabilities and facilities for collecting data and organizing them in a variety of useful formats to satisfy the researcher's needs. Special event-oriented data collections of this type can be as comprehensive or as narrow, in terms of data from associated disciplines, as the researcher desires.

Commission H - Session 1

Thursday A.M. 0900 - 1130
THEORY OF WAVES AND ANTENNAS IN PLASMAS
Chairman: T.N.C. Wang, Stanford Research Institute, Menlo Park, CA

1. WAVE CHARACTERIZATION IN MAGNETOPLASMA BY AN INVARIANT METHOD: H. C. Chen, Department of Electrical Engineering, Ohio University

An invariant method is presented in this paper to unify and systematize the analysis of wave characteristics in a magnetoplasma. The results, all in invariant forms, include (1) the dispersion equation of a magnetoplasma, (2) the polarization and the field vectors, (3) the Poynting's vector and energy density, and (4) the relationship among the wave vector surface, the group velocity vector and the time average Poynting's vector. The distinct advantage of the invariant method over the conventional one is that the former eliminates the necessity of coordinate systems. The results thus obtained are therefore general and easily correlated to experiments.

2. A TECHNIQUE TO PREDICT NONLINEAR PROPAGATION OF INTENSE ELECTROMAGNETIC PULSES THROUGH WEAKLY IONIZED PLASMAS: W. A. Seidler, Simulation Physics, Inc.

A technique which predicts the nonlinear propagation of intense electromagnetic signals in weakly ionized plasmas has been developed. Moments of the Boltzmann equation are solved simultaneously with the high frequency approximations for propagating electromagnetic fields using a modification of Gear's multistep techniques. Comparisons are made with linear propagation models. An example is shown of intense nonlinear propagation where collision absorption causes a propagating pulse to be almost completely damped. The stability and relative error analysis are discussed.

3. NONLINEAR INTERACTION OF WAVES IN BOUNDED MEDIA: J. C. Hassab, Naval Underwater Systems Center

The radiation of an intense wave into the ionosphere or ocean produces a nonlinear behavior in the medium which in turn influences the propagation characteristics of that wave. The self-interaction process changes the absorption and phase of the wave and also produces harmonics of its fundamental frequency. Methods for the theoretical analysis of such waves in nonlinear media are of interest. To permit an analytical description of the nonlinear interaction, simplifying assumptions are here made, where the medium is presumed to be isotropic with plane parallel boundaries. Some complications are included in the analysis, namely that of a bounded medium with varying properties. The wave-medium interaction process is mathematically depicted by a

nonlinear Fredholm integral equation of the second kind. Blithely applied, the method of successive approximations is known to lead to a divergent series solution. Here a new functional series representation of the solution is produced for a second order nonlinearity in the wave field. It is shown that the present series summation remains convergent outside the region of validity of the regular perturbation series. The bifurcation equation is produced and questions of uniqueness, of type and number of solutions are addressed. The form of the solution allows identification and characterization of order of contribution by the various physical phenomena.

4. COMPUTATION OF NON-LINEAR AND SHEATH TRANSIT TIME EFFECTS FOR AC PLASMA PROBES: J. Moron and H. Weil, The University of Michigan

A numerical procedure is explored to solve the coupled ion and electron Vlasov equations and Poisson's equation in the vicinity of a cylindrical surface immersed in a plasma. The surface potential is, at time t = 0, forced to vary sinusoidally about a fixed bias potential. The computations proceed from t = 0 using a field of initial values of the distribution function and potential obtained from steady state solutions. The method permits arbitrary amplitude of the forcing AC potential and arbitrary frequency so that non-linear plasma response can be studied as well as the effects of the non-zero time of transit of the ions and electrons across the sheath. The procedure involves expansion of the distribution functions in a finite series of products of Hermite polynomials in the radial and in the transverse velocities. The resultant space and time dependent equations for the expansion coefficients are integrated numerically using a Lax-Wendroff scheme. Self-consistancy of the equations is obtained by an iteration procedure. Appropriate normalization and an artificial damping term are used to accelerate convergence and reduce numerical instabilities. Results for number densities and potential in the sheath and for current drawn by the probe are presented.

5. EXACT FORMULAE OF THE CURRENT AND INPUT ADMITTANCE FOR A LONG ANTENNA IN A MAGNETOPLASMA: T. N. C. Wang, Stanford Research Institute

This paper presents an exact mathematical formulation of the antenna current and its input admittance for the antenna embedded in a uniform, multicomponent magnetoplasma. To facilitate the analysis, we consider an infinitely long, electrically thin and a perfectly conducting cylindrical antenna, with its orientation parallel to the static magnetic field. Two cases of the magnetoplasma model, cold electron and cold ions, and warm electron and cold ions, are considered. Exact formulae for the antenna current and the input admittance are derived. Limiting cases of the derived formulae are examined. As the electron temperature approaches zero, our solution for the plasma model with a warm electron species simplifies to that for the cold plasma model. Furthermore, as the plasma parameters degenerate to those in free space, the solution reduces

to the well-known expression derived by Hellén. In the analysis for the warm magnetoplasma case, our method can be extended to include any number of warm-particle species in the plasma.

Several physical predictions of the antenna current and its admittance can be obtained by simply checking the exact integral solution. The exact current formulae for a finite antenna in a magnetoplasma are still difficult to derive analytically. However, in certain cases the formal solution derived herewith can be used to justify neglecting the end-reflections. Under such conditions, our formulae become valid for predicting the current distribution for an antenna with a finite length.

6. ANALYSIS OF MICROWAVE SCATTERING FROM A PLASMA COLUMN USING THE FIRST BORN APPROXIMATION: S. E. Rosenthal and F. W. Crawford, Institute for Plasma Research, Stanford University

Linear microwave scattering from a cold, radially inhomogeneous plasma column is a potentially useful diagnostic of electron density: in principle, the radial density profile can be reconstructed from an analysis of the angular scattering spectrum. Using partial wave analysis, this inverse scattering problem requires considerable computational effort, since the indirect process must be carried out of iteration towards a self-consistent solution of a non-homogeneous Helmholtz equation which contains information on the profile. Direct inversion is possible, however, in the restricted case of weak scattering, when the first Born Approximation (BA) yields a Fourier transform relation between the angular spectrum and the radial density profile.[1] An appropriate validity criterion for the BA, which is less restrictive than the typical weak scattering criterion, $(\omega_0/\omega_i)^2 \ll 1$, has been derived as $(ka)^2(kR)^{-1/2}(\omega_0/\omega_i)^2 \ll 1$. Here, ω_0 is the maximum electron plasma frequency in the column, ω_i is the incident microwave frequency, $k = \omega_i/c$, a is the radius of the column, and R is the radial distance at which the angular spectrum is sampled. The Born-inversion technique has been investigated in a computer study, and has been found to agree well with exact partial wave analysis results when the validity criterion is satisfied.

1. Y. Midzuno, J. Phys. Soc. Japan 16, 971 (1961).

Commission B - Session 5

Thursday P.M. - 1400 - 1650
SCATTERING AND SHIELDING
Chairman: D. R. Wilton, University of Mississippi

1. A MATHEMATICAL METHOD OF CALCULATING AND MEASURING THE SHIELDING EFFECTIVENESS OF CYLINDRICAL ENCLOSURES: A. Rashid, General Dynamics Corporation, Convair Div.

The present method of measuring the shielding effectiveness of an enclosure by MIL-STD-1377 has raised many questions without answers, and, basically the method does not appear to have generated confidence in many personnel working in the EMC community. A new method is described to both calculate and measure the shielding effectiveness of cylindrical enclosures. In this method, the incident plane wave is expanded in cylindrical functions, and, by matching the boundary condition, the current on the outside wall of the enclosure is calculated for both the horizontal and vertical polarizations. The current on the inside wall is calculated based upon the work of King. The electromagnetic field inside the enclosure is expanded in terms of cylindrical functions and the coefficients of these cylindrical functions are calculated in terms of the currents on the inside wall of the enclosure. The open circuit voltage developed across a wire is calculated by assuming a sinusoidal current distribution on the wire, and, also by using the electric field along the wire, whose magnitude and phase varies along the length of the wire. The ratio of the open circuit voltage developed on the wire by a plane wave without the enclosure to the open circuit voltage developed on the same wire inside the enclosure is used to calculate the shielding effectiveness of the cylindrical enclosure. Experimental technique is described to collect data on shielding effectiveness of a tail cone. Both the theoretical and measured data are presented. The method may be extended to measure shielding effectiveness of enclosure of any other geometrically describably enclosures.

2. SCATTERING FROM FINITE AND THIN DIELECTRIC CYLINDERS: N. K. Uzunoglu, N. G. Alexopoulos, J. G. Fikioris, National Technical University of Athens.

The scattering from dielectric finite cylinders with arbitrary length and refractive index but with small radius to wavelength ratio is formulated, by using the Lippman-Schwinger equation for the scattering process. The free space Green's function is expanded in cylindrical wave functions, then by assuming for a thin finite cylinder the internal field to be constant over the cross section of the scatterer, a one dimensional integral equation is obtained for the internal field. In order to describe the internal field, several Fourier expansions are considered and convergence and numerical stability conditions are investigated. The formulation is applicable for any incidence and scattering direction. The scattering amplitude is obtained by an integration over the internal field multiplied by a plane wave.

The scattering, attenuation and depolarization of millimetric and centimetric waves from ice particles of needle shapes can be calculated using this method. Cross polar discrimination and attenuation for several frequencies will be presented. Especially the orientation of ice particles by strong atmospheric electrostatic fields can cause a limitation for satellite-earth communication.

3. A STUDY OF THE CHARGE AND CURRENT INDUCED ON AN AIRCRAFT IN AN EMP SIMULATOR FACILITY: C. D. Taylor, K. T. Chen, T. T. Crow, Mississippi State University.

A study of the aircraft skin current and charge is made for an aircraft under the illumination of the electromagnetic field produced by a nuclear EMP simulator. This work is motivated by the need to relate the response of an aircraft in the EMP simulator to the response of an aircraft under actual EMP illumination. The analysis is directed toward a specific EMP simulator at Kirtland AFB, New Mexico, however, the methodology presented is applicable to other types of simulator facilities.

A theoretical-numerical solution technique is developed to determine the current and charge densities induced on an aircraft by an electromagnetic pulse. To represent the aircraft the formulation uses an electromagnetic model formed with axial segments of bodies of revolution. Verification of the theoretical model is accomplished by extensive comparisons with measured data obtained by using scale models.

Measured and calculated data are also presented for an EC-135 aircraft in the ATHAMAS I (also called HPD) simulator at Kirtland AFB, New Mexico. In addition the EC-135 is considered to be illuminated inflight by a typical estimate of the nuclear EMP. Comparison of the inflight data with corresponding simulator data is made to investigate the possibility of general trends.

4. DIFFRACTION BY A SLOTTED, CONDUCTING SCREEN IN THE PRESENCE OF A FINITELY-CONDUCTING GROUND: C. M. Butler, R. D. Nevels, University of Mississippi, A. Q. Howard, University of Arizona

The purpose of this paper is to present the results of an investigation of the effects of the presence of a finitely-conducting ground, e.g., earth or sea, upon electromagnetic diffraction by a uniform-width, infinite slot in a planar, conducting screen. Equations are formulated for the cases of illumination being TE and TM to the slot axis, and data are obtained from numerical solutions of these equations. It is shown that the influence of the ground is less significant in the TE than in the TM case. In the TE case, the presence of the ground alters the magnitude but has little effect on the distribution of the electric field in the slot, whereas, in the TM case, both can be influenced. The modification due to the presence of the ground is highly dependent upon the slot width in the latter case but not in the former.

Infinite Sommerfeld integrals
→ see Howell

5. COMPUTATION OF THE CURRENT INDUCED ON A RECTANGULAR PLATE BEHIND A PLANAR SCREEN BY AN ELECTROMAGNETIC FIELD WHICH PENETRATES THE SCREEN THROUGH A SMALL APERTURE: A. W. Glisson, C. M. Butler, University of Mississippi.

Attention in this paper is addressed to the problem of determining the current induced on a rectangular plate located in the proximity of a small aperture in a conducting screen. Problems of this nature arise in EMP and shielding considerations. Vector integro-differential equations, which account fully for the coupling between the small aperture and the plate, are discussed and are solved numerically for several cases of interest. Currents induced on the plate are presented for cases involving small circular and elliptic apertures and plates of several sizes up to $1\lambda \times 1\lambda$; also the dependence of current upon the distance between the screen and plate is discussed. Comparisons are made with data obtained for cases in which the backscattered field in the aperture, arising from currents on the plate, is ignored.

6. CURRENT COMPUTATION BY THE FINITE ELEMENT METHOD: A. Sankar, T. C. Tong, W. A. Oliver, TRW Defense and Space Systems Group.

In spite of its origin in structural mechanics, the finite element method can be used as an efficient numerical method for solving complicated boundary value problems in many other fields. Here, the method is exploited to solve electromagnetic scattering problems on conducting structures.

The finite element method, as used here, is predicated on a variational principle governing the physics of the problem and an approximation procedure to carry out the variational expression integration. A variational principle is derived and found to involve a double integral. A transformation is then used to reduce the double integral into a repeated integral. This form is then used in conjunction with the finite element approximation to compute the induced currents on perfectly conducting thin wires and plates due to an incident plane wave. The wire and the plate are discretized into linear and triangular elements, respectively, and linear shape functions constructed from the nodal currents and local coordinates are used. The predicted currents are used to calculate the radar cross sections for both cases. The current and cross section predictions are then compared with other known results and the agreement is found to be excellent. The numerical results are tested for stability, accuracy, convergence, efficiency and economy.

Commission C - Session 2

Thursday P.M. - 1400 - 1650
SIGNAL PROCESSING
Chairman: B. D. Steinberg, University of Pennsylvania

1. INFORMATION THEORY AND RADAR DETECTION: A. Ephremides, Electrical Engineering Department, University of Maryland

The performance bounds and capabilities of radar detection system can be evaluated by casting the problem in a setting described by the entropy of the target motion. In most cases advantage is taken of the Markovian nature of the motion process. Detection is studied in discrete time and in discrete state space for the motion vector by partitioning the target area into finite cells.

The theory is applied to "Track while Scan" (TWS) radar which uses a tracking window for the detected target. The performance in finite time as well as the asymptotic characteristics are obtained for fixed false alarm rate. In the study of this problem several non-surprising connections to coding-decoding theory are pointed out. Each cell is modeled as a binary communication channel and use is made of the Shannon Information theorems. Many of the results generalize to multi-target environments.

2. AN EXACT ANALYSIS OF THE ACCURACY OF AN AMPLITUDE COMPARISON MONOPULSE RADAR: I. Kanter, Raytheon

The usually employed approximation for the effect of interference on the performance of an amplitude comparison monopulse radar yields the results that (i) the estimate is unbiased and (ii) the variance in the estimate is inversely proportional to the signal to noise ratio. This approximation is employed when the target is on axis, the signal to noise ratio is "large" (how large has never been established by analysis, since the approximation linearizes the monopulse ratio and the effect of neglecting higher order terms in the noise to signal ratio cannot be determined) and the interferences in the difference and sum channels are independent, zero mean thermal noises with equal average power.

The present paper gives an exact analysis of the non-linear problem when there are interfering targets as well as correlated, unequal average power noises in the difference and sum channels. It is thus applicable to multiple targets, multipath effects, clutter type interference and man-made noise sources. From the exact probability density function of the monopulse ratio, both the bias and the variance of the estimator are given and the results are compared to those of the approximate theory for arbitrary signal to noise ratio and arbitrary correlation between the difference and sum noises.

3. A MULTIPLE-PROCESSING DOPPLER FILTER: J. K. Hsiao, Naval Research Laboratory

In a radar (or acoustic system) the undesired clutter signal usually can be discriminated by use of a doppler filter. This filter can be either a stop-band and pass-band type (such as MTI in radar work) or a multiple-band filter (as a FFT filter). However, in many practical cases, this type of filter may not be adequate to achieve the desired clutter rejection. For example, when the radar return contains more than one type of clutter and each has a different doppler spectral distribution and their mean doppler may not be zero, a fixed pass-band and stop-band MTI filter certainly is not enough to filter out this type of clutter. On the other hand, due to the limitation of sidelobe level, a multiple-band filter usually does not have the capability to reject a strong and widespread clutter. To alleviate these problems, a cascaded system may be used. For example, to reject both surface and volume clutter simultaneously, one may use two MTI filters in cascade. A FFT filter may follow them to resolve target dopplers. This in general requires a large number of radar pulses. In the above example, if the two MTI stages are respectively 3 and 4 pulse cancellers while the doppler filter is an 8-point FFT, a minimum of 15 pulses is required. Due to data rate and other considerations, this number of pulses may not be obtainable in a radar system.

In this paper a multiple-processing system will be described in which the same set of radar pulses will be used to perform the filtering action in each filter stage simultaneously. It thus reduces the number of pulses required yet achieves the same performances. The performance of such a filter system will be analyzed and compared to a conventional multiple stage filter.

4. INFORMATION EXTRACTION USING PRONY'S METHOD: E. K. Miller, S. Aggarwal, Lawrence Livermore Laboratory

Prony's method is a technique for determining the coefficient (poles and residues in the frequency domain) of an exponential series. Recently, applications of this method have been considered in electromagnetics because of the possibility the method offers for obtaining the SEM poles of conducting objects from their transient response. In addition, Prony's method appears useful in offering insight into the general problem of extracting useful information from one-dimensional data.

In particular, Prony's method can be viewed as a transformation of data from one form to another. Many numerical procedures - for example, matrix inversion - can be similarly viewed. It is intuitively apparent that the information that can be extracted from the transformed data can at best remain the same or actually diminish. Clearly, retention of the greatest amount of information possible in the transformed data is desirable. Thus, in order to evaluate the information transformation process, some way of determining the amount of information contained in the original data and the transformed data must be considered.

These questions of information content and data transformation are considered in this paper. Concepts of data rank (number of poles from exponential data) and data precision are used to define information content. Prony's method is then studied from a data transformation viewpoint by first defining a waveform using pole-residue information, sampling the waveform to obtain the associated data, and then using Prony's method to transform the data and compare it to the original information content. Other numerical processes - in particular matrix inversion - are similarly examined. It is shown that problems of ill conditioning are related more to the data than to the process. Finally, applications of Prony's method to other physical problems with exponential solutions are also briefly considered.

5. TWO RECURSIVE ESTIMATES OF AUTHOREGRESSIVE MODELS BASED ON MAXIMUM LIKELIHOOD: B. Dickinson, Princeton University

The fitting of autoregressive models to time series data has received much recent attention. The use of high order autoregressive models for spectral smoothing and estimation, pitch estimation for voiced speech siganls, and as part of two-stage least squares identification methods for mixed autoregressive-moving average models has stimulated research on computational methods for this problem. The well-known Yule-Walker estimates obtained by a recursive algorithm due to Levinson, provide one method of estimation with key advantages for high order models: the number of arithmetic operations required grows only as the square of the model order, storage requirements grow in proportion to model order, and models are generated recursively in increasing order. This last property can be useful in deciding the "best" model to fit the data.

The Yule-Walker method can be viewed as a rough approximation to maximum likelihood estimation. In this paper we will give two additional approximate maximum likelihood methods and a recursive solution procedure resembling the Levinson algorithm. The first is a least squares method of Box and Jenkins, but the algorithm is new. The second is an approximation motivated by the structural features of the equations that permit their solution with recursive methods. Experimental results on real time series data will be presented.

6. MINIMIZED FOUR- AND FIVE-PLANE PROCESSORS: P. Carlson, R. Francois, University of Washington

Considering a Fourier transform analog processor as a minimized two-plane processor and a convolutional/correlation analog processor as a minimized three-plane processor, one can examine minimized four-plane and five-plane processors as basic processor elements. Using the Rayleigh-Sommerfeld propagation integral equation in the Fresnel zone case, the four-plane processor Kernel is the first processor kernel in the hierarchy of n-plane processors that is integral in form. The two- and three-plane processing kernels are simple non-integral, explicit, and relatively easy to interpret. A generalized four-plane kernel is not so easy to interpret, but it has several forms that can be compared to known information processing measures. One example is like the Woodward Ambiguity function, used for range and doppler signal analysis. Another four-plane example is an image erecting system for correcting geometrical distortions or oblique observation planes. The five-plane kernel is a new and interesting case that allows the development of new processing measures. To illustrate, the five-plane kernel can be arranged in the form of a triple complex correlation. An example could be a correlation over doppler and range variables of the transmitted signal, the received signal, and a reference library signal; or it could be of the transmitted signal, a received signal at time, t_1, and another received signal at time, t_2. All of these are examples of cases where the desire is to improve the signal-to-noise ratio and sophistication of information processing measures.

7. NEW FEATURES OF ADAPTIVE OPTICAL DATA PROCESSORS: P. Carlson, University of Washington

Adaptive optical/digital data processors have been developed and basically optimize the parallel structure of the optical processor and utilize the serial data reduction of the digital processor in the output or interface space. A simple processor for recognizing and counting blood cells has been developed utilizing a digitally sampled output space and simple linear regression model for predicting the count. This model has been extended to incorporate a minimum-mean-square-error filter in an intermediate Fourier plane. The basic concept is to enhance the desired signal-space and reduce the effect of the largely dominating noise processes.

A discussion concerning the changes in the linear regression model will be given to illustrate the flexibility of using various sampling strategies and independent variable selection. The relative worth of various vector components in the signal space will be demonstrated and compared with the earlier model development.

Experimental results for both methods will be compared and examples of the intermediate plane filters will be presented.

Commission E - Session 2

Thursday P.M. - 1400 - 1630
NATURAL RADIO NOISE
Chairman: G.H. Price, Stanford Research Institute, Menlo Park, CA

1. MEASUREMENTS AND NOISE EXCISION STUDIES OF ATMOSPHERIC NOISE FROM 1.0 TO 4.0 kHz: R. J. Dinger, J. R. Davis and W. D. Meyers, Communications Sciences Division, Naval Research Laboratory

Measurements of ambient atmospheric noise have been taken in a frequency range of 1.5 to 4.0 kHz at a site located near Tromsø, Norway. The measurement periods include data from summer and winter. The receiver consists of a broadband (untuned) loop antenna and low noise amplifier, a tape recorder that records four filtered narrow-band signals distributed across the bandwidth, and a real-time amplitude probability distribution (APD) computer. Preliminary analysis of the data indicates that at 3 kHz the summer Norway mean square noise level varies from a daily low of approximately -179 dB // 1 A/m/$\sqrt{\text{Hz}}$ (-179 dBH), attained during local afternoon, to a high of approximately -170 dBH, attained during local midnight. In winter, the corresponding noise levels are -182 dBH and -173 dBH. Brief periods (several hours) in which the noise is -165 dBH and higher have also been observed in summer and winter. The APD is log-normal between the 1% and 99% exceedance levels, except during the most disturbed periods. The results of a noise excision study using non-linear processing show that the effective noise level can be decreased by 8 dB by using a simple clipper.

2. REMOTE OBSERVATIONS OF IDENTIFIABLE ATMOSPHERICS FROM SEVERE THUNDERSTORMS: W. B. Zavoli, Stanford Research Institute

Using a directional HF antenna with a nominal beamwidth of 0.5^{o}, experiments were conducted to study remote atmospherics from severe thunderstorms. Information from National Weather Service severe weather forecasts and on-line ionospheric soundings provided guidance in scanning the California based directional antenna across midwestern regions of the country likely to develop tornadoes. Analysis of the data recorded during periods when severe storm events were sighted led to the discovery of a class of atmospherics significantly different from those radiated by normal thunderstorm activity. These atmospherics take the form of randomly occurring impulses. A data processing technique was devised to extract this class of atmospherics from the remaining radio noise background. Based on 23 hours of data, taken on four separate days, a statistically significant correlation between the reception of these impulses and the presence of remote severe thunderstorms was found.

3. H.F. ATMOSPHERIC NOISE MODELS FOR DISTRUBED ENVIRONMENT: G. H. Price and E. G. Bauman, Stanford Research Institute

Prediction of HF signal-to-noise ratios for disturbed conditions requires a noise model that permits assessment of the effects of the propagation disturbance on the noise power. This requirement precludes direct use of standard noise data. Formulation of the noise in terms of a few dominant discrete sources, although reasonably successful for many environments, becomes increasingly awkward for severly disturbed environments in which the presence of large propagation losses leads to the dominance of minimally attenuated noise sources. The use of thunderstorm occurrence statistics and a nominal cosmic-noise model to predict antenna noise temperatures under such conditions is described.

4. VHF RADIO EMISSIONS FROM LIGHTNING: J. B. Smyth and D. C. Smyth, Smyth Research Associates

A new theory of the electromagnetic characteristics of lightning (Radio Science December 1976) described the radio associated luminous observables of a lightning discharge. Terrestrial observations of VHF radio emissions at to to 30 kilometers have shown strong fields associated with the leader and weak to non-detectable fields associated with the return stroke. These and other phenomena here-to-fore undescrible theoretically and considered anomalies are shown to be the normal and expected characteristics of lightning discharges when examined and described on the bases of the aforesaid new theory.

5. RADIO FREQUENCY INTERFERENCE MEASUREMENTS AT 150 RURAL RESIDENCES: D. N. March, Electrical Engineering Department, Montana State University

Measurements of the RFI present at 150 rural residences along proposed EHV power line routes in Montana, Idaho, and Oregon were recorded during the summers of 1975 and 1976. A repeatable test procedure was developed that recorded the peak, quasi-peak, and average values of the signals and noise from 10 KHz to 1000 MHz. The bandwidth dependence of the noise was measured. The primary source of RFI at each residence was identified. The quality of the residents' tv and radio communications was observed and recorded where permission was granted. Other parameters, including weather data, were recorded at each site. The details of the measurement tests and a summary of the results are presented in the paper.

6. FIGURES OF MERIT FOR MICROWAVE RADIOMETERS: S. Sensiper, Self Employed Consultant

The increasing interest in microwave radiometers for imaging applications suggests that some measure of performance would be useful for comparing or even optimizing such systems. The relevant parameters such as antenna size, operating frequency and bandwidth, integration time, etc. are clearly parts of such a figure

of merit. A particular form of such a figure of merit is chosen and some examples are discussed where the influence of path or atmospheric loss on the frequency choice is shown.

In one form of the figure of merit the spatial cutoff frequency of the antenna aperture is immediately evident. This in turn recalls the various figures of merit applied to optical imaging systems. Some comparison of these with the radiometric figure of merit noted here as well as others is briefly discussed.

Commission F - Session 5

Thursday P.M. 1400 - 1700
RADIO METEOROLOGY
Chairman: A. T. Waterman, Electronics Lab., Stanford University

1. AEROSOL MEASUREMENTS IN THE MARINE BOUNDARY LAYER AT SAN DIEGO: D. R. Jensen

Measurements of aerosol size distributions have been made in the marine environment at San Diego since April 1976 using a PMS ASSP-100 knollenberg Spectrometer. Aerosol size distribution measurements from both ground based and airborne spectrometers have been made during different meteorological conditions including fog, haze and clear skies. Continuous observations during onset and dissipation of a Santa Ana related fog shows the aerosol particile size distribution and concentrations to be in general agreement with some theories of fog formation and dissipation. Aircraft observations show the horizontal and vertical variability of the aerosol distributions and are compared with simultaneous ground based measurements. Simultaneous drop size distributions measured by 1) two Knollenberg spectrometers and 2) a Royco and Knollenberg spectrometer have been made. These data will be presented and discussed.

2. MICROWAVE SENSING OF ATMOSPHERIC TEMPERATURE AND WATER: M. T. Decker, E. R. Westwater, and F. O. Guiraud, NOAA/ERL/Wave Propagation Laboratory

The feasibility of using a multi-channel microwave radiometer mounted on an ocean-based data buoy to remotely sense atmospheric temperature structure is being investigated theoretically and experimentally. Experiments are being conducted jointly by NOAA and the Jet Propulsion Laboratory on the California coast and aboard the Canadian ship Quadra in the Gulf of Alaska. Zenith measurements of thermal emission are made at three frequencies in the 50-60 GHz oxygen absorption band and corrected for the presence of cloud and water vapor by additional measurements near 22 and 31 GHz. Using statistical inversion, the resulting equivalent clear-sky radiation is used to obtain temperature profiles. Both theory and experiment indicate that useful measurements can be made under nearly all cloudy conditions except during rain. RMS differences between these temperature measurements and data from concurrent radiosondes range from less than 1 °C near the surface to about 2 °C at heights of about 8 km. In addition, these measurements are used to determine the line integrals of water vapor and cloud liquid in the pointing direction of the radiometer. Vertical profiles of water vapor are also determined and compared with data from radiosondes. In all cases, the observed differences are quite close to the theoretical prodictions which suggests that these techniques can be evaluated with confidence theoretically for various climatological and operational conditions.

3. A SIMPLIFIED OPTICAL RAIN GAUGE: T. Wang, K. B. Earnshaw and R. S. Lawrence, NOAA Research Laboratories

We describe a technique for measuring path-averaged rain parameters by analyzing the rainfall-induced scintillations of a laser beam. From the variance of the irradiance scintillation as seen by a line-detector, we are able to measure the average rain rate along the optical path. Though this technique does require a prior assumption of the raindrop-size distribution, the dependence is extremely weak. Sample experimental results show good agreement with conventional tipping-bucket rain-gauge data.

4. PRELIMINARY RESULTS FROM A LASER WEATHER IDENTIFIER: K. B. Earnshaw, T. Wang, and R. S. Lawrence, NOAA Research Laboratories

We have constructed and made initial tests of a prototype optical forward-scatter instrument designed to permit automatic identification of precipitation and other obscurations of visibility. We discuss the nature of the effects of various weather phenomena on a laser beam, with particular emphasis on the temporal power spectrum and the space-time correlation function of the intensity fluctuations of the direct beam and on narrow-angle forward scatter. Then we describe how these effects have influenced the design of the laser weather identifier. Finally, we present and discuss sample recordings made from the various outputs of the instrument.

5. OPTICAL C_n^2 AND WIND SENSING: THE EFFECTS OF SATURATION OF SCINTILLATION: T. Wang, G. R. Ochs and S. F. Clifford, NOAA Research Laboratories

Using an extension of the first-order perturbation theory of optical scintillation that accounts for the observed variance and covariance of the amplitude fluctuations in strong integrated turbulence, we analyze the experimentally observed changes in the operation of our optical path-averaged C_n^2 and wind sensors. The theory suggests a transmitter-receiver configuration that can nearly eliminate the performance-degrading effects of strong turbulence. Based on this analysis, we have developed saturation-resistant optical C_n^2 and wind sensors that maintain their calibrations and weighting functions throughout the observed range of integrated-turbulence values.

6. METEOROLOGICAL STUDIES USING THE SCANNING MICROWAVE SPECTROMETER: N. C. Grody, W. C. Shen, P. P. Pellegrino, National Environmental Satellite Service, National Oceanic and Atmospheric Administration

The scanning microwave spectrometer (SCAMS) aboard Nimbus 6 detects thermal radiation emitted by the earth in the oxygen band (52.85, 53.85, 55.45, GHZ) and water vapor region (22.23, 31.65 GHZ), with a 150 to 350 KM field of view and 2400 KM scan coverage on Earth. Atmospheric vertical temperature profiles and water content are the principal meteorological variables derived from SCAMS measurements in the oxygen and water vapor spectral regions, respectively. Horizontal temperature gradiants are used to obtain winds based on the geostrophic approximation. Because of the cloud penetrating property of microwave radiation, together with the high stability and sensitivity of the SCAMS instrument, many of the problems encountered with other remote sensing instruments are absent in the SCAMS measurements. Several synoptic and dynamical case studies are presented showing the impact of SCAMS measurements on the analyses of meteorological systems. Comparisons are made with conventional data sources such as radiosonde measurements and satellite cloud imagery as well as numerical prediction models developed by the National Meteorological Center.

7. LOW ELEVATION PROPAGATION MEASUREMENTS AT 30 GHz ON A SATELLITE-EARTH PATH: A. W. Straiton, B. M. Fannin and W. J. Vogel, Electrical Engineering Research Laboratory, The University of Texas at Austin

During a recent orbit change the ATS-6 satellite ascended over the horizon in Texas at a rate of about 1.3 degrees per day. To determine the effect of low elevation paths over water on the signal amplitude a receiver was set up at Port Aransas, Texas. It monitored daily for at least one hour the 30 GHz signal level. During that time the elevation angle changed from 1.5° to 17.3°.

Presented are the results of the data analysis performed on a total of 59 samples of 205 seconds each. Despite variations from sample to sample it was found that the mean dB attenuation can be approximated by (.8) times the number of airmasses traversed. The standard deviation showed some levelling off at about 6 dB below 4° elevation. Power spectra of the fluctuations were produced and their frequency dependence has approximately 8/3 as an upper limit to the negative exponent. Their variability points out the nonstationarity of the strong fluctuations observed at low angles. A rain attenuation event was observed and its influence on the signal is described.

8. ATS-6 IN-TRANSIT C-BAND MULTIPATH INVESTIGATION: J.P. Corrigan, ATS Project Office, H. Hanft and W. H. Asplund-Westinghouse Defense & Electronic Systems Center

Various propagation phenomena were noted during the initial drift period of ATS-6 from 94° W longitude to 35° E longitude to support European operations. The initial analysis

of the preliminary data indicated a unique geometry of the Indian Earth Station at Ahmedabad, India (used in the experiment) because its antenna was located on a hill overlooking a flat plain with no obstructions in the line of sight to the satellite. This resulted in the performance of a special propagation experiment during the return drift period when ATS-6 moved back from 35° E longitude to 140° W longitude. The experiment tests were made at low antenna elevation angles (under five degrees elevation) for C-band propagation paths over an essentially smooth earth.

9. AMPLITUDE SCINTILLATIONS OF 15-GHz SATELLITE SIGNALS AS RELATED TO METEOROLOGICAL VARIABLES: C.A. Levis, Advanced Study Program, National Center for Atmospheric Research

The amplitude scintillations of 15-GHz signals received at Columbus, OH, from the ATS-5 satellite are analyzed with respect to statistical distribution and temporal spectra. Since the satellite failed to despin, the data analysis is complicated, but the "on-off" nature of the signal as the satellite antenna pattern sweeps over the receiver allows the separation of relatively weak high-frequency scintillation components from system noise by a method previously reported by the author. In this paper, the statistical and spectral scintillation parameters observed on 17 summer days in 1970-71 are related to meteorological conditions. Particular attention is paid to the high-frequency (rapid scintillation) components at relatively high satellite elevation angles. The intent is to evaluate scintillation observations in terms of meteorological sensing, rather than for communications purposes.

Commission F - Session 6

Thursday P.M. 1400 - 1640
RADIO OCEANOGRAPHY, WAVE PROPAGATION AND REMOTE SENSING
Chairman: R. H. Stewart, Scripps Institute of Oceanography, La Jolla, CA

1. DIRECTIONAL OCEAN WAVE SPECTRAL ESTIMATES FROM HF RADAR BRAGG LINE STRENGTHS PARAMETRIC IN FREQUENCY AND AZIMUTH: D. B. Trizna, R. W. Bogle and J. C. Moore

Preliminary results are presented for experiments conducted in March, 1977, using the SEA ECHO HF radar on San Clemente Island, with its azimuthal coverage recently extended to 80°. Measurements of the first order Bragg lines were made with the radar after precision internal calibration and using an independent monopole repeater. These measurements were used in the radar equation to derive ocean wave spectral estimates over 80 degrees in angle, and between 0.144 and 0.5 Hz in wave frequency. For sea truth, omni-directional spectra derived from a Waverider buoy were available, as well as measurements of swell made by an array of underwater pressure sensors just off shore north of LaJolla, California. Results are presented for a variety of sea and wind conditions.

2. IONOSPHERIC EFFECTS ON SEA-ECHO OBSERVED AT SAN CLEMENTE ISLAND: J. B. Snider, National Oceanic and Atmospheric Administration

A series of over-the-horizon HF radar measurements of backscatter from the northeastern Pacific Ocean was performed at San Clemente Island during May 1976. These tests were conducted to determine the effects of system variables and ionospheric conditions upon the quality of Doppler spectra and to estimate the accuracy of ocean wave characteristics deduced from the spectra. In this paper, the radar system and experimental procedure are briefly described followed by a discussion of the more significant findings. Among the latter are:

a. Multimode propagation often contaminates second-order energy in the Doppler spectrum causing incorrect estimates of significant wave height and period.

b. Even in the presence of multipath, wave direction, inferred from relative amplitudes of resonant Bragg lines, can usually be estimated with good accuracy.

c. Ionospheric generalizations found suitable for communications circuits are often inapplicable to sea echo measurements.

The impact of these ionospheric effects upon OTH remote sensing of sea state over large areas is considered. Wave characteristics calculated from Doppler spectra are compared with available ground-truth information.

3. DIRECTIONAL OCEAN-WAVE SPECTRA BY INVERSION OF SECOND ORDER RADAR ECHOES: B. Lipa, Stanford Center for Radar Astronomy.

The spectra of high frequency radar echoes from the sea contain dominant peaks due to first order Bragg scatter and a structured continuum due to higher order scatter. Interpretation of the first order peaks is well established; however the derivation of sea-state requires the radar frequency and look angle to be varied at will which is seldom possible due to practical limitations on radar design. We show that interpretation of the Doppler continuum yields detailed information on sea-state from a single decameter radio wave-scatter observation.

The second order structure of the radar spectrum has been given in terms of the directional ocean wave spectrum through a two dimensional nonlinear equation. Inversion of this equation is shown to yield accurate estimates of the directional ocean wave spectrum, together with wind direction and wave height. Accuracy improves with higher sea states and/or radar frequencies. Results from representative model test cases indicate that the directional ocean wave spectrum can be obtained to within 10% and the wind direction within 5° from decametric radar scatter data. The method is illustrated by a test application to measured data. Results of inversion are compared with oceanic information from an in-situ tilt buoy and are found to agree within the estimated statistical error.

4. TOWARD A THEORY OF WAVE PROPAGATION FROM SATELLITES INTO THE PENUMBRA REGION OF THE EARTH: R. W. Harper, GTE Lenkurt, K. R. Carver, New Mexico State University

The theory of propagation of plane waves from a satellite into the penumbra region of the earth is important for practical prediction of multipath behavior over sea or terrain and for the estimation of channel reliability, when the receiving station is in the earth-edge zone. Earth-diffracted plane waves are expressed in terms of the spherical-harmonic expansions of the fields of equivalent vertical electric and vertical magnetic dipoles located above the earth. This takes advantage of the fundamental theoretical work of both B. van der Pol and H. Bremmer as well as that of V. A. Fock; in both cases, exact solutions have been reduced by means of contour integration to approximate solutions which can be numerically evaluated in the penumbra region. It is then shown that Fock's results, which were previously limited to transmitter/receiver heights less than about 100 km., can be extended to include geostationary satellite heights (36,000 km.) by introducing a virtual source at 100 km. above the earth with an earth horizon common to that of the satellite. This provides a general theoretical framework for treating such specific propagation problems as near-grazing incidence and scattering of VHF and UHF plane waves from the sea, where neither interference nor shadow-zone diffraction formulations hold.

5. PASSIVE MICROWAVE REMOTE SENSING OF NEAR-SURFACE SOIL MOISTURE:
E. G. Njoku, Jet Propulsion Laboratory, J. A. Kong, Massachusetts Institute of Technology.

The theory of microwave thermal emission from a non-scattering, half-space medium is developed for application to regions within nonuniform subsurface soil moisture and temperature variations. A coherent, stratified model is presented which is valid for nonuniform temperature profiles and rapidly varying moisture profiles, under which conditions the commonly used emissivity and radiative transfer approaches become inaccurate. For naturally occurring profiles, the stratified model gives more accurate results than the other approaches at frequencies below about 4 GHz. Experimental results from ground-based radiometric observations of a controlled target area compare systematically with brightness temperatures predicted from the theoretical model to within approximately 10^{o}K. Results of dielectric constant measurements of the sand are given at seven frequencies in the microwave range, and for moisture contents in the range 0 to 30% by volume. Using this model, the thermal microwave emission spectrum is computed for a number of representative moisture and temperature profiles in the frequency range 0.25 to 25 GHz. A regression technique is used to show that multifrequency data can be used to obtain moisture and temperature gradients in the soil when an estimate of the surface temperature is available.

6. MASSIVE HYDRAULIC FRACTURE MAPPING USING MAGNETIC INDUCTION:
J. A. Landt, Los Alamos Scientific Laboratory

The production of energy from hot dry rock depends on establishing circulation of a working fluid in a deep fracture zone. Massive hydraulic fracturing is presently being employed at the Los Alamos Scientific Laboratory to form large fractures in hard granite at depths of approximately 3,000 meters. Accurate determination of fracture orientation is required to permit a second hole to be drilled to connect with the fracture zone and thus provide the desired circulation system. It has been proposed that a magnetic induction technique be employed to map these fractures. This paper addresses the theoretical development of an instrument based on the magnetic induction technique, and experimental verification is provided. Fracture mapping is accomplished by detection of eddy currents induced in the conductive fractures by a downhole coil operating near 100 kHz. This instrument is compared to the conventional induction logging devices commonly used in the oil industry. Plans of ruggedized instrument construction are discussed briefly.

*This work was performed under the auspices of the Energy Research and Development Administration.

7. MINIMUM MEAN-SQUARE-ERROR ESTIMATION OF UNDERGROUND COAL BURN VOLUMES FROM REMOTE ELECTROMAGNETIC INDUCTION RESPONSES: E. A. Quincy, M. L. Rhoades, University of Wyoming.

Bayes minimum mean-square-error algorithms for estimating the radius of a subsurface coal burn volume are derived and their performance calculated. The algorithms are derived for noisy responses obtained at the surface by an electromagnetic induction system. The coal burn geometry is assumed to be cylindrical. Thus an estimate of the coal burn volume is provided if the cylindrical length is taken to be the distance between gasification wells.

Geophysical investigations of the Hanna Coal Gasification Site (Hanna, Wyoming) indicate that the sub-bituminous coal seam is a very poor conductor ($\sigma < 10^{-6}$ mhos/m) while the overburden is a poor conductor ($\sigma = 10^{-3}$ mhos/m). However, the burn creates a charred shell which converts the coal to a good conductor and the void fills with saline ground water ($\sigma = 1$ mho/m). These orders of magnitude difference in conductivities produced a sizeable anomaly in the induction response when probed from the surface at various locations.

Analytic and numerical radius estimator algorithms are compared for a linearized approximation to the cylinder response. The mean-square-error and bias are determined as a function of sample size for a family of "signal-to-noise" ratios. A priori knowledge of the radius was described by Rayleigh and Gaussian statistics. The additive noise was assumed to be Gaussian.

8. THE BOULDER ATMOSPHERIC OBSERVATORY -- A FACILITY FOR REMOTE-SENSING RESEARCH: W. H. Hooke, Wave Propagation Laboratory, NOAA.

The Wave Propagation Laboratory of NOAA, in cooperation with NCAR, is developing a test facility, some 20 km northeast of Boulder, for the evaluation and testing of remote-sensing equipment and the study of turbulence in the planetary boundary layer. The facility will include a 300-m tower, instrumented at eight fixed levels and on a movable carriage with three-axis sonic anemometers and fast-response temperature sensors. Some fast-response humidity sensors will also be available. In addition, three acoustic sounders (ultimately to have a Doppler capability), a laser-beam wind-sensing triangle and a microbarograph array will also be a permanent part of the site. Data processing will be handled initially by an existing computer facility able to do some processing of the tower data in real time; however, in one year this will be supplanted by a more sophisticated system, able to provide a good deal of real-time processing, including spectral analysis, to multiple users in a highly interactive mode. Additional data channels will be available to accommodate data inputs from outside groups. Use of the facility by outside groups is being encouraged.

Commission G - Session 3

Thursday P.M. - 1400 - 1630
ELF TO VHF PROPAGATION AND PROBING I
Chairman: O. G. Villard Jr., Stanford Research Institute

1. COMPUTER SIMULATION OF MULTI-MODE IONOSPHERIC PROPAGATION BETWEEN SPECIFIED TERMINALS VIA QUASI-SYMMETRIC RAY PATHS: S. Silven, GTE Sylvania Incorporated, Mountain View, CA

A fast economical computer program has been developed for estimating the parameters of the various ionospheric propagation modes between specified terminal locations. The terminal locations are specified in terms of latitude, longitude, and height above the earth's surface. The parameters describing the ionosphere (foF2, foE, Hmax, horizontal gradients, etc.) are either specified by the user or computed from the ITS-78 data tape at a sufficient number of locations to compute individually the parameters of each hop. Solutions involving high-angle rays are found in addition to the usual low-angle and multiple-hop solutions between the specified terminals.

The ionosphere is modeled as being nominally spherically symmetric in the vicinity of each reflection. Each hop is thereby computed to be nominally symmetric about its axis, though the various hops comprising the mode are not identical. The ray elevation angles, group-path lengths, phase-path lengths, and ground range between the subterminal points are computed on this basis to the specified homing accuracy. Also computed are the doppler shifts associated with each mode, resulting from motion of the terminal points. A derivation is presented for calculating the transmission loss for each mode directly from the homing procedure, thereby assuring that the effects of ionospheric focusing/defocusing are included. Also presented are derivations of procedures for estimating the effects of horizontal gradients in ionospheric electron density. These effects are computed as first-order variations from the nominal propagation parameters computed for the spherically symmetric model, and are seen to be functions of the nominal values themselves as well as of the gradients specified.

2. ON THE RELATIVE EFFICIENCY AND STABILITY OF IONOSPHERIC DUCTING CHANNELS: K. Toman, Electronic Sciences Division, Hanscom AFB and D.C. Miller, Arcon Corporation

Reasonable ionosphere cross-sections are computationally specified to study the relative efficiency of ducting in ionospheric channels. The effects of scattering are simulated by introducing

into the ray-tracing scheme successive aberrations in ray direction that are controlled by noise-like and scale-size dependent processes, the latter being related to electron density encountered by the ray. Both algorithms may eventually be modified to optimize their corresponding to physical reality. More realistic ionosphere cross-sections of a modified Polar Ionosphere Model are used to deduce by means of ray-tracing the ducting phenomenology and perhaps to infer how the presence of ionospheric ducting manifests itself on oblique forward- and backscatter ionograms.

3. PULSE BROADENING DUE TO PHASE FLUCTUATIONS IN AN HF IONOSPHERIC SCATTERING RADIO LINK: A. Malaga and R. E. McIntosh, University of Massachusetts, Amherst

It is well known that fluctuations in the index of refraction an an ionospheric scattering link introduce amplitude and phase fluctuations on monochromatic siganl transmission. When dealing with the transmission of signals used in digital data transmission, i.e., pulses, a measure of the distortion (jitter or broadening) introduced by deterministic and random spatial variations in the refractive index of the propagation medium is provided by the delay spread of the channel. In this paper, results which relate the amount of pulse broadening to the multipath spread and the dispersion factor (which is a measure of the dispersiveness of the medium) of a typical HF link are presented. The ionosphere is modeled as a two-layer inhomogeneous, isotropic plasma, whose index of refraction is a random function of space. The mean electron density profile of each layer is assumed to vary parabolically with height. The purely random part of the index of refraction is assumed to be statistically homogeneous and isotropic. It is found that broadening is primarily due to the discrete multipath of the transmission medium (due to the deterministic spatial variations in the refractive index). Additional broadening due to the randomness in the medium is significant only when the fluctuations are large and the transmitted signal is a chirp pulse with large bandwidth.

4. A SPECULAR REFLECTION MODEL FOR E-REGION FADING STATISTICS: P. R. Albee and D. H. Schrader, Washington State University

The statistical properties of E-region radio wave measurements have been used to argue for diffractive model descriptions of the E-region irregularities which produce fading. We show that for irregularity sizes required by the diffractive models, a simple model based on the interference of waves from multiple, specular reflections by an undulating surface leads to comparable statistics. These statistics are in agreement with our experimental measurements. Thus, a comparison of experimental amplitude fading data with statistical formula derived on the basis of a diffractive model does not resolve the question of adequacy of either the specular reflection or the diffraction approximations to the description of the E-region fading measurements.

5. ESTIMATING REFLECTION HEIGHT FROM DOPPLER MEASUREMENTS: K. Toman, Electronic Sciences Division, Hanscom AFB

If height changes in the ionosphere are assumed to occur uniformly over the region of interest, there exists a possibility that, for an oblique fixed-frequency radio transmission, a reflection height can be estimated using the Doppler method. Conventionally, a pulse-arrival-time difference is used for such an estimate. In the Doppler method, the ratio of the Doppler shifts for the one- and two-hop transmissions gives a plausible estimate of reflection height, provided that the radial motion of the reflection boundary is uniform. Since one- and two-hop signals are not reflected at the same height in the ionosphere an error is introduced. Ionization changes in the 'nondeviative' regime can also introduce Doppler shifts. Therefore, the ratio method will be more useful when the effects of such ionization changes are negligible. When ionospheric reflection-height changes are due to atmospheric waves, the method's accuracy deteriorates less the larger the wave. The method fails for a motionless ionosphere.

6. VERTICAL INCIDENCE ABSORPTION AS A DIAGNOSTIC FOR THE WINTER ANOMALY: E. K. Walton, L. G. Smith and E. A. Mechtly, Department of Electrical Engineering, University of Illinois at Urbana-Champaign

Al absorption measurements during the winter anomaly period as well as other seasons are examined using electron density profiles obtained on rocket flights. It is found that the measured values of absorption agree well with values calculated from simultaneous rocket measurements of electron density profiles, using the phase integral method, for a collision frequency model in terms of the pressure $p(Pa)$: $\nu_m = 6.0 \times 10^5 p$.

The absorption is calculated as a function of frequency in the range 1.7 to 3.0 MHz and found to be sensitive to the detailed structure of the electron density profile. It is also noted that, in some cases, sporadic-E layers are responsible for low values of absorption.

Commission B - Session 6

Friday A.M. 0900 - 1155
NUMERICAL METHODS
Chairman: E.K. Miller, Lawrence Livermore Laboratory, Livermore, Ca.

1. THE GREEN'S FUNCTION MOMENT METHOD APPLIED TO WIRE SCATTERING AND SLOT DIFFRACTION: W.A. Johnson, C.W. Prettie, D.C. Dudley, University of Arizona.

This paper develops a modified moment method for determining the current on a straight thin wire scatter. The singularities of the current's first derivative are extracted and the modified method is used to solve for the current. The same technique is applied to two-dimensional diffraction through a slot. For each problem sample data is given and comparison with other methods of solution is made.

2. REFLECTION COEFFICIENT CALCULATION FOR A PROBE-FED CAVITY-BACKED SLOT ANTENNA: A.J. Fenn, G.A. Thiele, Ohio State University ElectroScience Laboratory.

Previous work by the authors has been concerned with the development of a moment method technique for the far field pattern prediction of probe-fed cavity-backed slot antennas of arbitrary (rectangular) aperture size. The aperture distribution is treated as an unknown. The technique employed to determine the aperture distribution of the cavity-backed slot involves the application of Babinet's principle. The theory of images is used to remove the walls of the cavity resulting in two infinite arrays of dipoles behind the aperture plane which model the probe in the cavity. These two arrays are then the source of the incident field in calculating the generalized voltage matrix (V).

To accurately compute the far field it is only necessary to expand the aperture distribution in the wide dimension, considering the distribution to be constant in the narrow dimension. However, to accurately calculate the reflection coefficient, it has been found necessary to also expand the distribution in the narrow dimension whereupon matrix conditioning deteriorates. Incorporation of the inverse square root edge condition tends to alleviate the conditioning problem. Reflection coefficient and condition number results will be shown for various aperture sizes.

3. AN ASSESSMENT OF TEMPERATURE-PROFILE DETERMINATION USING FREQUENCY-DOMAIN REFLECTOMETRY: R.J. Lytle, G.K. Myers, Lawrence Livermore Laboratory.

It can be difficult to accurately measure the temperature profile in the region where oil shale is being retorted in situ, where coal is being gasified in situ, or where a geomthermal reservoir is being exploited. Thermocouples can be used, but since measurements at many locations are needed (to give good spatial resolution), the number of cables and thermocouples can become prohibitive and cost-ineffective. It is therefore desirable to be able to monitor the temperature profile with a single cable, along which a detailed spatial profile can be determined and displayed almost instantaneously.

This presentation concerns the use of reflectometry on a coaxial cable with an inner sheath of temperature-sensitive dielectric to ascertain the temperature profile along the cable. Of the suggested applications, in situ oil-shale-retorting problem is the most severe test. Characteristic temperature profiles encounted during in situ oil-shale-retorting process were thus considered in numerical simulation experiments.

For unambiguous interpretation of reflectometry data, a dielectric constant that varies monitonically with temperature for $30^{o} \leq T \leq 700^{o}$ C is needed. From theoretical considerations, high-silica glasses show promise of maintaining their dielectric properties over this temperature range and having a dielectric constant change that is at least an order of magnitude for the temperature range of 30 to 700^{o} C.

Modeling began with computer simulation of a transmission line with nonuniform loading (with the loading dependent on the local temperature), using a differential equation representation of the cable. By using this cable model, representative reflectometry data were generated. Several algorithms were considered for inverting reflectometry data to obtain the spatial distribution of temperature inside the temperature-sensitive cable. Sample results of an inversion technique that successfully infers the spatial temperature profile will be presented. The dependence of the results upon the initial estimate of the profile will be illustrated. It appears that a single cable holds promise for replacing many theromocouples to give adequate spatial resolution of temperature in geothermal, coal-gasification, and oil-shale energy programs.

4. ELECTROMAGNETIC MODELING OF COMPOSITE WIRE/SURFACE GEOMETRIES:
E.H. Newman, D.M. Pozar, Ohio State University ElectroScience Laboratory.

The application of the method of moments, in the form of thin-wire computer programs, is one of the most widely used tools in analyzing antenna and scattering problems. One of the most useful properties of these computer programs is the ability to model solid conducting surfaces using a wire grid or mesh. Unfortunately, it takes many wire segments and current unknowns to accurately model a solid surface. Thus, probably the most severe limitation of the thin-wire computer program is that it is not applicable to surfaces larger than a few square wavelengths. The maximum surface area which can be treated can be substantially increased by modeling the conducting surfaces by surface current densities, or the so-called surface patch modes.

This paper will describe a computer algorithm for modeling composite wire/surface geometries. The technique has the advantage that continuity of current is enforced on the wire, on the surface, and at a wire surface junction. Data will be presented which illustrates the efficiency of the computer program.

5. HYBRID COMPUTER APPLICATIONS IN ELECTROMAGNETICS:
E.L. Coffey, New Mexico State University.

In recent years, many digital computer techniques have been developed to solve problems in electromagnetics. Unfortunately, developments in computer technology have not kept pace with these methods, and frequently it is the computer rather than the method that defines the scope of problems that can be solved by using that particular method. For example, application of the method of moments is limited to problems which can be described by fewer than one or two hundred basis functions, not restrictions inherent in the method.

Recently, several investigators have been using the analog/hybrid computer as their primary computational tool. To illustrate the versatility of the hybrid computer this paper presents the results of several studies which have utilized hybrid computer programming techniques to reduce execution time and storage requirements. These studies include waveguide mode analysis, wave propagation in non-uniform media, two- and three-dimensional scattering, dielectric lens design, far-field antenna pattern calculations, and antenna range simulation -- especially mechanical dynamics of antenna structures and boresighting.

Results are presented using both digital and hybrid techniques, and a comparison is made of tradeoffs in each case. Finally, guidelines are developed to determine which machine is best suited to a particular electromagnetics problem.

6. A UNIFIED TIME DOMAIN ELECTROMAGNETIC AND CIRCUIT ANALYSIS CODE:
J.A. Landt, Los Alamos Scientific Laboratory.

Recent interest in the broadband response of antennas has lead to development and refinement of numerical time-domain techniques capable of high efficiency and accuracy. These techniques are easily modified to handle simple non-linear loads, and this work has been reported earlier. Hybrid approaches have been employed to assess the response of antennas connected to more complicated circuits. These techniques have found widespread use in the assessment of electromagnetic pulse effects, electromagnetic compatibility, radio frequency interference, and other applications.

A unified numerical procedure is discussed in this paper. The antenna portion of the computer code is based on the thin wire approximation to a time domain electric field integral equation. The circuit portion of the code is based on a simple time-domain nodal analysis. Application of the technique is demonstrated by consideration of several simple types of antennas connected to circuits containing linear and non-linear elements.

7. A COMPARISON OF METHODS FOR SOLVING SCATTERING PROBLEMS INVOLVING INHOMOGENEOUS DIELECTRIC BODIES: S. Govind, R.J. Pogorzelski, L.L. Tsai, D.R. Wilton, T.K. Wu, University of Mississippi.

In recent years many digital computer techniques have been developed for solving electromagnetic scattering problems. For the study of scattering from inhomogeneous dielectric bodies, one approach is to stratify the inhomogeneity into layers of homogeneous media. Among the techniques applicable in such an approach are the moment method, unimoment method and the recently proposed modification to the moment method. Thus, one is confronted with the selection of a suitable techinque for the problem at hand. The present paper deals with an attempt to expose the relative merits and demerits of each of the above techniques. A few of the points of consideration for this study include ease of programming, required core capacity, required CPU time and convergence rates. It has been found that the modified moment method has simplicity over the moment method and deals with smaller sized matrices. However, it is not as adaptable as the unimoment method when dealing with a variety of inhomogeneous scattering problems.

8. SCATTERING BY COMPOSITE METAL-DIELECTRIC BODIES OF REVOLUTION: T.K. Wu, L.L. Tsai, D.R. Wilton, University of Mississippi.

The scattering problem of either a conducting or a dielectric body-of-revolution has been solved using the surface integral equation and moment methods technique. In this paper, the previous method is extended to solve the scattering by composite metal-dielectric bodies-of-revolution. Specifically, appropriate integral equations are formulated at each boundary surface via Maxwell's equations, Green's theorem and the boundary conditions. The unknown surface current densities are then obtained by first Fourier decomposition and moment method Galerkin's procedure.

Of primary interest is the model comprising a finite length conducting cylinder attached to a homogeneous, lossy dielectric cylinder or cone-sphere. This model may be used to represent a missile in flight with a trailing plume. Numerical results which are in good agreement with the thin-wire model results will be presented and discussed for various plume shapes and constitutive parameters, ε (permittivity) and σ (conductivity).

9. SCATTERING SOLUTIONS FROM GAUSSIAN QUADRATURE: Y.L. Chow, M.D. Miller, T. Keshava-Murthy, University of Waterloo.

The Gaussian quadrature can be used to solve an integral equation through simply replacing the integral by a sum. The system of linear equations resulted, following Kantorovich's approximation, can be shown to be identical in form to that from the point matching moment method.

Despite such similarity, the Gaussian quadrature is inherently faster convergent. In solving scattering cross-sections, its fast convergent property is applied twice : one is to solve the integral equation of the current on the scatterer and the other is to apply the quadrature directly on the current to get the cross-section. The improvement in convergence is especially significant when the current has known singularities. An example of this in this paper is the current on a rectangular scatterer.

The Gaussian quadrature can be applied to scatterers not only with straight boundaries of finite lengths but also with curved boundary through a conformal transformation. With a little manipulation, the Gaussian quadrature can be made similar to the moment method with mixed basis functions and becomes applicable to boundaries of semi-infinite length.

Sometimes the quadrature used on the semi-infinite boundary may have to be made faster convergent through a deformation of the path of integration into the complex plane. An example of this is the scattering from an open-ended waveguide.

Commission C - Session 3

Friday A.M. 0900 - 1155
FREQUENCY STABILITY AND ITS APPLICATIONS TO
TELECOMMUNICATION AND TIME SERVICE SYSTEMS
Chairman: W.C. Lindsey, University of Southern California

1. SOME NOISE MODELS WITH APPLICATION TO FREQUENCY STABILITY MEASUREMENTS:
J.A. Barnes, National Bureau of Standards.

Typical noise models used to characterize the performance of electronic equipment, such as oscillators, are normally taken (1) to be gaussian in nature and (2) to follow a simple extrapolation from zero to infinite Fourier frequency. Recently, both of these assumptions have received some attention with some significant results. There is increasing evidence that a gaussian model is inadequate to characterize the detailed performance of the best frequency standards. The appearance is that of sudden and unexplained steps in frequency of a magnitude comparable to the other (gaussian) noises. There exist some interesting, non-gaussian models (e.g., sporadic noise) which might be good models for these oscillators.

The assumptions of performance at zero and infinite Fourier frequencies have major implications for the very concepts of measurability. The proper accounting for the possible problems arising at the extremes of the Fourier spectrum thus affords constraints on meaningful measurements. These problems have been directly addressed for the case of frequency instabilities, and significant results have resulted. Key among these results is a strong suspicion that estimates of the ordinary variance of many real, physical processes will fail to converge in a practical sense. Further, the ordinary variance is often not the quantity of greatest utility.

2. FREQUENCY INSTABILITY EFFECTS ON TELECOMMUNICATION SIGNALS AND SYSTEMS:
W. C. Lindsey, University of Southern California, C. M. Chie, LinCom Corporation.

A current problem of great interest in telecommunication, Doppler measuring, radar and ranging system design and performance verification is that of specifying system phase noise requirements due to instabilities associated with the carrier oscillation. Unfortunately, oscillator phase noise, unlike thermal noise which is well approximated by a delta correlated process, does not possess a constant power spectral density for all frequencies. Not only does this fact make it difficult to measure but makes it more difficult to develop a working theory from which performance can be predicted.

In a recent paper the authors developed the theory of oscillator instability in terms of a set of stability functions and interconnected this theory with frequency standards as set forth by Subcommittee on Frequency Stability of the Technical Committee on Frequency and Time. The purpose of our discussion is to show how this set of stability functions enter into

the theory of correlative tracking systems and show how frequency and phase instability enters naturally into telecommunication system performance equations. In addition, we show how other phase noise components due to channel turbulence (AM-PM conversion, media scattering, etc.) enter into the system performance measures of Doppler accuracy and bit error rate performance. Both τ-domain and f-domain performance characterizations are made and a Mellin transform theory is given. In order to demonstrate the utility of the theory, application is made to carrier tracking and one-way and two-way Doppler measuring systems.

3. SOME ASPECTS OF TIMING AND FREQUENCY CONTROL IN COMMUNICATION SYSTEMS: P. Kartaschoff, Swiss Post Office Research Division.

The impact of data communications on system design has lead to a review of the requirements on timing and frequency control in communications systems.

The wideband anology transmission using frequency division multiplex techniques the phase noise spectral density $s_{\varphi}(f)$ of the carrier generators must be kept very low. Values of 120 dB below 1 (radian) per Hertz for the voice frequency range ($300<f<3400$ Hz) are desirable for individual generators in extended networks.

In extended digital networks, the emphasis is on the timing properties of the network clocks and the establishment and maintenance of synchronism. Clock characteristics interact with the properties of transmission paths, each introducing random timing jitter and some systematic effects. Maximum time interval error has been proposed for specifying the network clock characteristics.

There is no upper bound on time interval error for arbitrary long time intervals. An additional specification may be stated in the form of a bound on allowable frequency drift and low Fourier frequency divergent noise (e.g. "flicker" - noise).

The required reliability of network timing and frequency control is to be obtained by means of redundancy and adequate network organization.

Relations between frequency stability parameters developed be metrologists and those required for system design are discussed emphasizing the need of more dialogue and further common studies among the various interested specialists.

4. JTIDS - A DIGITAL COMMUNICATIONS SYSTEM FOR THE DISSEMINATION OF TIME AND POSITION INFORMATION: R. Dell-Imagine, Hughes Ground Systems Group.

JTIDS (Joint Tactical Information Distribution System) is a communication navigation system under development by a Tri-Service program office to provide the military services with jam resistant capability during the 1980's. The JTIDS waveform utilizes a 5 MHz spread spectrum modulation to provide unambiguous location, identification, and timing information. When it is

deployed, JTIDS will provide both the military users, and, in a simplified configuration it could provide commercial airline users, with GMT to an accuracy better than 1 microsecond and position location information by multilateration to an accuracy better than 1000 feet.

JTIDS operates in the TACAN band without interference to the TACAN function by using a frequency hopped waveform over the 960-1215 MHz band for its high anti-jam mode and a fixed 969 MHz carrier for both low AJ secure and in-the-clear transmissions. The waveform includes the capability for transmitting intercomputer messages as well as digital voice and TTY data.

JTIDS represents one of the first applications of digital LSI and spread spectrum technologies to a large scale system. The ultimate number of JTIDS terminals deployed will depend on the cost savings attainable using LSI technology and the benefits to both military and non-military users.

5. PRECISION TIME TRANSFER USING THE GPS SATELLITE SYSTEM: J.J. Spilker, Jr., F.D. Natali, Stanford Telecommunications, Inc.

The planned Global Positioning System (GPS) offers, for the first time, the possibility of worldwide timing with accuracy on the order of nanoseconds. An operational network of 24 NAVSTAR satellites carrying on-board atomic standards and providing worldwide coverage is planned for the 1980's with the first six satellites to be launched in 1977. Satellites transmit wide-band signals for which unambiguous time of arrival can be measured accurately at the receiver. Data is transmitted from the satellite by which the user can compute satellite on-board clock errors from the system time as well as accurate satellite position. The received information allows the user to estimate propagation time and set a local clock. One of the largest error sources is anticipated to be due to uncertainties in ionospheric delay. A two-frequency ionospheric delay measurement is available for the users who require extreme accuracy.

This paper discusses the details of the time transfer process, expected accuracy, and equipment configurations. A relatively inexpensive user equipment will be capable of providing time transfer accuracies better than 100 ns. A more complex equipment will provide higher accuracies for authorized users. The relationship between the GPS system time and Universal Time Coordinates (UTC) will also be discussed.

6. APPLICATIONS OF PRECISION TIME AND FREQUENCY TO DEEP SPACE NAVIGATION AND VLBI: D. Curkendall, Jet Propulsion Laboratory

The influence of clock error on modern radiometric measurement, range and Doppler, is charted. Both coherent (two-way) and noncoherent (one- and three-way) systems are considered.

Examples of Doppler data corrupted by oscillator instability are shown. In the case of a crystal oscillator, their effect is clearly seen by directly inspecting the data itself. With an atomic standard, autocorrelation techniques are used to separate receiver noise from oscillator effects.

Current applications include supplying time and frequency to coherent ranging systems that can operate at the limits of the solar system. The 1981 Saturn encounter with the Voyager spacecraft will in part be made possible by carefully measuring the differential range to the spacecraft from each of the two stations separated by intercontinental distances. This demands very precise knowledge of the differential clock rate. Efforts to calibrate the differential rate or monitor hydrogen maser performance via Very Long Base Line Interferometry (VLBI) will be discussed.

VLBI itself may at once be the technology which demands the most stringent performance from future clock systems, and the technique of choice for determining and distributing time and frequency to worldwide nets. These issues will be discussed.

7. COMPENSATION FOR THE DEPOLARIZATION EFFECTS OF PROPAGATION THROUGH THE ATMOSPHERE BY ADAPTIVE POLARIZATION CONTROL TECHNIQUES: S.H. Durrani, NASA/ Goddard Space Flight Center, C.C. Allen, General Electric Company

The problem of recovering communications signals that have been depolarized will be addressed in this paper. Communications signals at Ku-band are especially subject to depolarization effects of various degrees of severity from light precipitation, rainfall, etc. Considerable loss of signal, signal variations, and fading, can result from these effects. Cross-polarization caused by propagation effects as well as antenna misalignment can also produce cross-coupling of received signals.

Adaptive polarization control techniques to compensate for adverse propagation effects, were developed in connection with a study of dual polarization for frequency reuse in a Ku-band communications system. These techniques recover the two depolarized signals, which were originally orthogonal when transmitted, and separate them into their respective output channels with maximum isolation and low loss. Circuits for implementing these techniques will be presented.

The circuit operation is based on the assumption that the two orthogonal transmitted signals have different pseudo-noise (PN) codes, that both signal codes are acquired at the receiver, and that synchronized reference signals are available. Adaptive processors are used to form two cross-polarized beams with the aid of the reference PN code sequences. The algorithm uses an estimate of the stronger signal for each beam as the reference, which causes the weaker signal to be rejected in the feedback path and restores the initial orthogonal polarization.

Commission F - Session 7

Friday A.M. 0900 - 1200
SCATTERING OF RADIO WAVES, THEORY AND EXPERIMENT
Chairman: W. Vogel, University of Texas at Austin

1. BACKSCATTERING FROM A PERFECTLY CONDUCTING, GAUSSIAN DISTRIBUTED, ROUGH SURFACE: G.S. Brown, Applied Science Associates, Inc.

The problem of scattering from a random surface possessing both large and small scales of roughness is considered. The analysis is specialized to backscattering from a perfectly conducting surface in order to more clearly illustrate the approach. The analysis employs a perturbation technique developed by Burrows (Trans. IEEE, AP-21, 241, 1973) wherein the small scale surface features act as a first order perturbation to the large scale dependent physical optics scattering. Thus, the surface height spectrum must be split into two parts, i.e., a large scale ($\lambda \geq \lambda_T$) and a small scale ($\lambda \leq \lambda_T$) part. Such a dichotomy is possible when the surface is jointly Gaussian in height, slope, curvature, etc. When the slopes of the large scale structure are not too large, a particularly simple expression for $\sigma^\circ(\theta,\phi)$ is obtained. That is, the result comprises a sum of the large scale dependent physical optics term plus a line broadened small scale Bragg result where the broadening is determined by the large scale structure. This latter result is identical to the well known tilted plane Bragg solution except for the presence of an additional term. This term is most important because it insures the continuous transition between the physical optics and Bragg scattering regimes. Of particular significance, is the finite (but small) contribution to the normal incidence return by the small scale surface structure. A specific spectral example is presented and the importance of λ_T is discussed.

2. BACKSCATTERING FROM A HALF-SPACE RANDOM MEDIUM WITH THE RADIATIVE TRANSFER APPROACH: L. Tsang, J.A. Kong, Massachusetts Institute of Technology

In active remote sensing with a radar, the effect of volume scattering has been studied with the model of a random medium with three dimensional correlation functions. Using a wave approach, the bistatic scattering coefficients have been calculated with the Born approximation. In this report we employ the radiative transfer theory by assuming incoherence and far-field interaction to calculate the backscattering cross-sections to second order in albedo with an iterative process. The first order result corresponds to single scattering and checks with previous results in the literature. The most significant consequence of the second-order result is the depolarization effect. This effect is easily appreciated by visualizing the induced dipole moments due to the incident wave as well as the scattered wave. While the first order moment generates scattered wave with the same polarization as the incident wave, the second order moment

is now capable of generating waves with polarizations differing from the original incident wave. The theory is applied to low loss and scattering dominant areas such as show and ice field, desert, and lunar environment. We illustrate the back-scattering results with various numerical examples plotted as functions of frequency and incident angles.

3. A NUMERICAL STUDY OF KIRCHOFF APPROXIMATION IN BACKSCATTERING FROM A RANDOM SURFACE: H.L. Chan, Naval Weapons Center, A.K. Fung, Electrical Engineering Department, University of Kansas

The backscattering characteristics of a completely known one-dimensional random surface are studied by computing the exact surface current distribution over the illuminated area by the moment methods and then the backscattered field by Gaussian quadrature technique. This computation is repeated 40 to 80 times (depending on the incident frequency) over different surface segments to obtain enough scattered field samples to estimate the average scattered power. If the surface current distribution over a surface segment is estimated by the Kirchhoff approximation, the above calculations may be repeated to obtain the average scattered power under the Kirchhoff approximation. By comparing these two average scattered powers at different frequencies, it is found that (1) the Kirchhoff approximation is valid over a range of frequencies; (2) over the range where the approximation is valid, the average backscattered power need not be proportional to the slope distribution of the random surface; and (3) further study is needed to establish the range of validity of the Kirchhoff approximation. Comparisons are also made between existing approximations to the Kirchhoff integral representing the average backscattered power and the numerically computed backscattered power under Kirchhoff approximation. It is found that the choice of approximations depends upon the incident frequency and the shape of the surface correlation function.

4. STATISTICS OF A CONSTANT VECTOR PLUS AN ALGEBRAIC - EXPONENTIAL VECTOR: J.L. Ekstrom, Amecom Division of Litton Industries

In many problems involving the mathematical modeling of various propagation and scattering phenomena, it is often necessary to compute the statistics of the random variable r obtained by the vectorial addition of a constant vector x_0 and a non-negative random vector x, the angle between the two vectors being assumed to be a random variable independent of r and uniformly distributed over $(0, 2\pi)$.

When the pdf of x is given by

$$f(x) = \frac{n}{\sigma \Gamma\left(\frac{m+1}{n}\right)} \left(\frac{x}{\sigma}\right)^m \text{ EXP } \left[-\left(\frac{x}{\sigma}\right)^n\right]$$

where m, n, and ρ are parameters of the distribution, the pdf of r may be expressed in two different forms (depending on whether $r > x_0$ or $r < x_0$), each involving an alternating infinite series of hypergeometric functions of the ${}_2F_1$ type.

The cumulative probability that r exceeds some threshold R_0 may, when $R_0 \leq x_0$, also be expressed in an alternating infinite series of ${}_2F_1$ functions. This series is absolutely convergent, and a technique for finding a term in the series beyond which the term magnitudes decrease monotonically is given; thus, if the series is summed to this term, the truncation error will not exceed the next term in the series; an asymptotic technique for estimating the size of this term is also given.

5. DELAY DOPPLER PROPERTIES OF THE OCEANIC L-BAND MULTIPATH CHANNEL: A.D. Thompson, Boeing Commercial Airplane Company.

An aircraft-to-satellite channel probe was conducted to investigate the oceanic forward scatter multipath properties at the delay-Doppler scatter function, $S(\tau, \omega)$ coordinate level. This function represents the distribution of diffusely scattered power arriving at the receiver with Doppler frequency ω and time delay τ. For the stationary, zero mean complex gaussian random scatter process, $S(\tau, \omega)$ completely characterizes the channel statistics. Data are presented to illustrate $S(\tau, \omega)$ and lower echelon parameters such as delay spectra, Doppler spectra, uni-dimensional spread parameter measures, auto-correlation functions, and rms total energy as a function of velocity vector direction, grazing angle and polarization. Results are compared to theory through use of the vector formulation for the physical optics very rough surface scatter model. In general, a high degree of correspondence between experiment and theory is in evidence.

6. RADIO SCATTERING LAWS AND THE LUNAR SURFACE: R.A. Simpson, G.L. Tyler, Stanford Center for Radar Astronomy.

Recent analysis of lunar bistatic radar data obtained during flights of Apollos 14, 15, and 16 has shown that mare surfaces can be reliably identified from radio information alone. Functions giving probability of surface slope occurence for tilt angles between 0° and 20° were derived from λ=13 cm data and found generally to agree best with a Hagfors scattering law. An exponential law is preferred in a small number of cases. A Gaussian scattering law, which has been used in earlier analyses, gives significantly poorer agreement than either the Hagfors or exponential laws for mare (seriously underestimating the population of highly tilted surface elements), though the difference in highlands is considerably less -- perhaps owing to the presence of large scale surface features which distort the data. Surface roughness on 10-20 m horizontal scales is as low as 4° in Oceanus Procellarum, based on the most recent estimates. Extension of these terrain identification techniques to Mars is being actively planned. A future study of Venus, where radio methods may be the only source of surface information, would also be of interest.

7. MICROWAVE THERMAL EMISSION FROM A BOUNDED MEDIUM CONTAINING SPHERICAL SCATTERERS: J.A. Kong, L. Tsang, Massachusetts Institute of Technology

In passive microwave remote sensing with a radiometer, theories have been developed to study subsurface scattering effects on observed brightness temperatures. Models of a random medium as well as a homogeneous medium containing discrete scatterers have been considered. In this report we investigate the radiative transfer theory applied to thermal microwave emission from a bounded layer of dielectric medium containing spherical scatterers. Brightness temperatures are calculated by using the Mie scattering functions and compared with Rayleigh results. Resonance phenomena that are characteristics of Mie scattering are revealed. Results computed from an iterative approach which accounts for single scattering are compared with that obtained from a numerical approach which accounts for multiple scattering. There are less oscillatory signatures when multiple scattering effects and particle size distributions are included. The theoretical results applied to ice and snow field, desert, cloud and rainfall, vesicular basalt, and lunar environment. The brightness temperatures as functions of observation angles and frequencies are examined for the vertical and horizontal polarizations and for different partical size distributions with numerical results illustrated and compared with experimental results.

8. CUMULATIVE ATTENUATION STATISTICS ALONG A LOW-ELEVATION ANGLE SATELLITE-EARTH PROPAGATION PATH: D.J. Fang, Propagations Studies Department, COMSAT Labs.

Rainfall statistics such as those specified by the Rice and Holmberg model are studied analytically to establish the relationship between precipitation at a point and along an earth satellite transmission path, i.e. a slant path extended from the point. Rain cells are assumed to be cylindrical, of finite ceiling height with the cell diameter decreasing with rain rate in accordance with known profiles, e.g., the mesoscale rainfall raincell profile, the C.C.I.R. raincell profile, etc. Cumulative attenuation statistics are then derived for a slant path based on stochastic considerations, accounting for the fact that a rain cell which intercepts the path in different ways will produce different amounts of attenuation.

Since the method given here is particularly effective in examining the dependence of cumulative attenuation statistics on elevation angle, it is especially useful in the determination of cumulative attenuation statistics for slant paths from earth stations operating at low elevation angles.

9. RAIN ATTENUATION OBSERVATIONS AT 11.7 GHZ WITH THE CTS SATELLITE:
L.J. Ippolito, NASA/Goddard Space Flight Center

Long term rain attenuation statistics utilizing the 11.7 GHz CTS beacon have been measured at NASA terminals at the Goddard Space Flight Center, Greenbelt, Maryland, and Rosman, North Carolina. Continuous monitoring of the circularly polarized beacon signal was accomplished with 4.5 meter antennas employing low noise parametric amplifier front ends. Meteorological support data, including rain gauges and dual frequency radars, were also utilized to develop prediction models and characterize the earth-satellite path.

The results of the first year of measurements are presented, including monthly, seasonal, and annual outage statistics; rain rate-attenuation correlation; and scintillation effects. The 11.7 GHz statistics are incorporated with 15, 20, and 30 GHz statistics measured with the ATS-5 and ATS-6 satellites to provide the first set of rain attenuation outage statistics and prediction curves derived from directly measured earth-space links.

Commission G - Session 4

Friday A.M. 0900 - 1150
ELF TO VLF PROPAGATION AND PROBING II
Chairman: A.J. Ferraro, Pennsylvania State University

1. AN EMPIRICAL, TIME-VARYING, IONOSPHERIC MODEL FOR VLF PROPAGATION CALCULATIONS: L.A. Berry, R.M. Davis Jr.

Calculations of the time availability of VLF and LF communications links using waveguide mode or wave hop propagation models require a model of the lower ionosphere that varies realistically with the relevent geophysical parameters. To develop such a model. we collected over 500 measured D-region profiles from the journal and report literature. These profiles were scaled and analyzed to produce a model of the form

$N(h) = N_0 \exp(\alpha(h-h_w))$, where α and h_w are simple functions

of local time, month, sunspot number, latitude and the presence or absence of ionospheric disturbances. The coefficients of the functions were determined using multi-parameter linear regression guided by VLF-LF propagation experience.

The model was validated by comparing propagation variations based on the model with measured VLF field strength variations. Some inadequacies in the data base and the form of the model are revealed. More elaborate models could be derived from the existing data base, but the value of doing so is debatable given the uncertainties, the sparseness, and the uneven distribution of the available profiles.

2. COORDINATED MEASUREMENTS OF ELF TRANSMISSION ANOMALIES AND THE PRECIPITATION OF ENERGETIC PARTICLES INTO THE IONOSPHERE: W.L. Imhof, J.B. Reagan, E.E. Gaines, Lockheed Palo Alto Research Lab., T.R. Larsen, Norwegian Defense Research Establishment, J.R. Davis, Naval Research Laboratory, W. Moler, Naval Electronics Laboratory Center

Stimulated by previous findings of a positive qualitative correlation between anomalous ELF signal levels and the occurrence of significant fluxes of precipitating energetic particles, a special coordinated exercise was conducted in March-April 1976 between satellite measurements of the precipitating particles and ELF transmissions between the U. S. Navy Wisconsin Test Facility and receiving stations in Maryland, Greenland, Norway, and Italy. During this time period significant fluxes of precipitating electrons were often measured with the Lockheed payload on the polar-orbiting satellite 1972-076B. Based on the fluxes, energy spectra, and pitch-angle distributions of the particles, ion-pair production profiles have been calculated and electron density profiles subsequently obtained with application of known effective electron loss rates. From these and coordinated data taken at other times, correlative studies between signal strengths and electron density profiles

are being performed with use of an ELF wave-guide-mode computer program developed at the Naval Electronics Laboratory Center. The propagation path to each station of interest is segmented into different regions with an averaging perpendicular to the direction of propagation of the wave-guide parameters. With the inclusion of data from several stations, the transmission signal strengths can be studied simultaneously under a variety of ionospheric conditions. The correlations between the enhanced electron densities and the measured and calculated ELF signal strengths will be presented.

3. TRANSIENT VLF PROPAGATION DISTURBANCES CAUSED BY WAVE-INDUCED ELECTRON PRECIPITATION FROM THE MAGNETOSPHERE: B. Dingle, Radioscience Laboratory, Stanford University

VLF propagation in the earth-ionosphere waveguide is subject to transient perturbations at night that coincide with the occurrence of whistlers or VLF emissions. A complete explanation of this phenomenon involves a wide range of magnetospheric and ionospheric physics. Whistler-mode wave bursts propagating in the magnetosphere scatter trapped energetic electrons, causing some of them to be dumped into a confined area of the lower ionosphere. There the electrons produce enhanced ionization which forms a bump on the bottom of the ionosphere. The bump scatters VLF waves traveling in the earth-ionosphere waveguide producing changes in signal amplitude and phase at remote receiving stations. When the electron precipitation ends, the excess ionization decays with a time constant determined by local chemical reactions. Much of the activity in this chain of events can now be described quantitatively. The results may be used for new methods of magnetospheric and ionospheric analysis, and for assessing effects on communication and navigation systems.

4. REFLECTION AND ABSORPTION OF ELF RADIO WAVES IN THE EARTH-IONOSPHERE WAVEGUIDE: R.A. Pappert, Naval Electronics Laboratory Center

As an aid to better understanding ELF propagation in the earth-ionosphere waveguide, full wave ELF modal height gains will be analyzed as regards regions of reflection and absorption. In particular, reflection will be examined primarily within the context of the Darwin-Hartree microscopic theory of reradiation. Frequencies between the Schumann band and 75 Hz will be discussed for representative day/night, ambient and disturbed ionospheres. Relative contribution to the earth ionosphere waveguide modal attenuations due to leakage and absorption will be discussed as will sensitivity of propagation parameters to D and E region ledge ionization.

5. ROOT FINDING METHOD FOR WAVEGUIDE CALCULATIONS IN TROPOSPHERIC DUCTING ENVIRONMENTS: C.L. Goodhart, Megatek Corporation, C.H. Shellman, Naval Electronics Laboratory Center

A crucial problem in analytical waveguide studies is whether or not all modes of consequence have been found. A recent mode search technique (ref. 1) developed particularly for ELF/VLF/LF propagation in the earth ionosphere waveguide finds all modes in any given rectangular region of the complex eigenvalue space. The utility of this technique for tropospheric ducting will be examined and compared with the more conventional Newton-Raphson scheme which was used in a recent work (ref. 2). Feasibility and ease of implementation will be the main concerns.

1. Morfitt, D.G. and C.H. Shellman, (1976), "MODESRCH," an Improved Computer Program for Obtaining ELF/VLF/LF Mode Constants in an Earth-Ionosphere Waveguide, Defense Nuclear Agency Interim Report 77T, prepared by Naval Electronics Laboratory Center.

2. Pappert, R.A. and C.L. Goodhart, "Case Studies of Beyond the Horizon Propagation in Tropospheric Ducting Environments," Radio Science, Vol. 12, No. 1, 75-87, 1977.

6. GENERALIZED CHARACTERISTIC FUNCTIONS APPLIED TO PROPAGATION IN BOUNDED INHOMOGENEOUS ANISOTROPIC MEDIA--RECIPROCITY AND ENERGY RELATIONSHIPS: E. Bahar, B.S. Agrawal, Electrical Engineering Department, University of Nebraska

The problems of radio wave propagation, in bounded inhomogeneous anisotropic media, can be expressed as sets of four simultaneous first order differential equations with variable coefficients [1]. When the problem can be reduced to two pairs of uncoupled second order differential equations, rigorous closed form analytic solutions can be found for special permittivity profiles. If the medium of propagation is slowly varying and devoid of critical coupling regions, the solutions can be expressed in terms of WKB type characteristic functions.

A nonsingular transformation matrix is introduced to diagonalize the coefficient matrix even when two or more of its characteristic values are equal [1].

Thus, the original set of differential equations for the transverse electromagnetic field components are converted into loosely coupled generalized characteristic functions. These generalized characteristic solutions are suitable for regions where there is strong coupling between the upward and downward traveling ordinary and extraordinary waves.

In this work, numerical solutions are presented for sixteen transmission and reflection scattering coefficients that characterize a bounded inhomogeneous plasma in an arbitrarily oriented magnetic field. These numerical solutions for arbitrary excitations are shown to be consistent with the reciprocity conditions for dissipative anisotropic media [2] and also with energy conservation for nondissipative media.

[1] E. Bahar (March 1976), Canadian Journal of Physics, Vol. 54, No. 3, pp. 301-316.

[2] D. M. Kerns (January 1976), NBSIR 75-824, Supt. of Doc., U.S. Govt. Printing Office, Washington, D.C.

7. OBLIQUE INCIDENCE OF A PLANE ELECTROMAGNETIC WAVE UPON AN ANISOTROPIC LAYER: M. Kisliuk, Department of Electronics, Tel-Aviv University

A rigorous solution for the oblique incidence of a plane electromagnetic wave upon an anisotropic layer (which has as yet not been obtained) is derived from two vector integral equations, which are equivalent to Maxwell's equations in a source-free region partially filled with material media.

For an anisotropic layer which μ and ε tensor's elements are constants, the integral equations are reduced to two sets of linear algebraic equations. One of the sets is equivalent to Maxwell's homogeneous field equations for plane waves in the considered anisotropic medium. It determines the complex refraction angles, the complex propagation constants, and the relations between the electric and magnetic intensities components of the four waves excited in the layer by an incident wave. The angle of incidence and the polarization of the incident wave are arbitrary.

The second set of four equations determines the complex amplitudes of each of the four waves inside the layer. Expressions are derived for the computation of the complex amplitudes of the reflected, and the transmitted waves.

Joint Session:
Commission G - Session 5
Commission H - Session 2

Friday A.M. 0900 - 1140
WAVE PHENOMENA IN IONOSPHERE AND MAGNETOSPHERE
Chairman: R.A. Helliwell, Radioscience Laboratory, Stanford University

1. CONTROLLED NONLINEAR WAVE-WAVE INTERACTION IN THE MAGNETOSPHERE: D.C.D. Chang, R.A. Helliwell, Radioscience Laboratory, Stanford University

Manmade whistler mode (WM) waves propagating along a geomagnetic field line in the magnetosphere and interchanging energy with energetic electrons often interact with other WM waves at nearby frequencies. Using the Siple Station transmitter an experiment was performed to determine the critical frequency separation within which wave-wave interaction (WWI) occurs. Several constant frequency waves were sent into the magnetosphere simultaneously. The frequency spacing between these waves was varied from 50 Hz to 5 Hz from time to time. Preliminary results showed that the rate of emission triggering by a group of such waves increased with the frequency spacing. This indicates that two waves with frequency difference less than 50 Hz are coupled to one another. One wave component may transfer its energy to another or it may suppress the growth of another. Coupling is attributed to overlap of the perturbed electron distribution functions associated with each wave. Each wave organizes electrons in a finite $v_{\parallel}$ range centered on the corresponding resonant velocity. When the $v_{\parallel}$ perturbation ranges of two waves overlap, the electrons in the region of overlap are 'shared' by the two waves and consequently their effectiveness for growth of one or the other of the two waves is reduced.

2. SIMPLIFIED COMPUTER SIMULATION OF MAGNETOSPHERIC VLF TRIGGERED EMISSIONS: T.L. Crystal, Radioscience Laboratory, Stanford University

The problem of the growth and triggering of coherent VLF waves in the magnetosphere is attacked using a new computer simulation. The program formulation is based on a simple physical interpretation of the interaction physics which aims to relate observed ASE characteristics to measurable flux parameters. The simulation introduces a monochromatic WM signal into a collection of electrons having equal perpendicular velocities ($v_{\perp}$) but a range of parallel velocities ($v_{\parallel}$) spread uniformly over a band around resonance. At first the associated electron density distribution is assumed uniform in $v_{\parallel}$ (the "flat top distribution" of earlier work). It is found that when a range of $v_{\parallel}$ exceeding a few trapping widths is included, the resulting phase bunched current, aligned with the stimulating wave's magnetic field, is negligible. In treating a 'tilted' distribution, this flat top contribution can properly be subtracted out of the total current integral. The simulation now involves only a narrow range of $v_{\parallel}$ (2-3 trapping widths) near resonance and thus requires substantially less computer memory and manageably short run times. The total wave-stimulated current at a single value of $v_{\perp}$ is now attributable to the

electron density slope near resonance. This current has a phase that is closely aligned with the wave's electric field and a damped oscillating amplitude. These new simulation results agree with both linear analytic treatments (e.g., Istomin and Karpman (1973)) and computer simulations using many more particles (e.g., Rathmann, Vomvoridis and Denavit (1977)) that also involve only single valued $v_\perp$. However repeating the simulation at several $v_\perp$ shows the necessity of including a range of pitch angles in any total stimulated current integral.

3. FAILURE OF LOCAL, LINEAR STABILITY ANALYSIS FOR ALFVEN WAVES IN THE SOLAR WIND: B. Abraham-Shrauner, Department of Electrical Engineering, Washington University

The growth rates of Alfvén waves (ion cyclotron branch) are discussed in local, linear stability analysis for solar wind, high speed stream data from IMP-7 [1]. Plasma parameters and growth rates are given for 17 measurements. The dispersion relation for magnetic field aligned modes has been solved numerically for proton and electron distribution functions which are each modeled by two drifted bi-Lorentzians. Although about a third of the measurements show the field aligned Alfvén mode is stable, arguments are given from previous work[2] to show that the waves are expected to be unstable for oblique propagation. The observed proton distribution appears stable but the e-folding time for the instability is at most several minutes leading to a failure of the local, linear stability analysis. A nonlinear Alfvén wave which is a stationary solution of the Vlasov equation has been proposed[3] to explain the discrepancy. A criterion for choosing an inhomogeneous distribution in lowest order is discussed.

1. Feldman, W.C. (private communication)

2. Montgomery, M.D., S.P. Gary, W.C. Feldman, and D.W. Forslund, J. Geophys. Res. 81, 2743 (1976).

3. Abraham-Shrauner, B. and W.C. Feldman, "Nonlinear Alfvén Waves in High Speed Solar Wind Streams" J. Geophys. Res. (in press).

4. LINEAR WAVE COUPLING AND GROWTH IN THE LONG DELAYED ECHO MECHANISM: T.L. Savarino, F.W. Crawford, Institute for Plasma Research, Stanford University

The phenomenon of long delayed ($\approx$ 10 s) radio echoes from the ionosphere has been a subject of interest since its discovery in 1928. Using a simplified model of the ionosphere, with a vertical electron density gradient, we have investigated some problems of linear wave coupling required by a mechanism previously advanced to explain the occurrence of these echoes.[1]

In the first step of this process, some energy from an ordinary wave is transferred to a right-hand polarized wave by electron density perturbations in the vicinity of the ordinary wave reflection point. The strength of this interaction is calculated using Fosterling's coupled equations. For a density perturbation of 0.1%, over 10% of the energy in the ordinary wave can be transferred to the right-handed wave.

Energy that has been coupled into the right-hand polarized wave can then experience amplification, and propagate with low group velocity ($\sim$ 1 km/s), via a beam-plasma interaction with electrons that precipitate along the earth's magnetic field lines. The quasistatic dispersion relation for the beam-plasma interaction has been evaluated using both a macroscopic approach and a low-temperature expansion of the microscopic theory. Growth rates and group velocities have been obtained numerically.

The amplified plasma wave couples to an ordinary wave which propagates to the ground. For plausible parameters for the beam-plasma interaction, and assuming a density variation as small as 0.1% in 100 meters, the coupling to an ordinary wave is approximately -60 db.

---

1. Crawford, F. W., Sears, D. M. and Bruce, R. L., J. Geophys. Res. 75, 7326 (1970).

5. IONOSPHERIC DIAGNOSTICS THROUGH MEANS OF COHERENT WAVE INDUCED PARTICLE PRECIPITATION: U.S. Inan, T.F. Bell, R.A. Helliwell, Radioscience Laboratory, Stanford University

Energetic electrons in the radiation belts are precipitated into the ionosphere through interaction with coherent VLF waves from ground transmitters. The particles interact with the waves in the cyclotron resonance mode, resulting in the amplification of the waves (up to 30 dB) and pitch angle scattering of the particles. A computer simulation approach used to study the particle scattering shows that energetic particle fluxes as large as 5 ergs/cm^2-sec can be precipitated by a wave with intensity of the order of 10 mγ. Complete equations of motion are employed in the simulation, and the results are compared with those of linear theory. The full distribution of particles is simulated by test electrons appropriately distributed in energy and pitch angle. By computing the scattering of these test particles, the precipitated flux is obtained. The method used is quite general and can be applied to any kind of particle distribution. The perturbation in the D region produced by the flux precipitated by a 10 mγ, 5 kHz wave is calculated for field lines both inside and outside the plasmapause and it is shown that significant perturbations can be produced in the nighttime

ionosphere. Thus, using controlled VLF wave injection experiments, it appears possible to study both chemical and transport processes in the ionosphere as well as coupling processes between the ionosphere and the magnetosphere. In addition, this tool offers a means to study the Trimpi effect in which precipitated particles affect the phase and amplitude of VLF waves propagating in the earth-ionosphere waveguide.

6. THE PLASMAPAUSE AS A SECONDARY SOURCE FOR PLASMASPHERIC HISS: W.J. Malloy, R.M. Thorne, University of California, Los Angeles

The effect of the plasmapause on whistler-mode wave propagation in the plasmasphere has been investigated with the use of a ray tracing model. If one assumes that the waves originate by cyclotron resonance with medium energy radiation belt electrons, the source region is expected to be confined to the geomagnetic equatorial region just within the plasmapause and the initial wave normal should be confined to a cone aligned along the magnetic field. The waves then generally propagate outward at oblique angles to the magnetic field until they reach the plasmapause. A major fraction of these waves are internally reflected and subsequently propagate to fill the plasmaspheric cavity with whistler-mode waves. This behavior is consistent with satellite observations that show a relatively steady band of turbulent ELF hiss throughout the plasmasphere. A small fraction of the wave energy is ducted along the plasmapause down into the ionosphere. Only a minor part of the wave energy incident at the plasmapause is able to escape from the plasmasphere.

7. COMPUTATIONS FOR IMPULSE PROPAGATION IN A MAGNETOPLASMA: R.J. Vidmar, F.W. Crawford, Institute for Plasma Research, Stanford University

The propagation of delta-function pulses in a magnetoplasma is being investigated analytically and numerically, using parameters appropriate to the ionosphere at a height of 450 km. The treatment includes the effects of magnetic field, positive ions, and momentum transfer collisions. The impulse propagation is studied for principal modes, which are represented in terms of inverse Laplace transforms. These expressions are evaluated analytically, or by appropriate asymptotic expansions.

Results will be presented for all branches of propagation parallel and perpendicular to the magnetic field. Some simple expressions have been found for the upper branch (right-hand polarization), and lower branch (left-hand polarization), for parallel propagation, and for the ordinary mode and the upper branch of the extraordinary mode, for perpendicular propagation. The remaining branches (whistler, ion cyclotron, upper hybrid, lower hybrid) are characterized by group velocities much less than the speed of light, and are best treated by asymptotic analysis, when the time of propagation is long. Computations for these branches will be presented.

Commission G - Session 5
Commission H - Session 2

8. VLF WAVE TRAPPING IN MAGNETOSPHERIC DUCTS: P.A. Bernhardt, Radioscience Laboratory, Stanford University

Electron density enhancement requirements for ducting of VLF signals in the magnetosphere are considered. Over 3000 ray trajectories have been calculated and catalogued for propagation in ducts of varying sizes. Gaussian ducts were used with L-shell half widths ranging from .01 to .08 earth radii. The duct enhancements vary from 5 to 30%. Rays were injected at the equator with ranges of initial wave normal angles and positions inside a duct. The trapping characteristics of ducts as a function of initial conditions and duct parameters are presented in the form of contour maps of the altitude where the ray leaves the duct. From this study we conclude that: 1) wider ducts require larger enhancement factors; 2) it becomes more difficult to trap rays as the wave frequency approaches one half of the equatorial gyrofrequency where theoretical cutoff in ducting is predicted, and 3) in a few cases, rays with frequencies above the equatorial half gyrofrequency can propagate from one hemisphere to another, crossing the equator in an unducted mode.

Commission B - Session 7

Friday P.M. 1400 - 1640
ANTENNAS
Chairman: G.A. Thiele, Ohio University, Columbus, Ohio

1. SIDELOBE REDUCTION AND ANGULAR RESOLUTION IN RANDOM, THIN ARRAYS: B.D. Steinberg, University of Pennsylvania, Philadelphia.

The angular resolution of a random, thin antenna array is determined primarily by the beamwidth and the average sidelobe level. The average sidelobe level relative to the main lobe is N^{-1} where N is the number of elements. Large numbers of elements, which implies high cost, usually are required to hold the sidelobes to an acceptable level. It is found that for the case of two targets of widely differing cross-section N may be reduced by a factor of the order of 3 or 5 without impairment of the angular resolution by subdividing a random array into statistically identical subarrays and multiplying their outputs. Theory and simulation results are presented.

2. RECTENNA DESIGN CONSIDERATIONS: Jefferson F. Lindsey, University of Houston, Houston, Texas.

The rectenna is the major element used in the conversion of a.c. microwave energy into a d.c. form of energy. Major design factors include efficiency, cost and the environmental effects. The efficiency is related to the antenna type, the materials used for fabrication and the power level which is rectified in the diode. The optimum antenna would be one which has a high radiation resistance compared with ohmic losses and one which occupies a small physical area and at the same time has a large electrical capture area. The helical element is suggested as a candidate and is compared with other types of antenna elements. Another limiting factor is the amount of power which is rectified by the diodes. Since the barrier voltage of a diode must be exceeded before the diodes act as conductors, the conversion efficiency is a function of power level. An opposing factor is related to environmental and biological effects of a sustained r.f. field at high levels. This includes effects on the ionosphere and trophosphere in the case of the proposed space solar power station and effects on plants and animals which may be in the path of the microwave energy. Finally, the cost is particularly important for large rectenna farms which may be several miles in diameter for power transmission from space. A recent proposal by NASA has called for a rectenna with an output of 5 GW.

3. CURRENT INDUCED ON AN INFINITE HORIZONTAL WIRE ABOVE A LOSSY EARTH BY AN ARBITRARILY-ORIENTED DIPOLE: D.C. Chang, A. Hoorfar, E.F. Kuester, University of Colorado, Boulder, Co.

An electric Hertzian dipole located above a plane lossy earth excites an infinite thin horizontal wire parallel to the air-earth interface. An integral equation for the current induced on the wire is obtained in the thin-wire approximation by requiring the total fields to satisfy the boundary conditions at the wire as well as at the surface of the earth. The solution of the integral equation can be written as the sum of discrete mode contributions as well as radiation components. Numerical results for the current have been obtained for various heights and orientations of the dipole, as a function of distance along the wire. These results are of practical interest in the design of guided radar systems, and also in studies of external interference with transmission lines, since the two-wire transmission line corresponds to the limiting case of a perfectly conducting earth.

4. OPTIMIZATION OF THE RECEIVING LOOP ANTENNA WOUND ON A CYLINDRICAL FERRITE CORE: T.L. Simpson, University of South Carolina, Columbia, S. C.

Abstract: The magnetostatic potential on the surface of a cylindrical ferrite rod subjected to an incident magnetostatic potential field is determined by numerical solution of Phillips' integral equation. The incident potential may arise from a distant source enabling the computation of the received open-circuit voltage available from a pick-up loop wound on the core. Alternatively, the incident potential may emanate from current in the loop itself in which case the self inductance may be determined. By employing the open-circuit voltage and the self-inductance in an equivalent circuit representing a broadband receiver, conditions are obtained for maximum power into the receiving load. A relation is found which expresses the ratio of the received power to the core volume and the optimum volumetric efficiency is determined for cores of various aspect ratios and permeability.

5. INPUT IMPEDANCE CHARACTERISTICS OF ANTENNAS ON FINITE GROUND PLANES: A.W. Glisson, D.R. Wilton and B.M. Duff, University of Mississippi, University, Mississippi.

The numerical modeling of antennas on finite ground planes and near bends or edges is of great importance since these situations arise frequently in practical applications, such as in modeling an antenna in a shipboard environment. In this paper the problem of determining the input impedance of antennas located on rectangular finite ground planes and near bends is considered. The electric field integral equation is solved numerically for plate and wire currents by employing an extension to a very successful scheme recently developed for handling surfaces with sharp bends. Features of the method are that it is simple, efficient, highly convergent, and is capable of treating small ground plane sizes (dimensions of the order of twenty wire radii or larger). Numerical and experimental results for antennas and flat ground plane structures of various sizes have been obtained and work is currently in progress for treating non-perpendicular antennas and antennas near bends and edges of finite ground planes. Results indicate that the impedance values for an antenna on a finite ground plane tend to oscillate about the value for the antenna on an infinite ground plane. The impedance values for small ground plane sizes differ significantly from other results which have appeared in the literature. For very small ground planes, the impedance approaches that of an end-fed antenna, as one might expect, and is almost completely reactive.

6. SOME EFFECTS OF SLOTS IN A GROUND PLANE UPON THE PERFORMANCE OF A MONOPOLE: S. Singarayar, C.M. Butler, and K.R. Umashankar, University of Mississippi, University, Mississippi.

The effects of narrow slots in a ground plane upon the characteristics of a monopole over the plane are assessed. Cracks and other narrow slots in a ground plane or screen alter the current distribution in the screen from what it would be without such apertures present, and, thus, they can influence the monopole current. In some cases, slots and cracks occur inadvertently due to fabrication of a ground plane and in other cases they may be introduced to accomodate probing of electromagnetic fields. In any event, the slot presence must be accounted for in an accurate investigation of monopole performance. The monopole in the presence of a slotted ground plane is investigated in this paper, and coupled, integro-differential equations are formulated for this problem with full account taken of the interaction between the monopole and slot. These equations are solved numerically and the effect of the presence of the slot upon the monopole current and input impedance is investigated for various cases of interest. In addition, transient currents on the monopole and the associate transverse electric field in the narrow slot are determined subject to EMP excitation.

7. THE EFFECT OF SMALL RADIAL GROUND SCREENS ON INTERMEDIATE FIELD STRENGTH OF HF ANTENNAS: Michael Jay Dick, Naval Electronics Laboratory Center, San Diego, California.

The effect of large radial ground screens is a well researched topic. However, the effect of small radial ground screens is relatively unstudied. This study utilizes standard numerical modeling computer programs interfaced with numerical solutions of the Sommerfeld integral to determine the effect of smallnumbers of radials on intermediate distance field strength of simple whip and dipole antennas. These models are made for various lengths and numbers of radials over a variety of ground types.

8. CHARGE AND CURRENT DISTRIBUTIONS ON CROSSED-MONOPOLE TRANSMITTING ANTENNA: William E. Beyatte, Lawrence Livermore Laboratory, Livermore, Ca. and Robert W. Burton, Naval Postgraduate School, Monterey, Ca.

Experimental measurements of charge and current density distributions on crossed-monopole antennas have demonstrated that the locations and electrical lengths of the cross segments have significant and widely varying effects on the distributions along the antennas. Crossed-monopoles may serve as models for fixed wing aircraft, and the empirical results obtained can advance the analysis of the currents induced on aircraft which have been exposed to electromagnetic fields such as those associated with the Electromagnetic Pulse (EMP). The addition of a cross arm to a base fed monopole results in a change in the feed point impedance as well as current and charge distributions. The change is a function of cross arm lengths and angle of intersection.

Charge and current density distribution data was recorded on a moderately thick ($ka = .2$) base fed crossed-monopole antenna constructed with a 45 degree angle of intersection. The results are compared with base fed monopole of the same height. Four configurations were investigated, each representing a different combination of charge and current maxima and minima at the junction.

The oblique intersection of the cross arm resulted in asymmetrical distributions on the antenna segments. The most prominent effects were present along the lower vertical and lower cross arm segments where two factors, the greater standing wave amplitudes and the close physical proximity, combined to produce large charge concentrations and current magnitudes.

Commission C - Session 4

Friday P.M. 1400 - 1600

TIMING AND CARRIER PHASE
RECOVERY IN DATA COMMUNICATION

Chairman: L. E. Franks, University of Massachusetts

1. CARRIER SYNCHRONIZATION IN COHERENT COMMUNICATION SYSTEMS:
W.C. Lindsey, University of Southern California

Central to the problem of coherent demodulation of bi-phase, staggered quadriphase and minimum shift keyed signals (BPSK, QPSK, MSK) is the establishment of carrier and clock references at the receiver. New signal designs of the suppressed carrier type are currently being planned for advanced satellite systems. They include unbalanced quadriphase shift signals (UQPSK) in which the power as well as the data rates in the I and Q data channels are unequal and vary over a wide dynamic range.

This talk will review the status of contemporary suppressed carrier recovery techniques and discuss new and alternate methods. Particular emphasis is placed on techniques of interest in satellite communications. The problems of filter bandwidth selection, phase ambiguity, false-lock and sync acquisition will be discussed as a function of the PCM baseband signaling format chosen (NRZ or Manchester). In addition, the effects which bandlimited nonlinear channels (TWTAs) produce on the carrier recovery process will be addressed along with the problems of low bit-rate demodulation and oscillator phase noise effects. If time permits techniques for incorporating AGC in the receiver and lock detection will also be discussed.

2. THE FALSE-LOCK PERFORMANCE OF COSTAS LOOPS WITH HARD-LIMITED IN-PHASE CHANNEL: M. K. Simon, Jet Propulsion Laboratory

The ability of a Costas loop to false lock on a data sideband is a problem which must be dealt with in the design of suppressed-carrier receivers which employ such loops for carrier reconstruction. For conventional Costas loops wherein the error signal is formed from the product of two analog signals, the false lock problem has recently been investigated by the author and others and is now well understood. For implementation reasons associated with the reduction of dc offsets, it is often desirable to hard limit the output of the in-phase channel and replace the analog multiplier which forms the above product with a chopper-type device. The false lock behavior of such a Costas loop with hard-limited in-phase channel is quite different from that of the conventional Costas loop and is the subject of investigation in this paper. Results are also presented for a modified version of the Costas loop wherein the quadrature arm filter is removed. This configuration has recently been suggested as a means of improving the false lock performance of the Costas loop with hard-limited in-phase channel.

3. HANGUP IN PHASELOCK LOOPS: F. M. Gardner, Gardner Research Company

Phaselocked loops (PLL's) occasionally exhibit unduly-prolonged phase transients during initial acquisition of lock. The loop appears to stick, temporarily, at a large value of phase error before settling to its normal tracking condition of small error. This phenomenon has been dubbed the "hangup" effect.

Hangup is associated with the reverse-slope null of the phase detector. The problem is caused by the small output voltage that occurs in the vicinity of the reverse null and by equivocation back and forth across the null.

Dwell time at the hangup point is finite--the loop cannot remain indefinitely at the unstable null--but even a short dwell time may be excessive for some applications. An example arises in TDMA communications where rapid acquisition is demanded for efficient usage of channel time. Failure of a PLL to settle within an allotted preamble time prevents correct detection of an identification marker and causes loss of the entire burst.

Recent practice in TDMA synchronizers has been to substitute narrowband, tuned filters for for a PLL in order to avoid the hangup effect. The resulting equipment tends to be overly complex and suffers from other unwanted characteristics. A hangup-free, phaselocked synchronizer would be preferable.

In this paper we examine the causes of hangup,and formulate necessary conditions for its prevention. Methods are suggested for implementing the conditions and a particular implementation is proposed.

4. FALSE LOCK IN BPSK AND QPSK CARRIER RECONSTRUCTION LOOPS: H. Chang, J. J. Spilker, Jr., Stanford Telecommunications, Inc.

One common problem encountered in BPSK and QPSK carrier reconstruction loops with closed-loop sweeping is false lock: namely, the loop locks to a sideband instead of the genuine carrier. The carrier reference constructed from a sideband locked loop is generally located at a multiple of the symbol rate divided by two (BPSK) or four (QPSK) away from the actual carrier frequency.

The false-lock sidebands are shown to be originated essentially from the modulation distortion effect. The more serious the modulation distortion effect, the larger the relative sideband magnitudes. If the power contained in the sidebands is sufficient and if the frequency sweep range is greater than one quarter (BPSK) or one eighth (QPSK) of the symbol rate, the result could be a false lock rather than the desired carrier lock. In the case of a Costas-type loop, modulation distortion is due mainly to the finite I/O filter bandwidth. It is analytically demonstrated and experimentally verified that by appropriate widening of the I/O filter bandwidth, the false-lock sidebands can be greatly suppressed. Possible means of preventing false lock other than suppressing the sidebands are also discussed.

5. HIGH-PRECISION DOPPLER TRACKING BETWEEN SPACECRAFT: J. J. Stiffler, Raytheon Company

A phase-coherent, dual-frequency link was established, during the Apollo-Soyuz mission, between the Docking Module that connected the two spacecraft and the Apollo Command Service Module. This link was used to perform Doppler measurements between the two modules to a millihertz frequency (in 10 to 100 seconds integration time). These measurements were made in an attempt to detect mass concentrations (mascons) in the earth's crust.

The link operated at 162 and 324 MHz. The master oscillators in the transmitter and receiver both had a frequency stability of 1.5 parts in 10^{12} (in 10 to 100 seconds integration time). Both receiver channels used phase-locked loops to minimize the errors introduced by additive noise. The outputs of these loops were processed digitally and the resulting information was encoded and recorded on magnetic tape for subsequent data reduction.

This paper describes briefly the instrumentation system concept and its implementation. It then summarizes the analysis used to estimate the Doppler measurement inaccuracies caused by various instrumental and propagation effects, including those due to multipath reflections from the earth's surface. The resulting error estimates are compared to those actually measured.

6. OPTIMUM RECEPTION OF DIGITAL DATA SIGNALS IN THE PRESENCE OF TIMING-PHASE HITS: D. D. Falconer, R. D. Gitlin, Bell Laboratories

Protection switching of microwave radio channels results in a timing-phase discontinuity and occasional long error bursts in the demodulated data signal. Using an idealized mathematical model we derive receivers which rapidly track such delay hits, whether or not a timing-pilot tone is used. Since the receiver is at a different physical location from the switch, the tracking algorithm must also sense the occurrence of a switch. A dual-mode data-directed structure is revealed as being optimum; a narrow-band tracking loop is used for steady-state operation, while a wideband tracking loop provides rapid recovery from the timing transient. An error-sensing non-linearity, which incorporates hysteresis, inhibits erroneous noise-induced mode transitions. Oversampling of the demodulated data signal rapidly establishes a coarsely-quantized optimum sampling phase, and permits the dual-mode tracking loop to operate in a data-directed manner. Data-directed operation permits greater loop bandwidths, since the data energy is not perceived as noise.

Simulation of a system employing a dual-mode data-directed and coarse-quantized timing loop has demonstrated dramatic reduction of the length of error-bursts following a protection switch. For example, at the data rate of 1.544 M bits/sec a conventional phase-locked loop with a 100 Hz bandwidth, when displaced half a symbol interval by a delay-hit, would typically sustain an error burst 15,000 bits in duration. When such a delay-hit stresses the dual-mode timing loop, simulation has indicated error bursts on the order of 15-bits in duration.

7. SIGNAL DESIGN FOR IMPROVED SYNCHRONIZATION IN CARRIER DATA SYSTEMS: L. E. Franks, University of Massachusetts

The use of highly efficient signal formats for carrier data systems, such as VSB/PAM and QAM/PAM with suppressed carrier and no additional pilot signals, presents special problems in connection with the recovery of the carrier phase and symbol timing information. The conventional approach involving independent estimation of carrier phase with a Costas loop followed by symbol timing recovery from the demodulated baseband signal can be shown to be completely ineffective for modulation schemes of this type. On the other hand, an approach based on joint recovery of the two types of timing parameters provides satisfactory, and sometimes close to optimum, performance. A data receiver structure, derived from the principles of joint maximum-likelihood estimation, is proposed. There are both open-loop and closed-loop versions of this structure for estimation of the two parameters.

A simplified expression for the receiver performance, in terms of r.m.s. jitter in the timing parameters, is presented. This expression allows a study of the effects of various parameters on the receiver performance. In particular, for sharply bandlimited systems, the shape of the data pulse has a strong influence on the amount of jitter and some results concerning optimum pulse shapes have been obtained. An evaluation of the "bandwidth vs. jitter" tradeoff is also considered.

Commission F - Session 8

Friday, P.M. 1400 - 1640

THEORETICAL AND EXPERIMENTAL STUDIES
OF RADIO PROPAGATION PROBLEMS

Chairman: C. R. Beard, Naval Research Laboratories, Washington, D. C.

1. ATMOSPHERIC REFRACTION COMPENSATION TRANSFORMATIONS: Dr. W. M. Cornette, Naval Weapons Center

A transformation to compensate for ray curvature due to atmospheric transmission is a very useful tool in evaluating first order effects of refraction on electromagnetic wave propagation. The transformation in use at the present time is the effective (or 4/3) earth's radius. Unfortunately, this transformation has been greatly misunderstood and misused. The classic derivation of this transformation is incorrect resulting in a transformation which is not conformal and does not map rays into straight lines. Using the same basic techniques used to obtain the effective earth's radius, an effective radius transformation is obtained which eliminates most of the errors inherent in the effective earth's radius. Finally, using the differential equations for curvature and ray tracing, the correct transformation is obtained and compared with the other two transformations.

2. BEAM PROPAGATION IN RANDOMLY PERTURBED LENS-LIKE MEDIA: A WAVE-KINETIC APPROACH: I. M. Besieris, W. B. Stasiak, Virginia Polytechnic Institute and State University, and F. D. Tappert, Courant Institute of Mathematical Sciences

A technique has been developed for extending conventional ray-tracing methods to incorporate both diffractive and refractive effects associated with the propagation of beamed signals through randomly inhomogeneous media. The formalism is illustrated by considering the propagation of partially coherent cw focused laser beams in randomly perturbed lens-like media (e.g., selfoc fibers, laser-induced plasmas, etc.). Physical observables such as position and angle variances, as well as the decay of mean power from the fundamental unperturbed mode and mean power transitions to higher modes, have been computed in special cases and numerical results will be presented. Finally, the possibility of beam stabilization by means of spatially dependent conductivity will be discussed.

3. PROPERTIES OF JOINT GAUSSIAN STATISTICS: D.L. Knepp, Mission Research Dorporation, and G.C. Valley, Hughes Aircraft Corporation

In this paper joint- or complex-Gaussian statistics are assumed to apply to the in-phase and quadrature components of an electromagnetic wave which has propagated through a turbulent medium, and the consequences of this assumption are compared to tropospheric, ionospheric, and laboratory propagation experiments. New curves for the cumulative probability distribution of intensity and for the variance of intensity versus the variance of the logarithm of intensity are presented. Joint-Gaussian statistics are shown to fit the total set of turbulence propagation results better than the Log-normal, Rice-Nakagami or Nakagami-m distributions. But a major feature of optical observations cannot be fit by joint-Gaussian statistics: straight-line cumulative intensity distributions in the saturation regime which reflect a large probability of occurrence of high intensity spikes.

4. SPECTRAL BROADENING IN A RANDOM MEDIUM WITH ANISOTROPIC IRREGULARITIES AND VELOCITY FLUCTUATIONS, R. Woo, Jet Propulsion Kaboratory, F. C. Yang, Dikewood Corporation, A. Ishimaru, University of Washington

When a monochromatic radio wave propagates through a random medium, it undergoes spectral broadening if the refractive index fluctuations are strong. These effects have, for example, been observed in planetary (including earth) ionospheres as well as the solar corona. In previous work we obtained a solution for spectral broadening by applying the Markov approximation to the parabolic wave equation and studying the Fourier transform of the mutual coherence function. The irregularities were assumed to be isotropic and their spatial wave number spectrum to be power-law with spectral index p. Because the irregularities tend to be anisotropic due to alignment with the magnetic field, we consider the effects of anisotropy in this paper. We show that while anisotropy increases the bandwidth of the spectrum, the shape of the spectrum remains unchanged for a given value of p. The increase is greatest when the magnetic field is transverse to the propagation path. When the axial ratio of the irregularities is less than two, the bandwidth increase is less than threefold. However, for larger axial ratios, an increase in bandwidth by as much as a factor of 10 is possible. It is also shown that wind velocity fluctuations cause slight increases in the bandwidth but do not change the spectrum shape.

5. RADIOMETRIC RECOGNITION OF COHERENCE IN THERMAL RADIATION THROUGH DIELECTRIC LAYERS: K. R. Carver, University of Kansas

The response of microwave and infrared radiometers to thermal radiation passing through a spatial filter may be described in terms of the observed degree of coherence and apparent emissivity. For example, an incoherent plane wave passing normally through a lossless dielectric sheet will in general be recognized as partially coherent, with the degree of coherence γ depending on the sheet thickness d and the bandwidth of the radiometer. The coherence length associated with a bandwidth Δf is given by $d_c = c/\Delta f$; if a dielectric sheet with constant ε_r has a thickness d, then it can be shown that the degree of coherence is given by $\gamma = (\sin X)/X$ where $X \approx (\bar{\beta}d)(\Delta f/f)$ with $\bar{\beta}$ being the midband phase constant of the dielectric. This means that incoherent thermal radiation passing from terrain or sea surfaces through dielectric slabs or films will in many practical situations be recognized as coherent by microwave radiometers but as incoherent by infrared radiometers. For example, a 69.8 GHz radiometer with $\Delta f = 1$ GHz which is used to observe oil films on sea water will recognize nearly complete coherence ($\gamma \approx 99\%$) and 50K brightness temperature oscillations as the film thickness varies; this has been verified experimentally by workers at NRL. A 13μ infrared radiometer with $\Delta\lambda = 1\mu$ which views the same scene would not see the interference fringes, since $\gamma \approx .01\%$.

6. RELATIONSHIP BETWEEN REFRACTIVE BENDING AND RETARDATION:* S. Weisbrod, L. A. Morgan, Teledyne Micronetics

The paper deals with the feasibility of using the radar as a sensor to accurately estimate range errors at low elevation angles. The underlying assumption is that the radar makes routine observations on cooperative transtropospheric targets such as satellites and/or celestial radio sources whose true positions are sufficiently well known to permit the determination of refractive bending to an accuracy of about .1 mr at elevation angles between 10 and 50 mr. It is also assumed that the surface refractivity is routinely measured or computed from temperature, pressure and humidity at the radar site.

It will be shown that this information is adequate to allow the determination of the range error as a function of the observed elevation angle of a noncooperative target down to the radio horizon with typical accuracies of better than two meters. For the purpose of this investigation, it has been assumed that the radar targets of interest are above the

troposphere and also that the radar frequency is sufficiently high so that no ionospheric correction needs to be made while tracking cooperative transionospheric targets. Neither of these assumptions is necessary, but they do simplify the error estimating procedures. Procedures described here can be extended to allow tracking the target down well into the troposphere. Similarly, adequate ionospheric corrections could be made at lower frequencies from routine topside and bottomside ionograms. Both of these points will be discussed in the paper.

---

*This work was performed under the sponsorship of the Rome Air Development Center, Contract No. F30602-76-C-0384.

7. ANTENNA-TO-ANTENNA ISOLATION ON SPACE VEHICLES: J. F. Lindsey, University of Houston, H. D. Cubley, NASA Johnson Space Center

Antenna-to-antenna isolation is an important parameter which significantly affects the design of receiver and transmitter filters used for sophisticated communication systems on space vehicles. When the antennas are located on a curved surface which is covered by dielectric thermal protection material, accurate theoretical determination of isolation becomes more difficult. In this paper, the use of several theories are combined to obtain a reasonable estimate for minimum isolation between the Space Shuttle Orbiter S-Band Quad Antenna and the Orbiter S-Band Payload Antenna. The theories include a plane surface model with a dielectric coating developed at the NASA-Langley Research Center and a curved surface theory developed at the University of Michigan. The results of the theoretical determination are then compared with measured data to substantiate the approach.

Commission G - Session 6

Friday, P.M. 1400 - 1640

RADIO EFFECTS OF IONOSPHERIC WAVES AND IRREGULARITIES

Chairman: T. Croft, Standord Research Institute

1. PHASE AND AMPLITUDE SCINTILLATION AT HIGH LATITUDE: C. L. Rino, E. J. Fremouw, Stanford Research Institute

The DNA Wideband Satellite was launched into a sun-synchronous 1000-km circular orbit on 22 May 1976. The satellite carries a multifrequency beacon with an S-band reference signal and phase-coherent transmissions at L-band, UHF, and VHF. Data have been recorded several times per week at Fairbanks, Alaska and Ancon, Peru (near Lima). In this paper we shall present a synoptic analysis of the high-latitude phase and amplitude scintillation data.

The measured standard deviation of phase follows a nearly perfect linear variation with wavelength (excepting the most severely disturbed passes) with no detectable Fresnel-radius dependence. Moreover, the phase spectra generally follow a power-law form from the lowest frequencies admitted by the filtering operation to the noise level. Thus, the signal phase spectrum is directly proportional to the ionospheric irregularity spectrum integrated over the scan direction.

The satellite orbit is such that many of the passes come very near the magnetic zenith. For all such passes we have observed a pronounced local enhancement of both the amplitude and phase scintillation, suggesting a geometrical enhancement due to field-aligned irregularities. A careful analysis shows, however, that the region of enhancement is longitudinally extended over that predicted by a simple cylindrically symmetric model. Sheet-like structures possibly explain this effect.

The phase scintillation spectral data are fitted with a log-linear power law to determine both the spectral intensity and the spectral index, P. The data show a high degree of variability in the spectral index. For the typically observed weak background irregularities, $P \sim -2.4$. During more disturbed conditions P achieves a value closer to the usually reported value of -3. On many occasions, however, the spectral index achieves value greater than -3.

2. INTERFEROMOMETER-MEASURED VELOCITY REVERSALS ASSOCIATED WITH AN ENHANCED SCINTILLATION FEATURE: R. C. Livingston, Stanford Research Institute

Spaced receiver measurements are being routinely collected in the auroral zone as a part of the Wideband satellite transmission experiment. The complex beacon signal at 413 MHz is received at each of three remote antennas, 300 m west, 600 m east, and 900 m south of the main station. Preliminary analysis, which has been directed toward obtaining diffraction pattern drift motion, has shown good agreement between the velocities estimated by correlation and cross-spectral methods using both signal intensity and phase. During quiet geomagnetic conditions, a velocity reversal is usually observed which corresponds to a distinct and consistent scintillation feature. This feature is often the only scintillation observed on an otherwise quiet pass, and has been observed in the pre-midnight sector over a narrow latitudinal but broad longitudinal range on successive nights. Two explanations of this feature have been suggested, a geophysical effect associated with the equatorward edge of the diffuse aurora, or an enhancement associated with the scattering geometry of field aligned sheets. The factors affecting the interpretation of the observed pattern velocity in terms of ionospheric irregularity structure and motion will be discussed for both of these cases.

3. IONOSPHERIC EFFECTS ON THE SEASAR SYNTHETIC-APERTURE RADAR BASED ON WIDEBAND SATELLITE DATA: W. D. Brown, Sandia Laboratories

Phase scintillation data at 1.24 GHz from the Wideband Satellite Experiment have been used to determine the expected performance degradations of SEASAR. These degradations are a result of propagation through ionospheric electron density irregularities. Values of the phase scintillation index were translated into estimates of the integrated sidelobe ratio by scaling from the detrend time to the synthetic aperture integration time. Values of other SAR performance parameters were obtained from the phase scintillation spectrum. On the basis of the data from Poker Flat, Alaska, it is demonstrated that SEASAR performance problems will occur for a significant fraction of the time in the polar region.

4. IONOSPHERIC BACKSCATTER REFLECTIVITY: G. S. Sales, RADC/ETEI, Hanscom AFB

HF backscatter radar data from the Polar Fox II system, which operated from a site in Northern Maine for a period of one year from November 1971 to November 1972, was used to determine the intrinsic backscatter characteristics of ionospheric irregularities of both auroral and non-auroral origin. The Polar Fox II system operated two days per week and produced, besides stepped frequency backscatter ionograms (6 to 26 MHz) at three azimuths every half hour, three fixed frequency, range vs azimuth maps of the auroral ionospheric regions. System calibrations were recorded with the data and detailed antenna patterns are available.

Several specific examples of this data have been selected and analyzed in an attempt to identify the propagation modes involved in reaching the clutter regions. The returned backscatter signals were then normalized for both the radar's operating parameters and the loss processes. Two specific reflectivities have been defined; one for land and sea surface scatterers and another for ionospheric volume scatterers. Three-dimensional ray-tracing techniques were employed, using available real-time ionospheric-vertical sounding data, as an aid in mode identification.

Surface reflectivities ranged from -20 to -40 dB (m^2/m^2) while ionospheric volume scattering reflectivities ranged from -50 to -80 dB (m^2/m^3) depending on the type of scatterer.

5. GHZ EQUATORIAL SCINTILLATION FROM A LOW-ORBITING BEACON SATELLITE: E. J. Fremouw, M.C. Cousins, R. C. Livingston, Stanford Research Institute

Ionospherically produced scintillation at GHz frequencies has been reported by a number of workers observing geostationary satellites at receiving stations near the geomagnetic equator. Among the explanations put forward for these initially unexpected observations is that the scintillations are produced by irregularities contained in a vast plasmaspheric region extending possibly to several earth radii. We report in this paper scintillations measured at Ancon, Peru on signals extending up to S band and transmitted from a beacon orbiting at 1000 km. While the measurements do not preclude a contribution from irregularities above 1000 km in the geostationary-satellite observations, they do demonstrate unequivocally that such irregularities are not a necessary condition for production of GHz scintillation. The measurements were made by means of the DNA Wideband beacon, which transmits ten coherent frequencies ranging from VHF (138 MHz) to S band (2891 MHz), the latter of which is used as a phase reference for measurements at the lower frequencies. The measurements reveal a diffraction-induced departure from the λ^2 frequency dependence of phase variance usually observed with Wideband, plus reduced correlation between scintillations (both phase and intensity) observed on UHF frequencies as closely spaced at 11.5 MHz.

6. A SPACED-RECEIVER INVESTIGATION OF EQUATORIAL SCINTILLATION AT UHF AND L-BAND: M. R. Paulson, R. U. F. Hopkins, Naval Electronics Laboratory

Scintillation amplitude measurements were made at Guam on signals from the GAPFILLER/MARISAT satellite simultaneously at UHF and L-Band during 1976. During July and September, spaced-receiver measurements were made using three UHF receivers giving 300, 700, and 1000-meter separations in a magnetic east-west direction. Two L-Band receivers were co-located with the outer UHF receivers. During August, October and November, one of the UHF receivers was operated by Naval Communications Station personnel in Guam, providing continuous information on scintillation activity over a five-month period.

Results of this investigation to be presented will consist of a comparison of scintillation at the two frequencies, including spaced-receiver cross correlations.

Cross correlation at UHF as a function of spatial separation will be shown as well as the variation of the correlation maximum with time.

Scintillation intensity will be compared with the apparent drift velocity of the irregularities for a number of cases.

Fade duration distributions will be shown and compared with some for earlier years.

Bit-error-rate measurements made over the satellite link during scintillating conditions will also be presented.

7. THE LOCALIZED ORIGIN OF EQUATORIAL IRREGULARITY PATCHES: J. Aarons, J. Buchau, Hanscom AFB, S. Basu, Emmanuel College, J. P. McClure, University of Texas at Dallas

An intensive study of nighttime irregularities of electron density in the equatorial ionosphere was performed in October, 1976, by making 50-MHz radar backscatter measurements at Jicamarca, Peru, and scintillation measurements of 249-MHz transmissions from LES-9 at two ground stations (Ancon and Huancayo, both in Peru), as well as by aircraft flying in the vicinity of the stations. The 137-MHz scintillations from the orbiting WIDEBAND DNA-2 satellite were also recorded at Huancayo. The results of the above co-ordinated measurements made on October 17, 1976, are discussed in the paper. It is found that on this particular night, a large scale irregularity patch evolved first in the west, as detected by the radar at Jicamarca, and drifted eastward to cause successive onsets of scintillation activity at Ancon and Huancayo. The observations indicate an east-west dimension of the large scale structure to be 400 km, drift-

ing eastward at a speed of 100 m/s, having a lifetime of at least 1½ hours, and containing a hierarchy of irregularity scale sizes in the range of meters to kilometers causing both radar backscatter at 50 MHz and scintillations at 249 MHz. On this night, another independent irregularity patch which could not be associated with either the radar maps or ground scintillation observations, was detected to the northwest of Jicamarca by airborne scintillation measurements. The DNA-2 observations of Huancayo revealed the presence of another irregularity patch with a latitude extent of at least 10° to the east of the ground stations. The measurements indicate the importance of local conditions for the generation of nighttime equatorial irregularities.

Commission G - Session 7

PROBING OF THE HIGH LATITUDE
IONOSPHERE AND MAGNETOSPHERE

Friday, P.M. 1400 - 1710

Chairman: M. Baran, Stanford Research Institute

1. OGO-3 OBSERVATIONS OF POWER LINE-INDUCED VLF CHORUS IN THE MAGNETOSPHERE: J. P. Luette, C. G. Park, R. A. Helliwell, Radioscience Laboratory, Stanford University

Very low frequency (VLF) chorus activity detected by the OGO 3 satellite was influenced by power line radiation (PLR) at high-order harmonics. Relative occurrence was highest in regions threaded by geomagnetic field lines that intersect industrialized areas. For spacecraft passes inside L = 10, PLR accompanied by interaction with chorus occurred at multiples of 60 Hz along North American meridians and 50 Hz along the Western Europe meridian. Interpretation of these results is based on radiated harmonics that leak into the magnetosphere and stimulate the recorded emissions through cyclotron interaction with trapped energetic electrons.

2. MORPHOLOGY OF THE F-REGION AT CHATANIKA, ALASKA: R. R. Vondrak, Radio Physics Laboratory, Stanford Research Institute

The incoherent-scatter radar at Chatanika, Alaska has been used to map out the two-dimensional (altitude, latitude) spatial variation of ionization in the high-latitude F-region. A region of approximately 600 km horizontal extent can be surveyed with a spatial resolution of about 10 km. Several such ionization maps can be made each hour. F-region phenomena that have been observed include the latitudinal dependence of the sunset decay of ionization, a post-sunset ionization increase associated with geomagnetic activity, and quasi-periodic spatial variations that resemble traveling ionospheric disturbances. The time history of ionization morphology is used to distinguish variations produced by transport mechanisms from those due to local production.

3. ESTIMATE OF THE RELATIVE IMPORTANCE OF JOULE HEATING AND THE LORENTZ FORCE IN GENERATING GRAVITY WAVES (AGW'S) FROM THE AURORAL ELECTROJET:
R. D. Hunsucker, Geophysical Institute, University of Alaska

The general problem of generation of AGW's by the auroral electrojet, and the relative roles of Joule heating and Lorentz force has been treated in theoretical developments by Chimonas and Hines [1970], Testud [1973] and Francis [1974 and 1975].

In their paper, Chimonas and Hines derive an expression which describes the relative contribution of the Lorentz force and Joule heating for generating AGW's from the auroral electrojet.

Data hitherto unobtainable permits us to make a new evaluation of their equation. Specifically, Pedersen and Hall conductivity have been obtained by Brekke and others using the Chatanika radar, and estimates of current density are available from simultaneous magnetometer data for six 24-hour periods. Twenty data sets for auroral electrojet peak values were used to evaluate the equation.

From analysis of these rather sparse data the following conclusions can be made.

1. The theoretical prediction of $\frac{L}{J} \simeq 0.1$ to 10 for "moderate disturbances" made by Chimonas and Hines appears to be true. The average value of $\frac{L}{J} = 2.37$ for an average electric field of $\simeq 43$ mV/m for our measurements.

2. Electrojet current peaks occurred for the period 1500 to 0800 AST for the data analyzed.

3. The only period when the "Joule contribution" dominates over the Lorentz contribution" for AGW generation is $\simeq$ (1500-1700 AST).

4. The period when the Lorentz contribution is strongest is at or near magnetic midnight.

5. There seems to be a tendency for the Lorentz contribution to be stronger post-magnetic midnight than pre-magnetic midnight.

6. There is at least a tendency for $\frac{L}{J}$ to converge on a value of $\simeq 2.5$ for auroral electrojet current densities of $\simeq 1.5$ to 2.5 amps/meters.

4. PLASMA LINES IN THE AURORAL E-LAYER: V. B. Wickwar, Radio Physics Laboratory, Stanford Research Institute

The first successful measurements of plasma lines in the auroral E-layer were made in January 1976 using the Chatanika Incoherent-Scatter radar. While the magnitude of the typical ion component signal is 150 K, the magnitude of the largest plasma-line signal measured was only 7 K. Both upshifted and downshifted plasma lines were observed. Their frequencies were between 3.8 and 6.0 MHz; their altitudes were between 100 and 135 km. The resultant plasma lines were enhanced between 4 and 30 times above the thermal level. The observed intensities are compared to predicted intensities arising from secondary electrons. The range of intensities and their altitude variation are consistent with excitation by secondary electrons.

5. DISTRIBUTION OF FIELD-ALIGNED CURRENT AND ELECTROSTATIC POTENTIAL AROUND ARUORAL ARCS: O. de la Beaujardiere, R. R. Vondrak, Stanford Research Institute

The Chatanika incoherent scatter radar has been used to measure the variation of ionospheric parameters in and near auroral arcs with a spatial resolution of a few kilometers. The measured parameters include the current, the electric field, the differential energy flux of the incoming auroral electrons, and the electron and ion temperatures. The data indicate that there is an intense upward Birkeland current within the arc of 3 to 40 $\mu A/m^2$. A return current of approximately the same magnitude is also observed. Within the arc the differential energy spectra of the incoming electrons are Maxwellian distributions that have been accelerated through an electrostatic potential of up to 5 kV. The arc is an "inverted-V" structure that extends over only a few tens of km in latitude. The north-south potential in the ionosphere is calculated from the measured electric field variations across the arc. The energy flux due to electron precipitation has its maximum within the arc (30 $ergs/cm^2$ - s). In contrast, the Joule heating maximum occurs outside of the arc (10 $ergs/cm^2$ - s). The electron temperature follows quite closely the precipitating energy variations, whereas the ion temperature follows the Joule heating variations.

6. THE EQUATORWARD BOUNDARY OF THE DIFFUSE AURORA--WIDEBAND SATELLITE/CHATANIKA RADAR SIMULTANEOUS OBSERVATIONS: O. de la Beaujardiere, M. D. Cousins, Stanford Research Institute

Coordinated experiments between the Chatanika incoherent scatter radar and the Wideband satellite are done on a routine basis. The Chatanika radar is used as a diagnostic tool to help determine the conditions necessary for the development of scintillation producing irregularities and plasma instabilities. At the equatorward boundary of the diffuse aurora the electron-density profile presents on some occasions an F-region maximum. This enhancement is at about 250 km altitude and extends over about one degree in latitude. The differential energy spectra of the incoming primary electrons are obtained from the radar data. Preliminary results indicate that the electron energy distributions are Maxwellian. The characteristic temperature E_o, and the total energy flux show a sharp increase at the boundary. The horizontal electric fields and currents as well as the field-aligned currents can also be derived from the radar data. Their latitudinal variations associated with the diffuse aurora will be examined.

7. OBSERVATIONS OF THE IONOSPHERIC TROUGH: M. D. Cousins, O. de la Beaujardiere, Stanford Research Institute

Ionospheric total electron content measurements made using the Wideband satellite beacon and a receiving station near Fairbanks, Alaska clearly show the ionospheric trough. The measurement technique applies the coherent Wideband beacon to determine dispersive phase and second difference of dispersive phase at UHF compared to an S-band reference. Total electron content is then found through its linear relation to dispersive phase. The poleward boundary of the trough is a particularly repeatable feature seen in the data through the summer, fall, and winter of 1976. The spatial gradient of total content in the trough poleward boundary is investigated for both night and daytime data. The behavior of the ionospheric trough position, its detailed structure, and its relation to pertinent geophysical parameters are examined. The nature of the vertical electron density distribution in the trough is determined via Chatanika radar data obtained in coordination with Wideband satellite passes.

Commission H - Session 3

Friday, P.M. 1400 - 1650

WAVES IN PLASMAS

Chairman: F. W. Crawford, Institute for Plasma Research, Stanford University

1. LOWER HYBRID HEATING OF A HOLLOW CATHODE ARC PLASMA: W. P. Ballard, S. E. Rosenthal, D. B. Ilic, F. W. Crawford, Institute for Plasma Research, Stanford University

In the experiments to be described, the highly-ionized, inhomogeneous plasma formed by a hollow cathode arc discharge in argon is being used to investigate the rf heating of the plasma by waves propagating almost radially near to the lower hybrid frequency (5-15 MHz). A subsidiary coaxial anode is used to start the arc and serves, in conjunction with the core of the arc, as an antenna to excite a quasi-coaxial, azimuthally-symmetric pump wave. The finite antenna excites a pump wave with $k_{\parallel}$ sufficiently large for the lower hybrid resonance layer to be accessible.

The loading of the rf pump source by the plasma is being studied with a specially-constructed homodyne receiver, which displays the locus of the reflection coefficient in the complex plane as the pump frequency is swept. The resulting CRT (or X-Y plotter) display serves to indicate the range of discharge parameters and pump frequencies where efficient coupling of rf energy into the plasma is achieved, and the effects of pump power level on the coupling efficiency.

Triaxial probes are being constructed to study the pump wave propagation in the plasma, and conversion at the lower hybrid resonance layer.

2. AN ANTENNA FOR SLOW WAVE COUPLING TO THERMONUCLEAR FUSION PLASMAS:* S. Bernabei, W. M. Hooke, R. W. Mosley, F. J. Paoloni, Plasma Physics Laboratory, Princeton University

The damping of large amplitude slow waves in the lower hybrid frequency range is very promising as a plasma heating method for thermonuclear fusion studies. A major difficulty for this approach lies in the coupling of the wave to the plasma, since the wave requires a refractive index (along the confining magnetic field) greater than unity in order to penetrate the plasma. At PPPL we have been studying[1] an antenna composed of an array of parallel waveguides which proved to be very successful in coupling to these waves in a toroidal plasma.[2] Transmission efficiencies of up to 90-95% have been achieved. In addition, this antenna proved to be naturally matched

to the plasma, thus eliminating the need for a complex matching system. In this paper we will discuss the importance of the various parameters involved in the coupling and present the results from a recent experiment.[2]

*Work supported by the US ERDA Contract E(11-1)3073.

[1] S. Bernabei, M. A. Heald, W. M. Hooke and F. J. Paoloni, Phys. Rev. Lett. 34, 866 (1975).

[2] S. Bernabei, C. Daughney, W. M. Hooke, R. W. Motley, M. Porkolab, T. Nagashima and S. Suckewer, Proceedings of the Symposium on Plasma Heating in Toroidal Devices, Varenna, 1976, (to be published).

3. SPECTRAL DENSITY OF ION ACOUSTIC PLASMA WAVES: D. B. Ilic, K. J. Harker, F. W. Crawford, Institute for Plasma Research, Stanford University

The detailed spectral density, $S(\underline{k},\omega)$, of ion acoustic plasma waves in a collision-dominated positive column is obtained from measured frequency sweeps of the complex cross-power spectra. The cross-power spectra are recorded for different probe separations, and a two-dimensional spatial Fourier transform is performed on a digital computer to yield sample points, $S(k_r, k_z, \omega)$. The spectral density is compared to the predictions of linear theory for low levels of turbulence; the values of correlation lengths and times are also derived. Integrating out the wave-number dependence yields power spectra which agree with those measured by a single probe. Further integration of the frequency dependence gives wave energy density normalized to thermal energy of about 10^{-4}, weakly decreasing with increasing pressure.

Knowledge of the fluctuation spectrum allows various transport coefficients to be calculated. In particular, a general expression has been derived for the component of the diffusion coefficient due to turbulent wave fields, valid for any ratio of the correlation and collision times. For our experiment, the resulting turbulent diffusion coefficient is predicted to be about 1% of the diffusion coefficient due to electron-neutral collisions.

4. SCATTERING OF LOW FREQUENCY SOLAR RADIO BURSTS BY INTERPLANETARY PLASMA IRREGULARITIES: J. S. Hornstein, R. R. Weber, Computer Sciences Corporation, R. J. Fitzenreiter, J. Fainberg, NASA/Goddard Space Flight Center

Scattering by irregularities in the interplanetary plasma broadens and displaces the images of solar radio bursts, and lengthens their time profiles. These effects on low frequency (25-5000 kHz) radio bursts are being studied by ray tracing, using a Monte Carlo technique to model irregular refraction. Our method includes two special techniques which significantly reduce the computation required. These two techniques are: a scaling law for images and time profiles, applicable in a plasma whose average density varies as the inverse square of the distance from the Sun; and a method of stacking images so that all the launched rays can be used in image forming, assuming the averaged medium is spherically symmetric. For type III bursts, emitted at twice the local plasma frequency, we find that rays are intensely scattered in a small region surrounding the source, and propagate freely once they emerge from this region. Brightness distributions and image displacements have been computed for source-observer configurations appropriate to observations by HELIOS-A and -B and RAE-2, allowing the inferred trajectory of the high energy electron streams exciting the bursts to be corrected for regular and irregular refraction.

5. OBSERVATIONS OF A FREE PLASMA DOUBLE-SHEATH: J. S. Levine, D. B.Ilic, F. W. Crawford, Institute for Plasma Research, Stanford University

A free double-sheath is a combination of an electron and an ion sheath in close proximity, localized in an otherwise geometrically uniform region of the plasma. In our unmagnetized, 2.5 cm diameter, argon positive column, at a neutral pressure of about 1 mTorr, the voltage-current characteristic is observed to be nearly flat for currents less than 5 A, and then rises sharply, effectively limiting the current. This current limitation is accompanied by large voltage spikes at the anode, with the cathode grounded. The double-sheath is identified as a 1 cm length of the plasma, with a 10 V ($\approx$ twice the electron temperature) potential step, which generates these pulses. Intense wall heating and a sharp transition in the luminosity of the plasma occur there.

Double-sheath formation is studied by pulsing the column from about 2 A to about 6 A, with 300 μs pulses, at a repetition rate of 1000/s. The current is limited to 5.6 A at approximately 150 μsec, consistent with the dc column. Time-resolved studies show that the rf emission, as received by single-loop wire antennas 2 cm upstream and downstream of the double-sheath,

grow and saturate at the time when limitation of the current pulse occurs. Signals below 10 MHz are about 5 db higher on the anode side of the sheath; signals above 16 MHz are unaffected by the sheath.

In an additional experiment, an electron-beam probe is being used to investigate the possible presence of double-sheaths in the "meniscus" region of a discharge, where the cathodic electron beam is broken up by rf beam-plasma interactions.

6. EXPERIMENTAL INVESTIGATION OF THE ABSORPTION OF ENERGY FROM AN EMP PROPAGATING THROUGH A PLASMA: R. N. Carlile, University of Arizona, W. A. Seidler, Simulation Physics, Inc.

We have built a plasma machine which allows us to experimentally investigate the propagation of an EMP through a nitrogen plasma of low energy electrons. The direction of propagation is along a DC magnetic field. Scaling laws are discussed which allow the experimental results to be applicable to a scaled EMP propagating in a scaled nitrogen plasma. To date, we have observed the absorption of energy from an EMP and the distortion of its wave-shape due to its interaction with the plasma. These results are discussed. Scaling certain of these results to a nitrogen ionosphere, we conclude that an EMP of approximately .05 microsecond half-width and weak amplitude will have half of its energy absorbed while it travels 60 meter at 110 KM altitude.

One of us has developed a theory which we have used to predict our experimental results. This theory makes use of the fluid model of a plasma with a transformation from real to retarded time. This theory has been able to predict experimental results to within 20%.

AUTHOR INDEX

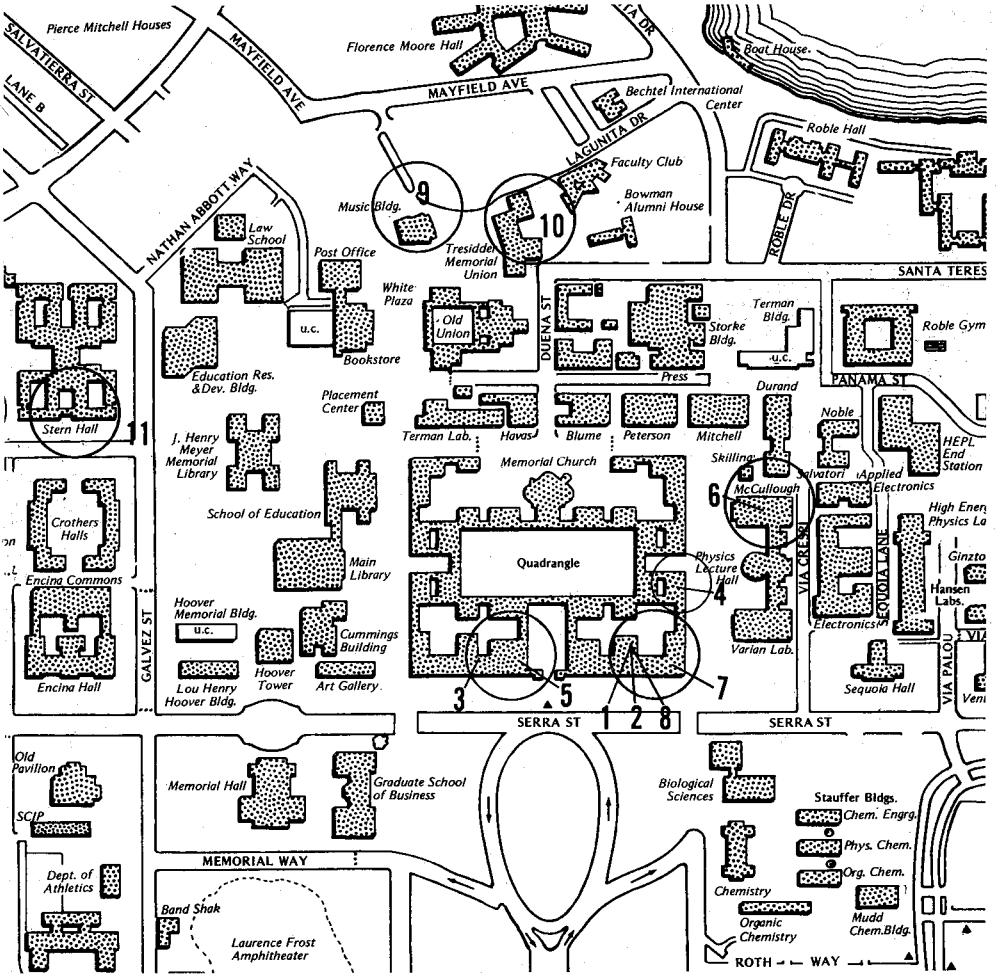

MAP LABEL	MEETING TYPE	BUILDING	ROOM
1	I	Jordan	040
2	II	Jordan	041
3	III	Political Science	161J
4	IV	Quad	370
5	V	120	121
6	VI	McCullough	134
7	VII	380 - Math	380Y
8	VIII	Jordan	050
9	Combined session (URSI IEMS, IEEE APS, USNC/URSI)	Music Building	Dinkelspiel Auditorium
10	Conference Registration and Message Center	Tresidder Union	270
11	On-Campus Residence and Dining	Stern Hall	